Seasonal Structure of the Gulf of St.Lawrence Upper-Layer Thermohaline Fields during the Ice-free Months

By Patrick Doyon

Department of Atmospheric and Oceanic Sciences
McGill University, Montréal

July 1996

A Thesis submitted to the Faculty of Graduate Studies and Research in partial fulfillment of the requirements for the degree Master of Science.

ISBN 0-612-19807-3

Abstract

The interactions between the atmosphere and the oceans play a critical role in determining our climate. These generally consist of various exchanges of heat, mass and momentum between the two media through the air-sea interface. Therefore, the physical state of the upper few meters of the oceans influences the rate at which these exchanges take place. Furthermore, these surface waters are of importance in affecting the primary biological production of the seas. In this context, knowledge of the upper-layer monthly averaged thermohaline state, i.e. temperature (T) and salinity (S) as a function of latitude-longitude and depth, is necessary for further climatological/oceanographic studies in the Gulf of St.Lawrence (GSL). The primary goal of this research is to produce, using basic statistical analyses, monthly mean fields of T and S and related quantities at various depths throughout the GSL. The historical hydrographic dataset covers the last 75 years.

Objective fields of sea surface temperature (SST), salinity (SSS) and chlorophyll-a (Chl-a) were also computed and compared with other similar climatologies (when available). Due to the enhanced observational coverage of SST and Chl-a resulting from the use of recent satellite-derived data, these interpolated fields reproduced several known physical surface characteristics of the GSL with a very small relative interpolation error. Using the aforementioned SST maps in combination with usual atmospheric fields and satellite-derived (ISCCP) monthly averaged cloud cover data, the surface heat budget was computed over the entire GSL for the 7 ice-free months.

Monthly means of mixed-layer depth (MLD), upper-layer heat content (HC) and upper-layer static stability (E) were obtained for 15 sub-regions of the GSL. Using simple 1D calculations (heat transfer, mixed-layer deepening rates, stratification change rates, heat storage rates), the seasonal evolution of the upper-layer thermohaline structure was studied. It was observed that "qualitatively", the upper-layer could be relatively well modeled for most areas by considering only the vertical processes. Inclusion of horizontal effects (e.g., slow advection of buoyancy from runoff) should lead to better results, particularly in the western and northern Gulf.

Résumé

Les interactions entre l'atmosphère et l'océan jouent un rôle critique envers le climat. Celles-ci se composent de différents échanges de masse, de momentum et d'énergie à travers l'interface air-mer. Par conséquent, l'état physique des eaux à la surface des océans influence de façon critique le taux auquel ces échanges ont lieux. De plus, ces eaux de surface sont d'une très grande importance en ce qui concerne la production biologique océanique. Dans ce contexte, une connaissance approfondie des caractéristiques thermohalines mensuelles moyennes de cette couche de surface, i.e.: température (T) et salinité (S) en fonction de la profondeur et de la latitude-longitude, est requise pour toute autre recherche océanographique et climatologique dans le Golfe du St-Laurent (GSL). Cette recherche avait donc comme objectif premier, à la suite d'un long processus de "filtrage et nettoyage" des données, de produire ces champs mensuels moyens de T et S à l'aide de méthodes statistiques de base. Les données hydrographiques historiques couvrent les 75 dernières années.

Les champs horizontaux de T, S et chlorophylle-a en surface (SST, SSS, Chl-a) furent calculés via méthode d'analyse objective, et comparés ensuite avec d'autres climatologies similaires. Grâce à une densité accrue d'observations de SST et Chl-a via l'utilisation des récentes données satellite, ces champs reproduisirent fidèlement la plupart des détails physiques observés via télédétection (eaux plus froides dues à l'upwelling, gradients thermiques latéraux, etc.). A l'aide des champs SST mentionnés ci-haut, et grâce à 8 années de données satellite de nébulosité mensuelle (ISCCP), le bilan de chaleur de surface fut calculé pour les mois sans glace. Les moyennes mensuelles de la profondeur de la couche limite (MLD), de la quantité de chaleur des eaux de surface (HC) et de la stabilité statique (E) furent aussi calculées pour 15 sous-sections du GSL. A l'aide de calculs 1D simples (transfert de chaleur, conservation de volume et d'énergie), l'évolution saisonière de la couche supérieure du Golfe (T, MLD, E) fut étudiée. De façon générale, son comportement mensuel fut relativement bien prédit pour l'ensemble du Golfe malgré la simplicité des calculs (1D, vertical). Cependant, de meilleur résultats pourraient être obtenus, particulièrement au nord et à l'ouest du GSL, si l'on tenait compte des effets horizontaux, tels l'advection d'eau douce provenant des rivières.

Acknowledgements

First, I should thank my supervisor, Dr. Grant Ingram, who, despite being on sabbatical during my thesis, supported me morally and financially throughout this work, particularly during my few months stay at the hospital due to a climbing accident. He also gave me the opportunity to "go to sea" during one of the JGOFS hydrographic cruises. Merci.

Merci also to my folks (Maman et Papa), for a great part of what I am today, I take it from them. They also helped me, via constant "telephone" kicks in the behind, to finish this work. Again, merci.

Finally, merci to my girlfriend (Mamour) who supported me (emotionally, morally and etc.) during the last year of my thesis. She's also become one of my best friend. xo

And to all the others - data providers, anonymous internet correspondents, friends and colleagues, and especially to the anonymous external reviewer for his useful comments - merci.

Table of contents

Figures and Tables

Figures

Tables

Un jour je vis passer, debout au bord des flots mouvants,

Passer, gonflant ses voiles,

Un rapide navire enveloppé de vents,

De vagues et d'étoiles;

Et j'entendis, penché sur l'abîme des cieux,

Que l'autre abîme touche,

Me parler à l'oreille une voix dont mes yeux

Ne voyaient pas la bouche:

" Poète, tu fais bien! Poète au triste front,

Tu rêves près des ondes,

Et tu tires des mers bien des choses qui sont

Sous les vagues profondes!

La mer, c'est le Seigneur, que, misère ou bonheur,

Tout destin montre et nomme;

Le vent, c'est le Seigneur; l'astre, c'est le Seigneur;

Le navire, c'est l'homme."

Victor Hugo
Juin 1839, Les contemplations

A maman (à qui je ressemble tant), à papa (qui me garde toujours bien droit), à ma blonde (que j'aime gros comme le Monde)

Chapter 1

Introduction

1.1 The Physical Environment: *The Gulf of St.Lawrence*

"Petit océan ou grand estuaire" is a question often asked by oceanographers studying the Gulf of St.Lawrence, a large semi-enclosed sea (approximately 226 000 km^2) located at mid-latitudes (approx. 46-51°N and 55-70°W). Lying between the Appalachian Mountains and the highlands of the Canadian Shield, it receives the discharge from the St. Lawrence River, whose length (3060 km) and the size of its drainage basin (1344000 km^2 excluding the Gulf), place it among one of the largest rivers on earth. This complex hydrographic system drains one of the world's largest freshwater masses, the Great Lakes, and plays a critical role in the environmental as well as economic life of the North American continent.

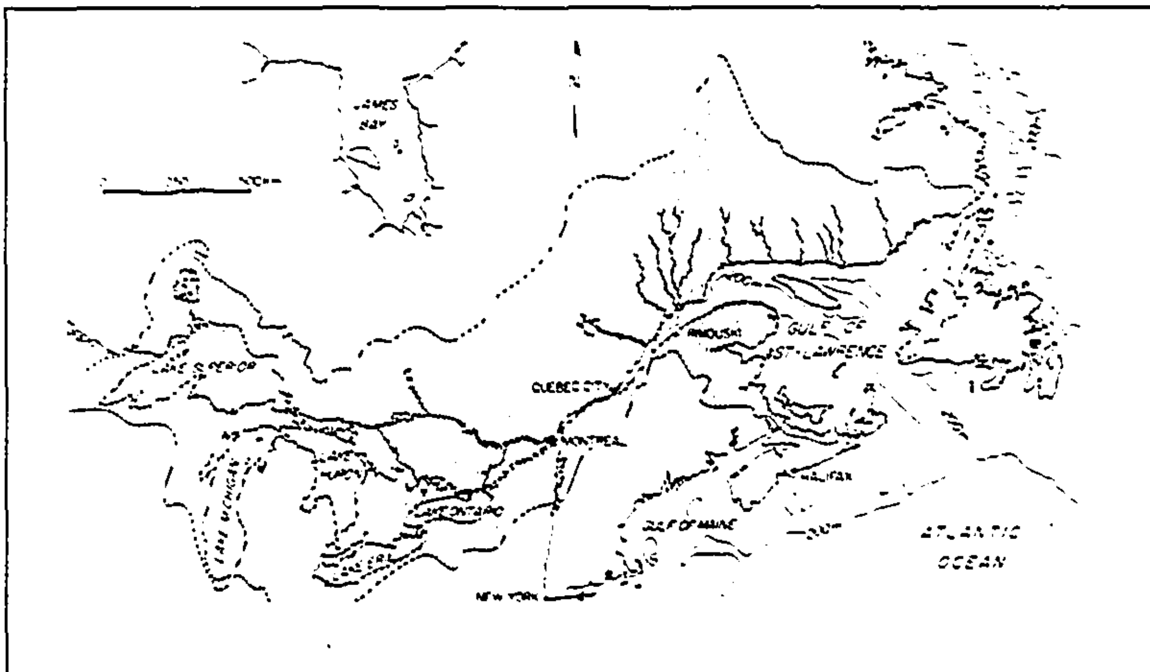

fig. 1.1: *The Gulf of St.Lawrence and its watershed* (from Koutitonsky and Bugden, 1991)

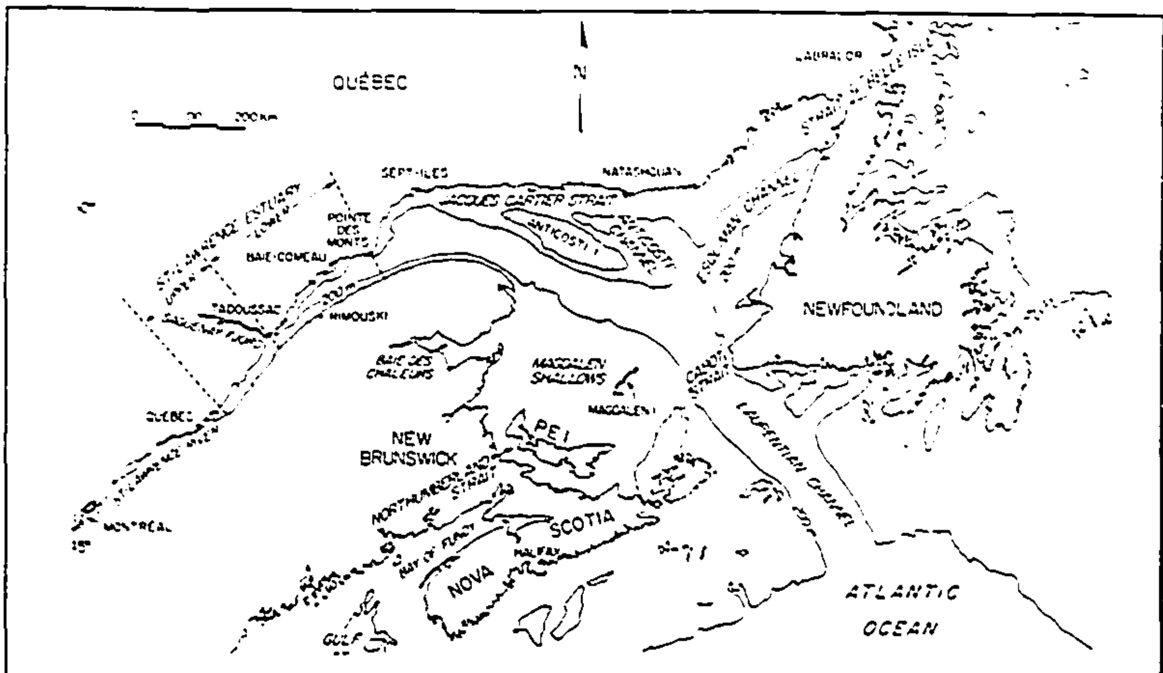

fig. 1.2: Physiographic features of *the Gulf of St.Lawrence* (from Koutitonsky and Bugden, 1991)

Runoff and bathymetry:

The Gulf of St.Lawrence (GSL) consists of a reservoir of considerable volume (34500 km^3, Forrester, 1964) and complex shape. Its bathymetry is profoundly marked by a deep trough of 500m maximum depth, the Laurentian Channel, extending from the Saguenay River to the Atlantic Ocean (defined by the 200m isobath on fig. 1.1 & 1.2). Two smaller trenches branch out from this main channel towards the northwestern and northeastern region of the Gulf: the Anticosti and Esquimain channels. An equally important bathymetric feature of the GSL is the Magdalen Shallows. The depth of the water column there ranges from 50 to 80 meters and forms a large shallow plateau covering nearly the entire southern part of the Gulf. The basin receives a considerable amount of freshwater runoff from the St.Lawrence River and its tributaries. This massive inflow of water exhibits a strong seasonal signal, with maximum discharge values during the spring. It is believed that this input of freshwater throughout the year is responsible for the typical estuarine density-driven circulation pattern in the Gulf (when averaged laterally, see Koutitonsky and Bugden, 1991, for schematic diagram and for monthly runoff values).

General horizontal and vertical circulation patterns:

A similar vertical thermohaline structure can be observed throughout the Gulf: it consists of a permanent deep, salty layer of oceanic origin (2 to 5°C, 33-35 PSU), an intermediate cold layer (-1 to 2°C, 32-33 PSU), which is the product of both in-situ wintertime cooling and advection through the Strait of Belle-Isle (Petrie et al., 1988), and a surface layer (roughly 50m deep) undergoing strong seasonal variations of temperature (T) and salinity (S) during the ice-free season but merging in T-S characteristics with the intermediate layer during the winter. As mentioned earlier, the laterally averaged circulation is characterized by a fresher surface flow towards the ocean with a weaker and saltier return flow at depth, through the Laurentian channel (Koutitonsky and Bugden, 1991). At the surface, the water currents exhibit a large-scale counterclockwise circulation pattern with strong horizontal velocities along the Gaspé Peninsula (the Gaspé current) and a broader more diffuse flow over the Magdalen Shallows (El-Sabh, 1976).

Surface temperatures, ice coverage and climate:

As Déry (1992) reports, the Gulf of St.Lawrence is one of the few semi-enclosed seas below the Arctic circle which experiences seasonal ice formation. While most of this ice is produced locally in the estuary and in the Gulf, some enters the GSL through the Strait of Belle-Isle. The surface coverage increases rapidly in January, usually spreading from the east and from the northwest into the central Gulf, to reach its maximum in early March. The prevailing spring winds and currents, combined with melting, help to rapidly break up the remaining ice and transport it onto the Scotian Shelf via the Cabot Strait. As will be discussed in the next chapter, the presence of an ice cover has important effects on the oceanography of the region. Monthly mean surface air temperatures over the water exhibit a strong annual cycle, with maximum values reaching, on average, roughly 12° to 18°C in July-August and minima ranging from -4° to as low as -14°C in January. In general (see chapter 4) there is usually (on the monthly time scale) a 3° to 6°C difference between the northern and southern Gulf (see section 4.1 for monthly climatological maps). Consequently, the sea surface temperatures display a strong seasonal signal, with their maxima (10° to 16°C, but as low as 8°C in the estuary) and minima (freezing point of sea water) occurring roughly a month later than those of the air (see chapter 5 for a description of these fields).

Oceanic forcing and tides:

The St.Lawrence is not recognized as having a strong tidal flow (tidal currents rarely exceed 30 cms^{-1} for the Gulf region, Koutitonsky and Bugden, 1991). However, Pingree and Griffiths (1980) demonstrated in a numerical model study of the M_2 component that, in some areas of the GSL, particularly in narrows and straits and/or shallower regions, tidal streaming may increase substantially and lead to mixing of the entire water column by the effect of bottom friction stress. Consequently, they suggested that, on the basis of the Simpson-Hunter parameter computation (see Pingree and Griffiths, 1980, for a definition), well-mixed waters might be observed in the Jacques-Cartier Passage, and the Northumberland and the Belle-Isle Straits. The M_2 constituent (with its amphidromic point near the Magdalen Islands) and the K_1 constituent (amphidromic point slightly to the south-east of Cape-Breton Island) dominate tidal elevations. Tidal heights are rather low in the Gulf (0.2 to 0.5m) but increase significantly in the Estuary. In terms of oceanic forcing, the Gulf of St.Lawrence is connected to the Atlantic through Cabot Strait (min. width: 104 km, max. unrestricted depth: 480m, min. x-section area: 35 km^2) and to the Labrador Sea via the Strait of Belle-Isle (min. width: 16 km, max. unrestricted depth: 60m, min. x-section area: 1 km^2, from Déry, 1992). The inflows and outflows of water through Cabot Strait are more significant for the oceanography of the Gulf than through the Strait of Belle Isle. In general, currents are found to be seaward near the surface and along the Cape-Breton side, whereas an upstream flow from near the surface down to the bottom is characteristic of the Newfoundland side of Cabot Strait (Trites, 1972). The flow pattern through Belle-Isle Strait is rather complex, with the direction of inflow/outflow dependant on variations of sea level pressure, following the geostrophic balance, across the strait (Garrett and Petrie, 1981). The hydrographic influence of both straits on the T-S characteristics of ambient waters will be discussed in chapter 5.

Atmospheric forcing:

The principal meteorological forcing influencing the Gulf's oceanography are as follows: the winds, the clouds, the air temperature and moisture, precipitation and solar radiation. Since these factors are described in chapter 4 in greater detail, only a brief discussion will be given here. Although the presence of the Gulf certainly affects the spatio-temporal evolution of these meteorological variables (e.g.: air temperatures milder in winter and cooler in summer, coastal and frictional steering of the winds, influence on cloud formation, humidity, surface albedo, etc), it is fair to say that, for the time and length scales involved in the present study (see chapter 2), this semi-enclosed sea is mainly driven by the atmosphere (and not the contrary). Consequently, an understanding of the seasonal evolution of the GSL surface waters must rely on a rather detailed knowledge of the atmospheric systems passing over the Gulf. For example, the prevailing winds for this region are mainly from the west (Saunders, 1977) with wind speeds stronger during the winter and minimum during the summer (see section 4.2). Consequently, this dominant surface atmospheric flow pattern advects continental masses of air, hence influencing the air temperature, relative humidity and cloud cover over the Gulf. Moreover, the atmospheric processes directly affect the rate at which the exchanges of mass, momentum and energy take place across the air-sea interface (section 2.2 & chapter 5).

1.2 Recent Oceanographic Climatological Studies in and near the Gulf of St.Lawrence

There have been several previous studies of the Gulf's oceanography and climate, particularly the excellent review paper by Koutitonsky and Bugden (1991) which thoroughly examines most physical processes occurring in the St.Lawrence in light of previous hydrographical studies (recent and less recent). Moreover, partial results of several investigators that will be used for comparison in the following chapters have been obtained directly from Koutitonsky and Bugden's review work. An important study dating back to 1964 by Forrester, and later reviewed by Trites and Walton (1975) was one of the first global oceanographic syntheses of the Gulf of St.Lawrence. More recently, researchers (Petrie, 1990, Vigeant 1984, Bugden et al., 1982, Weiler and Keeley, 1980) have investigated the surface thermohaline fields of the GSL in greater detail. In fact, as discussed in later chapters, Petrie's data report (1990) on the monthly-depth distribution of temperature and salinity throughout the Gulf proved to be very useful for this research and, to the author's knowledge, constitutes perhaps the most complete climatological study to date of the GSL T and S fields.

Previous studies concerning surface heat budget in the GSL are rare and Bugden's (1981) work constitutes the only recent study involving surface heat flux computations. In his study, Bugden segmented the Gulf into four large areas - the Estuary, the Northeast, the Northwest and the Southcentral GSL - for which he then calculated monthly averages of temperature, salinity, and other atmospheric parameters. This enabled him to estimate the energy fluxes across the surface of each area. These results are of interest for the present study since they constitute the only known surface heat budget with which comparisons can be made.

Although this research is not directly concerned with the Gulf's circulation, a knowledge of the current velocities is useful in explaining the possible causes of the upper mixed-layer behaviour and water mass modifications. The results of El-Sabh (1976) provide a widely accepted estimate of the Gulf's surface currents. More recently, Toro (1991) calculated the three-dimensional density-driven circulation throughout the GSL by diagnostic modelling. However, no full modelling study of the entire Gulf's circulation is yet available. It is also worth mentioning the work of Gan (1995) on the upper-layer modelling of the Baie-des-Chaleurs/Gaspé current, and that of Reynaud (1994) concerning the dynamics of the northwestern Atlantic Ocean. Although these two authors were investigating oceanic areas adjacent to the Gulf, their contributions can only help the understanding of the dynamical/physical processes occurring at the GSL boundaries.

Finally, four other studies have been selected as relevant to this research. First, Déry (1992) completed an exhaustive study on the variability of the Gulf's ice-cover while DeTracey (1993) continued Déry's work in modelling the sea-ice response to various types of physical forcing (air and water temperature, winds, mixed-layer depth, etc). Since the present research was primarily concerned with the ice-free months (May to November), Déry's and Detracey's results might be useful in "closing" the annual cycle and understanding the influence of winter ice-cover on surface waters in the following spring. Furthermore, Petrie and Drinkwater (1993) and Bugden (1991) investigated the extraseasonal temperature and salinity variability of water masses in and near the Gulf. Bugden studied deep Laurentian Channel waters while Petrie and Drinkwater were concerned with surface waters near Cabot Strait and on the Scotian Shelf. Knowledge of the climatological fluctuations of these waters helps the understanding of the seasonal formation of the Gulf's thermohaline fields as well as their fluctuations in time.

1.3 Objectives of the Present Study

The interactions between the atmosphere and the ocean play a critical role in determining our climate. These generally consist of various exchanges of heat, mass and momentum between the two media across the air-sea interface. Consequently, the physical state of the upper few meters of the oceans influences the rate at which these exchanges take place. Furthermore, these surface waters are of importance for the primary biological production in the seas. In this context, a general knowledge of the average seasonal state of the surface layer in the Gulf of St.Lawrence is desirable for any further studies on climatic fluctuations and their related effects.

Although much of the work done in this research involves "cleaning-up" the oceanic dataset for the GSL, another goal is to describe and understand the climatological state of the upper mixed-layer in the Gulf. Ultimately, this may assist in the integration of all the oceanic constituents (physical, chemical, biological) for the GSL within its climatic context. More specifically, this study has the following objectives:

- To produce an updated version of Petrie's original monthly-depth averages of temperature and salinity throughout the Gulf for the same sub-areas but using an improved (larger and with less errors) oceanic dataset (provided by K. Drinkwater).

- To form updated composite and Gulf-wide T-S relationships and discuss the various water masses (three layers) observed in the GSL.

- To calculate monthly averages of mixed-layer depth (MLD), upper-layer heat content and static stability during the ice-free season (May to November) for the same subsections used by Petrie, and discuss their seasonal evolution in light of the other atmospheric variables (mainly air temperature and wind).

- Using objective mapping techniques, in combination with various data sources (hydrographic and satellite derived), to produce monthly fields of sea surface temperature (SST), salinity (SSS) and chlorophyll-*a* (Chl-*a*) for the seven ice-free months.

- Using these SST fields as well as all other necessary atmospheric data (chapter 4), to compute a detailed climatology of the surface heat budget (shortwave, longwave, sensible, latent and net heat fluxes), again, for the ice-free months.

- To assess, using simple 1D calculations (heat transfer, mixed-layer deepening rates, stratification change rates, heat storage rates), which mechanisms are mainly responsible for the observed monthly upper-layer thermohaline structure throughout the Gulf.

- To process all the hydrographic data collected in the GSL during the 9 CJGOFS (Canadian Joint Global Ocean Flux Study) cruises and compare them with the appropriate climatologies previously computed in order to characterize the water mass changes at these stations over the annual cycle.

Chapter 2

The Physical Structure of the Upper Mixed Layer: *Review of Current Knowledge & Related Literature*

2.1 Introduction

The important role played by the oceans in affecting the global climate is now generally accepted, and has received considerable attention in the last decade by the scientific community (Mysak and Lin, 1990). The inherent thermodynamic properties of seawater compared to those of air clearly depict the enormous differences in volumetric

	Specific Heat Capacity (C_p)	Density (ρ)	(ρC_p)
air	$\approx$ 1000 $Jkg^{-1}K^{-1}$	$\approx$ 1 kgm^{-3}	$\approx$ 1000 $Jm^{-3}K^{-1}$
seawater	$\approx$ 4000 $Jkg^{-1}K^{-1}$	$\approx$ 1000 kgm^{-3}	$\approx 4\times10^{6}$ $Jm^{-3}K^{-1}$

Table 2.1: *Typical heat capacities for air and seawater (at around 35 psu and 10°C).*

thermal inertia between both fluids. As illustrated in the third column of table 2.1, the heat capacity of air is roughly 4000 times smaller than that of seawater.

Furthermore, it is the combined action of the atmosphere and the oceans that renders the climate so complex. As Phillips (1981) noted in his book on upper-ocean dynamics, "*The transfer of momentum and energy* [and mass] *across the air-sea interface provides the source of almost all oceanic motions. The immediate local reaction to these fluxes is to be found in the disturbed surface layer; their distribution and persistence on global scale results ultimately in the great oceanic circulations*". This surface layer (also called the Wind-Mixed Layer, or the Mixed-Layer, or simply the Upper-Layer) consists of the top few tens of meters of the ocean, going from the surface down to the seasonal thermocline (or pycnocline when referring to density) approximately, within which scalar properties like temperature (T), and most often salinity (S) (hence density (ρ)) are nearly homogenous due to the vertical mixing action of turbulence. The depth to which it extends is usually marked by a shallow region of very sharp temperature gradient, the thermocline (from here on, we will consider only temperature, unless mentioned otherwise). It is also very sensitive to coastal upwelling, but for the present, as well as for the scope of this research, an offshore mixed-layer will be considered. Energy, mass and momentum are being constantly exchanged across and within the mixed-layer (ML).

Since this research has for its ultimate goal a study of the seasonal evolution of the upper layer T-S fields, it is important to first try to understand how these near-surface waters behave and to what extent the physical processes involved control the evolution, on different time scales, of the mixed-layer. This chapter will attempt to clarify most of the physical mechanisms (figure 2.1) that determine the vertical thermohaline structure of the ocean adjacent to the surface. It must be kept in mind that, although the action of these different processes may look rather simple when studied individually, their combined actions render the situation much more complex.

2.2 Description of the Various Physical Mechanisms

Since we are constantly referring to the term "mixed" layer (for this manuscript, the term mixed-layer - oceanic - refers to the one adjacent to the sea surface), it is appropriate to mention some important points about the origin of this "mixing" and its overall effect. As a starting point, it is convenient to look at the different sources of energy producing the turbulent motions that are responsible for this mixing action, and their relative location. These various mechanisms can be classified (according to Turner, 1981) as:

- The generation of turbulence can be either "*mechanical* " or "*convective* ". For example, in the former case, the breaking of surface waves and the instability of shear flows at the thermocline are typical situations related to the mixed-layer. In the convective case, the vertical motions leading to turbulence usually originate from a locally unstable stratification as in the case of night-time or winter-time surface cooling.
- A further classification depends on the source of the mixing energy, i.e.: "*internal* " or "*external* ". For the case of the mixed-layer (ML), the input of energy is usually done externally, at both interfaces (surface and thermocline), and the mixing produced extends towards the interior of the layer.

With this in mind, it becomes easier to look at the following mechanisms remembering that they generally act to transfer some of the energy from their source into turbulent motion, and then, by vertical mixing, to produce a nearly uniform layer in terms of its temperature, salinity, density, and other scalar properties (Rodi, 1987).

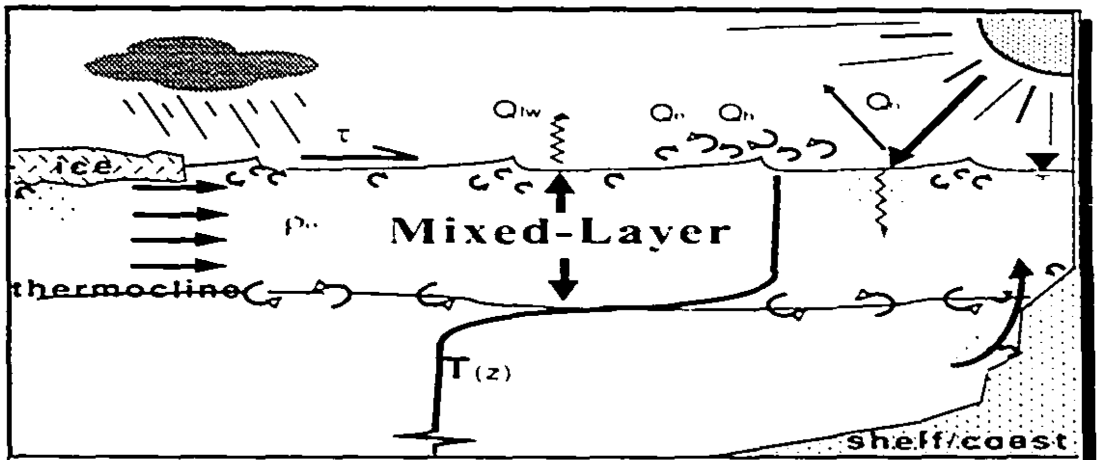

fig. 2.1: *Schematic diagram of the mixed-layer and main physical processes.*

Figure 2.1 illustrates schematically the different factors that play a role in the development and maintenance of the wind mixed-layer: the four heat flux components (Q_{sw} and Q_{lw} - short and longwave radiation, Q_h and Q_e - turbulent transfer of latent and sensible heat), the wind stress (τ) as well as the influence of an ice cover, coastal upwelling, clouds and water turbidity. This chapter will therefore consider qualitatively most of the important physical processes that originate from both principal energy sources for mixing: the wind and the buoyancy flux at the surface.

2.2.1 Surface Wind Stress

The motion of the air above the sea surface carries a certain amount of kinetic energy. Due to the viscous nature of air, the presence of a boundary (the sea) will generally affect the neighbouring flow by slowing it down. The shear increase is usually considered to be inversely proportional to the distance from the sea surface and that the air motion immediately above it has a logarithmic velocity profile (Gill, 1981). This effective loss of momentum is transferred downward to the sea via surface stresses. It is equivalent to say that the effective force per unit area required to slow the air down is the same as the one applied, again per unit area, onto the ocean surface (Kraus, 1972). This transfer of energy depends on many factors - air and surface water temperature (T_a, SST) and wind speed (U_a) - (Blanc, 1985) and is calculated using a highly parametrized approach (Liu and Schwab, 1987; Smith, 1988). Chapter 5 and section 2.5 on turbulence will treat these so-called bulk aerodynamical formulae in more detail and briefly discuss the surface stress in terms of velocities (Donelan, 1990). Nevertheless, it is fair to say that the air motion may be affected in the following ways: first, skin friction will act to slow the winds immediately above the sea surface in a fashion analogous to a fluid flowing on a flat plane experiencing momentum transfer against its velocity gradient; secondly, due to the physical topography of the surface waves, form drag will result from the pressure forces applied onto the rough air-sea interface (Blanc, 1985); finally, the air-sea temperature difference (T_a - SST) may influence the stability of the air layer immediately above the surface and thus affect the intensity of turbulence in that region. This can be summarized by the relation for the surface stress of air, $\tau_a = C_d \rho_a \bar{u}_a |U_a|$, where the drag coefficient $C_d = f(|U_a|, T_a\text{-SST})$.

The various pathways that the wind-stress energy may take once transmitted to the water body will be considered qualitatively. Most of the wind-induced momentum is used to generate surface waves (Dobson, 1971). The fate of this wave energy is divided into different oceanic motions, some of it, as Denman and Miyake (1973) reported, is advected away, "some is dissipated or transported into turbulence through wave breaking in the upper few meters, and some is transferred into a drift current". Therefore, only a fraction of this momentum energy loss to the sea will go into turbulence and result in vertical mixing of the near surface waters (Pond and Pickard, 1991). This is schematically summarized by figure 2.2, where a surface stress is initially applied to a linear temperature profile and, at some time later, a mixed-layer has developed as result of the stirring action of turbulence.

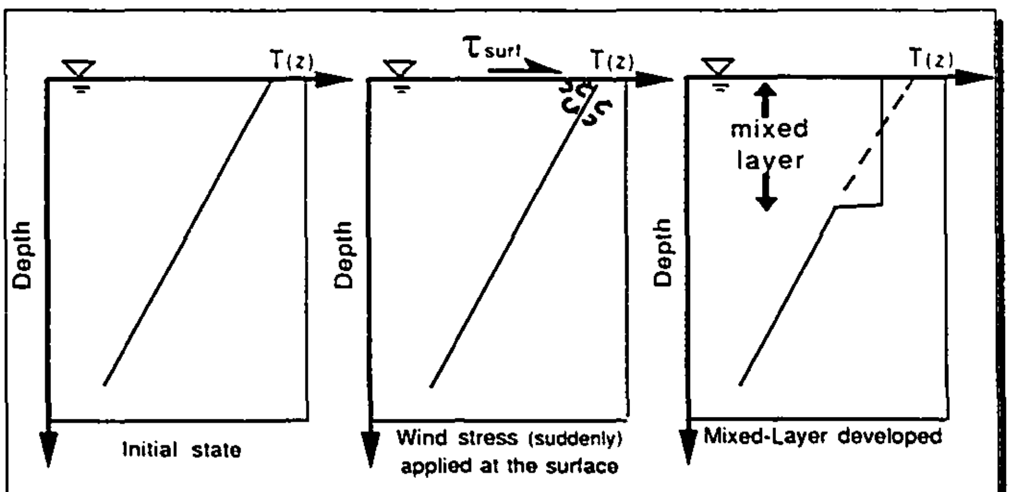

fig. 2.2: *Schematic diagram of ML behaviour experiencing surface wind stress.*

The kinetic energy input of the wind has then been used to alter the $T(z)$ profile by mixing the warm surface water with the heavier colder one immediately below it, thus forming a homogenous upper-layer colder than the initial SST.

Although described above in a relatively simple manner, the consequences of this stress imposed on the sea surface lead to much more complicated phenomena which are not yet fully understood. In fact, the fraction (m) of the eolian energy transformed into turbulent motions is not known in detail but is strongly dependant on sea-state (e.g.: Denman and Miyake (1973) found m=0.0012; Kato and Phillips (1969) observed m=0.0015 experimentally and Turner and Kraus (1967) calculated m=0.01 from field data). Researchers have tried to isolate the processes in laboratory experiments. Kato and Phillips (1969) used a rotating disk to apply a constant stress to a circular tank of fluid, initially at rest and with a uniform density gradient. As the underlying fluid was progressively entrained near the turbulent surface, a mixed layer developed. They then related the entrainment rate to the external parameters, namely the buoyancy frequency, N, (Turner, 1981) and the mixed-layer depth. Although several more experiments tried to relate the various mixing parameters to the surface stress (Ellison and Turner, 1959; Turner, 1981), some discrepancies still remained between each result as well as between the underlying theoretical assumptions. In a review paper on mixing processes, Turner (1981) proposed, from dimensional arguments, that the entrainment velocity producing a well-mixed layer in a stratified fluid undergoing a mechanical surface stress (without heating) should be proportional to the overall Richardson number ($R_{i*} = g\,\Delta\rho\,h / \rho_w\,u_*^2$). ($g$, $\Delta\rho$, h and ρ_w are the gravity acceleration, the density difference across the MLD, the depth of the mixed-layer and the ML density, respectively. u_*, the friction velocity, will be defined in section 4.2.3 along with the concept of mixing energy). This agrees with most current entrainment theories, although some authors choose various scales to define the corresponding Ri. All these experiments resemble one another in that they all apply a sudden stress to an initially quiescent fluid. This rather complex initial value problem will be further discussed in section 2.3.

Finally, an important aspect concerning the action of the wind is that several different oceanic motions (inertial motions, inertial waves, drift currents, Langmuir circulation, etc.) are directly related to this surface stress, and they are likely to influence the behaviour of the surface water by processes at various time/length scales. Consequently, this section does not provide a full treatment of the wind-ocean interactions, but simply tries to relate the formation of a well mixed-layer under the influence of wind stress.

2.2.2 Solar Radiation, Penetration, and Backradiation

The second major factor contributing to the seasonal formation and destruction of the upper-layer is the sun, or, more precisely, the amount of energy gained and lost at the sea surface by radiation. This section will describe the effects of this incoming solar radiation, explain how the ocean returns part of this energy in the form of longwave radiation, and briefly discuss how this incoming energy penetrates below the sea surface. For the picture to be complete, the following section will treat the turbulent fluxes of heat and mass transfer across the air-sea interface, thus providing all four terms needed to estimate the net heat fluxes at the sea surface.

A more complete treatment of the fundamentals of radiant energy and the associated budgets can be found in Budyko (1974) and other meteorological physics textbooks (e.g.: Houghton, 1985; Peixoto and Oort, 1991). This section is restricted to an explanation of short and longwave energy, the various environmental factors that influence their strength and the resulting impact on the surface waters of the ocean.

First, from a climatological perspective, and because the amount of uncertainties and fluctuations involved in various other physical quantities are considerable, the sun's radiation intensity may be assumed constant (Peixoto and Oort, 1991) such that the incident energy flux reaching the earth is referred to as the solar "constant" (S_o = 1360 Wm^{-2}). Consequently, the total energy reaching the top of the atmosphere for a particular area will depend on its latitudinal location and the time of the year. Budyko (1974) computed monthly average clear sky solar fluxes (in Wm^{-2}) for latitude bands of ten degrees, going from 90° south to 90° north. From this tabulated data, a small geometric correction can be applied (Bugden, 1981) to accurately estimate the monthly average incoming flux at the top of the atmosphere.

As this energy enters the atmosphere, several factors will affect its transmission. Because of the presence of air, aerosols, water vapour and clouds, and other atmospheric constituents, some of the energy will be scattered and reflected, some will be absorbed and reradiated back according to the temperature of the absorber. This influences the actual amount and type of radiation reaching the ocean surface. A complete picture should therefore consider several atmospheric parameters such as: cloud amount, cloud base and top height, cloud optical thickness and temperature, relative humidity and air temperature, aerosol and other gaseous constituents, etc. This makes the calculations extremely complicated and requires the use of far more sophisticated methods, such as complex radiative transfer models (Frouin and Gauthier, 1988). Although such a full analysis is very difficult to perform and not feasible within the context of the present study, one should nonetheless assess which of these factors have the greatest impact on the radiation budget and try to incorporate them using simpler empirical relationships.

Several authors (Budyko, 1974; Houghton, 1985; Frouin and Gauthier, 1988) have considered these aspects with various levels of complexity. For the present study, only the effects of cloud cover, surface air temperature and relative humidity will be taken into account. Although this is largely due to the data availability, these three atmospheric parameters are considered to be of the utmost importance for the radiation analysis and are generally included in global climate studies (Bunker, 1976; Hsiung, 1986; Hakkinen and Cavalieri, 1989) and modelling experiments (Oberhuber, 1992). In fact, the simple inclusion of the monthly cloud cover, C_n, in the short and longwave heat flux relations has been investigated by several researchers. The exact dependence of these two radiation terms on the cloud cover is still uncertain. Some studies suggest a linear dependence on C_n while others use the third power of C_n. More details will be given in chapter 5 of the methods used in the heat budget calculations. Once it has reached the surface, the shortwave radiation is then multiplied by the factor $(1 - \alpha)$ where α is the albedo of the sea surface (Budyko, 1974).

Although the sun's incoming rays penetrate to substantial depths, the bulk of this radiant energy [0.3 - 1.0 μm] is absorbed within the top few metres of the ocean (Phillips, 1981). On average, for the world's ocean, between 60% and 80% of the entering light energy will be absorbed within the first one and ten metres, respectively (Duxbury and Duxbury, 1991). This rapid decay with depth, influenced somewhat by scattering, but mainly affected by absorption caused by suspended particulate matter and dissolved materials, may be expressed by the exponential relation, $I(z) = I_0 \exp(-kz)$. I_0 and $I(z)$ correspond to the radiant intensity at the surface and at some depth, z, and k represents the attenuation coefficient for a particular water type (Pickard and Emery, 1990). Although this extinction coefficient varies with the wavelength (Pickard and Emery, 1990), it is possible to define an average value for k allowing adequate use of the exponential relation mentioned above (Denman and Miyake, 1973). Paulson and Simpson (1977) made further irradiance measurements in the ocean on the basis of an effective radiation band, which allowed them to define various types of waters according to their transmissivity.

Corresponding to this incident solar flux, there will be a response from the mixed-layer in the form of long wave energy, emitted according to the temperature of the sea surface (SST). This backradiation is assumed to take place within a very thin layer at the sea surface (Denman and Miyake, 1973). Thus, one can consider the SST as the only oceanic parameter involved in this heat flux component. Unfortunately, the atmospheric counterpart needs further attention. Reradiation by the atmosphere (by the layer of air above the sea surface, by the clouds and by the aerosols, etc.) plays a complex role in the radiation budget. Hence the need for an empirical relation in terms of cloud cover, C_n, air temperature, T_a, and relative humidity. It is not clear as to the exact role played by the humidity and the cloud cover terms in this infrared radiation budget (there are significant differences in the longwave equation between authors; see Pickard and Emery, 1990; Gill, 1981; Budyko, 1974). Qualitatively, the ocean will respond in an manner analogous to the land for the longwave term, namely: clear sky nights are known to be colder than cloudy nights due to the increase in infrared radiative cooling of the earth surface (Ahrens, 1991; Pickard and Emery, 1990). Clouds and humidity tend to absorb the longwave energy lost by the surface and emit it back, thus slowing the effective radiative cooling.

2.2.3 Turbulent Surface Fluxes

It can be said that the air motion near the sea surface is most likely to be turbulent (Pickard and Emery, 1990). Difficulties arise when using the simple bulk aerodynamical formulae in order to estimate how much heat and moisture is actually transferred across the air-sea interface by turbulent fluxes. Although these bulk transfer coefficients have been given considerable attention by several researchers (see Blanc, 1985, for a partial review), and despite striking similarities in most experimental approaches, as well as empirical relationships, large discrepancies from one scheme to another remain when computing C_h and C_e (latent and sensible heat coefficients, respectively). Blanc (1985) found differences as high as 45% and 70% for average fluxes of latent heat (±40 Wm-2) and sensible heat (±25 Wm-2). Nevertheless, these two fluxes - Q_h and Q_e for latent and sensible heat respectively - constitute two critical terms in the net energy budget at the air-sea interface. In fact, because they are strongly dependant on wind speeds and air-sea temperature differences, they have important fluctuations in their magnitude on both the seasonal and the interannual time scales.

The difficulties associated with the eddy transfer of properties arise from a more general problem: the complex nature of fluid turbulence. Although this is far from being fully understood, the conclusions drawn by several "air-sea interaction" experimentalists have yielded considerable insights as to which factors do influence these transfers. It is believed by many that the stability of the air immediately above the sea surface greatly affects the turbulent intensity and, hence moisture and heat transfer. For example, if the air-sea temperature difference is such as to give an unstable or "buoyant" atmospheric surface layer, air parcels will constantly tend to rise, thus increasing the intensity of turbulence and its ability to remove moisture and heat from the sea surface. Conversely, in the situation where the sea is actually cooler than the atmosphere, the surface layer of air becomes denser as it loses heat to the ocean, thus inhibiting convection and reducing turbulent transfer (Pickard and Emery, 1990; Smith, 1988). Furthermore, this air-sea temperature difference has a somewhat "double" influence: not only does it arise in the bulk formulations (see chapter 5 for formulations), but it also affects the values of the bulk coefficients under various atmospheric conditions (eg.: Kondo, 1975; Liu et al., 1979; Smith, 1988 and 1990) as C_h and C_e are functions of $|U_a|$ and (T_a - SST).

Another controversial aspect concerning these turbulent transfer coefficients is the wind speed. Dynamically speaking, an increase in the wind velocity will generally result in a more turbulent flow (Gill, 1981). The problems arise at both low and high speeds. Smith (1990) and Wu (1990) disagreed on whether one should use a continuous or discrete transition between aerodynamically smooth and rough flows. They also argued about the exact location of such transitions on the basis of several external parameters. Wu (1980) mentioned the possible effect of surface "ripples" on waves during strong winds which could prevent or delay the airflow separation observed in laboratory for "smooth" surface waves. Furthermore, higher wave activity for faster wind speeds is believed to increase the sea spray and lead to a greater transfer surface area (Roebber, 1989). Finally, although no consensus yet exists as to the exact dependence of C_h and C_e on $|U_a|$ and (T_a - SST), C_h is generally considered to be smaller than C_e ($C_e \approx 1.16\ C_h$: Smith, 1980; Blanc, 1985). In conclusion, large uncertainties remain when using bulk aerodynamical formulae and a conservative approach should prevail until more experimental evidence is available. Qualitatively, Q_e and Q_h are important in affecting both the atmosphere and the ocean (Cayan, 1990 and 1992a,b). Their direct influence on the net heat budget of the Gulf of St.Lawrence will be presented in chapter 5.

All four terms of the surface heat budget have been discussed - namely the incoming shortwave radiation, Q_{sw}, the effective longwave backradiation, Q_{lw}, and the turbulent fluxes of sensible and latent heat, Q_e and Q_h . We arithmetically sum them ($Q_{net} = Q_{sw} - Q_{lw} - Q_h - Q_e$) in order to obtain the net heat flux entering or leaving the sea surface each month. Heat gained by the sea is taken as positive. Although each constituent of this

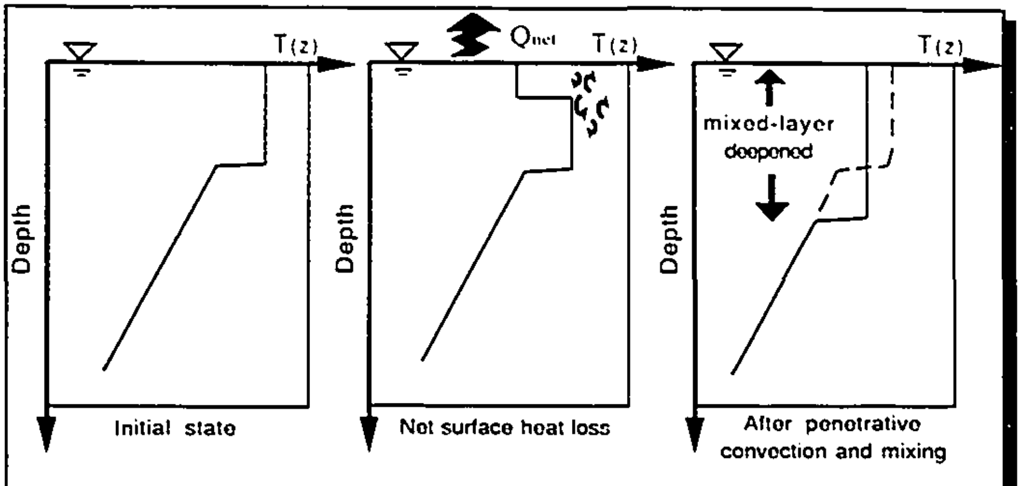

fig. 2.3: *Schematic diagram of ML behaviour undergoing a heat loss.*

budget is extremely important, it really is the net flux of heat at the air-sea interface that has critical consequences for the mixed-layer. The following pictures (figs. 2.3 and 2.4) examine two possible scenarios - net gain and loss of heat by the ocean surface - and explain qualitatively the corresponding effects of both cases on the ML development.

Figure 2.3 describes the response of a mixed-layer undergoing a net loss of heat to the atmosphere. Obviously, in such a situation, the temperature of the water immediately adjacent to the surface will decrease and, consequently, the density will increase. As this process takes place, surface waters become heavier than the layers just below and will sink, a process called penetrative convection. In doing so, these sinking plumes will entrain surrounding water and, as they break down into more turbulent water parcels and mix properties (T, S, suspended matter, etc.) with their immediate environment. It is this mixing that will redistribute the heat content of the surface layer with waters immediately below the mixed-layer depth, thus deepening the ML and making it colder.

In the second case (fig. 2.4), the ocean is gaining heat, a situation corresponding to the summer months (chapter 5 and Bugden, 1981). The surface waters now become lighter than the waters underneath, thus stabilizing the upper layer and inhibiting convective overturn, penetration and vertical mixing. Nevertheless, if mixing occurs at the surface (due to the wind action, the breaking of waves, etc.) this will again result in a redistribution of heat in the mixed-layer (Turner, 1981; Pickard and Emery, 1990) as depicted by the third panel of figure 2.4.

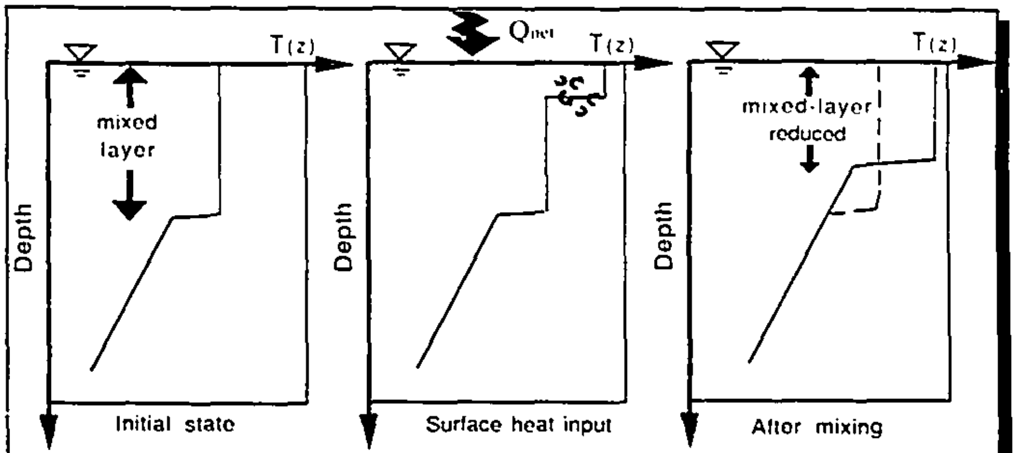

fig. 2.4: *Schematic diagram of ML behaviour undergoing a heat input.*

Although the arguments here may seem rather simple and obvious from a thermodynamic point of view, efficiently relating overturns and penetrative convection to a net "mixing" effect is a much more complex task (Galbraith, 1992). The penetrative nature of this mixing is still the subject of debate (Turner, 1981). Gill and Turner (Turner, 1981) have argued in favour of a non-penetrative heat loss during the cooling period and, under this assumption, concluded that little entrainment resulted from this. For the discussion to be complete, these processes are generally discussed along with the concept of buoyancy flux, which includes the effects of precipitation and evaporation. The next section will attempt to clarify this notion in parallel with the consequences of fresh water input and ice.

2.2.4 Precipitation/Evaporation, Runoff and Ice: *Buoyancy Input*

So far, radiative heat fluxes and turbulent transfer of mass, momentum and heat have been considered. This section will discuss other environmental factors that also influence the upper-layer thermohaline structure as they alter the stability of surface waters and thus affect vertical mixing.

Surface buoyancy flux:

Buoyancy is defined as "ρg" and links density differences and gravity together, which can produce or inhibit water motion (often defined as "$-\rho g$" because a water parcel is said to be more buoyant when it has less weight). In essence, it can be viewed in terms of water layers of different densities overlying one another. Their relative vertical position as well as their density difference lead to the well-known notion of water column stability.

Consequently, fluxes of buoyancy (negative or positive) at the sea surface will make the surface-layer more or less stable in comparison with waters immediately underneath. Gill (1981) defines the surface buoyancy flux by

$$B \equiv Cp^{-1}\, g\, \alpha\, (-Q_{net}) + g\, \beta\, (E - P)\, S,$$

where Cp, α $(-\rho^{-1}\, \partial\rho/\partial T)$ and β $(-\rho^{-1}\, \partial\rho/\partial S)$ are the heat capacity and the thermal and haline expansion coefficients of sea water, (E - P) is the difference between evaporation and precipitation, and g, S and Q_{net} are the gravity, surface salinity and the net heat flux (taken as positive upward in Gill, 1981), respectively. Hence from B, one can assess changes in potential energy to the water surface through fluxes of heat (1st term) and mass (2nd term). Motion induced by buoyancy contrasts are due to differences in both temperature and salinity. Evaporation contributes to a increase in buoyancy in two ways: via evaporative cooling, included in Q_{net} (the first right-hand side term of B), as well as by increasing the surface salinity, as expressed by the second term of B (refer to chapter 5 for the specific formulation of Q_{net}). Finally, for mid-latitude oceanic conditions, temperature differences generally result in stronger density changes than salinity (Gill, 1981). However, this might no longer hold true for the estuarine region of the Gulf where water is considerably fresher than in the rest of the basin. This is related to the fact that both temperature and salinity influence the value of α and β (Prinsenberg, 1982). Apart from the surface heat flux and the evaporation, the environmental factors affecting buoyancy and hence stability are rain/runoff, ice melt and ice formation.

Ice cover:

Not only will the presence of an ice cover be significant in terms of buoyancy flux as well as in affecting the transfer of momentum, mass and heat, but its growth and disappearance, and the rate at which these two phase changes take place may also be important. We consider first the freezing of the surface waters. As crystals form and agglomerate, salt is rejected (Pickard and Emery, 1990). This increases the ambient density and, in turn, leads to sinking and replacement of this adjacent layer. Therefore, as ice is formed, it results in a positive buoyancy flux (according to the definition of B above: Gill, 1981) near the surface due to an increase in salinity. The exact amount of buoyancy generated through this process will depend on how fast the layer of ice formed. A rapid freezing may trap more salt within the crystalline structure, forming pockets called brine cells. In the spring, the reverse situation occurs: the ice cover melts and generates an important "pulse" of relatively fresh water, hence leading to a more stable surface layer via a negative flux of buoyancy. It is extremely difficult to assess the quantitative importance of this process for it is a function of several parameters which are often not known. For example, in the Gulf of St.Lawrence, although the seasonal and interannual horizontal cover of ice is relatively well documented (Déry, 1992, DeTracey, 1993), little is known about the distribution of ice thickness and hence the actual volume/mass of sea-ice. Secondly, since the rate of freezing will influence the amount of seawater trapped as brine cells, it is difficult to estimate what will be the concentration of salt in the melted ice in the spring. Thirdly, it is believed that the time of the year at which ice forms may inhibit the surface thermal loss to the atmosphere, hence trapping more (or less) heat within the upper water column. The dates at which ice is formed are generally known (Garrigues, 1995; McGill Univ., personal communication), but there are no correlation studies relating the upper-water heat content to the ice formation. Finally, winter evolution of the temperature underneath the ice depends on the heat conduction of the entire sea-ice cover which is a function of the amount of snow that accumulates on the surface. Ice cover not only insulates the water surface, but also reduces the transmission of kinetic energy from the wind stress, thus affecting upper-layer turbulence and mixing. There is, however, a stress at the ice-sea interface induced by the ocean currents . Prinsenberg (1982, 1983) considered the effects of such ice-sea stress in Hudson Bay and concluded that, from McPhee's (1979) ice-ocean stress relation, $\tau_{iw} \approx 0.01\ V_w^{1.78}$ (V_w is in cms^{-1}), a tidal current of 20 cms^{-1} would generate a friction velocity, u_*, of around 1.42 cm s^{-1}, which roughly corresponds to the effect a storm would produce in interacting with the sea surface. Therefore, ice cover may cause mixing of the surface water which should consequently influence the winter evolution of the mixed-layer extent and the associated T and S profiles. Finally, Lepage and Ingram (1991) report that this ice-ocean stress becomes negligible when the ice is not land fast but free to move with the surface currents.

Runoff consequences:

A second important environmental factor directly linked to the surface buoyancy flux and the stability of the upper-layer is the runoff. Similar to the effects of ice melt, runoff contributes to buoyancy variations by supplying fresh water. For instance, following the melting of lake ice and snow within the Gulf of St-Lawrence watershed, there will be an increase in freshwater runoff to a seasonal maximum during late spring - early summer (Koutitonsky and Bugden, 1991). Not only will this fresh water pulse affect the stability of the surface layer, but it is generally believed that the the GSL density gradients resulting from river runoff "maintain a basic state of motion" (Koutitonsky and Bugden, 1991) much like the typical density-driven circulation of estuaries. Moreover, year-to-year fluctuations of the river discharge result in considerable changes in the surface salinity. Bugden et al. (1982) and Lauzier and Bailey (1957) have compared average Gulf-wide salinity fields between high and low runoff years and found significant differences at the surface, especially along the Gaspé shore and in the Magdalen Shallows. These effects can also be felt relatively far downstream from the river source (El-Sabh, 1976; Sutcliffe et al., 1976; Koutitonsky and Bugden, 1991). Finally, Prinsenberg (1983) reports that an increase in runoff can significantly increase the surface stability, thus reducing the deepening rate of the mixed-layer and keeping the winter salinity and pycnocline depth at values lower than normal. From a combination of modelling results and hydrographic observations in Hudson Bay, Prinsenberg (1983) concluded that an increase in freshwater discharge could result in "a tendency to produce more ice" by a decrease in winter surface T and S. However, this latter consequence might not hold true in different oceanographic basins. For example, Déry (1992) found no significant correlation between the ice cover and runoff in an interannual study of the GSL ice cover, which indicated that several factors interact in a more complex fashion.

Precipitation and evaporation:

After ice effects and runoff, precipitation and evaporation and the corresponding surface salinity decrease/increase cause the next largest changes in surface buoyancy in the GSL. Although the amount of heat addition associated with precipitation is relatively small (approximately 100 times smaller than the net summer heat flux for the GSL - Bugden, 1981), it may however have, in certain regions of the world ocean, an important impact on the surface stability by the flux of buoyancy. It is well known that precipitation over the tropical oceans generally results in a colder, fresher and more stable surface layer (Miller, 1976; Price, 1979). During a field study near the west coast of Florida, the formation of a "new" shallow mixed-layer as a result of a strong rainfall was observed ($\approx$ 6 cm in < 2h; Price, 1979). It this case, the strong, "nearly impulsive" negative buoyancy flux yielded, 3 hours after the storm passed, a new halocline at a depth of about 10 metres which eventually merged with the existing mixed-layer (MLD $\approx$ 30 m). It is important to note that not all precipitation events will have such a dramatic influence. During the BOMEX (Price, 1979) field program, (as well as in the Gulf of St.Lawrence during the JGOFS5 hydrographic cruise, May-June 1993), no significant mixed-layer and surface salinity response to rainfalls were observed, leading to the conclusion that much stronger events may be required in order to have a substantial impact on the upper-layer. Finally, evaporation also contributes to changes in the surface layer stability. In the warmer regions of the world's ocean, this process plays a major role in generating density gradients by removing water from the sea surface and rendering it heavier due to the salinity increase, as well as because of the associated loss of latent heat. Miller (1976) also showed that, in areas (e.g. tropics) where the pycnocline was influenced by changes in both T and S, the latter should be included in ML models in order to accurately predict the deepening rate.

2.2.5 Other Processes

In this last section, we briefly discuss some oceanographic processes that also affect the physical structure of the mixed-layer but play a less important role within this study. The reasons for not considering them are numerous and vary greatly: some of them are simply not relevant from a monthly climatic perspective; others are not quantifiable or apparent within the present dataset; finally, some of these processes are believed to be important to some degree but, due to limited time or improper tools of analysis (computer models, satellite imagery, missing datasets, aliasing, etc.), they will be neglected in this research. It should be kept in mind that the following brief discussion on the oceanographic processes constitutes a rapid and rather incomplete overview, and the topics are presented in no particular order:

Tidal mixing :

The sun contributes to the gravitational pull generating the tides, but the moon's effect is stronger by a factor of two (Pond and Pickard, 1991). For the GSL, tides are sustained by external forcing from the Atlantic Ocean (Koutitonsky and Bugden, 1991). Tidal currents rarely exceed 30 cm s^{-1} for the Gulf region. Nevertheless, in shallower and/or narrower areas, tidal currents may be sufficiently high to mix part of the water column as a result of bottom friction stress (see section 1.1). Again, the ambient stratification will inhibit this vertical mixing action from being felt throughout the water column (in this case, turbulence is generated at the bottom and its effects propagate upward). Therefore, only those situations where bottom generated mixing might be strong enough the reach the thermocline and/or the surface (hence affecting the characteristics of the mixed-layer) are important (Pingree and Griffiths, 1980).

Coastal upwelling :

Since the prevailing winds generally blow from the west over the GSL, one would therefore expect to see wind-driven Ekman upwelling along the north shore of the Gulf as well as on the south side of Anticosti Island (refer to fig. 1.1). From conservation of mass, and remembering that waters underneath the mixed-layer are relatively cold, one would also expect to see surface signatures of these upwelled waters (a nice schematic diagram can be found in Peixoto and Oort, 1991, p.180). In fact, the presence of cold coastal waters can be clearly observed in these Gulf regions with the aid of satellite imagery (Anonymous, 1991). Rose (1988) and Bourque and Kelley (1995) also observed upwelling events in the north-east sector of the GSL due to alongshore wind stress. The offshore distance to which this upwelled water will spread is related to the *internal Rossby radius of deformation* , λ_i (Pond and Pickard, 1991). For a two-layer system, λ_i can be defined as, $\lambda_i = f^{-1} (g'(h'h/(h+h'))^{1/2}$ (Csanady, 1982), where h and h' correspond to the depths of the upper and lower layer, respectively, f is the Coriolis parameter, and the reduced gravity is expressed by $g' = g\Delta\rho/\rho_0$. Assuming the following typical depth scales ($h \approx 30$ m and $h' \approx 70$ m), and a density difference, $\Delta\rho$, of 2 kgm^{-3}, yields typical λ_i values of the order of 4-7 km for the Gulf of St.Lawrence (Bourque and Kelley, 1995) . This gives a measure of the horizontal extent of upwelling events and indicates how far from the coast one might expect to observe the signature of such processes.

Surface processes:

Langmuir circulation is an example of the complex and non-linear nature of the interactions between oceanic motions (Pickard and Emery, 1990). This circulation has convergence and divergence patterns and associated zones of downwelling and upwelling. These features affect the upper-layer T and S profiles by entraining (and detraining) surface and subsurface waters, thus blending their scalar properties.

Thermocline processes (internal waves, inertial motion, erosion) :

Movement of the thermocline is also important for the mixed-layer. The presence of a continuously stratified fluid supports a wide range of internal motions. However, several laboratory and model studies disagree on the form of physical mechanisms that occur within a simplified two-layer system, i.e.: a sharp, nearly discrete density interface (Phillips, 1981; Turner, 1981; Gregg, 1987 and 1991). Gregg (1987) reports that internal waves evolving into dynamical instabilities constitute a major factor in generating mixing in the thermocline. This mixing may also result from interfacial shears in situations where sharp density gradients exist along with a change of velocity across the interface (Turner, 1981). Krauss (1981) observed and successfully modelled the upper ocean response to the passage of a sequence of severe storms in the Baltic Sea. His conclusions, supported by similar ones from Price's (1981) model study of a hurricane in the Gulf of Mexico, suggests that thermocline erosion resulted from the strong shears of the storm-generated inertial waves. Further evidence of internal wave-induced mixing has been reported by Galbraith (1992) in studying the effects of internal tide and solitons at the head of the Laurentian Channel. The entire topic of mixing in the ocean interior constitutes a complex subject. However, it is nevertheless important to note the two significant sources of energy for this mixing, i.e.: breaking internal waves, and interfacial shear, as a result of dynamical instabilities (Pickard and Emery, 1990). This topic will be further discussed in sections 2.3.1 and 2.3.2.

Diurnal effects :

A distinct daily cycle can generally be observed in the surface heat budget on calm and clear days. If the wind action remains weak, this cycle will result in stabilization of the upper ocean during the day followed by a positive (according to Gill's definition, 1981) buoyancy flux associated with the night time cooling (Turner, 1981). The main difficulty lies in determining if this increase in potential energy can lead to sufficiently strong penetrative convection during the night and therefore affect the mixed-layer. Woods and Barkmann (1986) and Woods and Strass (1986) investigated this phenomenon numerically and predicted a maximum variation of the early spring upper-layer extent ranging from a daily depth of 35m to 135m at the end of the night. In another model study, coupled with high resolution hydrographic observations, Price et al. (1986) report similar daily features but of much shallower extent. Furthermore, they noted the opposing effects of stabilizing mid-day buoyancy flux with an often seen concurrent maximum wind and its associated mixing action. Hence, both winds and the ambient water column stability can greatly influence these diurnal effects. They also observed the presence of a diurnal jet within the mixed-layer, whose cycle strongly corresponded to that of the wind.

Advection :

Although most earlier mixed-layer studies (mainly 1D models) assumed that the horizontal advection would have negligible effects compared to the vertical mixing occurring near the surface, this assumption can only be truly validated by exact knowledge of the existing currents or with the help of more sophisticated multidimensional models. In fact, in areas where horizontal motions are large (Gaspé current in particular), one should expect that local surface properties (T, S, plankton concentration, etc.) might be carried sufficiently fast to adjacent location such as to modify the upper-layer structure there. One must now distinguish between the "slow" horizontal displacement of oceanic properties (e.g.: advection of nutrients, or salinity minimum as is the case in the GSL, from the Gaspé coast towards Cabot Strait; Koutitonsky and Bugden, 1991) and the "dynamical" effects of stronger currents on the deepening of the mixed-layer. In the first case, the advection may certainly have an observable influence on the ocean over longer time scales, say weeks to months, by changing the heat input and/or influencing the stratification. In the second case, it is the velocity difference across the thermocline (i.e.: shear value between the surface and sub-surface currents; Gan et al., 1995) that will be important in terms of production of turbulent mechanical energy and hence, entrainment at the base of the mixed-layer. This will be discussed in greater detail in the next section.

2.3 Temporal Considerations of the Mixed-Layer

In the previous section, the most important upper ocean processes which influence the seasonal evolution of the mixed-layer and its corresponding temperature and salinity characteristics were discussed. Attention will now be given to the temporal evolution of the mixed-layer, more particularly to the different time scales over which various processes act and to the energy balance. Although the first widely known study of the oceanic upper layer dates back to Ekman (1905), and that the first realistic thermocline model including the effects of stratification was that of Munk and Anderson (1948), a significant evolution in the field of mixed-layer study can be attributed to Kraus and Turner (1967). They formulated a successful and realistic model of the seasonal thermocline and supported their results from laboratory experiments. Since then, considerable research efforts were made in order to understand the immediate response of a quiescent fluid to an imposed surface stress and heat flux. This led to a series of laboratory experiments (Kato and Phillips, 1969), theoretical studies (Pollard et al., 1973, Niiler, 1975) and numerical simulations (Denman, 1973), as well as an increasing number of hydrographic observations (Denman and Miyake, 1973). Consequently, the present section will cover three topics:

- First, after having briefly reported on the historical evolution of the upper layer study, we will focus on the "initial value problem" (IVP) of mixed-layer deepening, referring in particular to three significant contributions (Denman, 1973; Pollard et al., 1973 and Niiler, 1975). The notion of energy balance within the context of mixed-layer dynamics will be introduced.
- Next, we will relate the conclusions from these IVP studies to more realistic environmental conditions. In particular, the effects of storms on the upper ocean will be considered. Numerical, as well as observational studies, will be presented.
- Finally, the seasonal evolution of the upper mixed-layer will be discussed, with special emphasis on the balance of energy associated with this longer time scale, as well as a description of this seasonal cycle from observations.

2.3.1 The Deepening of the Mixed-Layer - Energetic Considerations

As mentioned earlier (see schematic pictures of sections 2.2.1 and 2.2.3), considerable insights might be gained from the rather simple-looking problem of an initially quiescent fluid body undergoing a sudden surface stress and heat flux. Since this research focuses on the seasonal evolution of the upper mixed-layer through monthly means of various quantities, emphasis will be placed here on the fact that, although the theoretical ML deepening behaviour deals with relatively short time scales (from hours to a few days - see section 2.2.3), it has nonetheless significant implications on what the ocean will look like on seasonal time scales. The ML deepening problem is the subject of much debate among oceanographers. This can be explained by the fact that, regardless of the scales of interest (both spatial and temporal), turbulence is the ultimate agent transferring properties in the upper-ocean and thus will determine the temperature and salinity fields near the surface. More precisely, the results presented below result from one-dimensional analyses/models and, unfortunately, require the use of several (debatable) parametrizations of physical processes (entrainment, energy dissipation, inertial motions, turbulence closure, etc.).

Denman and Miyake (1973) were one of the first to successfully predict the observed time dependant modifications of the upper mixed layer (for sub seasonal time scales) with a generalization of the Kraus-Turner one-dimensional integrated model. Since the goal here is to qualitatively describe the ML response, the model descriptions will be left aside - refer to Niiler and Kraus (1977) for a complete discussion on the subject, and a brief overview in section 2.4. One feature of Denman's model was the sensitivity of the results to the mixing energy produced by the wind stress, as well as by the absorption rate of solar radiation, which varied significantly with the extinction coefficient, k (see section 2.2.2). An important aspect of this model is the exclusion of rotation: consequently, Denman's physical explanations of ML deepening will differ somewhat from those of Pollard et al. (1973) and Niiler (1975) (whose models include rotation but lack observational comparisons/simulations). Denman concluded that the mixed-layer extent was dependent on both wind stress energy and water column stratification, and that the initial deepening rate was proportional to $t^{1/3}$ (where t is time), as reported by Ellison and Turner (1959) and Kato and Phillips (1969) in laboratory experiments. Denman suggested that diurnal effects were too small to be clearly noticed. He also observed that during strong summer wind conditions, surface heating was less important but should be considered during relatively calm wind periods.

In a more complex mathematical treatment, Pollard et al. (1973) found that rotation was important in limiting ML deepening after one half inertial period, as strong inertial oscillations prevented further deepening. Their results suggested that the maximum depth of the mixed-layer depended on wind, rotation and stratification as $MLD_{max} \approx u_* (Nf)^{-1/2}$. Furthermore, they argued that, on the seasonal time scale, surface heating/cooling would be dominant. A few years later, Niiler (1975) integrated both Denman's and Pollard's results and showed that both inertial motions and surface wind stirring were important in the initial stages of the mixed-layer. In his model study on the asymptotic ML deepening regimes, he extended the work of his predecessors by incorporating three layers - a surface mixed layer, a thermocline zone of perturbation energy production, and a quiescent abyss, and considered two possible sources of turbulent kinetic energy (TKE): the wave-induced shear of the surface currents and the turbulent entrainment at the thermocline (a natural extension of Niiler's work is the well known and now widely used 2 and $^1/_2$ layer model , e.g. Gan, 1995; Gan et al., 1995). Again, a rapid deepening followed by a subsequent slower erosion was observed; Niiler attributed this response to the initial input of TKE from surface processes (until 1 pendulum hour), and presumably followed, on time scales of a few hours, by the action of inertial motions. Similar to Denman, Niiler also noticed that the deepening rate was strongly dependant on the extent of the mixed-layer at the time of wind onset. For the seasonal cycle, heating and dissipation should play an important role.

In conclusion, a rapid initial deepening of the mixed-layer followed by a slow erosion has been observed and simulated by several researchers, but the exact mechanisms explaining the partition of energy amongst the different processes is still debated. The lack of understanding of turbulence in a stratified medium resulting in different assumptions and/or parametrizations can probably help explain the different conclusions and slight variations in the obtained results. In essence, different processes may dominate at different stages. Nonetheless, a nearly common feature in all these studies is the consideration of the balance of TKE inputs against the changes in potential energy and dissipation within the surface layer. Consequently, for the simplified yet realistic theoretical case of a sudden stress applied to the surface of a quiescent linearly stratified fluid body, four distinct dynamic stages were identified by Niiler (1975) and deSzoeke and Rhines (1976). Assuming no heating or energy dissipation, the TKE equation for the ML can be expressed as:

$$\frac{1}{2}\frac{\partial h}{\partial t}\left(\zeta U_*^2 + \frac{N^2h^2}{2} - |\delta V|^2\right) = mU_*^3$$

A	$0.5^{dh}/_{dt}\,(\zeta\, U_*^2)$	The storage rate of turbulent energy in the mixed-layer
B	$0.5^{dh}/_{dt}\,(N^2h^2/2)$	The rate of increase of potential energy due to entrainment from below
C	$0.5^{dh}/_{dt}\,\lvert\delta V\rvert^2$	The rate of production of turbulent mechanical energy by the stress associated with the entrainment across a velocity difference $\lvert\delta V\rvert$
D	mU_*^3	The rate of production of turbulent mechanical energy by surface processes

Table 2.2: *ML deepening stages and the corresponding balance of energy.*

(Turner, 1981) where h represents the MLD, ζ and m are fractional dimensionless coefficients, and where each energy term is explained in the previous table. As a result of the sudden stress impulse, the fluid body will exhibit four successive behaviours according to the dominant balance of energy:

- A ↔ D: *(Initially, up to a few minutes)*

  First, there will be an immediate reaction of the mixed-layer in "storing" a fraction of this turbulent kinetic energy produced by the surface winds. The mixed-layer will usually grow to a few metres very rapidly.

- B ↔ D: *(A few minutes, up to an hour)*

  If this process continues, the surface TKE production will, within the first hour, contribute in changing the potential energy of the entire ML, resulting in a characteristic thermocline (typically a few tens of meters deep; Turner, 1981) and increased upper layer horizontal velocities.

- B ↔ C: *(Until a time scale of half a pendulum day)*

  Meanwhile, the surface currents have been accelerating as well as the shear value increasing across the thermocline; consequently, rotation will have a stronger influence on the mixed-layer motions, resulting in an energy balance between the TKE produced at the surface and that generated by the inertial shear stress and characterized by entrainment at the base of the mixed-layer. This balance should dominate on a time scale of half a pendulum day. After this time, the MLD can be expressed in terms of U_*, f and N. Different authors proposed varying formulations of this depth dependence (i.e.: Turner, 1981), but these will not be presented explicitly.

- B ↔ D: *(Longer-to-seasonal time scale)*

  Finally, the inertial currents decrease and a slow ML erosion follows, thus restoring the initial balance between the mixed-layer potential energy change and the turbulent kinetic energy rate produced by the wind stress.

Note: (Longer-to-seasonal time scale)[1]

1: Although the seasonal time scale is usually taken to be of the order of a month in the literature, it is here referred to time scale of processes roughly greater than a pendulum day (Turner, 1981). This can be explained from the following energy balance: as the mixed-layer deepens from a sudden wind stress, it goes through three distinct stages specific to different time scales, processes and energy balance (A:B, B:D and B:C). The ML then undergoes a slow and steady erosion, with relatively no change occuring as for the dominant processes taking place. Unless the surface forcing suddenly changes, this energy balance will be dominant in determining the evolution of the mixed-layer on longer time scales (month to month), hence the somewhat misleading name "**seasonal**". However, this energy balance does not include the effect of

Although it is uncertain as to which dynamical criteria should be used to close this IVP, similar qualitative behaviours were obtained with different model formulations. Most of the methods used relate the entrainment to the shear across the thermocline with various formulations of the Richardson number as an independent criterion. Kundu (1980) noted the lack of vertical structure resulting from these "bulk" models and conducted similar studies on the mixed-layer response to wind stress by using the turbulent closure model. The improvements from such an approach are the ability to resolve velocity shears in the upper-layer and the assessment of the turbulent diffusion influence along the water column, but, overall, the ML behaviour remains qualitatively the same.

2.3.2 Typical Mixed-Layer Deepening and the Consequences of Storms

After having introduced the various response stages of the upper-layer to a suddenly applied wind stress, some results will be presented as well as their relations to typical environmental conditions. First, Denman (1973) modelled the mixed-layer behaviour resulting from a Gaussian shaped surface stress. The purpose was to represent the effect of a storm and its associated wind fluctuations. As depicted on figure 2.5, the wind velocity varied from calm, increased to a maximum of 15 ms^{-1} and decreased back to zero within a period of 4 days. As a consequence of this, the mixed-layer, whose initial depth was 10 m, started increasing slowly during the first day, reached a maximum deepening rate which corresponded to the strongest surface stress, and continued deepening but at a slower rate. The important aspect depicted here by this theoretical storm was the irreversible nature of the wind mixing that took place: as the winds increase, the ML deepens - but continues to do so and remains at this new depth when the winds cease. In spite of the highly idealized nature of this numerical experiment, one might wonder what would happen if a series of "stormy" events were to occur. Most probably, the sum of these synoptic weather events superimposed onto a background surface heat flux cycle constitutes the two critical factors affecting the seasonal evolution of the mixed-layer.

In a more local study, hydrographical observations were taken by Roche-Mayzaud et al. (1991) at three different locations in GSL, along a transect across the Gaspé-Anticosti channel. On figure 2.6, three graphs of salinity and temperature (for each location) are displayed, each consisting of two profiles - one before (avant) and one after (après) the passage of a storm. The events occurred over a two day period, with winds reaching a maximum of 13 ms^{-1}. These three sets of T and S profiles correspond rather

---

surface heat flux, a process found to be important on the monthly time scale (Haney and Davies, 1976).

well with previous theoretical results (Denman, 1973; Pollard et al., 1973). The MLD before the storm was about 20 m and varied from around 40 to 65 m after the storm.

Several other researchers have reported similar responses to synoptic weather forcing event (Krauss, 1981; Price et al., 1978). However, upon comparison of field observations and numerical modelling results, Price et al. (1978) found no evidence supporting the theory that storm-induced deepening events would be driven by wind stress only. They suggested that beyond a certain time scale (during the second half of the inertial period) the deepening rate would decrease along with the interfacial shear in spite of a continued increase in surface wind stress. Consequently, both processes - heat flux and wind stress - need to be considered for the seasonal time scale (Haney and Davies, 1976).

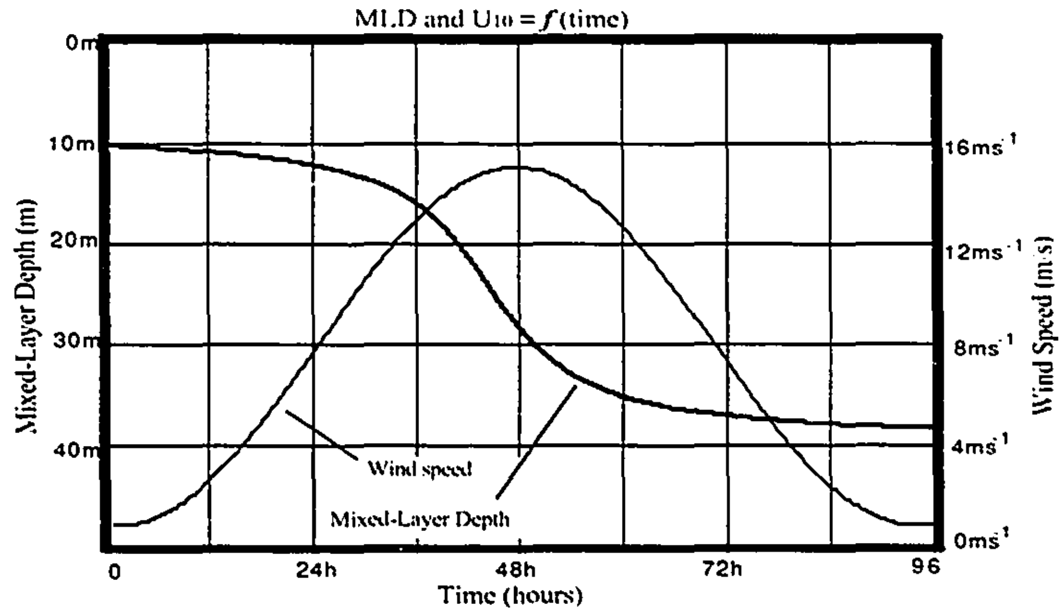

fig. 2.5: *Deepening of the MLD for a Gaussian wind (adapted from Denman, 1973)*

2.3.3 The Seasonal Evolution of the Mixed-Layer

Having described most of the surface processes in section 2.2, and explained the various stages exhibited by a mixed-layer under a surface stress, an explanation of the seasonal structure of the upper layer of the ocean will now be given. Although several researchers have studied the annual cycle of the upper ocean, laboratory and model studies by Turner and Kraus (1967) were most used in mixed-layer studies, as they were the first to model the seasonal ML variation with the use of a "bulk" model. Many of the concepts proposed by them are still in use today (with various degrees of modifications, e.g. the general circulation model of Oberhuber, 1993). In their study of the seasonal thermocline,

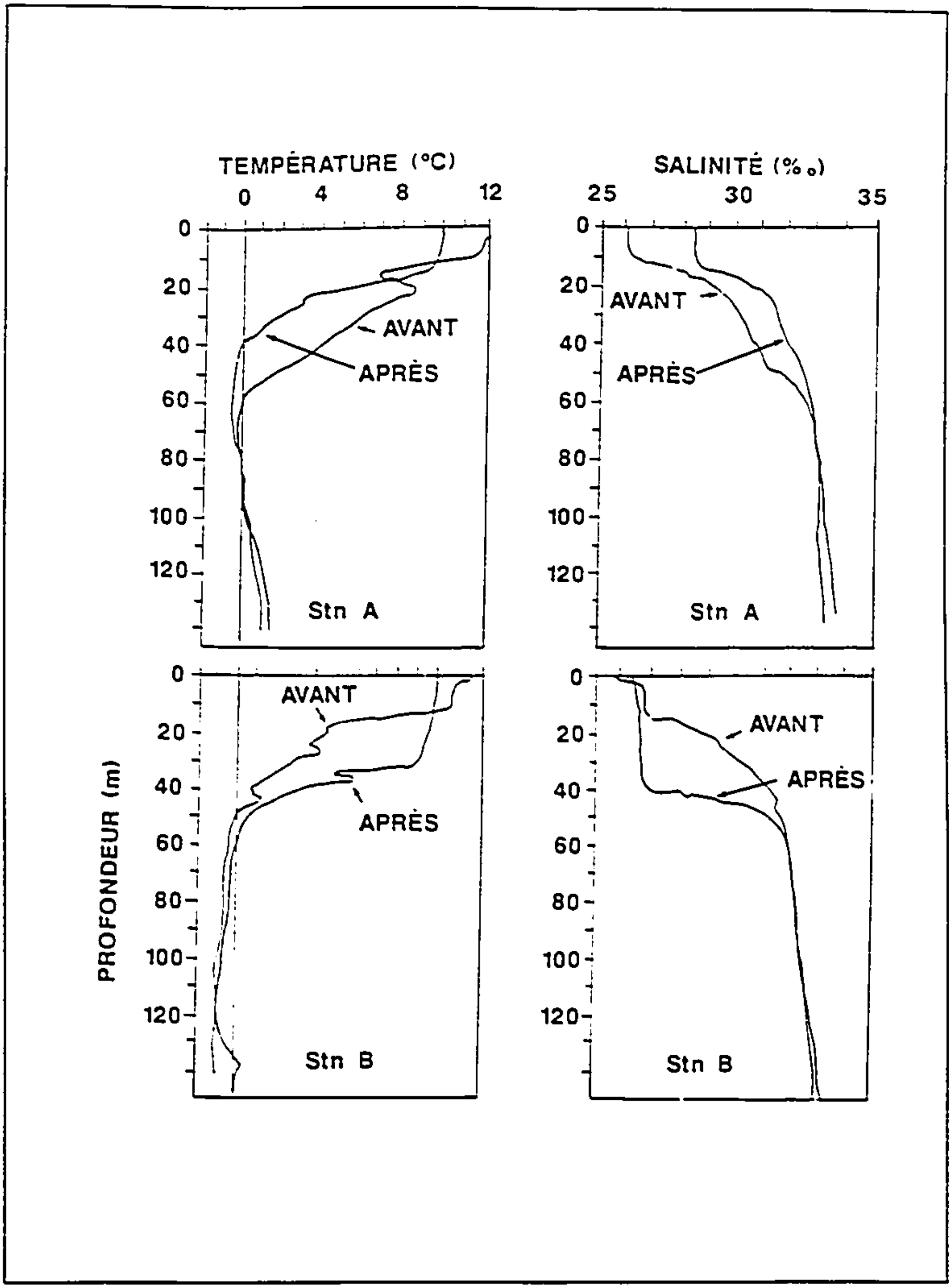

fig. 2.6: *T and S profiles between Anticosti Island and the coast of Gaspésie taken before and after the passage of a storm (from Roche-Mayzaud et al., 1991)*

Turner and Kraus (1967) had first hypothesized that, "if all the kinetic energy of stirring is used to change the potential energy of the system, one can calculate the temperature and the depth of the well-mixed surface layer as a function of time, given the heat input". That such an energy balance is indeed dominant throughout most of the year for mid-latitude oceanic regions was later confirmed by several other studies (see Stevenson, 1979). Difficulties with this oversimplified treatment arise during the winter months, when net cooling at the surface leads to a input of buoyancy and results in penetrative convection ($B > 0$, ref. to section 2.2.4). But before discussing the specific problems associated with the various model formulations and assumptions, let us first consider the climatological structure of the upper ocean in terms of a specific example of temperature-depth-month relationships for the Gulf of St.Lawrence (see figure 2.7 on the next page, adapted from Petrie, 1990).

The two graphs of figure 2.7 - temperature-depth-months - contours (top) and profiles (bottom), were adapted from Petrie's monthly "box" climatology for the GSL (1990) and are from the central part of the Laurentian Channel, just south of Anticosti Island (box #9 in Petrie, 1990). The top figure corresponds to the monthly evolution - from left (Jan) to right (Dec) - of the T-z values for a fixed area. From this graph, a distinct warming of the sea surface to a maximum around July-August as well as the establishment of a seasonal thermocline are clearly visible. The corresponding temperature profile graph (bottom part) emphasizes the development of a "summer" mixed-layer. This is depicted again by the formation of a sharp thermocline from May to August, followed by deepening and cooling of the ML in the September and November profiles. By December, the mixed-layer has substantially cooled and completely merged with the intermediate waters of the Gulf. Both graphs reveal a significant aspect of the annual structure, i.e.: the seasons are not felt beyond a certain depth ($\approx$ 100 metres) below which the temperature values remain essentially constant.

To understand why this repeating cycle occurs, it is instructive to look at some of the concepts discussed earlier. First, in their theoretical scenario, Niiler (1975) and de Szoeke and Rhines (1976) suggested, like Turner and Kraus (1967), that the mixed-layer response on longer time scales (seasonal) would be dictated by the energy balance between the surface processes and the associated change in potential energy of the upper waters. This presumes that the wind mixing effects are constantly balanced by the buoyancy flux

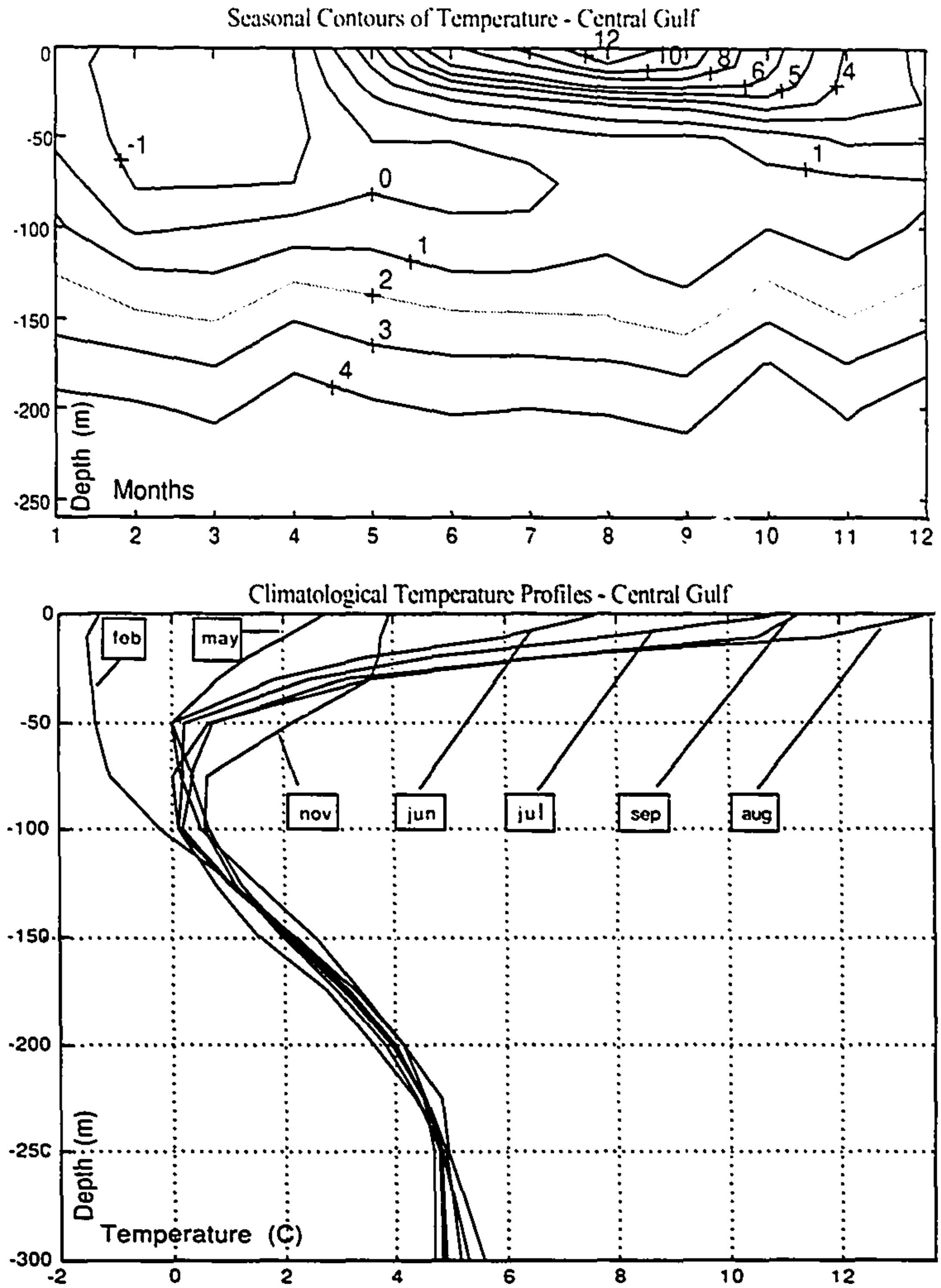

fig. 2.7: *Seasonal evolution of the temperature fields for central GSL (from Petrie, 1990)*

(for they consider no heat flux in their rather simplified case). The buoyancy flux no longer opposes the surface stress during the "winter" months because of the net heat loss experienced by the sea. In fact, in their model and an analytical study of mixed-layer deepening, Pollard et al. (1973) suggested that the ML seasonal evolution would be dominated by heating/cooling taking place at the surface rather than inertial entrainment occurring via interfacial breaking. On the other hand, Haney and Davies (1976) concluded, from results of a 1D eddy diffusion model integrated for several hundred years, that surface mixing played a critical role in reproducing important features of the upper-ocean monthly thermal structure. Consequently, a more realistic situation should consider both mixing and the formation of cold/heavy water at the surface but, as observed in several climatological (annual) model studies, the mixed-layer depth reaches infinity at the end of the cooling season if no other mechanisms are considered (Stevenson, 1979).

Leaving aside the even more complex thermodynamic situation of sea-ice formation, the problem now lies in determining which additional factors come into play in order to prevent this unrealistic "numerical" deepening and close the annual loop (cycle). Stevenson (1979), in a theoretical review, stated that a number of such physical processes limit ML deepening: TKE dissipation, internal gravity wave radiation from the ML bottom, a net annual positive (negative according to Gill's, 1981, formulation; see section 2.2.4) buoyancy flux, upwelling, etc. After studying several parametrizations of such processes in mixed-layer models, he concluded that "the dissipation must be able to balance the wind generation of TKE in absence of a surface buoyancy flux; and that the dissipation must exactly balance the TKE generated by the wind and released by convection near the end of the cooling season". In other words, wherever the TKE had been produced, it could not be "absorbed" simply by changes in ML potential energy. Therefore, to complete the annual cycle, dissipation should be considered. This leads us to an even more complicated situation: what is the value of TKE dissipation in the upper ocean (as a function of both depth and time)? Some aspects of this will be briefly discussed in the next section.

2.4 Miscellaneous Aspects of the Mixed-Layer

This final section serves one purpose: to introduce briefly two additional aspects which are not directly related to this research but are of significance to most mixed-layer studies. Since it has been stated that turbulence is central to the process of mixing, this will be discussed first. Then, as most conclusions drawn so far concerning the upper ocean physics come from various model studies, some introductory notes on 1D mixed-layer modelling will be presented.

2.4.1 Turbulence within the Surface Layer *(Assumptions & Observations)*

Much has been written about turbulence (e.g. Tennekes and Lumley, 1972). Consequently, only a few aspects of turbulence that have already been mentioned in relation the mixed-layer will be described. We leave aside the rather long historical background of turbulence research, and purposely avoid trying to define it, but consider the generation of turbulence in the ocean. Monin and Yaglom (1972) considered the following possible mechanisms in their well-known book on statistical fluid mechanics:

- Instability of vertical velocity gradients in drifting flow.
- Overturning surface waves.
- Instability of vertical velocity gradients in stratified large scale oceanic flows.
- Instability of local velocity gradients in internal waves.
- Convection in layers with unstable density stratification.
- Instability of vertical velocity gradients in a bottom boundary layer.

Next, a useful expression in describing oceanic turbulence and often used to derive some of the quantities that characterize microstructure data is the turbulent kinetic energy (TKE) equation. In its approximate form (see Oakey, 1985), it reduces to

$$\frac{d}{dt}\left(\overline{\tfrac{1}{2}q^2}\right) = \underset{(1)}{-\overline{u'w'}\frac{\partial U}{\partial z}} - \underset{(2)}{\varepsilon} - \underset{(3)}{g\frac{\overline{\rho' w'}}{\rho}}$$

where $\frac{1}{2}q^2$, the rate of change of TKE per unit mass, is the sum of three quantities: *1*- the rate of generation of TKE by the interaction of the Reynolds stress with the mean shear, 2- the viscous dissipation rate of TKE per unit mass, and 3- the potential energy rate of change due to buoyant production/destruction of TKE. In this equation, transport terms of TKE due to divergence are ignored, and averaging (denoted by the bars) and Reynolds decomposition into mean (unprimed) and turbulent parts (primed quantities) has been used.

For isotropic turbulence, the dissipation is often written as

$$\varepsilon = \frac{15}{2}\upsilon\left(\overline{\frac{\partial u'}{\partial z}}\right)^2$$

where υ is the kinematic viscosity (Oakey, 1985). This expression becomes of central importance since the turbulent shear (term in the brackets) is a directly measurable quantity. Recalling Stevensons' deductions (1979) in the previous section about the significance played by dissipation in the seasonal evolution of the mixed-layer, an accurate values of ε near the surface could greatly help in formulating "less intuitive" models and thus improving one's conclusion about the upper-ocean behaviour.

Oakey (1985) carried out several microstructure measurements during the 1978 JASIN experiment (see Pollard et al., 1983, for a summary) and, found a strong correlation between the surface wind forcing and the dissipation rate. As will be seen in chapter 4, the surface energy flux from the wind can estimated by $E_{wind} = \rho_a C_{10}(U_{10})^3$, where U_{10} is the wind speed at a 10 meter reference height, and ρ_a and C_{10} are the air density and drag coefficient, respectively. Furthermore, as argued by Pollard et al. (1973), turbulence could also be generated from inertial shears in the mixing layer. Nonetheless, since the inertial current intensity depends on the wind speed as well, both sources of turbulence would be imbedded in the $(U_{10})^3$ - ε correlation, thus reinforcing Stevenson's suggestion that dissipation is essential to the seasonal evolution of the ML.

In order to further investigate the physical significance of turbulence data, one can assume the ocean surface to behave essentially like a constant-stress boundary layer (e.g., Turner, 1981). For such a case, the shear layer can be expressed as $\partial U/\partial z = u_*(kz)^{-1}$, where u_* is the friction velocity (see chapter 4 for a definition) and k (≈ 0.4) is the well-known Von Karman's constant. Returning to the TKE equation, if the dissipation and production of energy are in balance, it follows that

$$\varepsilon = u_*^2\frac{\partial U}{\partial z} = \frac{u_*^3}{kz} = \left(\frac{\rho_a}{\rho_w}C_D\right)^{3/2}\frac{U_{10}^3}{kz}$$

(Oakey, 1985). From this, the dimensionless quantity, $\varepsilon z(U_{10})^{-3}$ can be formed to compare with results obtained elsewhere. One should also note in this equation that the dissipation, when assuming a constant stress layer, is inversely proportional to the depth, z. Grant et al. (1962 and 1968) were amongst the first to successfully measure turbulence quantities in the ocean. From their observations of the occurrence of turbulence in and above the thermocline, they reported the following results:

Depth (m)	Average ε ($cm^2\ s^{-3}$)	% of turbulent water
15	2.5×10^{-2}	100
27	5.2×10^{-3}	100
43	2.3×10^{-3}	100
58	3.7×10^{-3}	≈78
73	1.0×10^{-3}	≈55
89	3.4×10^{-4}	?
90	3.1×10^{-4}	≈35
90	1.5×10^{-4}	?

Table 2.3: *Observations of the occurence of turbulence near the surface (results from Grant et al., 1968).*

Although their observations were mainly descriptive, it is interesting to note that the dissipation rate seems to exhibit an inverse proportionality with depth, as stated earlier. In addition, the vertical distribution of turbulent waters during their hydrographic measurements seem to be confined essentially within the mixed-layer and the thermocline. Furthermore, their observed turbulence spectra (Grant et al., 1962) were found to match Kolmogoroff's $k^{-5/3}$ law and, from their measurements in a tidal channel, proposed a value of 1.5 for Kolmogoroff's constant in $E(k) = 1.5\ \varepsilon^{2/3}\ k^{-5/3}$ (here, k represents the wave number).

Figure 2.8 displays vertical profiles of various oceanographic parameters in the Gulf of St.Lawrence (June 19, 1994, lat. 49.66N, long. 66.06W) during a JGOFS cruise. Noteworthy are the signatures of a surface mixed-layer defined by the sharp thermocline and halocline (hence pycnocline, 1st panel from the left) as well as the much larger values of turbulent dissipation corresponding to this surface mixed-layer (ε, 4th panel from the left).

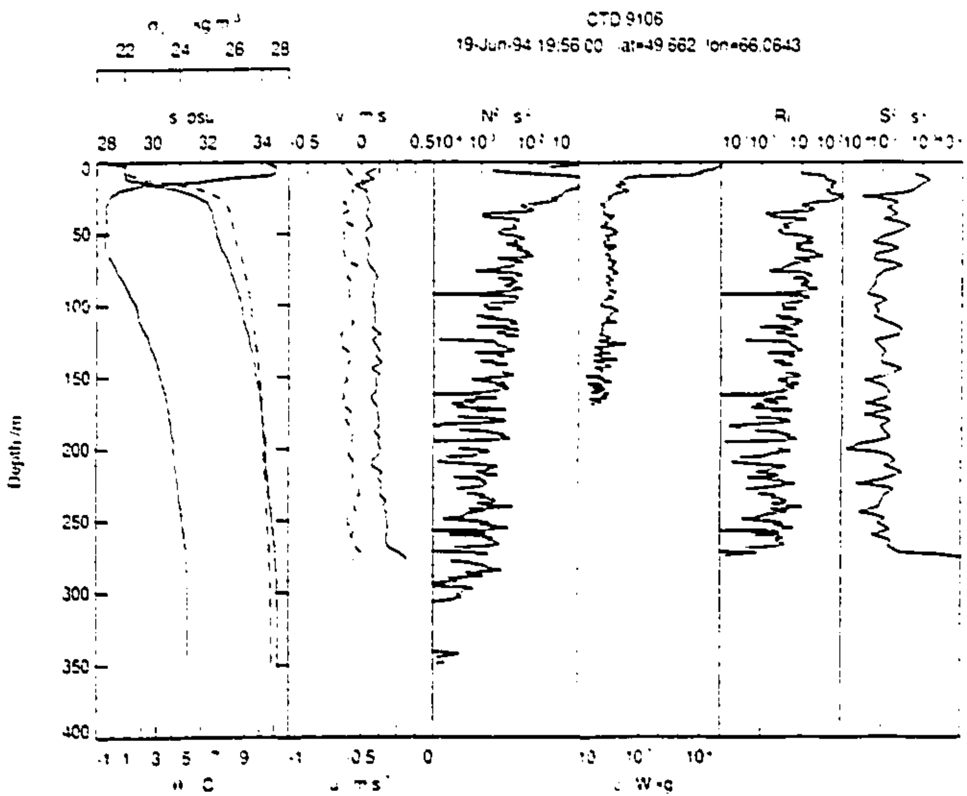

fig. 2.8: Vertical profiles of various oceanic parameters measured in the GSL (June 19th, 1994 - 49.66N, 66.06W) during a JGOFS cruise (J. Wesson, McGill Univ.; pers. comm.). Please, focus on the 4th panel.

2.4.2 Brief Overview of One-Dimensional Mixed-Layer Modelling

The intention here is to provide a brief overview of the physical numerical implications involved in most of the models discussed so far. It should not be considered, in any sense, as a complete and detailed description of one-dimensional (1D) mixed-layer modelling, but rather an attempt at introducing how some of these one dimensional models are formulated with respect to other types of models. To do so, we will follow the arguments proposed by Niiler and Kraus (1977) in their review article: "One-dimensional models of the upper ocean".

The basic rationale behind most 1D ML models is that "Bulk" T and S vary more along the vertical, on scales of 100m as opposed to the horizontal, which scales are of the order of 1000km in the open ocean (Niiler and Kraus, 1977). Consequently, "where vertical processes are dominant, one can assume that the vertical exchanges across the sea-air interface, as well as vertical mixing within the water column will affect the local state of the upper layer much more rapidly and effectively than the horizontal advection and horizontal mixing", state Niiler and Kraus (1977) in their review paper. Furthermore, the temperature as well as the depth of the mixed-layer probably are more important to the prediction because of the central role they play in the dynamics of climate as well as biological productivity. The fundamental physical equations (mass, momentum, heat, etc) must be approximated. To do so, two approaches are often used:

• *Differential approach:*

In this case, the entire set of primitive equations - salt, heat, momentum, TKE - are considered in their differential forms and treated numerically according to various finite difference (or other) schemes. The advantage is to not make any implicit assumptions as to what the ocean should look like, but the numerics of the associated set of algebraic equations are very complex.

• *Bulk or Integrated model:*

Here, the conservation equations are integrated from the surface to the "bottom" of the mixed-layer such that the physical variables involved now carry "bulk" properties which are valid over the entire mixed-layer depth.

In both approaches, however, the resulting set of equations are not closed, i.e..: there are too many unknowns for the number of available equations. One must therefore find explicit relations for the turbulent fluxes involved in order to "close" the set. This is usually referred to as the "closure problem". Following is a list of four commonly used methods of closure, with a very brief description of each.

Deterministic Solutions	Numerical solutions of the "full-blown" Navier-Stokes eq's on a fine spacial grid, with very short incremental time steps, and specified initial conditions.
Turbulent Closure Models	Parametrization of the higher moment products in which the Reynold's fluxes are expressed.
Eddy Coefficient - Mixing Length Method	Classical (and relatively old) method based on the analogy between the turbulent transports and molecular diffusion.
Mixed-Layer Model	Vertical integration of the basic set of governing equations throughout the surface layer, leading to expressions of the turbulent transports in terms of the external inputs and the mean quantities.

Table 2.4: *Commonly-used methods of closure in numerical modelling.*

As Mellor noted (in Niiler and Kraus, 1977), the mixed-layer models (4^{th} method) are somewhat disconnected from the existing methods of analysis of boundary-layer theories but, on the other hand, reveal insightful physics and simplicity due to their specific applications to the surface oceanic/atmospheric cases. An important difference between the more popular turbulent closure models and the mixed-layer models lies in their treatment of the turbulent kinetic energy (TKE) transport. The equilibrium closure models omit triple correlations, and set the mechanical energy flux arbitrarily to zero whereas in the mixed-layer models, the TKE, usually received at the surface by the action of the winds, works against gravity near the bottom of the ML, where denser water is entrained upward. Therefore, the existence of a flux of TKE is essential to the mixed-layer models, as for the 2^{nd} order turbulent closure ones, since deepening of the ML can only occur if there is a local supply of energy. This makes the ML models especially appealing and adequate for the diagnostic of the mixed-layer depth.

Mixed-Layer Model Assumptions:

- T, S and the horizontal current velocities (u) for the ML are quasi-uniform.
- For the depth and time scales (h, t), there is a practically discontinuous change in T, S, u across the lower interface (thermocline) as well as the air-sea interface.
- Rates of change of local turbulent velocity variance are small compared to the turbulent dissipation and generation.
- Changes in T due to frictional dissipation change are small and neglected.

The first assumption, represented by the vertical integration of the temperature, salinity, and the horizontal velocity, leads to expressions of bulk parameters (T_o, S_o, U_o) in terms of the neighbouring layers influence (T_o, S_o and U_o refer to temperature, salinity and current speed for the entire mixed-layer). The system is, however, not closed because of the introduction, when integrating the basic equation from z=0 to z=-h, of a time dependent parameter, the mixed-layer depth, h(t). Since there is no mean vertical velocity ($w = 0$), any subsequent deepening of the ML should be induced by fluid entrained within the surface layer. According to Phillips (1981), entrained flow can "only" be directed towards the more turbulent fluid (region), in this case, upwards into the ML.[2] This translates into :

$$w_e = \frac{dh}{dt} \text{ for } \frac{dh}{dt} > 0,$$

where w_e is the entrainment velocity. Finally, to close the system, w_e is calculated from the integration throughout the ML of the TKE in its balanced form (i.e. d/dt = 0), and knowledge of the flux boundary conditions (at z=0 and z=-h) is then required to evaluate these integral equations. In conclusion, simple 1D models are indeed valuable tools of analysis used to study the behaviour of mixed-layers. But it should be kept in mind that, although practical and effective, they are limited and do not yet reproduce nature's complexity. In short, as Turner (1981) reports, "... the models seem to have run ahead of the physical understanding on which they should be based".

2: Although the idea of entrainment occuring against the gradient of turbulent intensity is generally well explained by current turbulence theories, some upper-ocean models do, however, allow both entrainment and "detrainment" (Kraus, 1972) to take place in their formulations (e.g., see Gan et al., 1995).

Chapter 3

Oceanic Data and Analysis Methods

3.1 Introduction

In this chapter, the data used to produce the oceanic climatologies and to compute various related physical fields will be described as well as the procedures and methods (statistical as well as both objective and subjective analysis) taken to ensure quality of the resulting interpolated set of oceanic T and S profiles. The database for the St.Lawrence Gulf and Estuary was kindly provided by Dr. Ken Drinkwater from the Bedford Institute of Oceanography, N.S., Canada. It consists of 43601 stations (T and/or S profiles mainly obtained by mechanical, expendable and digital bathythermographs, conductivity-temperature-depth (CTD) probes and reversing bottles) encompassing 809585 records (values at a specific depth). Although some of these measurements were taken during the earlier part of the century (~1915-1930's), the bulk of the dataset lies roughly within the

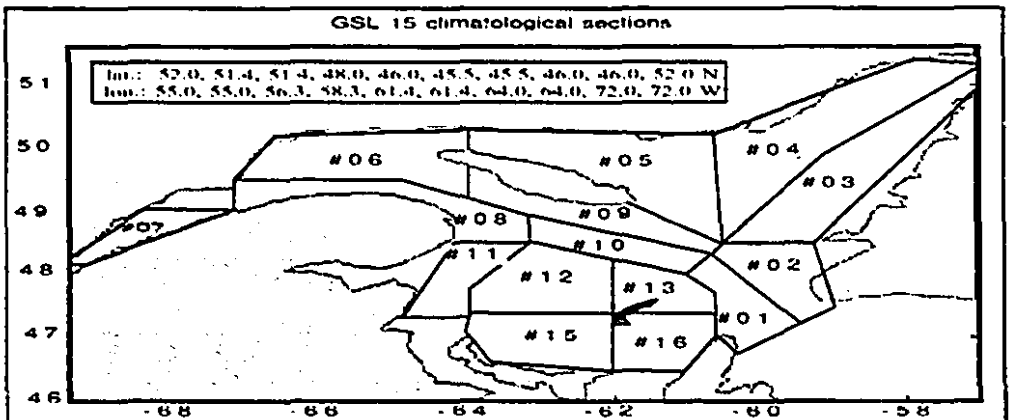

fig. 3.1: *The 15 areas (same # as Petrie) for which monthly fields were computed.*

1945-1990 period, and is believed to be the most complete historical archive of temperature and salinity profiles for the GSL to date. Its domain range is defined in fig. 3.1.

Obviously, not all data have been used for the present study, the spatial range of this research being smaller and focusing strictly on the Gulf of the St.Lawrence (GSL). The GSL was first divided into 17 areas (the same as those used by Petrie, 1990). This would allow the use of Petrie's box climatologies as a reference in order to determine rapidly if inaccurate data were present and/or if errors had been committed in the averaging process.

area#	Jan	Feb	Mar	Apr	May	Jun	Jul	Aug	Sep	Oct	Nov	Dec
01	154	56	39	54	325	414	257	341	157	135	362	9
02	178	116	70	52	251	277	137	301	114	147	380	50
03	269	37	7	35	155	210	189	280	183	140	283	25
04	56	36	5	62	87	130	128	134	151	109	162	23
05	48	52	8	34	140	219	187	130	150	124	144	8
06	45	56	9	81	206	236	142	392	162	173	257	46
07	49	58	35	150	203	271	756	363	364	194	90	47
08	30	46	25	60	195	507	523	429	545	278	372	48
09	12	29	8	40	77	92	83	127	88	70	219	28
10	31	13	5	42	152	112	43	106	69	19	56	4
11	15	10	0	30	337	604	319	546	744	261	42	5
12	12	14	10	48	510	727	194	612	375	116	120	17
13	24	9	0	11	158	162	54	159	122	23	50	0
14	8	0	0	7	151	429	439	444	427	198	18	0
15	26	2	2	33	372	596	392	571	379	140	134	20
16	22	4	0	17	301	388	200	643	305	130	91	1
17	50	4	1	9	220	660	562	534	278	134	72	50
total	1029	542	224	765	3840	6034	4605	6112	4613	2391	2852	381

Table 3.1: *Distribution of hydrographic observations (per area and per month).*

Finally, this geographical segmentation of the entire database into 17 sub-areas "on the basis of topography and physical oceanography of the Gulf" (Petrie, 1990) and the spatio-temporal hydrographic coverage makes possible the construction of time series in order to later investigate longer period (extraseasonal) climatic fluctuations and

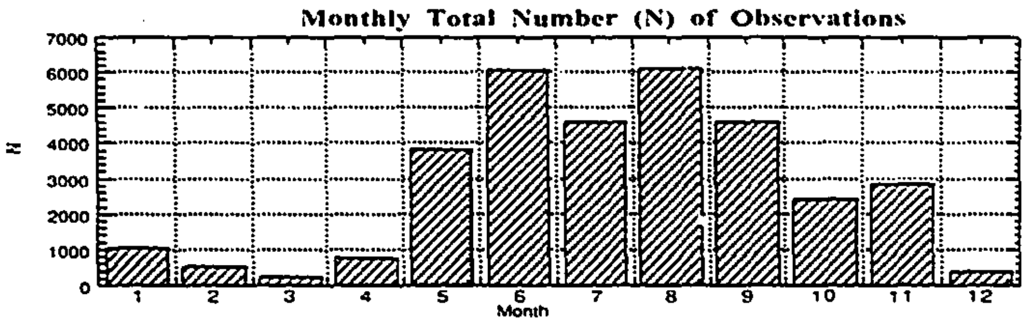

fig. 3.2: *Monthly histogram of the number of hydrographic observations in the dataset.*

again compare with pre-existing knowledge of such variations (Bugden, 1991; Petrie and Drinkwater, 1993). Displayed in Table 3.1 and figure 3.2 are the monthly and per area distribution of hydrographic observations initially contained in the original dataset. A direct relation may be observed between the number of observations and the absence of ice cover (from May to Nov).

3.2 Initial Filtering of the Data

The first procedure was to filter out unrealistic temperature and salinity values, or determine a "global" range within which all measurements should fall. The limits were bounded by zero-surface depth and by the maximum depth prescribed by the GSL bathymetry. Then, a characteristic T-S envelope was defined (using Forrester, 1964, as a guide) by a set of maximum and minimum allowable temperatures and salinities, independent of its geographical location, depth or time of the year. These were:

Tmin	Tmax	Smin	Smax
- 2.0°C	25°C	0 psu	35.5 psu

Although this initial criterion may seem rather conservative from a physical point of view, a surprisingly large number of records were deleted for these conditions.

The next step consisted in vertically interpolating each individual profile to predetermined standard depths, thus allowing intercomparison between similar reference levels. Again, despite the fact that this procedure, commonly used by oceanographers, is relatively simple, serious difficulties (which will be described in section 3.3) were encountered and required a cautious approach to this problem. The reference depths used for interpolation are the same as those used by Petrie, except that additional levels have been designated within the upper 100 meters to better define the details of the mixed layer. The 20 levels are: 0, 10, 20, 30, 40, 50, 60, 70, 75, 80, 90, 100, 125, 150, 175, 200, 225, 250, 300 and 400 meters. The choice of a 10m vertical resolution yielded a proper balance between retaining as many profiles as possible, according to quality criteria, while having (hopefully) a fine enough vertical resolution to properly characterize the upper ocean. After all profiles were brought back to these reference points via the interpolation method described in the next section, the second and perhaps most important stage of filtering was performed. It consisted in separating every T and S value according to its respective location, time and depth, and then comparing it with the corresponding climatological value obtained by Petric (1990). Although Petric's results were obtained with a less complete set of data (Petric, personal communication) and using a much coarser interpolation technique (zeroth order "bin" method), they nevertheless constitute the best guess of the monthly mean physical state of the GSL. To do so, each comparison was allowed to differ from Petric's average value within a predetermined "window", i.e.: ± some ΔT or ΔS, but always within the "absolute" T-S envelope defined earlier. This is summarized as follow:

	T allowable window	S allowable window
0m≤depth≤100m	$[T_{Petric} - 5\ ^{\circ}C] \leq T_{obs} \leq [T_{Petric} + 5\ ^{\circ}C]$	$[S_{Petric} - 4\ PSU] \leq S_{obs} \leq [S_{Petric} + 4\ PSU]$
depth > 100m	$[T_{Petric} - 3\ ^{\circ}C] \leq T_{obs} \leq [T_{Petric} + 3\ ^{\circ}C]$	$[S_{Petric} - 2\ PSU] \leq S_{obs} \leq [S_{Petric} + 2\ PSU]$

This "window" method of filtering was chosen instead of the conventional statistical approach where the observed data point is allowed to lie within ± N standard deviations from the mean calculated with all the original points at that reference depth. (The problem with the latter is that it is difficult to assess what N should be.) Each profile was then checked "visually" via an animated computer program in order to rapidly verify whether any spurious data had bypassed the filtering procedures. Nonetheless, following external suggestions, the original dataset was "refiltered" twice (independently) for a few areas (01, 04 and 10), keeping only data points falling within ±1, and ±2 standard deviations from the standard level mean. For the monthly averages, no differences greater than 5% were observed (i.e.: $\Delta Ti/(mean(Ti)) < 0.05$, where Ti is in °C).

Finally, before computing the monthly means for each box, all profiles that were taken during the same year, for a particular month and area, were first averaged out to a single observation, and then treated as such when grouped with the other profiles to compute the climatological means. By doing so, it avoided biasing the monthly average of any area to a specific year, when perhaps more observations had been taken. It also allowed the construction of monthly time series, per area and per depth, having then only one observation point per month for the entire time range. Although this is believed to represent more accurately the monthly average T and S state of the GSL waters, it reduced the total number of observations by first averaging together all profiles taken during the same month-year-area, hence diminishing somewhat the monthly spatial coverage of hydrographic observations. Consequently, this procedure was only done when computing the 15 box-climatologies, whereas all interpolated profiles were kept intact when computing the objectively analyzed fields (section 3.4).

3.3 Analysis Methods for the Vertical Hydrographic Profiles

The motivation for vertically interpolating profiles of oceanic quantities results from the discrete and non-homogenous depth distribution of observations, i.e: temperature and salinity. This vertical distribution depends on several factors: the type of instrument used, the purpose of the hydrographic measurement, the condition of the sea when the observation was taken, etc. Furthermore, when dealing with historical archives of measurements such as those of this dataset, the researcher has no way of knowing what were all the prevailing environmental conditions associated with these observations. Therefore, once an objective/subjective filtering procedure has been applied, each data point is considered as representing the water state for that particular site and time. From these remaining discrete T and S depth-values, the values at other depths (predetermined reference levels) can be determined by the chosen interpolation technique.

3.3.1 The Problem of Vertical Interpolation

Since the underlying goal of this research is to study the physical aspects of the oceanic upper-layer and their climatic implications, greater care must then be given to these near surface observations. More specifically, it is the "geometric" signature of the mixed-layer that is important to preserve from the set of initial discrete observations and their corresponding interpolated values. As mentioned in chapter 2, the extent of this mixed-layer usually corresponds with a relatively thin zone of density change, the pycnocline, in the upper water column. Although characterized physically by a density change (which is determined by both temperature and salinity), observation of several typical T and S profiles in the GSL during the ice-free months showed that the signature of this gradient is also clearly defined in the temperature-depth curves for the ice-free season. In addition, temperature measurements were substantially more numerous such that the resulting set of density observations were too small for a climatological study. Therefore, attention will be given to the interpolation of the T(z) curve and the difficulties associated with determining the mixed-layer depth from it.

In figure 3.3, a typical distribution of "raw" temperature values corresponding to a profile section contained in the historical database (area 01, August) are displayed. From a general knowledge of physical oceanography and of the Gulf's waters, it is relatively simple to deduce what this temperature profile should more or less look like in a continuous fashion. As illustrated, warmer, and lighter waters constitute the first 25 meters, followed

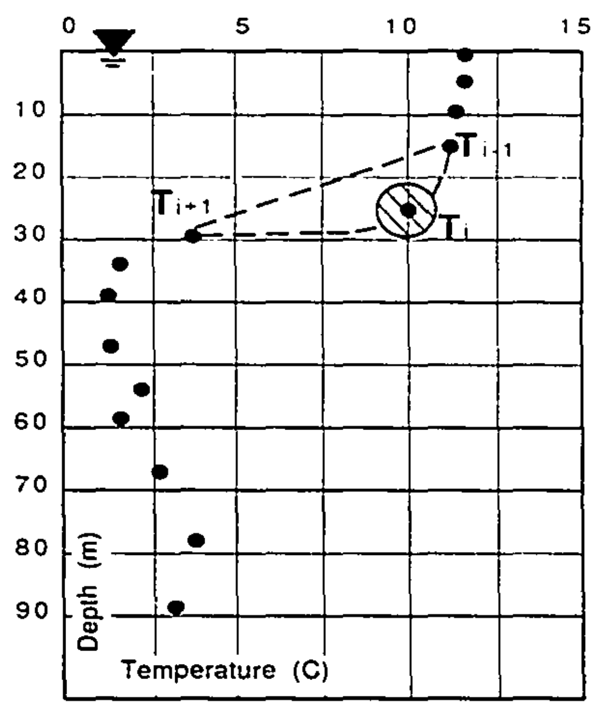

Fig. 3.3: *Typical T(z) discrete measurement (•) distribution (area 01). Shaded area and dashed lines are discussed in text.*

by an abrupt temperature gradient in which the water column cools from about 10 to approximately 2 °C within 10 meters. This typical distribution can be observed in most T(z) profiles during the May to November period, with some variations in the depth of the thermocline and/or in the magnitude of its gradient. It is this "curvature" in the T field that will be critical in determining the extent of the ML, thus influencing the evaluation of quantities like the heat content of the upper layers, the biological production, the stability of the water column, etc. Hence, a major aspect concerning the choice of a proper algorithm regards the persistence of the interpolated results if some observational points were to be removed at random. In fact, one might explore this scenario for the profile displayed on figure 3.3 by excluding (or not) the circled T value. In general, the thermocline region contains critical information required for this study and thus requires a more precise interpolation, whereas at the other end of the profile (below a depth of 100m), both T and S have relatively less structure, and are consequently easier to interpolate. It is therefore appropriate to have a method whose numerical criteria and features are *local* and do not first require pre-processing of the entire profile. As will be demonstrated later, surprising and rather different results will be obtained for the two cases. But before discussing specific numerical experiments, it is important to enumerate the various "computational" characteristics the algorithm should have to be suitable for processing the entire dataset.

1. The method should be "robust" numerically.

When an instrument like a CTD remains quasi-stationary at some depth, or when it undergoes a very slow descent, the resulting profile often contains clusters of discrete T and/or S points for some vertical sections. Although these dense accumulations of observations could depict various microphysical processes taking place, there is no realistic way to assess the true nature of these local phenomena within a large dataset. Consequently, these points represent valid hydrographic information and must therefore be included in the computation. Unfortunately, they are difficult to process numerically due to the sharp localized gradient features they exhibit. Third and higher order splines generally "blow-up" in these situations by generating unrealistic "zig-zag" curves and poor interpolated results.

2. The interpolating scheme should be "flexible" graphically.

By flexible, it is meant that the resulting interpolation should link all points by a set of piecewise smooth and continuous curves in accordance with the general orientation of the discrete measurements. Obviously, the natural relation between T_{i-1} and T_{i+1}, as illustrated in figure 3.3, runs through the value T_i. It is therefore expected that a "flexible" numerical scheme would yield a similar smooth link from T_{i-1} to T_{i+1} as it did between T_{i-1}, T_i and T_{i+1}.

3. The chosen technique should be relatively "natural" and "easily manageable".

By natural, it is meant that the numerical algorithm used to compute the interpolation on the basis of neighbouring points should be as simple as possible. Several methods exist to do such task, all having various degrees of complexity. In particular, there exist numerous modifications to the standard spline curves, all introducing external and/or artificial computational factors in order to modify their graphical behaviour (e.g.: "tension" parameter, "clamped" boundary conditions, external points and statistical weights for splines, all of which can be tuned manually for different purposes and therefore constitute computational attributes that complicate the algorithms; Kincaid and Cheney, 1991). Moreover, as in the case of the common cubic spline, most of these interpolation techniques require the use of all the profile points in a first computation, usually to determine some additional parameters (statistical structure, n^{th} order derivatives, skewness, weight, etc...), an aspect that is extremely undesirable for such a heterogenous situation as with oceanic vertical profiles. Most difficulties will occur near the surface where sharp property gradients are encountered and this is why caution should be taken.

Keeping these features in mind (robust, flexible, computationally simple and natural), three interpolation methods have been tested on the hydrographic dataset: the simple linear interpolation (also known as a 1st order spline), the "natural" cubic spline (Kincaid and Cheney, 1991), and the parametric-cubic curves. The first two techniques are commonly used numerical procedures, while the third scheme is somewhat more original in the field of hydrographic data analysis. It is a relatively novel alternative using local piecewise and smooth cubic constructions in parametric form. Like the spline method, the parametric equations are of the cubic order, and generate their interpolating curves using four neighbouring points. Their intended graphical characteristics are essentially the same as those of the cubic spline except that the associated computational algebra is much simpler, more robust, and requires the use of only 4 local points per interpolating interval. Its numerical formulation is described in the appendix. Some additional criteria concerning the minimum number of points, the maximum gradients and the allowable depth between two points are also included in the interpolating algorithms in order to fully cope with all realistic and unrealistic temperature and salinity distributions. The results were then compared for monthly climatologies, anomaly time series and individual profiles.

In general, the three methods yielded similar results for the climatology case, and showed only small discrepencies for the anomaly time series. However, looking at individual profiles reveals that the three schemes behave differently. For example, the upper section ($\approx$ 125m) of a typical summer T(z) profile was extracted from the dataset for area 01. Shown in figure 3.4, this profile was chosen because it exhibited three characteristic oceanic features that were important in choosing an appropriate interpolating technique. In zone 'A' (fig. 3.4, left-hand part), the transition from the upper mixed quasi-isothermal layer to the thermocline is depicted by the first four $T(z_i)$ points. Although only four measurements cover this zone, the parametric-cubic method clearly yields the best interpolated curve; the linear scheme oversimplifies the thermocline structure by generating colder temperatures and a much shallower mixed-layer depth. As for the cubic spline technique, an interesting erroneous behaviour can be observed: this characteristic extreme "overshoot" originates from the imposed "local" boundary conditions. In fact, since this method requires the 1st and 2nd derivatives to be preserved, a slight displacement of one data point is enough to change the curvature sign of that interval, thus forcing the 3rd order polynomial to go in a completely opposite direction, to curve, and come back to the next point, all this while preserving the local slopes given by the vertical distribution of observations. The problems associated with this reversal of curvature can sometimes lead the cubic spline method to "blow-up" numerically if neighbouring data points form a too closely packed cluster with successive changes in their 2nd derivatives. As illustrated by zone 'B', this cluster distribution shows nothing abnormal for both the linear and the parametric-cubic techniques, but forces the cubic spline curve to literally "zig-zag" through this dense array of points. In this situation, the method did not yield any numerical singularities, but nevertheless misinterpolated the thermocline zone.

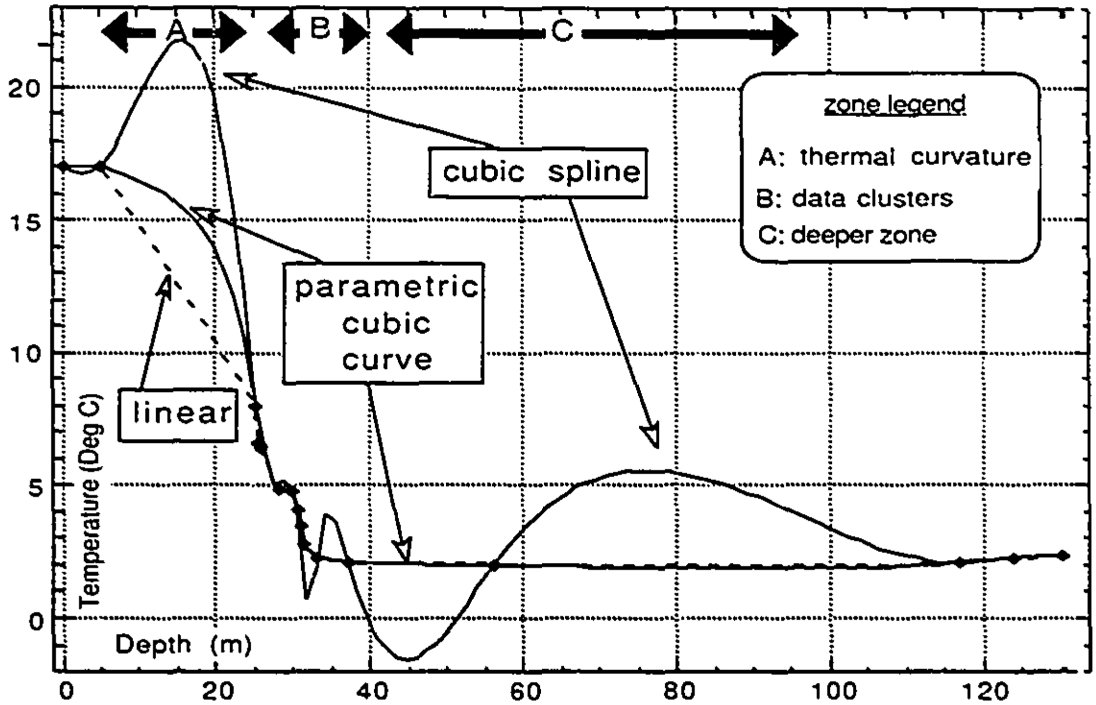

fig. 3.4: *Typical summer T(z) profile (area 01) interpolated with 3 different techniques.*

As for the deeper portion of the profile (zone 'C' on figure 3.4), a quasi-linear variation of temperature with depth characterizes both T and S profiles. Consequently, both linear and parametric-cubic methods yield interpolated results corresponding to the expected (quasi) straight line behaviour. The cubic spline algorithm carried the influence of the curvature condition a few points beyond the cluster section into zone 'C'.

In light of these results, the parametric-cubic method was chosen over the other three schemes for it is robust and flexible, yet simple enough to process accurately a large number of data. Perhaps its most important characteristic is to represent adequately the curvature observed in the near surface T(z) profiles as well as yield straight line interpolations where expected.

3.4 Analysis Methods for the Oceanic Horizontal Fields

Once all profiles were interpolated to the 20 reference levels, an objective analysis was performed on the surface fields in order to produce a horizontal description of various climatological parameters (SST, SSS, Chl-*a*, etc...). By objective analysis, it is meant that the fields interpolated from the initial observation were obtained through computer programs/numerical algorithms, and not based on the analyzer's personnal craft (Daley, 1991). Several methods currently exist, most of them arising from geology, meteorology and geometrical modelling. Although Lorenc (1986) reviewed eight analysis methods in the context of numerical weather prediction, three of these schemes that are often used in oceanography will be briefly discussed. They are listed in the diagram below, with some of their advantages and disadvantages. Afterwards, the method of successive corrections (MSC), the optimal estimation method (OEM) and kriging will be briefly introduced.

3 Common Methods of Objective Analysis

Empirical Schemes: MSC (Method of Successive Corrections)	Variational Interpolations: SOI (Statistical Optimal Interpolation), Kriging	Geometrical Methods: MCM (Minimum Curvature Method), Splines
Advantages:		
Easily performed numerically, intuitive, computationally inexpensive (no matrix inversion)	Derived from basic principles (Baysian), allows for error field estimation, optimal in a least-squares sense, use of mixed data	Produces smooth fields of noisy data by minimizing curvature, requires no a priori knowledge of the field, relies on information contained in 1 realization
Disadvantages:		
Empirical (intuitive) in its formulation, difficult to assess interpolation error (but feasible), implementation is also empirical (decreasing radii of influence, etc.)	Requires a priori knowledge of the field statistics, computationally intensive, sensitive to the covariance structure, often assumes isotropy, homogeneity and functional form of covariance	Known to have problem in extrapolating, or near the boundaries, difficult to assess interpolation error (but feasible)

3.4.1 The Objective Analysis Methods

The Method of Successive Corrections (MSC):

Simple yet efficient, this iterative scheme consists in assuming an initial guess field for the variable to be mapped (T, in this case), and correcting this field with a distance-weighted average of the difference between the observation, T_i, and the guess value,

T_{guess}, within a certain area of influence (denoted by a radius R, for the case of a circle). This can be expressed formally by:

$$T = T_{guess} + \frac{\Sigma WQ}{\Sigma Q}, \text{ where } Q = T_{guess} - T_i,$$

$$W = 0 \text{ for } r > R, \text{ and } W = \exp(-4r^2/R^2) \text{ for } r < R$$

The weighting function, W, similar to that used by Levitus[1] (1982), assumes a decreasing Gaussian-shaped radius of influence, where **r** = the distance between the observation and the analyzed grid point. This iterative process is performed successively with smaller radii, **r**, using the previously corrected field as the new guess, T_{guess}, until the resulting difference is less than a prescribed error, and/or until a maximum number of iterations has been reached. The common practice of systematically reducing the influence radius has, for rationale, to analyze for the long wavelengths first, and then build in details of the smaller scales (Achtemeier, 1987).

Originally, the monthly SST and SSS fields described later were processed with the MSC with six successive radii of influence (400, 200, 100, 50, 30 and 20 km) to meet a predetermined error criteria (less than 1°C and 1 PSU total RMS difference; Haltliner and Williams, 1980). Afterward, the analyzed fields were smoothed with a 9 point Hanning-type filter (Haltliner and Williams, 1980). Smoothed temperature and salinity values at every point are replaced by a distance-weighted average of the surrounding nine points, hence preserving their initial field features and property gradients while smoothing the overall map.

Although empirical in nature, Bratseth (1986; see also Lorenc, 1986, for a more complete review) showed that, with some modifications to the weights (W), the fields interpolated with the MSC coincides with those of the optimal interpolation in the limit of some iterations. He also notes that this modified formulation of the MSC allows for the inclusion of observational error statistics and multivariate analysis. Although the time needed to perform the analysis will depend on the number of iterations required for convergence, this technique offers the advantage of necessitating no matrix inversion.

---

[1]This scheme was used by Levitus (1982) to uniformly map the oceanic fields of the world, as well as by Michaud and Lin (1992) and Lin et al., (1992) in the Northern Atlantic and Pacific, by Reynaud (1994) in the Northwestern Atlantic and the Labrador Sea, and by DeTracey (1993) in the Gulf of St. Lawrence, to only name a few.

Optimal Estimation Method (OEM) and Kriging:[2]

Kriging is sometimes discussed in the literature along with smoothing splines and surface functional interpolation, but since the latter method was not used in this thesis, and due to the striking similarities of its formulation with OEM (Lorenc, 1986; Thiébaux and Pedder, 1987), they will be introduced together. Several types of kriging exist, but the main difference between the two methods is: while both (OEM and kriging) seek the best interpolation estimate (in a least-square sense) through a linear combination of observations that minimizes some error variance (also called a penalty or cost function) between the interpolated and observed field, kriging can accomplish this using a measure of spatial association (often called variogram) in the observations given only one realization (Madden and Katz, 1994). In contrast OEM does so using the expected value and covariance of both the estimated field and the observations (McIntosh, 1990). Therefore, OEM requires knowledge of the spatial correlation structure of the field to be interpolated, hence several realizations, and kriging may be done with only one realization of the process (although modifications of variogram estimation allow the use of repeated observations through time to better represent the spatial structure; Madden and Katz, 1994).

A last point of interest concerning these methods: McIntosh (1990) showed that OEM and splines were formally equivalent. Moreover, Lorenc (1986) and Thiébaux and Pedder (1987) reported that Kriging and splines may also be shown to be equivalent. Finally, as was mentioned earlier in this section, Bratseth (1986; and also Lorenc, 1986) showed that, in the limit of some iterations, interpolation using the empirical method of successive corrections (MSC) coincided with OEM results. Consequently, despite rather different formulations of the above methods, they can all be shown to be mutually equivalent (within the framework of Bayesian probabilistic arguments; Lorenc, 1986). Hence, one may not say that a method is better than another, but perhaps that a particuler situation lends itself better to the use of one technique rather than another, given the context within which the analysis is performed.

---

[2]: The goal of this section was to briefly describe the methods used to objectively analyze the horizontal fields, as well as to mention some important features concerning the use of these techniques. Detailed derivations may be found in McIntosh (1990) and in Thiébaux and Pedder (1987) for OEM and splines, in Bratseth (1986) for MSC, and in Marcotte (1991) for kriging.

3.5 Hydrographic Data during the 9 JGOFS Cruises in the GSL

This last section describes the hydrographic data obtained during the 9 JGOFS (Joint Global Ocean Flux Study) cruises in the Gulf of St.Lawrence. Several types of measurements were collected during this field experiment (biological, chemical, microphysical, etc.) but the purpose of this study was to mainly focus on temperature and salinity. These were obtained using CTD profilers from 1992 to 1994. On average, profiles were done every 1 to 3 hours during at least one daily cycle (except a few stations). This was done to minimize the aliasing effects of shorter scale processes (diurnal heating and motions, internal tides, etc.).

cruise	station 1	station 2	station 3	station 4	station 5	station 6
#, yr	49.7°N 66°W	49.7°N 62°W	47.7°N 60°W	47.2°N 62°W	47.8°N 64°W	49.3°N 58.8°W
J1, 92	7 (24/07) 16h		7 (27/07) 21h	5 (29/07) 4h	14 (26/07) 19h	
J2, 92	13 (02/10) 23h	20 (04/10) 40h	7 (06/10) 16h	13 (08/10) 22h	16 (09/10) 26h	
J3, 92	10 (26/10) 14h	11 (27/10) 15h	12 (29/10) 14h		10 (03/11) 14h	
J4, 92	31 (11/12) 52h	18 (14/12) 32h	3 (16/12) 2h	13 (08/12) 25h	17 (09/12) 25h	
J5, 93	9 (02/06) 27h			8 (31/05) 23h		7 (28/05) 16h
J6, 93	14 (10/07) 29h			15 (15/07) 29h		26 (12/07) 46h
J7, 93	11 (01/12) 32h			12 (27/11) 28h	12 (29/11) 32h	
J8, 94	16 (11/04) 32h	18 (14/04) 28h		12 (16/04) 43h	17 (18/04) 26h	
J9, 94	14 (19/06) 26h	12 (21/06) 34h	11 (24/06) 21h	14 (15/06) 33h	12 (17/06) 35h	

Table 3.2: *Summary of hydrographic observations (per station) during the 9 JGOFS cruises in the GSL. Included in the table are the number of CTD profiles taken at each station, the date on which the first CTD was taken, the amount of time spent at the station, as well as the station coordinates, and the cruise year.*

The original data quality was excellent for temperature, but some of the salinity profiles were "spikey". This is perhaps due to a slow response time of the conductivity sensors in comparison with the descent rate of the CTD instrument. Consequently, great care was required for the data processing. Both T and S profiles in the raw database were sampled every 1 m and further interpolated at every 5 m interval starting with the surface. Due to the high vertical resolution of the T data, we used a simple "bin" method (zeroth order) including all measurements within 1 m of the interpolated depth. Due to the rather "quiet" atmospheric and oceanic conditions during most cruises, investigation of the depth-averaged variance (per station/cruise) revealed very small standard deviations in the "daily" sampling cycle.

For the salinity case, no objective interpolation schemes were found satisfactory and processing of the entire dataset was done manually. Since T and S were observed to covary for each station/cruise (based on the good and noise-free data), one could easily "guess" what the true salinity profiles would look like, despite the "spikes". Therefore, for each S(z) cast, "dubious" spikes were removed individually. This significantly reduced the amount salinity points, but the overall number of S(z) observations was sufficient to produce an interpolated salinity profile for each station/cruise using a 3 m "bin" interpolation. Both T and S standard deviations compared favorably and were very small. This enabled us to represent each station/cruise observations by one average T and S profile with a 5 m vertical resolution. A summary of the hydrographic information from the 9 JGOFS cruises is provided in table 3.2, and the averaged T and S profiles are included in the appendix.

Chapter 4
Atmospheric Data and Analysis Methods

For climate studies in or near the Gulf of St.Lawrence, atmospheric datasets are available from the AES Canada (Atmospheric Environment Service) and consist of archived daily records from their network of weather stations surrounding the GSL. The Gulf of St.Lawrence is a relatively small basin and is well covered by approximately 12-15 regional coastal weather stations, as shown in figure 4.1. These weather stations are primarily used for operational meteorology, i.e.: to produce weather forecasts for both surrounding lands and waters, as well as in conjunction with the Coast Guard in case of marine emergencies. It is, however, costly and time-consuming to access the large amount of atmospheric data for these stations from AES Canada. Consequently, most of the atmospheric datasets used in this thesis have been obtained from other sources (e.g., Internet public domain, library disks, library atlases, NMC/NCAR CD-ROM disks, collaborators, etc.).

4.1 Air Temperature and Precipitation

The data used to evaluate the monthly climatological fields of air temperature (T_a) and precipitation (P_r) were extracted from the WorldWeatherDisk CD-ROM (Anonymous, 1988). This small subset consists of monthly time series of T_a and P_r for 13 weather stations located around the Gulf of St.Lawrence (fig. 4.1 and Table 4.1). Although the record length for each station is not the same and various gaps exist in the temporal coverage of T_a and P_r, enough data were available to produce reliable monthly averages for each location. After examination of several time series, the dominant fluctuation scales were found to be essentially seasonal, interannual, with smaller variations at the interdecadal scale (see Daoust, 1991, for more details). Time series length, as well as location for each station are included in Table 4.1. The weather station on Anticosti Island (ANTI) was moved from one end of the island to the other, approximately halfway through

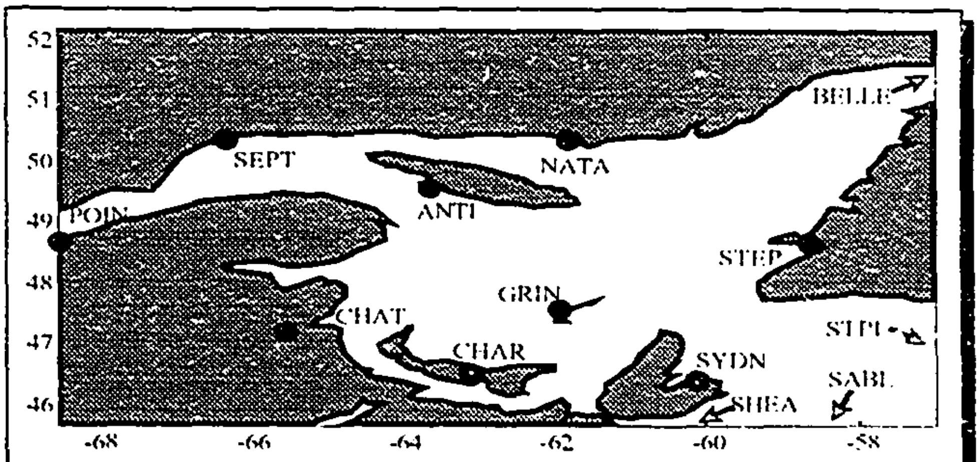

fig. 4.1: *Positions of the 13 weather stations used to produce Ta fields.*

its record. To circumvent this problem, individual monthly observations were first interpolated onto a regular grid[1] (0.75 °lat x 1° long), and monthly averages for each

Station name	code	location	time range (+/- 1 yr)	length
Pointe-des-Monts	POIN	48.5N 68.5W	1877-1951 & 1957-1972	≈ 91 yrs
Sept-Iles	SEPT	50.2N 66.3W	1944-1988	≈ 45 yrs
Anticosti (Isl.)	ANTI	49.4N 63.6W	1882-1955	≈ 74 yrs
Natashquan	NATA	50.2N 61.8W	1922-1942	≈ 21 yrs
Belle-Isle	BELLE	51.9N 55.4W	1911-13, 18-29 & 31-70	≈ 53 yrs
Stephenville	STEP	48.5N 58.6W	1942-1988	≈ 47 yrs
Grinstone (Isl.)	GRIN	47.4N 61.9W	1941-1972	≈ 32 yrs
Charlottetown	CHAR	46.3N 63.1W	1874-1886 & 1890-1971	≈ 95 yrs
Chatham	CHAT	47.0N 65.5W	1943-1988	≈ 46 yrs
Shea	SHEA	44.6N 63.5W	1944-1988	≈ 45 yrs
Sydney	SYDN	46.2N 60.1W	1940-1988	≈ 49 yrs
St-Pierre (Isl.)	STPI	46.8N 56.2W	1942-1988	≈ 47 yrs
Sable Island	SABL*	43.9N 60.0W	1890-1989 only for comparison	≈ 99 yrs

Table 4.1: *Weather stations names, abbreviations, location and time range of data records.*

[1]: An interpolated field was produced only when a sufficient number of stations were present, in conjunction with a certain spatial distribution of observations. For example, the minimum total number of stations required was set to 9, but extrapolated values were also removed from the final time series.

independant grid point were computed. With the resulting set of monthly averaged grid-point values, the monthly mean fields of T_a and P_r produced. Throughout this process, an inverse distance interpolation scheme was used (several methods were used - inv. dist., minimum curvature, universal kriging, etc., - but since extrapolation was not allowed in the analysis, the results were essentially identical). Finally, the resulting fields were compared with those produced by directly interpolating the station monthly means T_a and P_r, assuming the ANTI station to be located in the middle of Anticosti Island, and again no important differences were noticed.

The resulting T_a and P_r climatology fields, per station are displayed in figures 4.2. The temperature field in the 12 graphs (fig. 4.2, solid line) shows a strong seasonal trend at all stations, namely colder in the wintertime with minima ranging between -5° and -15°C (January-February), and warmer during the summer months (July-August maxima vary from +10 to +20 °C). A similar seasonal cycle occurs for all stations. Although each temperature value for the same month varies notably from station to station, as seen in the T_a-Months graphs of fig. 4.2, the similarity of the temporal evolution patterns suggest that, on the monthly time scale, the air mass modification over the Gulf is basin-wide[2]. Concerning the horizontal distribution of T_a, the northern part of the GSL is generally colder than the Magdalen Shallows, a situation that prevails all year long in the thermal fields (on the monthly time scale).

The P_r values are plotted in figure 4.2 (circles) as mm of precipitation[3] in histogram form. Study of each individual location could probably explain their specific seasonal characteristics, but no clear monthly signal, common to all stations, could be observed, as was the case for T_a. Furthermore, when comparing time series of P_r (monthly values and monthly anomalies) for various locations, the signals showed no significant correlation between all twelve series. Similarities were found only between neighbouring stations, which suggest that the precipitation structure, on the monthly time scale, might be of more local influence, i.e.: no consistent Gulf-wide pattern.

---

[2]: Indeed, comparisons of anomaly time series between various stations yielded no correlation coefficients smaller than 0.8.

[3]: The Pr values are those of "melted" precipitation, i.e.: if it consisted of snow, then the amount was divided by 10.

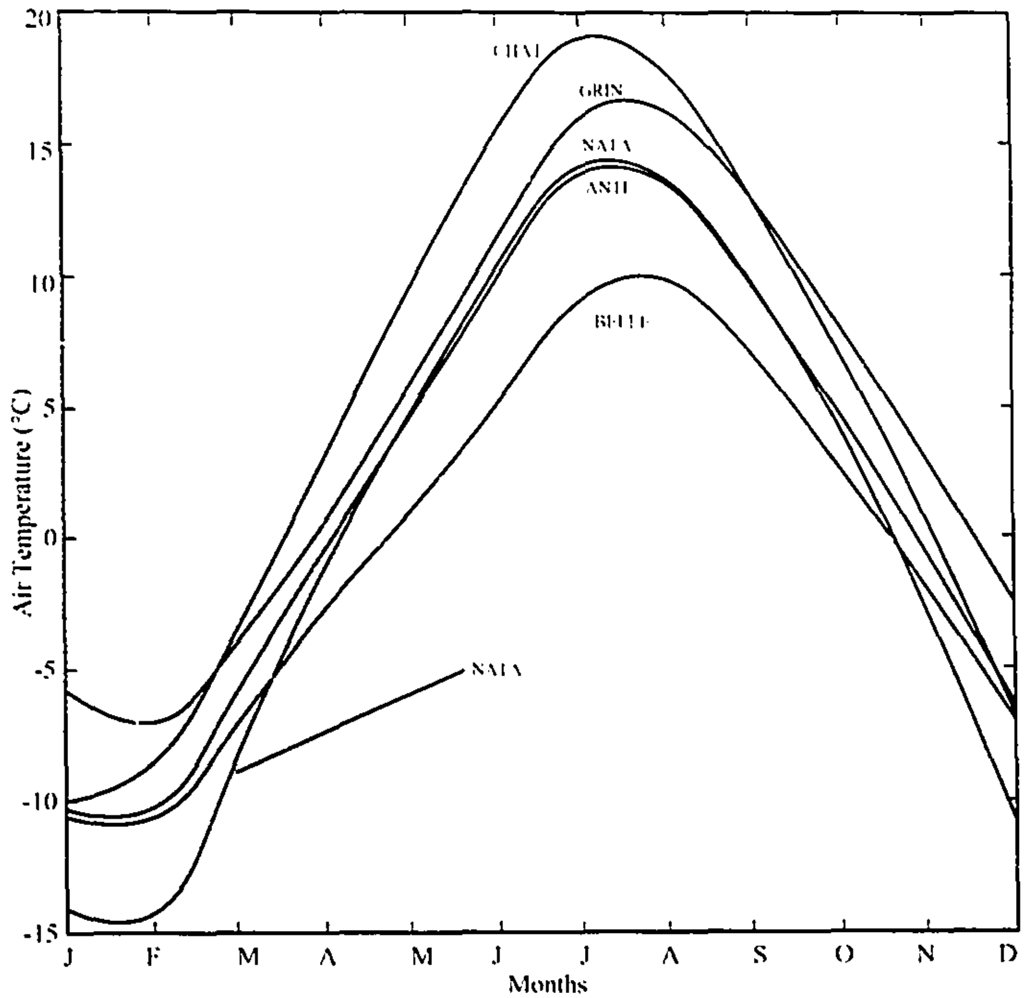

fig. 4.2: *Typical monthly averages (per station) of air temperature (°C). (The shaded sections represents months with sea ice.)*

4.2 Geostrophic Winds

As mentioned in chapter 2, one of the important physical processes acting upon the surface waters is the mechanical mixing action of the wind. Again, despite the Gulf's relatively small scale combined with the broad observational coverage by 13-15 land and island stations, assessing the actual winds (direction and magnitude) over the water is difficult. Koutitonsky et al. (1986) report differences between observed wind speeds and directions and those obtained using the geostrophic method, and suggest that orographic steering may play an important role in affecting the wind field (see also Herfst, 1984). Another problem is the availability of a complete set of accurate records, long enough and for all stations, in order to properly estimate the climatological winds. Since the purpose of this study is not directly concerned with the dynamics of the Gulf circulation but deals primarily with the thermohaline structure of the surface waters and the heat exchange across the air-sea interface, the magnitude of the wind would be sufficient to properly estimate the amount of mixing taking place, thus avoiding the difficulties associated with its direction. This assumption is valid only offshore, where coastal upwelling is not important. For these reasons, geostrophic wind data will be used.

The sea-level pressure data used to compute the geostrophic wind was extracted from (compact disc) the National Meteorological Centre (NMC) Grid Point Data, version II (1990), a subset for the northern hemisphere archived by the National Centre for Atmospheric Research (NCAR). It consists of twice daily (00 and 12 UTC) gridded data for various atmospheric variables (pressure, height, etc...) at pre-selected vertical pressure levels (sea level, 850 m, 700mb, etc..). These parameters, displayed on a 1977 point (47x51) octagonal grid and equally spaced when viewed from a stereographic projection centred at the north pole, are based on the NMC final analyses tapes and include data received up to about 10 hours after the data time. If the final analyses were not available, data were filled in with operational results, which have a data cutoff of 3 hours 20 minutes after the data time. The assimilation system used by the NMC to treat the heterogenous global dataset is based on updating a nine-level primitive equation prediction model by a local, multivariate, three-dimensional, statistical interpolation method. Updating is performed at 6 hour intervals and observations are weighted according to estimates of the observational error from different sources.[4]

In order to calculate the geostrophic wind climatologies, time series of sea-level pressure for sixteen (16) points covering the Gulf were extracted from the database. This array of observations covers the study area with a 4x4 grid of approximately 275 km wide square cells. The time records include data from 1946 to 1989. For each instantaneous pressure field, a corresponding geostrophic wind field was calculated, and a specific wind observation was then interpolated to the desired location using a Bessel 16 point central difference scheme. The process was then repeated for the following observation (12 h later), thus yielding a twice daily time series of 42 years in length. This is believed to be long enough that the climatological fields deduced from this dataset would not be overly affected by interannual and interdecadal fluctuations.

4.2.1 Spatial and Temporal Variations of the Wind Field

The aspect of temporal and spatial variability has already been addressed by some researchers (e.g., Saunders, 1977) and their results have been reported by Koutitonsky and Bugden (1991). Nevertheless, it remains difficult to know exactly how often and at which locations in the Gulf the wind speed should be recorded in order to properly estimate its action on the oceanic surface? The horizontal extent of the GSL arises when trying to determine whether the aeolian structure is essentially local or whether the winds are induced by large scale pressure fields. Variations taking place on shorter time scales, such as diurnal effects, cannot be included in this analysis. The simplest procedure would be to take hourly observations in as many different locations as possible. Unfortunately, computational as well as data limitations, do not allow such an approach for this study.

To examine spatial differences, three points were chosen - northwest GSL (49.5N-66W), central (48N-62W) and northeast GSL (50N-59W) - for which the monthly mean geostrophic wind speeds were computed from their respective 42 year time series. The results (monthly averages) showed no significant differences from one location to the other (less than 0.75 m s^{-1}). To ensure that the computed climatologies were accurate, the central point geostrophic time series were also compared with those produced by the Canadian Climate Program (Swail, 1985) at a location slightly to the east (48N-63.5W). A very good

---

[4]: For more information about the the NMC global data assimilation system (improvements of schemes, comparative studies), see: McPherson et al. (1979), Kistler and Parish (1982), and Dey and Morone (1985).

correlation was found between these records over a 33-year period. Furthermore, when the geostrophic wind magnitude was reduced to approximate the near-surface conditions and the wind stress calculated (see section 4.2.4 and fig. 4.4), they also compared well with existing climatologies (Saunders, 1977).

Times series of geostrophic winds (twice daily) were computed for the 1963-89 time period on a 21 point (1°x1°) grid, and principal component analysis (empirical orthogonal functions or EOF analysis: Peixoto and Oort, 1991) was then performed. The results, as displayed in figure 4.3, show that the first two modes, which explain 84 % of the total variance, are essentially homogenous. Since the geostrophic wind vectors can be reconstructed by linear combinations of the principal component fields (Preisendorfer, 1988) in accordance to their respective weight (% of variance), it is fair to say that, at any instant of time, the geostrophic wind conditions (speed and direction) are virtually the same over the entire Gulf. This can be appreciated intuitively when looking at the characteristics of sea-level pressure maps covering the study area. Typical length scales for synoptic pressure patterns, hence geostrophic motions, usually range from hundreds to thousands of kilometres (Ahrens, 1991), thus encompassing the area studied. The geostrophic wind was used on the basis that atmospheric motions were effectively synoptic over the GSL. Consequently, although diurnal[5] and local effects might actually be present, especially nearshore, it is believed that such features (e.g.: land-sea breeze, valley winds) do not extent far enough offshore to disturb the air motion, thus justifying the choice of a homogenous geostrophic wind sampled twice-daily at the centre of the GSL.

[5]: The 12 h sampling resolution in the geostrophic time series corresponds to the minimum Nyquist frequency required to resolve diurnal processes (Peixoto and Oort, 1991).

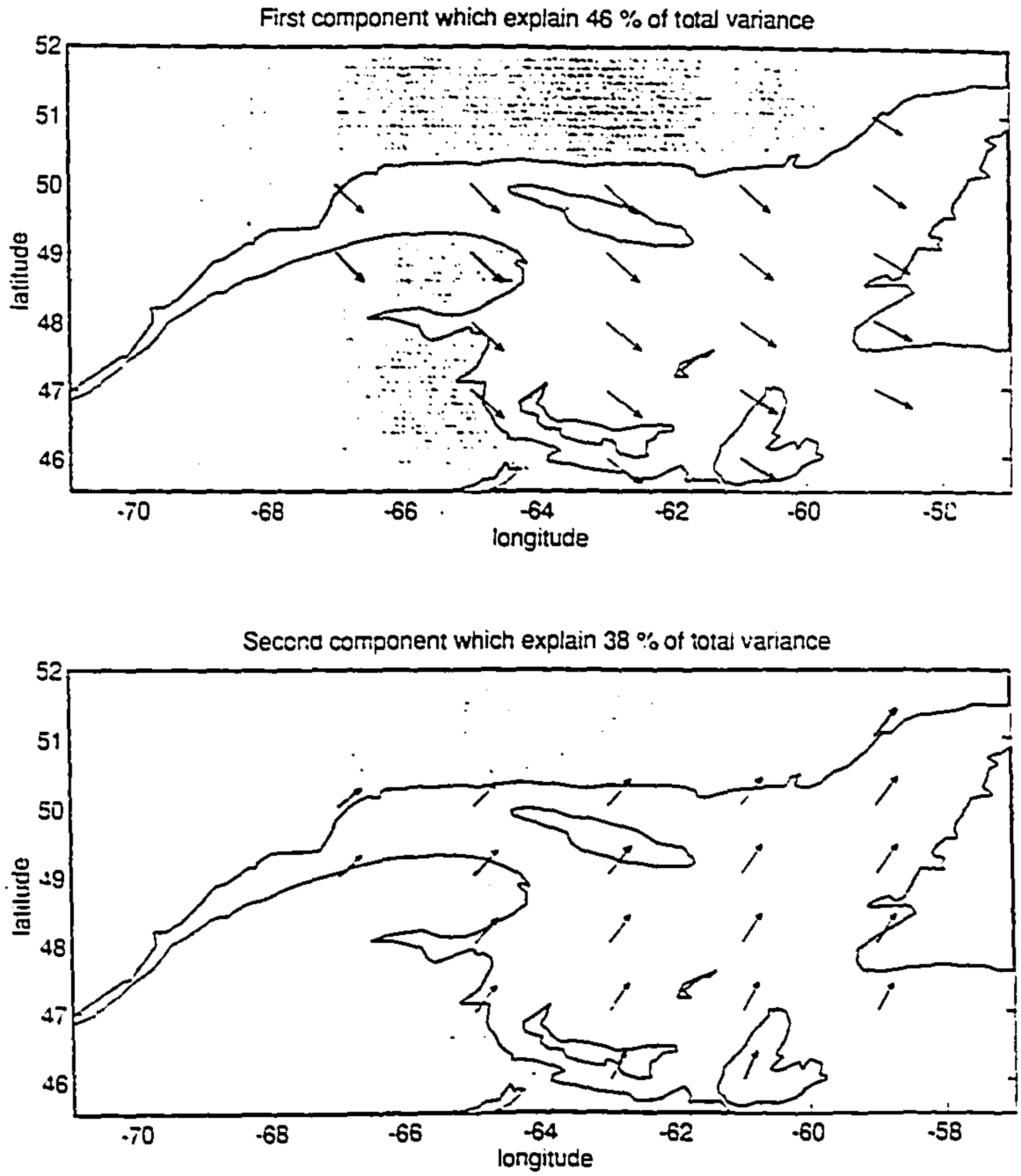

Fig. 4.3: *First two EOF spatial components of the geostrophic wind field.*

4.2.2 The Climatological Wind Stress

As mentioned before, a primary objective of this study is to determine the climatological thermohaline state of the surface waters, and the extent to which various atmospheric processes influence this temperature and salinity structure. Consequently, one main concern is to estimate the mixing action of the Gulf's wind regime. Numerous studies have addressed the question of turbulent kinetic energy transfer from the wind surface stress to the ocean surface. Although it is relatively simple to estimate the energetics of a specific wind regime, it is more complicated to know how much of this energy is transferred to the ocean, and what are the resulting motions. Ellison and Turner (1959) and Kraus and Turner (1967) followed by a number of similar laboratory studies (Kato and Phillips, 1969), numerical simulations (Pollard et al., 1973) and oceanic observations (Denman and Miyake, 1973) tried to relate the mechanical mixing effect of a surface stress to various oceanic parameters such as entrainment rate, mixed-layer depth and deepening rate, Richardson number, etc. As reported by Turner (1981), in an excellent review paper on mixing processes, most mixed-layer studies base their models on "energy arguments that balance the inputs of turbulent kinetic energy (T.K.E.) against changes in potential energy and dissipation".

According to a common formulation introduced by Turner and Kraus (1967), and summarized in Denman (1973), the rate of work done by the wind (usually taken at a reference height of 10m) on the water surface is given by

$$E_a = \tau U_{10} = \rho_a C_{10} U_{10}^3,$$

where E_a represents this rate of working, and τ, ρ_a, C_{10} and U_{10}, are the wind stress, air density, drag coefficient and wind speed, respectively. In this formulation, the wind stress term and the associated drag coefficient are defined by

$$\tau = \rho_a C_{10} U_{10} |U_{10}|$$

$$C_{10} \sim 0.63 \times 10^{-3} + 0.66 \times 10^{-6} |U_{10}|,$$

where the empirical formula used to estimate C_{10} is from Smith and Banke (1975), as used by Saunders (1977) in his wind stress study, and assumes that neutral conditions prevail over the water surface. Although it is well known that the air-sea temperature difference plays an important role in influencing the turbulent exchanges of momentum, heat and moisture across the air-sea interface (Saunders, 1977; Large and Pond, 1980), the use of this simpler relation for C_{10} was motivated by its independence on the near surface atmospheric stability, a parameter that was available only for later years, but for a period much shorter than the wind records used in the present calculations. It is then possible to define a friction velocity scale, u_*, (Denman, 1973) for the surface waters,

$$u_* = \left(\frac{\tau}{\rho_w}\right)^{1/2} = \left(\frac{\rho_a}{\rho_w}\right)^{1/2} C_{10}^{1/2} U_{10},$$

such that an estimate of the rate of transfer of turbulent kinetic energy downwards, E_w, below the ocean surface can be made:

$$E_w \sim u_* \tau = \left(\frac{\rho_a}{\rho_w}\right)^{1/2} C_{10}^{1/2} U_{10} \tau = \left(\frac{\rho_a}{\rho_w}\right)^{1/2} C_{10}^{1/2} E_a.$$

Making use of the expression for E_a combined with that for u_*, E_w can be expressed in terms of the friction velocity scale or in terms of the directly measurable reference wind speed, U_{10}, as follows:

$$E_w = \rho_w u_*^3 = \frac{\rho_a^{3/2}}{\rho_w^{1/2}} C_{10}^{3/2} U_{10}^3.$$

From this last relation, it is clearly evident that the rate at which the energy available for mixing is transferred from the wind to the ocean surface is proportional to the cube of the wind speed, U_{10}^3. Hence, any evaluation of the monthly value of E_w will require adequate treatment of U_{10}. Knowledge of the monthly mean wind speed will not be sufficient to properly estimate the corresponding monthly average of E_w but will necessitate analysis of daily or twice daily U_{10} time series. This is shown by the relation:

$$\overline{E_W}\Big|_{monthly} \sim f\left(\overline{U_{10}^3}\right) \neq f\left(\overline{U_{10}}\right)^3.$$

On the basis that the overbar notation designates monthly averages,

$$\overline{U_{10}^3} > \overline{U_{10}}^3.$$

The problem associated with the use of monthly mean wind speeds and stresses has been addressed by Oberhuber (1993) in the development of a coupled sea ice-mixed layer-isopycnal general circulation model. When estimating the amount of atmospheric turbulent kinetic energy input in his model, Oberhuber noted that:

> "monthly u_*^3 determined only from the monthly mean absolute wind U_{10} is much smaller than the required [monthly average of] u_*^3".

Furthermore, he suggested that:

"the effective u_*^3 must be determined by the additional use of the monthly mean standard deviation of the absolute wind, $\sigma(U'_{10})$," as indicated by the following approximation:

$$\overline{u_*^3}\Big|_{\text{Oberhuber}} \sim \left(\frac{C_{10}\rho_a}{\rho_w}\right)^{3/2} \overline{U_{10}}\left(\overline{U_{10}}^2 + 3\sigma^2(U'_{10})\right).$$

Consequently, three ways of calculating the monthly averages of u_*^3 were compared (1- directly from the u_* time series, 2- from the monthly means of u_*, 3- from Oberhuber's method). It was observed that the last two methods yielded monthly u_*^3 values much lower than the first one. We now discuss an often debated parameter that has either been experimentally determined or simply adjusted "manually" for numerical purposes, the fraction (m) of E_a used to increase the potential energy of the upper ocean as a result of mixing. A first estimate of this fraction can be obtained by neglecting the effects of dissipation, thus expressing it as the ratio of T.K.E., E_w, used for mixing to the total T.K.E. of the wind, E_a,

$$m \sim \frac{E_w}{E_a} = \left(\frac{\rho_a}{\rho_w}\right)^{1/2} C_{10}^{1/2}.$$

A simple scale analysis assuming that $\frac{\rho_a}{\rho_w} \sim 0.001$ and that C_{10} is of the order of 10^{-3} yields

$$m \sim \left(\frac{1}{1000}\right)^{1/2} (1\times 10^{-3})^{1/2} \sim O[1\times 10^{-3}],$$

which is approximately of the same order as that used by Denman and Miyake (1973).

Figure 4.4 summarizes the monthly mean wind-related statistics computed from equations described above, using wind speed approximated from geostrophy, at a central GSL location. Although different in magnitude, a distinct (and typical) seasonal cycle may be observed, with stronger winds in winter and minimum values during summer. To estimate the actual wind magnitude in the marine surface layer, Zverev (1972) suggests that the wind speeds be scaled down to 70 % of that of U_g. For the present study, geostrophic wind statistics (Ug, |U|, u_*, Ew, etc.) were computed for both 0.7|Ug| and 0.8|Ug| so as to define a "window" within which the real wind speeds are likely to fall.

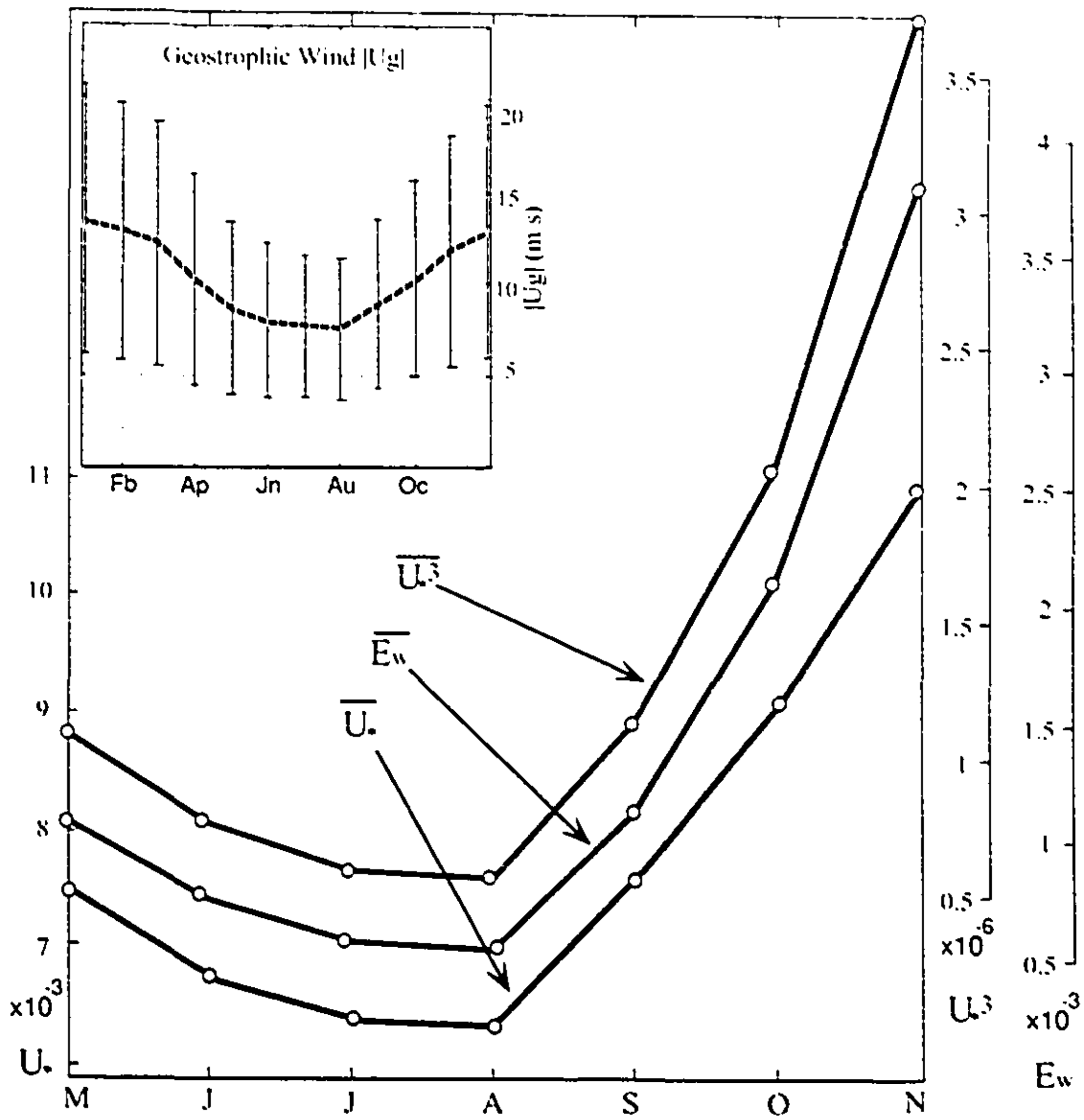

Figure 4.4: *Monthly geostrophic wind statistics: The smaller graph (top left) represents the geostrophic wind speed (|Ug|) calculated at the center of the GSL. In the main graph, the 3 solid curves correspond to monthly means of the friction velocity (U_*), the friction velocity to the 3rd power (U_*^3) and the water mixing energy (Ew), as computed from the 0.75x|Ug| time series. The shaded area represent the [0.7-0.8]xU_* window - a measure of the "true" wind speed window (as explained in the text. The corresponding units for the 3 parameters are: U_* (10^{-3} x m/s), U_*^3 (10^{-6} x m^3s^{-3}) and Ew (10^{-3} x W/m^2).*

4.3 Clouds

As mentioned in section 2.2, the cloud cover is an important factor which influences the heat transfer across the air-sea interface. This direct and very sensitive dependence of the cloud fraction on the total incoming solar radiation will be shown later in the computation of the net surface heat budget (see chapter 6). In fact, until the magnitude and seasonal evolution of all the terms of the net heat flux are known, and one assesses the sensitivity of each term to the atmospheric and oceanic variables involved in the heat calculations, it is nearly impossible to determine the accuracy required for each dataset. Consequently, an assumption will be made that the spatial structure of the cloud cover is of critical importance to properly determine the heat budget at the surface of the GSL, thus justifying the choice of the best cloud cover dataset available.

4.3.1 Intercomparison between Various Data Sources

When choosing the kind of cloud parameter needed for later computations, several options were considered. First, a monthly mean value for the entire Gulf taken at one central point location would be the simplest choice on the assumption that the spatial extent of the entire basin is small enough to be represented by one single observation. However, despite the relatively short length scale, i.e.: approx. 500 km from Gaspé (Québec) to Stephenville (Newfoundland), there is a strong east-west gradient in the monthly cloud fraction throughout the entire Gulf, thus rendering inappropriate the single-point approach. For the next alternative, cloud data from the several (approx. 13 to 15) weather stations surrounding the study area could be analyzed in order to form a monthly "land" climatology and then be interpolated over the GSL. This method was also rejected because of two problems: first, the entire atmospheric data set for these 15 AES stations were costly and would take a long time to obtain and analyze; secondly, the cloud data were not taken in the same fashion throughout the network of Canadian AES stations, some using fractions (/4, /8 or tenths), and the measurements were not taken at the same time of day.

The third option considered was to use NCAR's global cloud atlases for land and sea (Warren et al., 1986 & 1988). Unfortunately, only two data points were available from both atlases, one to the west, near Baie-des-Chaleurs, and one to the east, near Stephenville. The spatial resolution of both atlases was considered too coarse to adequately represent the horizontal structure of the cloud cover. However, these atlases have been used quite extensively in larger scale global climate studies and constitute therefore a valid source of "coarse" data to be used for comparison. In Table 4.2, Warren's monthly mean values of cloud cover (in %) for the two observation points within the Gulf are shown. The land atlas data were deduced from weather station observations reported during the period of 1971 to 1981. The oceanic counterpart consists of ship data averaged over the 1952-1981 interval (Warren et al., 1986 & 1988). An obvious feature displayed by the results of Table 4.2 is a net increase in cloud cover from west to east. As mentioned in section 4.2 (Koutitonsky and Bugden, 1991), the dominant winds over the Gulf generally blow towards the east. This motion leads to an advection of continental masses of air over approximately 500 km of water, thus altering the stability and humidity content of this air mass and promoting cloud formation.

	Land atlas (west) (≈ 48N, 65W)	Ocean atlas (west) (≈ 48N, 63W)	Ocean atlas (east) (≈ 48N, 60W)	Land atlas (east) (≈ 48N, 58W)
May	67 %	66 %	71 %	73 %
June	64 %	64 %	70 %	72 %
July	63 %	63 %	71 %	74 %
Aug.	58 %	61 %	66 %	70 %
Sep.	59 %	60 %	62 %	67 %
Oct.	65 %	67 %	70 %	73 %
Nov.	71 %	76 %	79 %	77 %

Table 4.2: *Monthly mean cloud cover, in % (from Warren, 1986 & 1988).*

In fact, within the first 50 km or so from the land the first convective cloud cell has already had enough time to form. (R. Davies, McGill University, personal communication).

4.3.2 Cloud Cover Climatology for the Ice-free Months

In order to overcome the problem of the coarse spatial resolution, the use of satellite data was therefore considered. This dataset was obtained from the International Satellite Cloud Climatology Program (ISCCP). It consists of an international scientific collaboration using a large array of both geostationary and orbiting satellites, and the monthly mean cloud amount from July 1983 through June 1991 were extracted as a subset from this larger global dataset (Rossow and Schiffer, 1991). The resolution is a 2.5 degree square, which yields a total of 15 observation points over the Gulf in an array of 5° by 3° (long. by lat.). In total, 8 years of data were available for each month. The data were averaged together into a mean for each month. The resulting climatology (figure 4.6) was contoured onto a interpolated grid of 1/12° resolution (only contour lines over the water are considered accurate).

The results compare (qualitatively) well with those of Warren (table 4.2). The cloud amount, on the monthly time scale, is very close in magnitude. The zonal increase, as noted earlier, is also reproduced. Two aspects of the satellite climatology should be noticed. First, the finer and more homogenous resolution necessarily yields a more accurate picture of the horizontal cloud structure over water. Secondly, a strong (also present in other monthly time series) interannual fluctuation in the cloud amount, observed even using monthly averages (fig. 4.5).

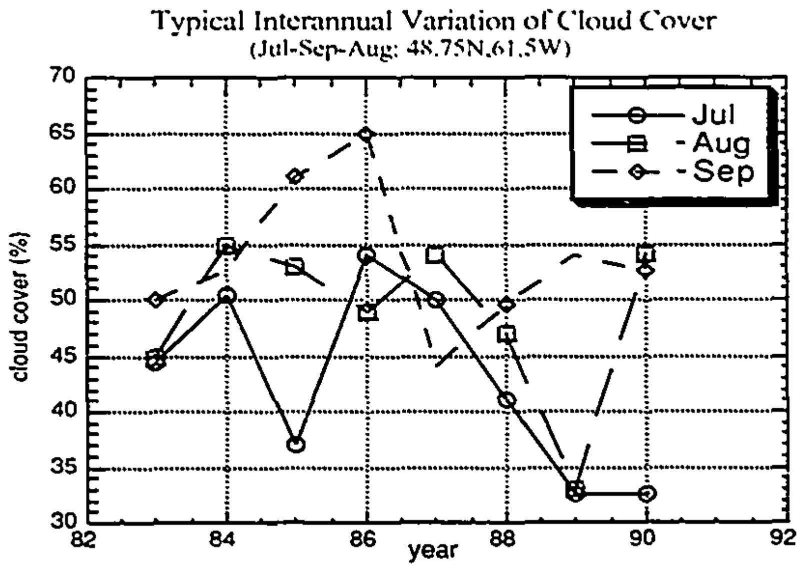

fig. 4.5: *Interannual time series of the ISCCP-derived cloud cover in Central GSL for the months of JUL, AUG & SEP.*

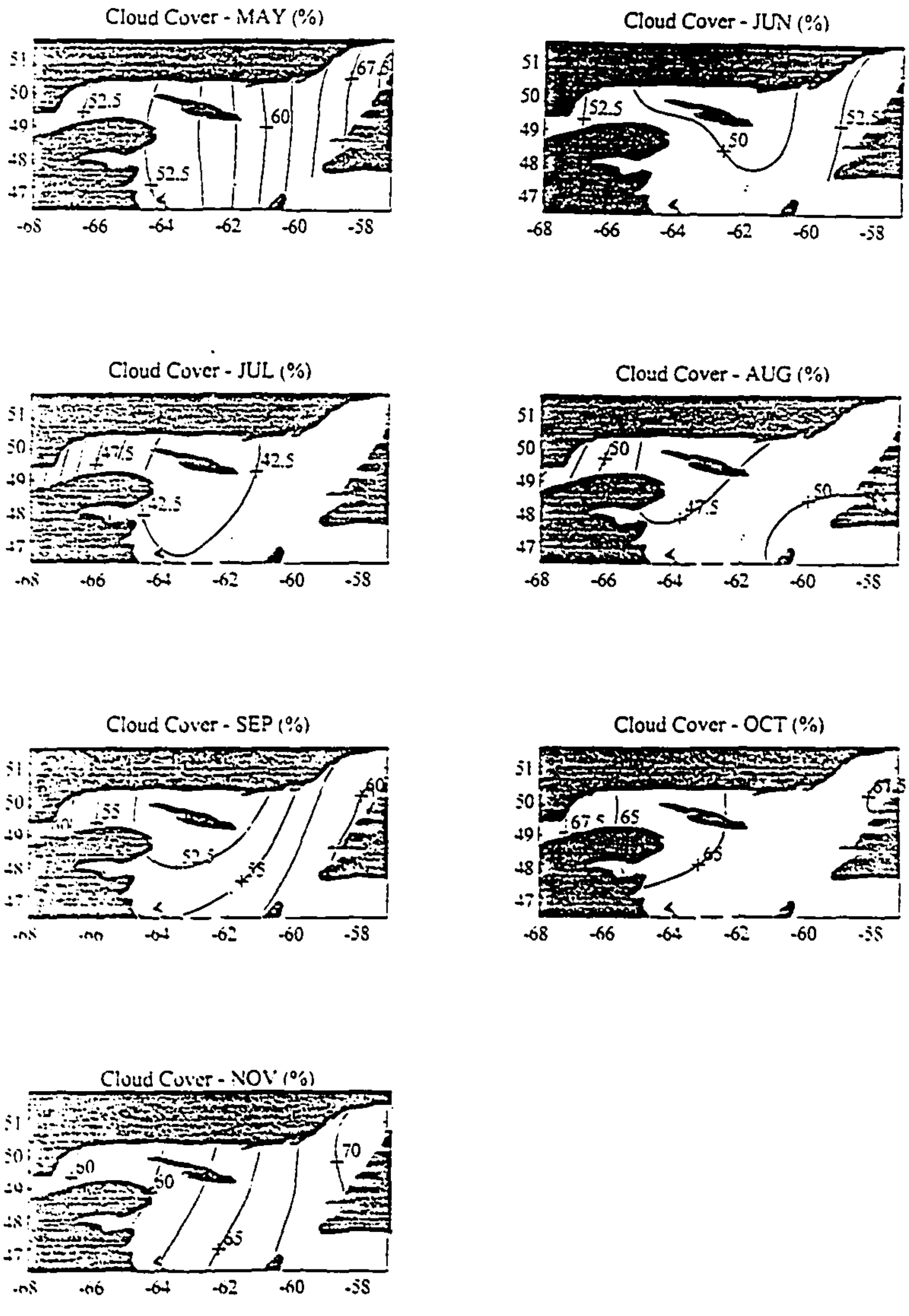

fig. 4.6: *Monthly averaged ISCCP-derived cloud cover fields (%) for the 7 ice-free months.*

4.4 Hourly Wind and Air Temperatures

As mentioned earlier, one of the main objectives of this study is to provide a "climatological picture" to be used when comparing results obtained during the Canadian JGOFS program in the Gulf of St.Lawrence. Consequently, hourly wind and air temperature data corresponding to the 9 JGOFS cruise periods (see chapter 3) were purchased from the AES. Again, one of the main problems was dealing with the interpolation over water using shore-based measurements. These difficulties were "somewhat" tolerable for the case of T_a but various tests of wind interpolation yielded completely erronous results due to the "vectorial" nature of the field analysed. Fortunately, Besner (1994) devised a regression method to estimate hourly air temperature and wind (speed and direction) based on land-based observation and air-sea temperature difference. In his analysis, Besner (1994) created "virtual" weather stations at fixed locations throughout the Gulf and the Estuary and, using historical archives of co-registered hourly weather observations on ships of opportunity and shore stations, was then able to deduce appropriate regressions for both wind and air temperature at these "virtual" locations. Luckily, these matched closely the locations of the 6 hydrographic stations used during the GSL JGOFS cruises. In this way, we were able to obtain (through analysis of AES) hourly wind speeds and air temperature (both corrected to a 10 m reference height) for each day/station during the 9 JGOFS cruises. These results are presented in the appendix.

Chapter 5
Monthly Surface Climatology during the Ice-Free Season

In this chapter, monthly horizontal climatologies of several fields (SST, SSS, Chlorophyll-a, Qnet) will be examined. First the monthly spatial autocorrelation structure of sea surface temperature and chlorophyll-a concentration (Chl*a*) will be discussed and objectively analyzed fields of monthly SST, Chl*a* and SSS will be presented, along with a discussion on their associated interpolation errors. Finally, the surface heat budget will be computed for the 15 regions covering the Gulf.

5.1 Surface Climatology during the Ice-Free Months

5.1.1 Monthly Spatial Autocorrelations

As mentioned in chapter 3, a central feature of most statistical objective analysis schemes is the "a priori" knowledge of the covariance of the parameter interpolated (McIntosh, 1990). Ideally, one would like to know how an observation, say SST, at some location (i.e., a point in time and space) is related to the surrounding observations (again in space and time). This is often referred to as the covariance of the field, or sometimes as the autocorrelation. For most climatological studies, this covariance is usually extremely difficult to obtain because of the poor data coverage (in both time and space). Consequently, the covariance structure is often assumed to obey some functional form (e.g., Gaussian). In this study, due to the availability of high quality and good resolution satellite-derived monthly images of SST and Chl*a* for 7 recent years (Anonymous, 1994), it was possible to calculate the spatial autocorrelation structure for each of these two fields (fig. 5.1). Theoretically, the "unbiased" correlation structure of a physical variable should be 4-dimensional, i.e.: it should include the dependence of all three spatial directions as well as time. Practically, this was impossible to do for various reasons (please refer to Daley, 1991, for a complete discussion). In this study, once again due to data limitations, stationarity as well as isotropy and homogeneity have been assumed when calculating the correlation structure. The first approximation may not be so bad (Thiébaux and Pedder, 1987). However, as will be seen later, the last two assumptions impose a somewhat severe restriction on the optimal interpolation method. Coastal areas are well known for their anisotropic behaviours (Denman and Freeland, 1985), and a study area like the Gulf of St.Lawrence is likely to have regional differences in its correlation structure. However, as pointed out by McIntosh (1990), it is far better to assume isotropy and homogeneity and calculate a "true" spatial autocorrelation structure than to simply assume some functional covariance and proceed with the interpolation. This last point is critical since the entire "power" of the statistical interpolation method depends on this covariance structure (Thiébaux and Pedder, 1987). More important to note is the fact that, without the use of the monthly satellite-derived data for the 7 recent years (1979 to 1986, 1987 and 1990), the hydrographic database alone would not have permitted the assessment of the correlation structure. In such a case, empirical methods like that used by Levitus (1982) are perhaps more appropriate.

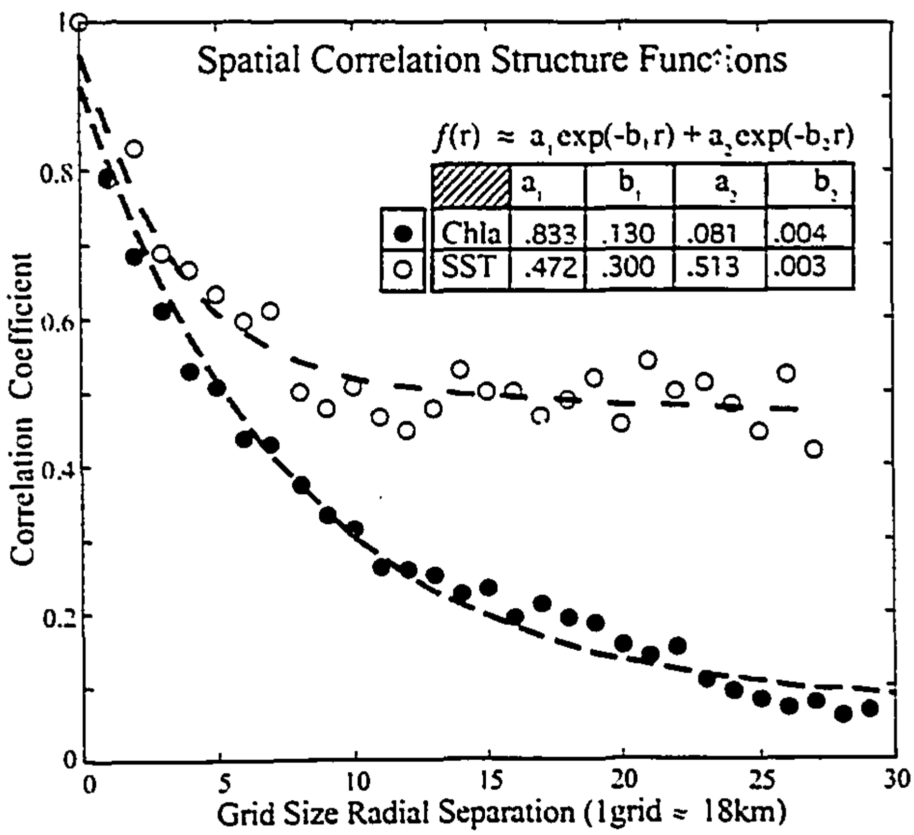

Fig. 5.1: *Spatial correlation structure function of satellite-derived monthly SST and* Chla *anomalies averaged over 1 pixel separation (≈ 18km radial distance). (The thick dashed lines correspond to the structure function, f(r), fitted to data points). The coefficients $a_{1,2}$ and $b_{1,2}$ are the non-linear fit (in a least-square sense) of f(r). The structure function f(r) assumes spatial isotropy and homogeneity.*

On figure 5.1 are displayed the spatial autocorrelations of both SST and Chl*a* as calculated from the monthly satellite-derived images (unfortunately, the hydrographic dataset did not render possible such a computation for the sea surface salinity data). A typical aspect of this relation is the "near" perfect [1] correlation at zero "spatial" lag followed by a distance dependent decay in the correlation. Monthly Chl*a* data do not seem to "plateau" like its SST counterpart, and decorrelate a little more rapidly than the temperature signal (figure 5.1). However, nature does not necessarily behave in an exact manner, and due to the previously mentioned assumptions, these spatial autocorrelation trends should be used with caution, especially near the coast and when considering different time scales.

Figure 5.2 displays typical error fields resulting from the objective analyses. Only June and September are shown since all 7 ice-free months were very similar. As expected, the largest interpolation errors for the SST and Chl*a* maps are found near the (north) shore. This is likely to result from the isotropic/homogenous assumption mentioned earlier. Moreover, since the overall resolution of the satellite-derived images is only 18 km, oceanographic features of comparable or smaller scales can simply not be captured by the analysis. As for the case of surface salinity, the optimal interpolation should be considered valid only over the Magdallen Shallows due to the lack of adequate data coverage elsewhere. Most of its interpolation errors occurred in the data poor regions.

A last note on the objective analyses concerns the functional covariance form used in the present study. Based on the results of figure 5.1, three correlation structure functions were tested: *1.* a classical Gaussian (see Denman and Freeland, 1985); *2.* a double exponential (as expressed by the algebraic relation on figure 5.1); and *3.* a modified exponential in which the first term is similar to method #2 but where the second exponential term has been replace by a constant. All three functions were fitted to match as closely as possible the spatial correlation points of figure 5.1 (for both SST and Chl*a*, successively), and a background error (Denman and Freeland, 1985) of 10% (0.1) was assumed for all fields and months. Although it was difficult to assess which functional covariance was better, based only on the relative interpolation maps, the double exponential was chosen for it matched the spatial correlation points better than the other two. As for salinity, we used covariance forms and scales similar to that for SST.

---

[1]: We used the term "near perfect" because the "self" correlation coefficient is indeed 1 at zero distance lag, but it is common practice to assume a background error associated with the observations (Denman and Feeland, 1985).

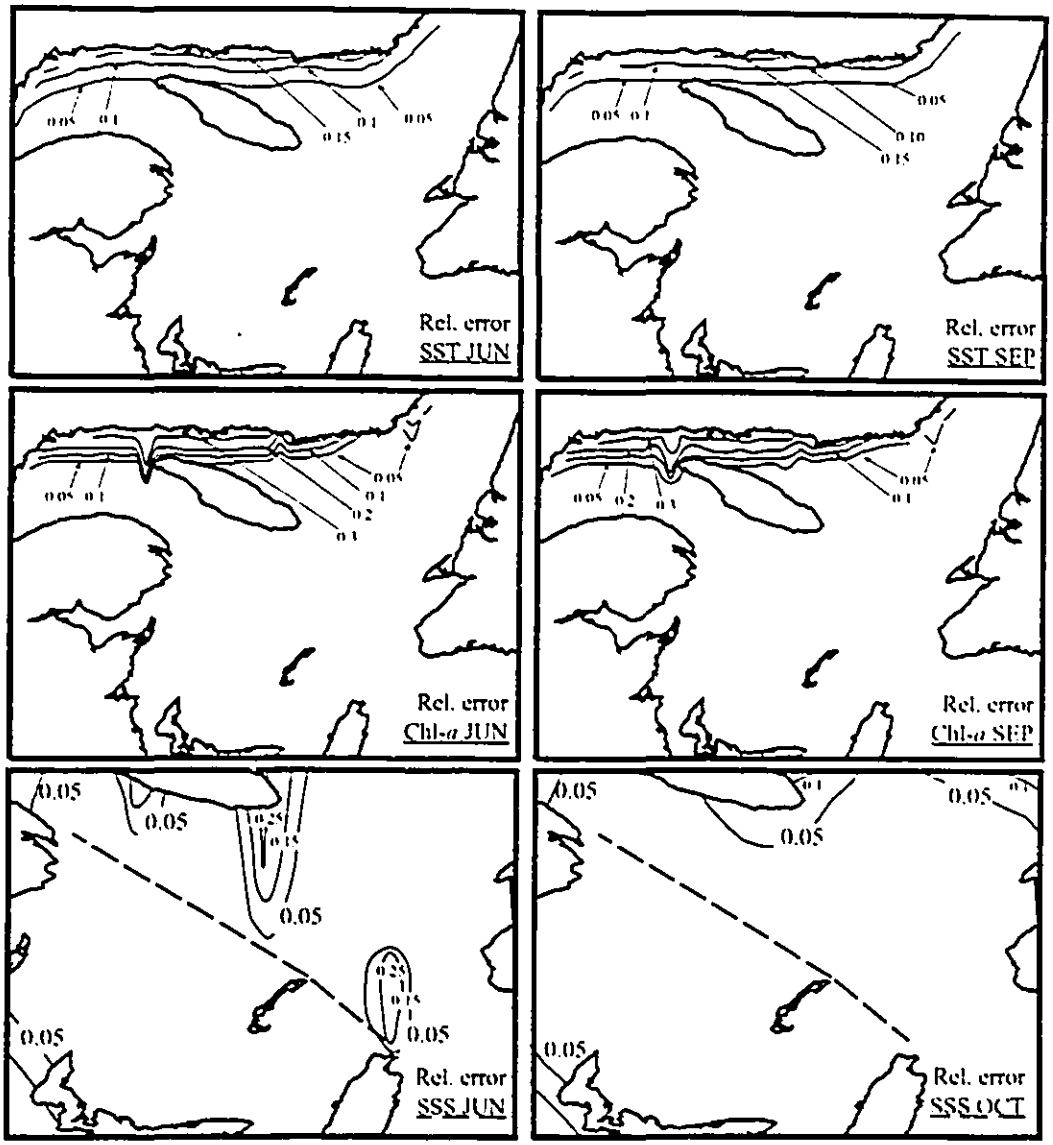

Fig. 5.2: *Typical relative interpolation error fields for the monthly surface temperature - June and September. Error values range from 0 to 1. Error maps for only 2 months are plotted since the 6 monthly maps (May to Nov.) were very similar. The oblique dashed line on the two error maps of surface salinity denotes the boundary between the Magdalen Shallows and the Laurentian Channel. The density of SSS observations is greatly reduced north of this limit.*

5.1.2 Monthly Objective Surface Fields (SST, SSS, Chl_a)

The approach used here was to produce the best objective fields given the spatial distribution of the hydrographic observations contained in the database. For the surface Chl*a* maps, roughly 2000 observations with a spatial resolution of 18 km were available for each month. They were satellite-derived (Anonymous, 1994) and covered the years 1979 to 1986. For SST analyses, a combination of remotely sensed data (again at 18 km homogenous resolution) and hydrographic measurements yielded a total monthly coverage of over 3000 surface observations (roughly 2/3 of these were satellite-derived). Finally, surface salinities were far less numerous and originated from the hydrographic database only (chapter 3). General and specific features of these monthly averaged surface fields (SST, Chl*a* and SSS) are now discussed, with the corresponding figures following the text, i.e.: figs. 5.3a-c (SST), figs 5.4a-b and 5.5 (Chl*a*), and figs 5.6 and 5.7 (SSS).

General Features

The surface thermohaline and chlorophyll-a features observed throughout the Gulf are discussed in light of the present objective analyses as well as in comparison with other similar studies[2]. In general, the following overall SST and SSS characteristics can be deduced from the corresponding figures: The Magdalen Shallows have the warmest surface waters found in the Gulf throughout the ice-free season (excluding the regions covered by area 14 and 17); the coldest summer SST values can be found in the Lower Estuary and along the north shore of the GSL, roughly from the Strait of Belle-Isle to the Mingan Archipelago. For the surface salinity field, the freshest waters usually appear in the Lower Estuary due to the strong runoff from the St-Lawrence. Although they are somewhat more saline than those of the Estuary, relatively fresh waters can also be found near the mouth of Baie des Chaleurs, and along the Gulf's north shore where rivers supply an important fraction of the total freshwater discharged in the GSL (Koutitonsky and Bugden, 1991). Finally, surface waters occupying the east-central GSL are usually the most saline. In terms of temperature characteristics, the waters there are somewhat colder than those found further west over the Shallows, but are not as cold as the surface waters along the north shore and in the Lower Estuary. The Chl*a* fields do not constitute "thermohaline" fields per

[2]: Vigeant (1987) produced monthly SST maps from ship measurements; Bugden et al. (1982) studied surface layer salinities; Petrie (1990) plotted contour maps of SST and SSS from his area-based monthly climatologies; Koutitonsky and Bugden (1991) included some satellite images of surface temperatures during the summer.

se, but since an excellent dataset was available from the NOAA-NASA Pathfinder program, and since they are of interest for the JGOFS program in the Gulf, they were also analyzed. Generally, there is an overall east-west gradient in the Chl*a* fields for most months (northwest-southeast more precisely), the western Gulf exhibiting higher surface Chl*a* concentrations (similar to previous studies: Dunbar et al., 1980; de Lafontaine et al., 1991). It is characterized by higher monthly chlorophyll values along the north shore, near the Estuary, and at the mouth of Baie des Chaleurs. When averaged over the usual 15 areas (excluding area 07), some interesting features become apparent: First, the northwestern areas (06, 08 and 11) clearly show higher concentration values than the rest of the GSL, as well as higher Chl*a* in May and September, which is perhaps indicative of a spring and autumn bloom. As will be presented in chapter 6, the strong upper-layer stratification of these regions, in conjunction with a relatively constant supply of nutrients from the St.Lawrence (de Lafontaine et al., 1991) might be responsible for such increased surface biological activity. Also interesting (fig. 5.5) is the overall monthly trend observed throughout the GSL, where Chl*a* values are high in spring, decrease to minimum values during mid-summer and increase again in September, a behaviour which is opposite to that of the mixed-layer depth. Finally, Chl*a* values in November show a rapid decrease in northern and western areas while the surface concentrations continue to increase in the southern regions (area 01, 02, 13, 15, 16). (NOTE: due to the poor data quality of most November images, averages for this month have not been computed).

Specific Features

SST fields exhibit horizontal temperature differences oriented along the south-west to north-east direction during these two months such that warmer waters cover the Shallows (around 4 to 6°C in May and 8 to 12°C in June), while SST values for the Esquiman Channel range from 0 to 4°C in May and 3° to 7°C in June. An interesting feature in the objectively analyzed fields of SST is that, despite the overall gradient, they preserve the more local temperature differences across the Esquiman Channel axis such that waters along the north shore of the GSL are slightly colder than along the Newfoundland coast. This is in accordance with the known circulation patterns for this area where currents going northward tend to advect warmer waters along the coast of Newfoundland, whereas the incoming surface flow through the Strait of Belle-Isle tends to follow the Gulf's north shore (El-Sabh, 1976). Relatively cold pools of surface water along the GSL north shore are also observed. As mentioned earlier, these colder areas are likely to be the result of coastal upwelling (see Rose, 1988). In examining the salinity fields, distinct surface features can be seen. However, one must be careful because of the coarser resolution of this set of hydrographic observations (see appendix). In general, regions near the Estuary and the mouth of Baie des Chaleurs are characterized by fresher surface layers (SSS ranges from 26 to 29), whereas the eastern section of the GSL (although much less sampled) exhibits more saline waters (31 to 32). Also apparent in the surface waters of the southern Gulf, is a freshening from May to October, which is likely caused by the slow advection of the freshwater pulse associated with the spring runoff from the Estuary (Koutitonsky and Bugden, 1991). The summer season, along with the month of June, generally provide the best hydrographic dataset for the oceanic variables (fig. 3.2). Again, a region of colder waters persists in the Estuary and along the north shore of the GSL, where temperatures range from 9 to 10°C in July-August, and go as low as 5 to 6°C in October. SST maxima are still found in the southern part of the Magdalen Shallows (16-17°C). The warmest month is August. During the summer season, the prevalent horizontal gradient of sea surface temperature assumes an approximately north-south orientation in the central GSL, where SST isotherms extend from the western part of the Gulf (near Cap Gaspé-Baie des Chaleurs) and follow their course into the Esquiman Channel, indicating the presence of warmer waters on the Newfoundland side of the channel (from 1 to 4°C warmer). The sea surface salinity fields in the north-east section of the Gulf, despite the better distribution of observations, still remain considerably less sampled than in the Shallows or the Estuary. Nevertheless, relatively fresher surface waters is indicated in the Estuary and near the mouth of Baie des Chaleurs. In general, the seasonal cycle of SSS, although much weaker, assumes a shape opposite to that of SST, where surface salinities decrease to a minimum in August and then, begin to increase again. For example, SSS values for the Magdalen Islands are around 31 during the late spring period (May-June), decrease during the summer to reach a minimum of around 29 in August, and increase again to surface values near 31 in November. Finally, the same overall spatial characteristics of surface temperatures and salinities can be observed during the October-November period but with generally cooler SST and slightly higher SSS than in August. The Magdalen Shallows are still covered by the warmest waters throughout the Gulf (8-11°C in October and 4-8°C in November), with the surface isohalines (29-30-31) extending from the Baie des Chaleurs-PEI (Prince Edward Island) region slightly beyond the edge of the Shallows in October. The surface fields near the western part of the Gulf exhibit the same coastal signatures of fresher waters (although not as fresh as before) due to runoff from the St-Lawrence.

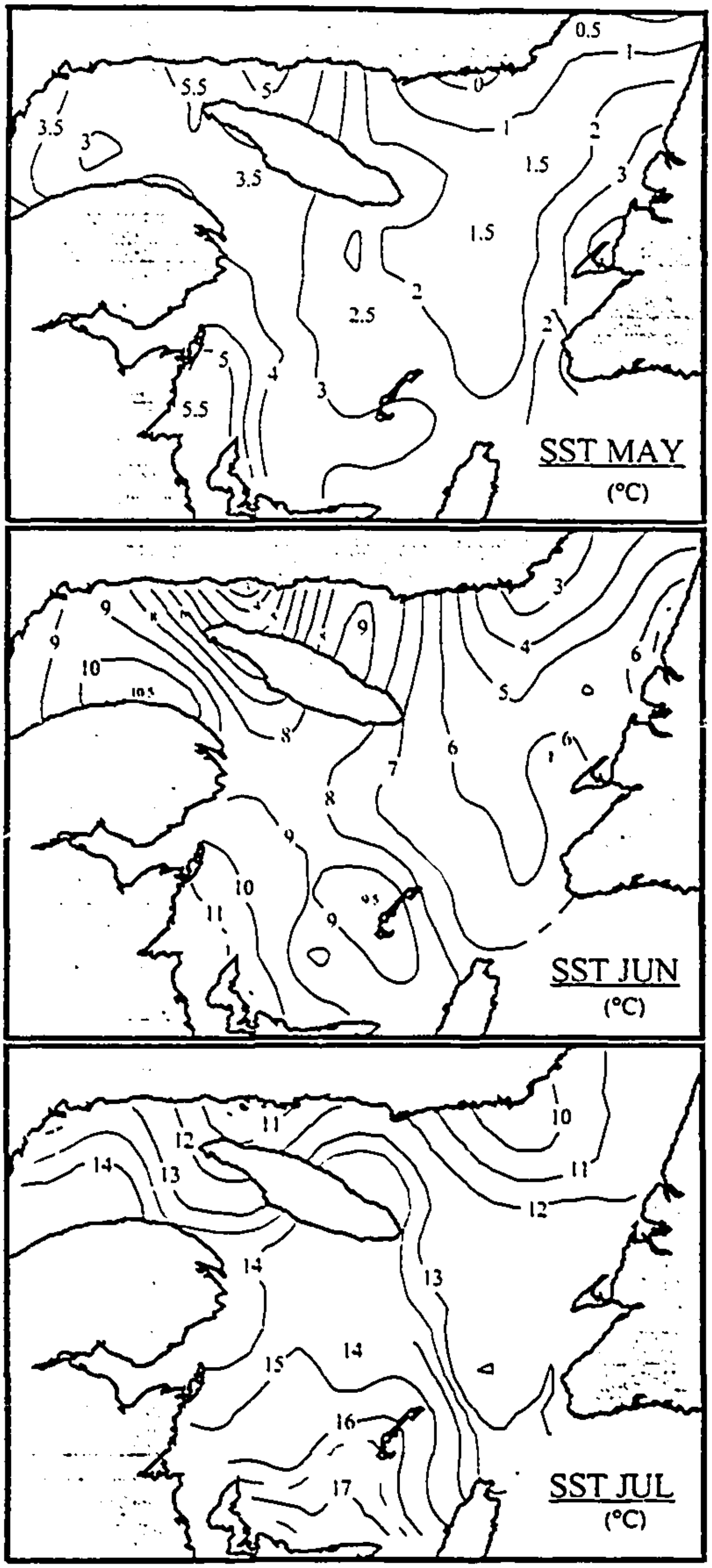

Fig. 5.3a: *Monthly climatology (MAY, JUN, JUL) of sea surface temperature (SST, °C). Contour lines are 0.5 °C apart.*

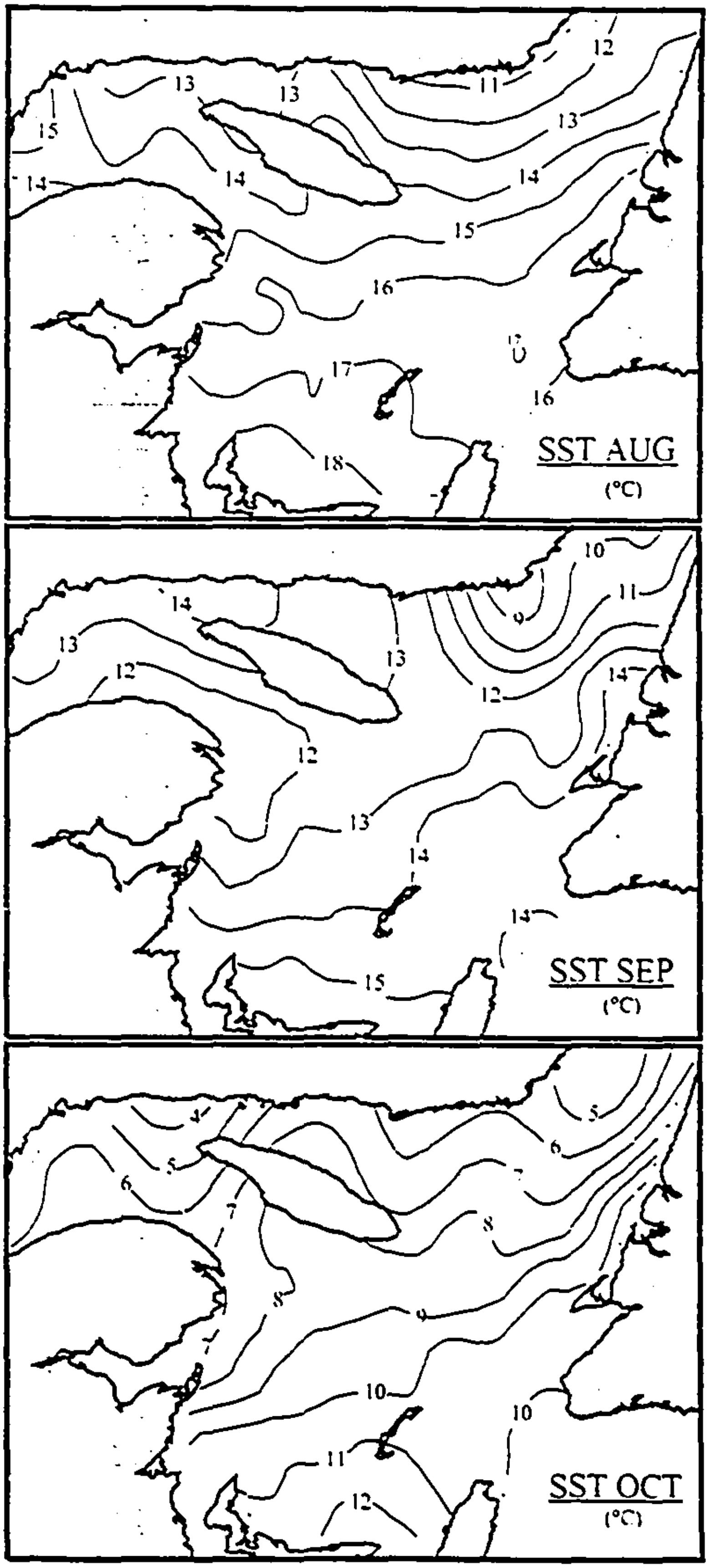

Fig. 5.3b: Monthly climatology (AUG, SEP, OCT) of sea surface temperature (SST, °C). Contour lines are 0.5 °C apart.

Fig. 5.3c: *Monthly climatology (NOV) of sea surface temperature (SST, °C). Contour lines are 0.5 °C apart.*

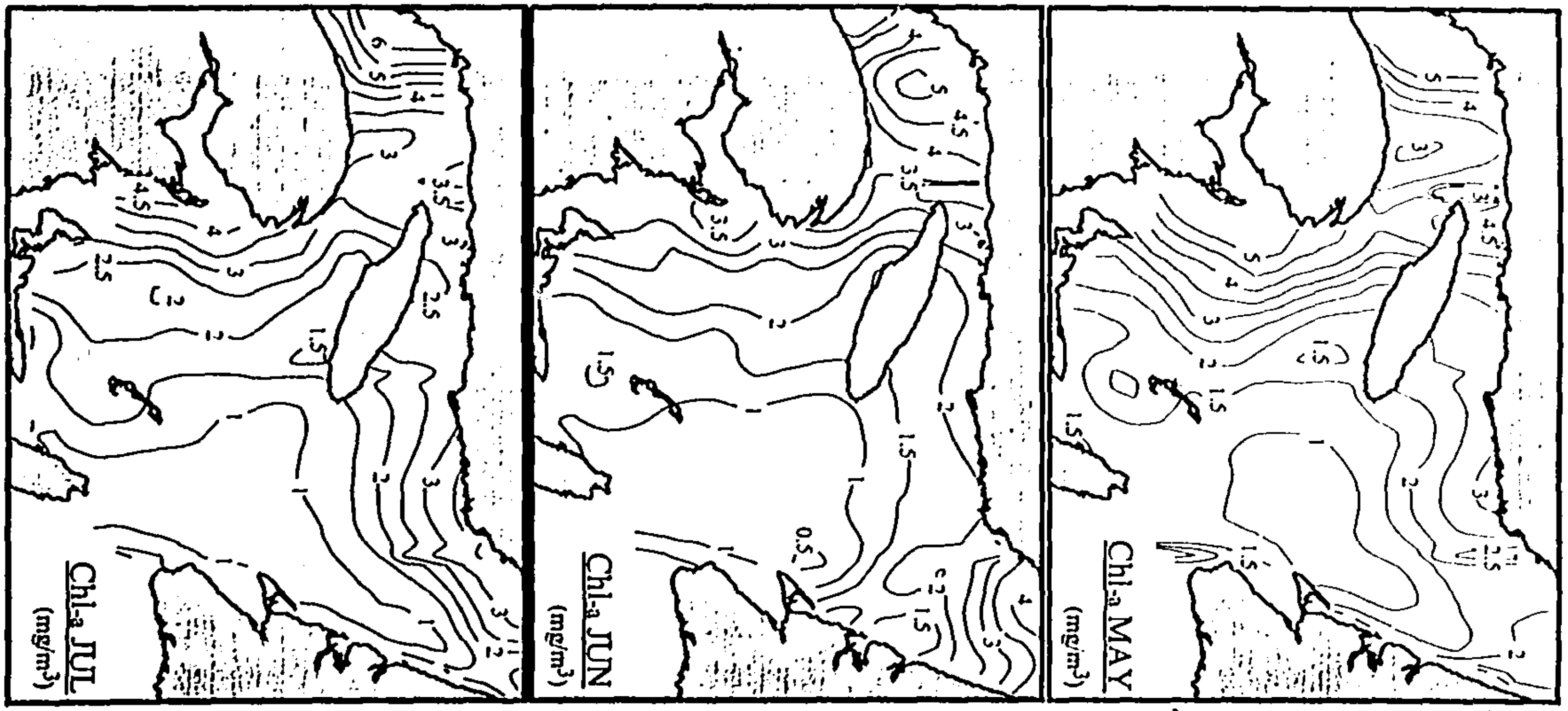

Fig. 5.4a: *Monthly surface climatology (MAY, JUN, JUL) of satellite-derived chlorophyll-a concentrations (mg/m^3). Contour lines are 0.5 mg/m^3 apart. Monthly maps were obained from statistical objective analyses of 7 years of Nimbus/CZCS derived monthly Chl-a images with a 18km pixel resolution.*

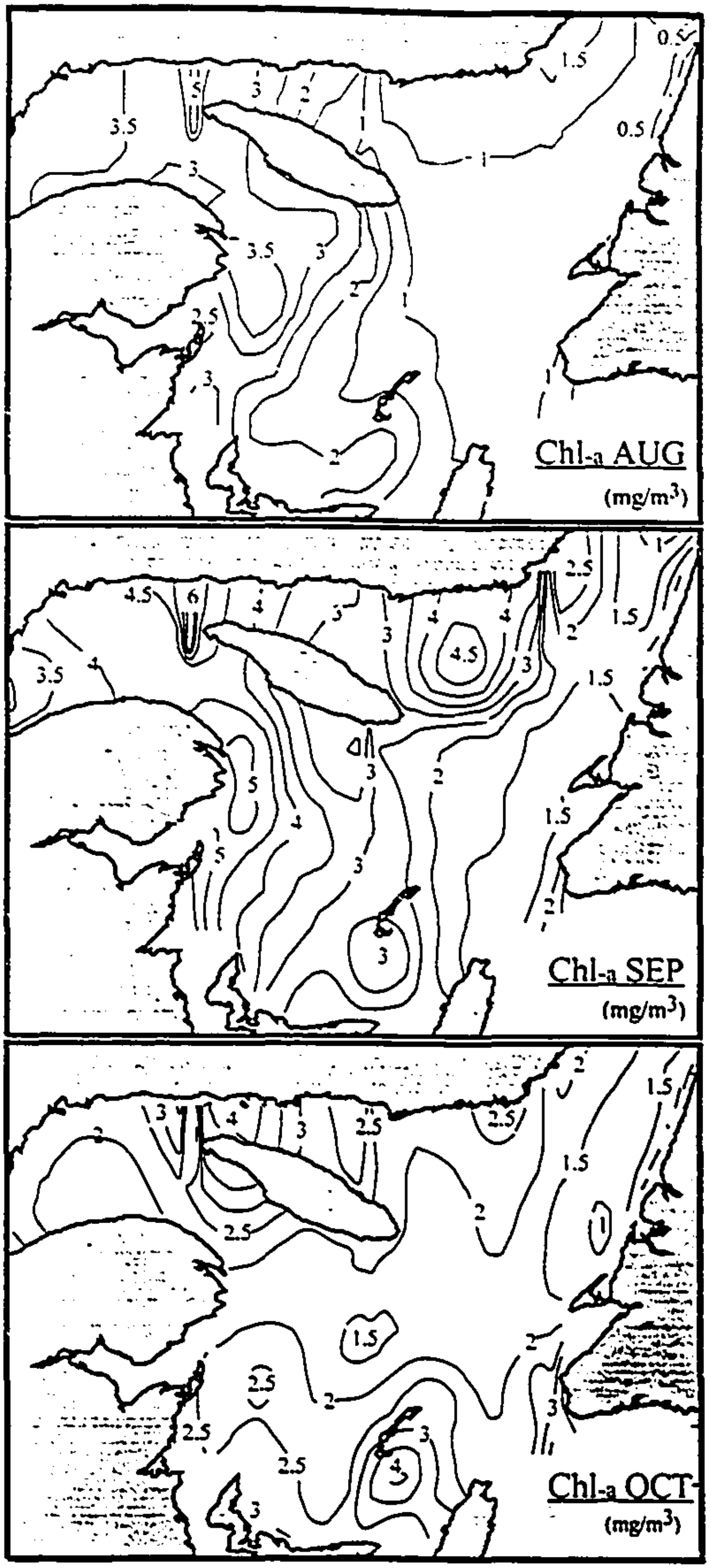

Fig. 5.4b: *Monthly surface climatology (AUG, SEP, OCT) of satellite-derived chlorophyll-a concentrations (mg/m^3). Contour lines are 0.5 mg/m^3 apart.*

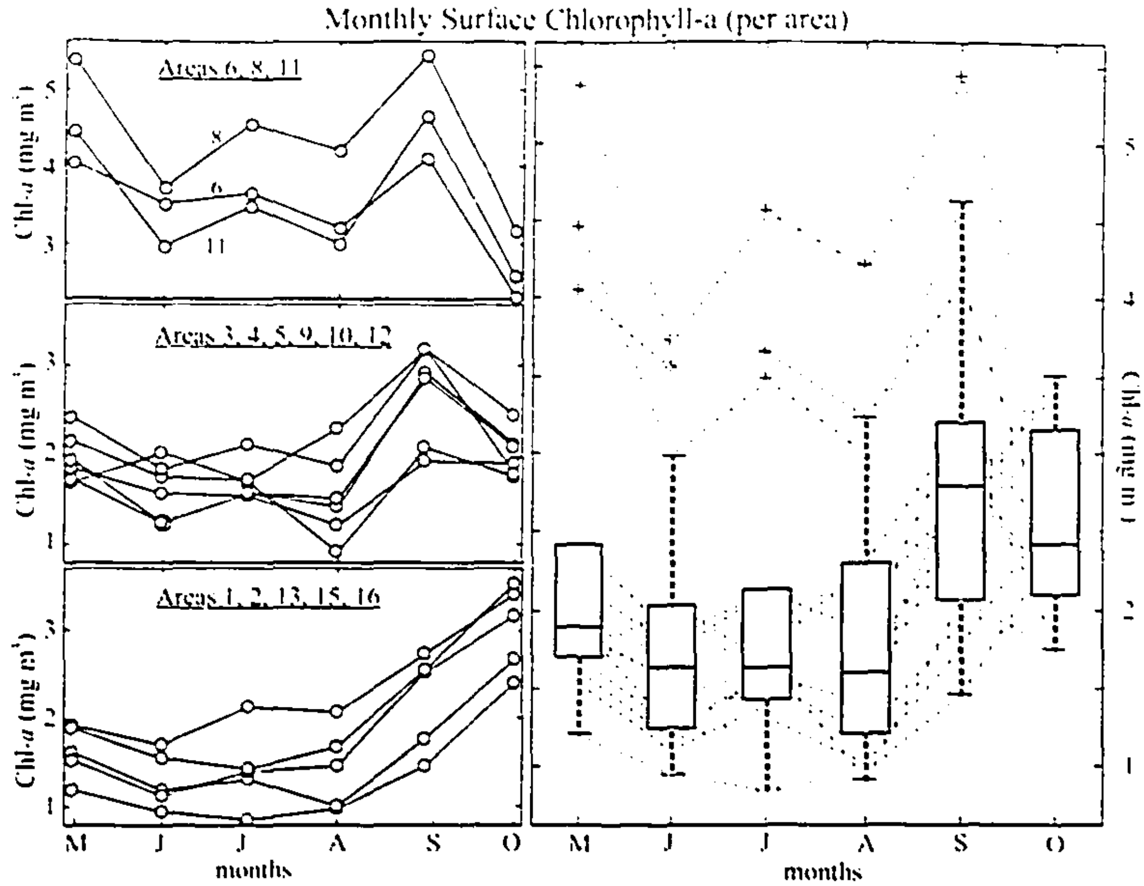

Fig. 5.5: *Monthly surface Chlorophyll-a concentrations (mg m^{-3}), per area (3 panels on the left). A boxplot of monthly surface Chl-a for all 14 areas (right graph) shows the monthly spatial spread of the data. The boxes have horizontal lines at the lower quartile, median, and upper quartile values. The whiskers are dashed lines extending from each end of the box to show the extent of the rest of the monthly data. Outliers (denoted by the crosses '+') are Chl-a values beyond 1.5 times the interquartile range (IQR). The IQR is formed by subtracting the 25th percentile of the data from the 75th percentile of the data, and is a robust estimate of the spread of the data since changes in the upper and lower 25% of the Chl-a values do not affect it.*

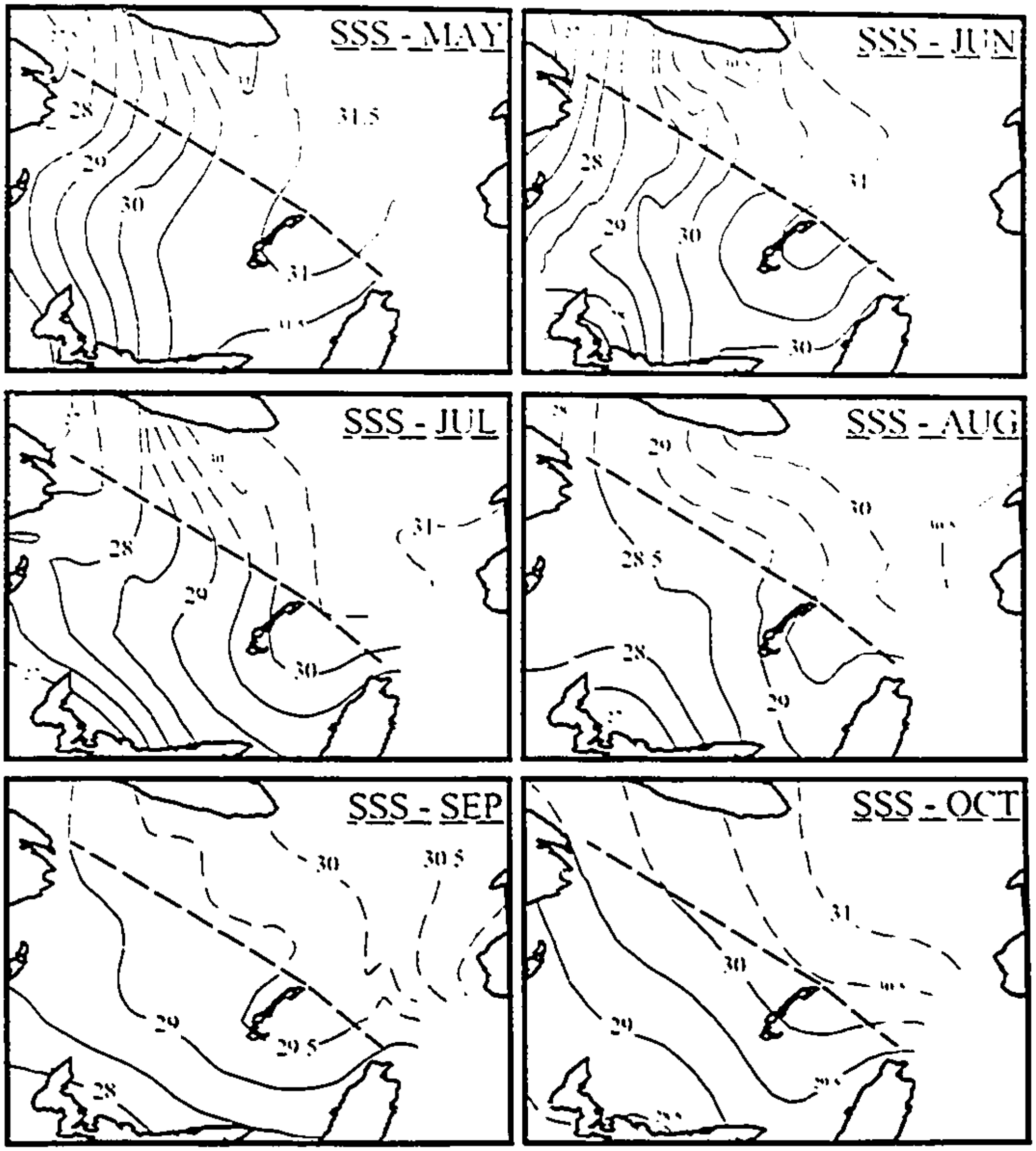

Fig. 5.6: *Monthly climatology (MAY to OCT.) of sea surface salinity (SSS, psu). Contour lines are 0.5 psu apart. The oblique dashed line denotes the boundary between the Magdalen Shallows and the Laurentian Channel. The density of surface salinity observations is drastically reduced north of this limit. Consequently, the dashed isohalines should be considered less accurate.*

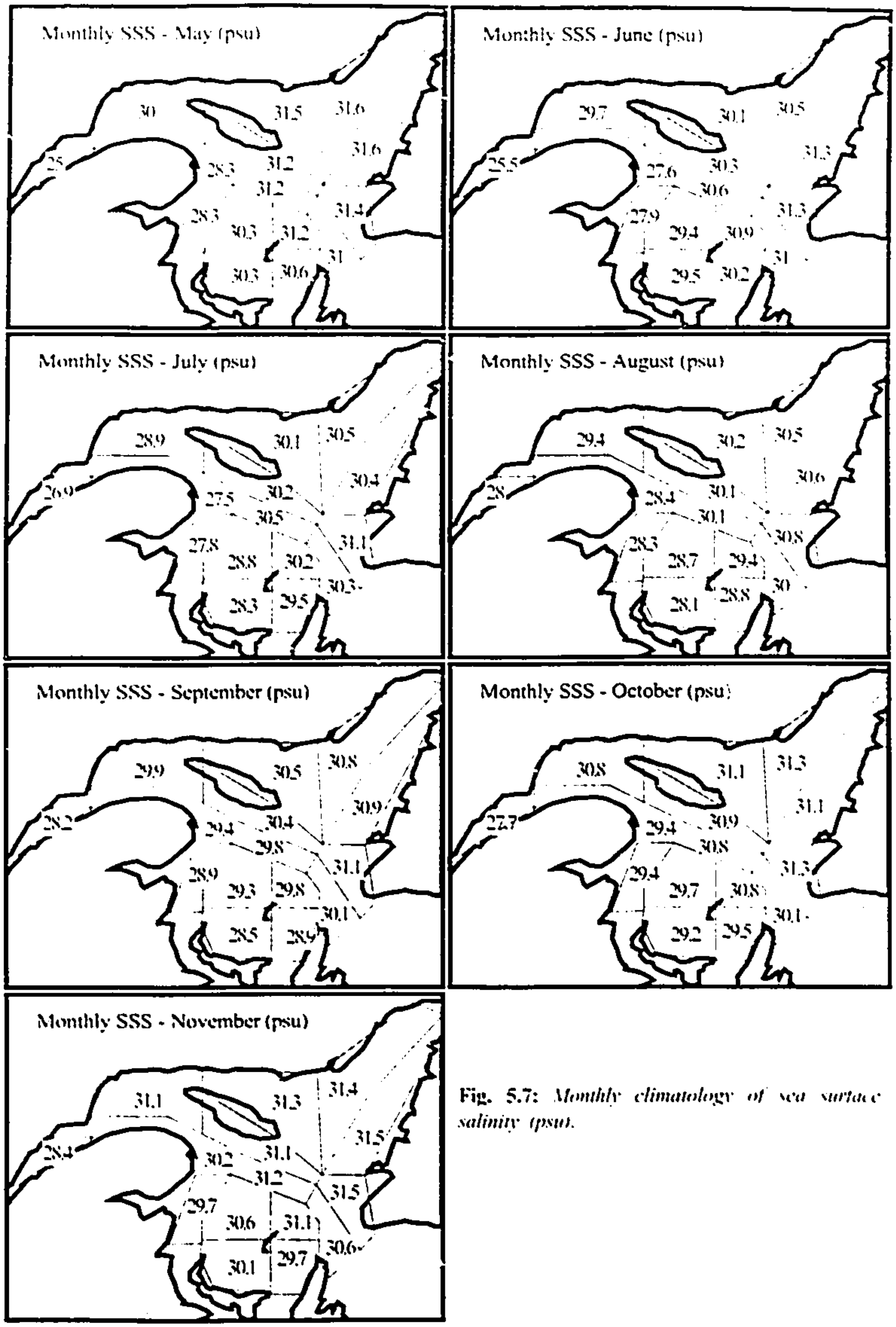

Fig. 5.7: *Monthly climatology of sea surface salinity (psu).*

5.2 Monthly Surface Heat Fluxes

Having computed reliable maps of sea surface temperature, these will now be used along with several other atmospheric fields to compute the net heat budget at the surface of the GSL. To do so, the four heat flux components (Q_{sw}, Q_{lw}, Q_e, and Q_h) will be calculated on a similar grid (18 km) to that for the SST, from which the resulting net surface heat (Q_{net}) will be deduced. Finally, the four surface heat flux (Q_{sw}, Q_{lw}, Q_e, Q_h) as well as Q_{net} will be averaged over the usual 15 areas.

5.1.1 Incoming Shortwave and Outgoing Longwave Radiation Fluxes

The most important component entering the net heat flux calculation is the amount of energy received by the ocean surface from the sun. Although it is easy to evaluate the amount of solar radiation hitting the top of the atmosphere given the time of the year and the geographic location, it is much more difficult to assess what happens to this incoming shortwave energy as it travels through the atmosphere on its way to the ocean surface. As mentioned in section 2.2, one must consider both direct and diffuse surface irradiation under a clear sky, which requires an accurate knowledge of the atmospheric transmissivity. Furthermore, cloudiness, along with several other factors (cloud height, type and temperature, aerosol content, surface albedo, sun spot cycle, etc), will affect the amount of solar radiation received at the surface. All these involve uncertainties at each stage of the estimation and, for lack of adequate knowledge of these aspects, one usually relies on empirical relationships of various degrees of complexity.

For the present study, two methods have been used: the first one is the same formulation used by Bugden (1981) and proposed by Budyko (1974). Although this parametrization does not represent adequately the influence of all atmospheric constituents, it is generally believed that the cloud cover has the strongest influence on Q_{sw} (Perry and Walker, 1977). Consequently, the use of a better cloud dataset (finer resolution, more recent and better spatial coverage) should yield more reliable results concerning the spatial distribution of monthly incoming radiation. The solar radiation, Q_{sw}, at the GSL surface is given by:

$$Q_{sw} = Q_o (1 - \alpha)(1 - aC_n - bC_n^2)(\cos\theta / \cos\theta_o)$$

where α (= 0.1) is the albedo, C_n is the monthly cloud cover, and θ is the latitude. In this formulation, Q_o is the monthly clear sky solar radiation for the θ_o (= 50°N) latitude, and a and b are empirical constants. Q_o, a, and b were obtained from Budyko's tables (1974) for the desired months. However, some aspects are worth noting concerning the cloud correction factor. Since several authors offer different formulations (Hsiung, 1986) in which the dependence on C_n ranged from $C_n^{0.7}$ to C_n^{3}, and that it is not clear from the literature whether these formulations were deduced from monthly averaged values or from smaller time scales observations, one should avoid any non linear cloud cover dependence when using monthly averaged C_n simply because of the sub-monthly variability of the cloud fraction. Consequently, the second method used, consisted in estimating the daily incoming short wave radiation and using this result to compute the averages for each month. The second scheme is from Reed (1977):

$$Q_{sw} = Q_o\,(1 - \alpha)\,(1 - 0.62C_n + 0.0019h)\,(\cos\theta / \cos\theta_o),$$

in which h now represents the noon solar elevation in degrees. The daily clear sky radiation was computed using the procedure by Seckel and Beaudry (1973) and depends on the day of the year, and the latitude. This method, used by Umoh and Thompson (1994) and Gilman and Garrett (1994), has recently been reviewed by Schiano (1996), who found it to agree well with direct measurements. Finally, although both surface Qsw fields showed some minor differences, these were almost absent after the area averages had been done.

The most obvious aspect to note is the common seasonal fluctuation in the Q_{sw} fields. A perhaps more surprising characteristic concerns the spatial distribution of the incoming shortwave radiation. Within an area the size of the GSL, one might expect a small latitudinal variation in Q_{sw} in a decreasing fashion towards the North (given by the $\cos(\theta) / \cos(\theta_o)$ correction), and a rather homogenous zonal distribution of irradiation. However, due to the effect of cloudiness, the main feature observed in the Q_{sw} maps is an east-west gradient (not shown), in accordance with the satellite cloud cover climatology of section 4.3. More specifically, differences as strong as 50 Wm^{-2} in Q_{sw} can be observed for two different locations within the same month (fig. 5.9). Finally, knowing that it is the sun that "drives" the atmosphere-ocean engine (Gill, 1981), one should note that the use of adequate cloud cover climatology with a simple empirical relation results in rather important spatial variations of the Q_{sw} fields, even for an area the size of the GSL.

The outgoing radiative flux exhibits the weakest seasonal fluctuation from the four heat flux terms of the surface energy budget (fig. 5.9). This longwave backradiation, Q_{lw}, was computed following Brunt's formulation (Budyko, 1974) with a correction factor for air-sea temperature differences such that:

$$Q_{lw} = \varepsilon\sigma T_a^4 (0.39 - 0.05\, e_a^{1/2})(1 - 0.71 C_n^2) + 4\,\varepsilon\sigma T_a^3 (SST - T_a)$$

where $\varepsilon = 0.97$ and $\sigma = 5.67 \times 10^{-8}$ $Wm^{-2}K^{-4}$ is the Stefan-Boltzman constant. T_a and SST correspond to the air and sea surface temperature, respectively. C_n is the cloud cover fraction and e_a (mb) is the atmospheric vapour pressure (see Budyko, 1974). No particular spatial pattern in the monthly fields of Q_{lw} were observed. In fact, the longwave radiation fluxes (positive when leaving the surface) appears to be rather homogenous for each month and show little variation throughout the ice-free season. Monthly Q_{lw} values lie within the 40-80 Wm^{-2} range.

5.1.2 Sensible and Latent Heat Fluxes

The fluxes of sensible (Q_e) and latent (Q_h) heat are computed from bulk aerodynamical formula.

$$Q_e = \rho_a C_p C_e |U_{10}| (T_a - SST)$$

$$Q_h = L\, C_h |U_{10}| (e_{sat}(Ta) - r\, e_{sat}(SST))\, 0.622 / P_a,$$

in which C_p (= 1005 J $kg^{-1}K^{-1}$) is the heat capacity of air, r the relative humidity[3], P_a the sea surface atmospheric pressure and ρ_a is the air density, computed from air temperature (T_a) the sea-level pressure and using the ideal gas equation with an adequate correction compensating for the moisture of air. In these two flux equations, the saturation vapour pressure e_{sat} was determined following Bolton's formula (Rogers and Yau, 1989),

$$e_{sat}(T) = 6.112 \exp(17.67\, T / (T + 243.5)),$$

where e_{sat} is in mb and T in °C, and where the latent heat of evaporation, L, was chosen to vary (linearly interpolated) with T_a according to the following table (Rogers & Yau, 1989).

L (J g^{-1})	2525	2501	2489	2477	2466	2453
T_a (°C)	-10	0	5	10	15	20

Table 5.1: *Latent heat of evaporation (L) for various air temperature (T).*

The last aspect concerning these two bulk formulae deals with the choice of the turbulent transfer coefficients, C_e and C_h. As Blanc (1985) reported in his review paper on transfer coefficient methods, there is "no single, universally accepted bulk transfer coefficient scheme". In reviewing 10 bulk transfer coefficient schemes published between 1973 and 1982, Blanc noted that "the most reliable bulk schemes should be those based on

[3]: "r" was obtained from the Canadian Climatological Atlas produced by the AES.

direct observations, i.e.: eddy-correlation measurements". Nevertheless, "we have no way of knowing which of the bulk schemes, if any, is correct. There are almost as many opinions on the subject as there are experimentalists. Prudence, therefore, requires that we take a serious look at the typical worst case results in order to properly gauge the potential seriousness of the situation." For the present study, Smith's (1988, 1990) formulations of C_e and C_h were chosen for they considered both the effects of wind speed and air-sea temperature differences, and yielded reasonable values of the coefficients (i.e. not too high nor too low in comparison to values obtained with other schemes). Moreover, this method was based on strong experimental evidence using the eddy-correlation method, and compared well with other schemes. Smith used field data near Sable Island (south of Nova-Scotia), which perhaps, of all other existing field-deduced transfer coefficients, represents oceanic conditions closest to those encountered during the summer in the Gulf of St.Lawrence.

In figures 5.9 and 5.10, both Q_h and Q_e were plotted as positive for heat leaving the sea surface. Although they differ in value, one interesting aspect regarding the Q_h and Q_e fields is the striking resemblance in their spatial distribution pattern throughout the ice-free season. Moreover, this seasonal trend was observed (but not shown) to follow closely that of the air-sea temperature difference throughout the GSL, a characteristic that was also observed in a much larger scale heat flux study by Hsiung (1986). This can be better appreciated by looking at figure 5.8. Plotted on these two graphs are the dependence of sensible and latent fluxes of heat on both wind speed and air-sea temperature difference (air-sea differences of specific humidity are plotted for Q_h, but it can be shown that this follows very closely air-sea temperature differences.). The monthly Q_h and Q_e values for four typical regions of the GSL denote clearly a stronger influence of ΔT than on U. For example, assuming a mean state (i.e.: $\Delta T = 0$ °C, $\Delta q = 1$ g/Kg, U = 6.5 m/s), perturbation changes of ± 5 °C and ± 2 g/Kg would result in ΔQ_e and ΔQ_h of around 55 W/m^2 and 60 W/m^2, respectively, while the heat flux lines of the four areas tend to follow the isoQ_e and isoQ_h contours when for varying wind speeds.

Finally, Q_h and Q_e ranged between -20 to 100 and -30 to 80 Wm^{-2}, respectively, showing a tendency to increase during the summer and to reach maximum values in November for both latent and sensible heat fluxes, which are of the same order of magnitude as the longwave backradiation. Although this seasonal variation is not as strong as that of the incoming shortwave radiation, its variability is however more important than that of Q_{lw}.

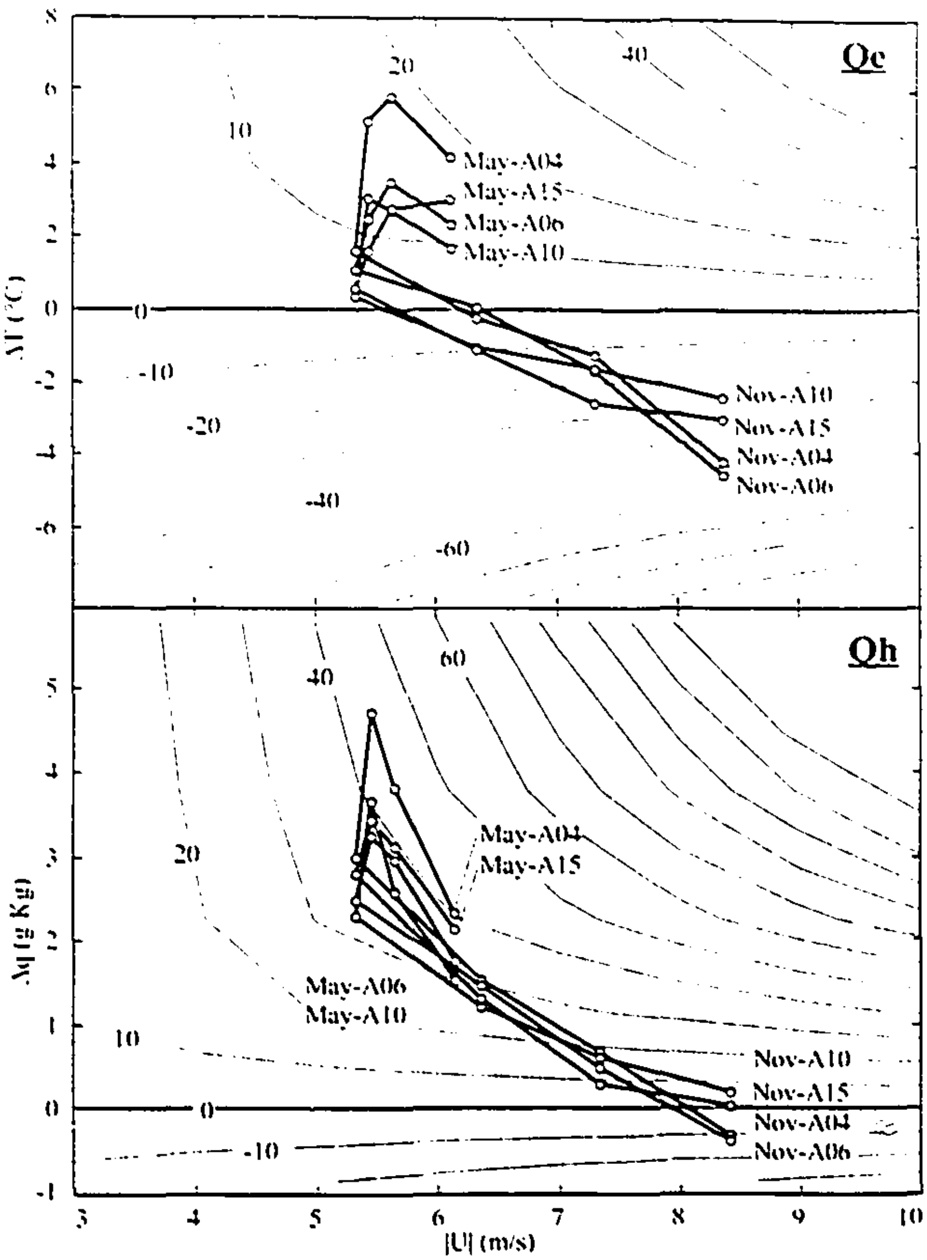

Fig. 5.8: *Sensible (top) and latent (bottom) heat flux dependence on wind speed (|U|) and air-sea differences of temperature (ΔT) and humidity (Δq). Monthly means of Qe and Qh are also plotted for 4 areas of the Gulf: Northeast (A04), northwest (A06), central (A10) and southern GSL (A15). Iso-heat flux lines are 10 W m⁻² apart.*

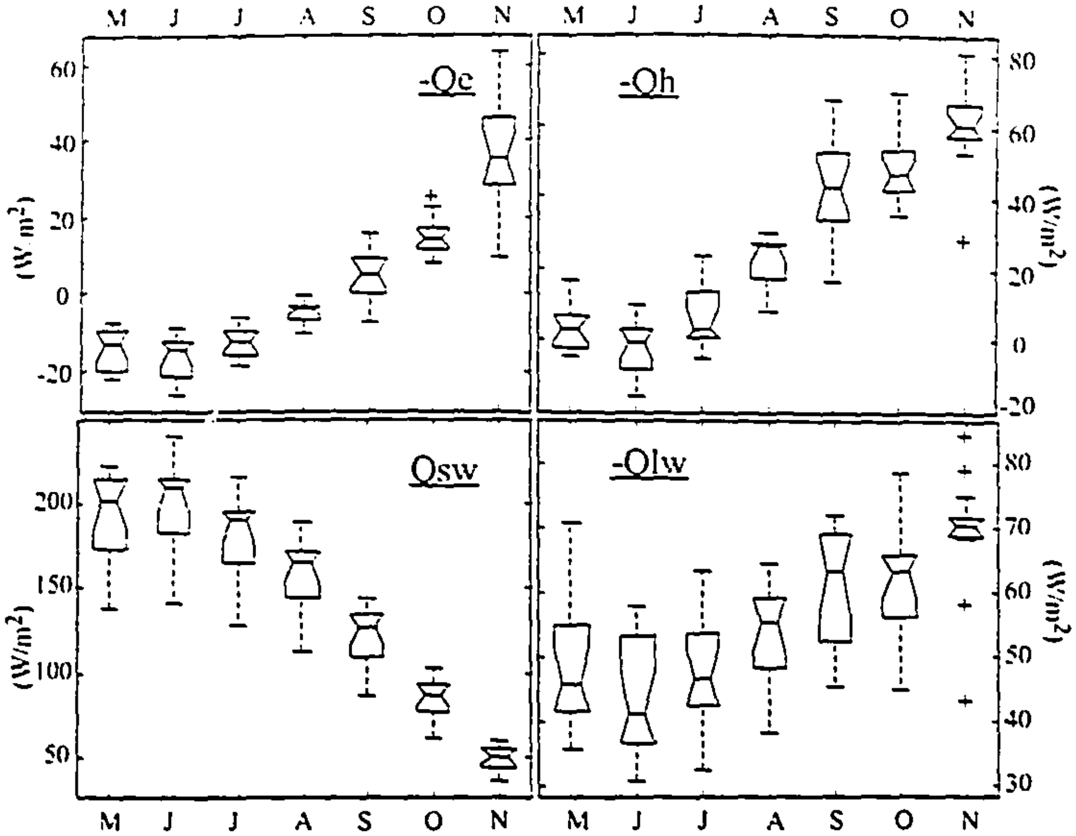

Fig. 5.9: *Boxplots of the 4 heat fluxes (Qe, Qh, Qsw, Qlw), showing the monthly spatial spread of each component (calculated from the 15 area monthly averages). Boxes on all plots have lines at the lower quartile, median, and upper quartile values. The whiskers are lines extending from each end of the box to show the extent of the rest of the monthly data. Outliers (denoted by the crosses '+') are heat flux values beyond 1.5 times the interquartile range (IQR). The IQR is formed by subtracting the 25th percentile of the data from the 75th percentile of the data, and is a robust estimate of the spread of the data since changes in the upper and lower 25% of the data do not affect it.*

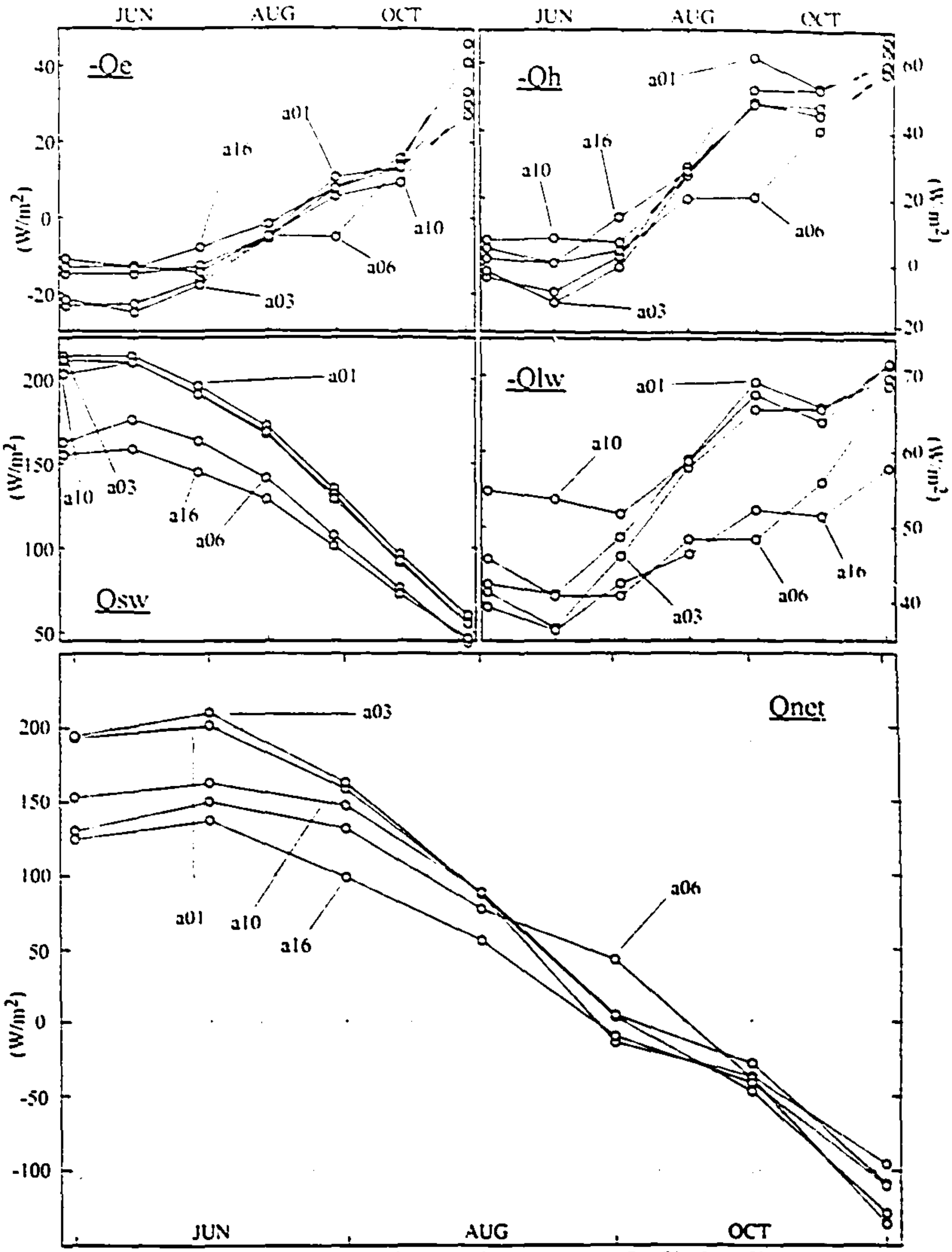

Fig. 5.10: *Typical monthly patterns for the 4 heat flux components (Qe, Qh, Qsw, Qlw - top 4 panels) as well as for the net surface heat flux (Qnet - large bottom graph), for 5 regions of the GSL: (Cabot Str.: area 01; northeast: 03; northwest: 06; central: 10; and southern Gulf: area 16).*

5.1.3 Net Surface Heat Fluxes

As Phillips (1981) reported in his book on the dynamics of the upper-ocean, "for most dynamical purposes in oceanography, the energy balance is important only in as far as it determines the rate of generation of buoyancy at the surface." Consequently, this last section is of critical importance not only in understanding the seasonal evolution of the Gulf's upper-layer, but as an essential starting point for further studies on the dynamics of the GSL circulation, climate and biological properties. The net flux of heat entering or leaving the sea surface is obtained by summing the four heat flux components as follows:

$$Q_{net} = Q_{sw} - Q_{lw} - Q_c - Q_h$$

In this algebraic formulation, the incoming solar radiation is defined positive as it enters the sea surface, whereas, the remaining terms are defined positive as heat lost is from the ocean to the atmosphere.

Figures 5.10 display the monthly evolution of the four heat fluxes and of Q_{net} for 4 areas of the Gulf, whereas figure 5.11 show the 7 monthly averaged Q_{net} fields. As Bugden (1981) noted in his box-model study, the usual seasonal cycle of net surface heat flux can be observed, starting with moderate values of Q_{net} for the month of May, reaching a maximum around July and decreasing thereafter until the fluxes reverse. This occurs as early as September for some regions but during October-November for the entire Gulf. Although the Q_{net} fields of the present study have a better spatial resolution than Bugden's box estimates, they nevertheless exhibit similar monthly averages. Looking at monthly fields of Qnet (fig. 5.11) reveals interesting features concerning the heat flux spacial structure. Perhaps the first aspect worth noting is the overall "heterogeneity" within each monthly field. For example, southern areas (01, 02, 13 and 16) exhibit a net heat loss in September while the rest of the Gulf is still gaining heat.

Estimating the "quantitative" errors associated with this heat budget is extremely difficult to do, since several factors cause uncertainties in the heat flux calculations. These can generally be classified as random (which decrease with the number of observations) and systematic (Gilman and Garrett, 1994). The random errors cannot be estimated in this study for they require "simultaneously" measured time series of all parameters involved in the calculations. As Gilman and Garrett (1994) report, "systematic biases in the observations result from changes in the instrumental practices [and] are quite difficult to quantify". Although great care have been applied to the filtering and interpolation of most quantities, a complete error analysis for the heat budget lies outside the scope of this study.

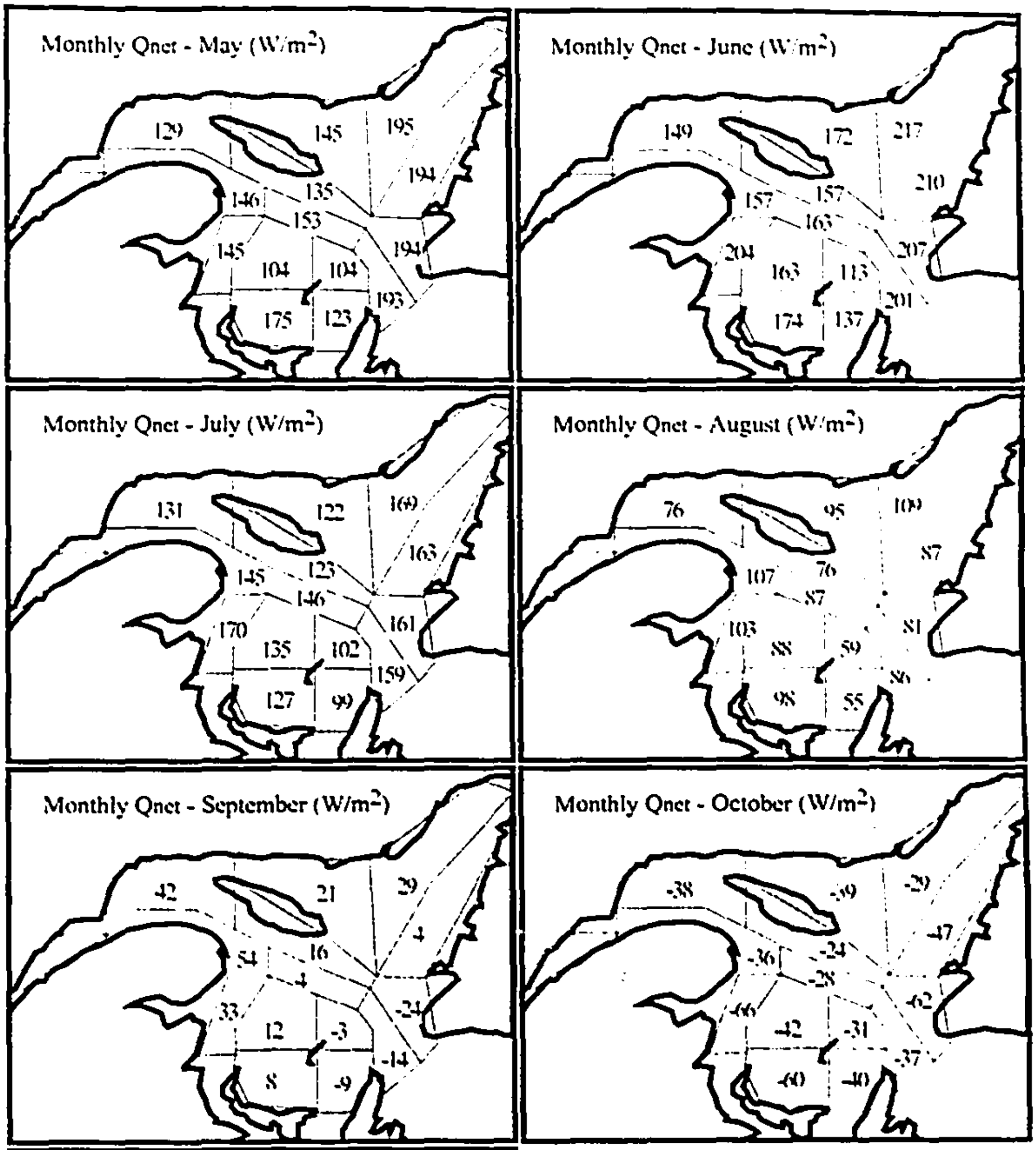

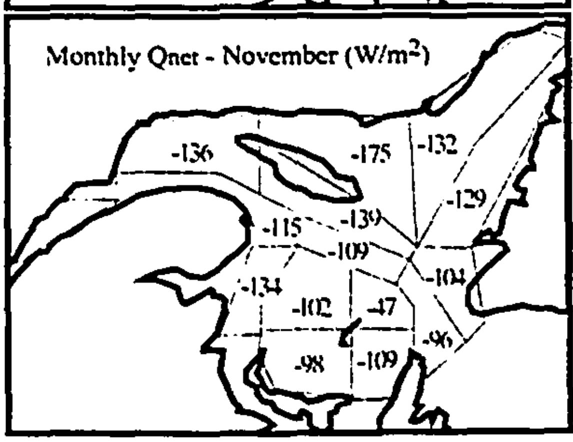

Fig. 5.11: *Monthly net surface heat flux (Qnet, in W/m^2) for 14 areas of the Gulf (The estuary has been excluded since the objective analysis did not produce SST maps for this area). Positive values mean the ocean is gaining heat.*

Finally, during the first phase of this research, attempts were made to approximate the net surface heat fluxes over the GSL with the widely-used Haney-type (1971) relation ($Q_{net} \approx \xi\ (T_* - SST)$), where ($T_* - SST$) is the difference between an "equivalent" atmospheric temperature and SST, and ξ is some arbitrary monthly average coefficient. This was tried for the 4 large areas employed by Bugden (1981), using SST and T_a values mentioned in chapters 4 and 6, as well as the surface flux values computed by Bugden (1981). The goal was to approximate the net heat flux with fewer variables, hence rendering possible the formation of time series of Q_{net} anomalies, given the various dataset lengths. In trying to match Bugden (1981) values of Q_{net} with the monthly means of T_a and SST through a simple linear relation of the form $Q_{net} \approx A\ (T_a - SST) + B$, no consistent result was obtained from one area to the other, or from month to month.

Chapter 6

Monthly Vertical Structure of the Upper-Layer Thermohaline Fields (May to November)

Following the description of the surface fields (T, S and Chl*a*) of the GSL in the previous chapter, we will now examine the monthly evolution of the upper-layer vertical thermohaline structure and related quantities. More precisely, climatological monthly depth distributions of T and S will first be described, followed by a discussion of monthly averages of mixed-layer depth (MLD), upper heat content (HC) and upper-layer static stability (E). Using the previously obtained surface heat fluxes in conjunction with a few simple 1D calculations (heat diffusion, MLD and stratification) the seasonal evolution of the upper-layer thermohaline fields (i.e.: T, MLD and ρ) will be discussed. Finally, a preliminary study of the variability of some upper-layer physical fields (SST, MLD) in relation with various atmospheric forcing (Ta, |U|, Qnet) will be introduced.

6.1 Monthly Distributions of the T and S Fields with Depth

As mentioned earlier, the first procedure performed for this climatological analysis was to segment the oceanic database into 15 geographical areas[1] and calculate the monthly means of T and S obtained earlier by Petrie (1990). In doing so, a first comparison would allow us to validate the dataset quality as well as to detect any errors that could have occurred during the analysis. The second motivation for dividing the Gulf into subsections was to allow a sufficient number of T and S profiles to be regrouped within the same area to produce, after averages were computed, multiyear time series of monthly temperature and salinity anomalies at various depths[2].

---

[1]: Areas 14 and 17 were excluded from the analysis for a few reasons: 1- their spatio-temporal coverage is not very good compared to the other areas; 2- some of the assumptions made throughout this thesis do not apply these coastal areas; 3-because they constitute narrow and shallow regions of smaller scales than the other areas; in particular, it is difficult to determine whether the physical processes governing the Gulf's upper waters play a similar role in Northumberland Strait region.

[2]: This would render possible the study of interannual fluctuations within the GSL. These time series have been produced for all sections at all reference depths, but have not been analyzed statistically.

Several investigators have *recently*[3] studied the Gulf's mean characteristics: Bugden (1981) computed means of T and S for 4 large areas and 4 distinct vertical layers in the Gulf; Bugden et al. (1982) studied the influence of runoff on sea surface salinities; Vigeant (1984) produced SST maps from ship data; and Petrie (1990) calculated monthly-depth climatologies of T and S for 17 GSL subareas. However, a complete understanding of the average physical and dynamical state of the GSL is not available. Hence there is a need for a more comprehensive temperature and salinity climatology (Bugden, personal communication). An accurate description of temperature and salinity as function of depth, time of the year and latitude-longitude, is important for many areas of oceanographic research. The calculated fields presented in this chapter are believed to form the most complete and up-to-date climatology produced for the Gulf (Bugden and Drinkwater, personal communication). The overall characteristics observed throughout the Gulf's 15 monthly-depth distributions of T and S will first be discussed, followed by an investigation of local thermohaline features.

6.1.1 Gulf-wide and Specific Features

In regard to ocean temperature, the formation of a distinct warm surface layer from May until November can be observed in all areas. Its thickness varies considerably from month to month (from 10-20m in May to around 50m in November) as well as from one area to another. The associated SST maxima (usually occurring in July-August) range from around 17-18 °C in the shallows (areas 12-15) down to about 10 °C in upwelling areas (05, 06 & 09) and as cold as 6-8 °C in the lower estuary (07). The presence of a cold (<2°C) intermediate layer (Koutitonsky and Bugden, 1991) below the mixed-layer is apparent nearly everywhere. During the winter months, this layer merges with the upper one to form a region of cold water extending to the surface. Finally, below a depth of approximately 100 m, the seasonal fluctuations of temperature nearly disappear, but strong interannual variations are present (Bugden, 1991).

For salinity, the vertical structure is less dramatic, showing a monotonic increase of S with depth, accompanied by a weak signature of the upper mixed-layer (weak in

[3]: In the 1950's, the work of Lauzier and coworkers (Lauzier and Bailey, 1957; Lauzier et al., 1957; Lauzier and Trites, 1958; and Tremblay and Lauzier, 1940) was probably the first real attempt to look at the vertical and horizontal T-S structure in the Gulf of St.Lawrence. However, due to the difficulty in obtaining the original manuscripts, and since their results have been largely included and summarized in the review papers of Trites and Walton, 1975, and, more recently, in Koutitonsky and Bugden, 1991, only the latter two will be acknowledged.

comparison to the temperature profiles). The surface and near surface annual salinity cycles are opposite to that for temperature (SSS minima occur in summer) with a typical range of around 2 PSU, except near the estuary (compared to about 18 °C). The salinity minimum is strongly affected by runoff from the St.Lawrence River and from its major tributaries. It occurs at slightly different times for various locations due to the relative distance from the freshwater sources. Finally, the bottom waters of the GSL, characterized by salinities of 33 to 35 (<150m), result from the inflow of slope water from the Atlantic Ocean entering through Cabot Strait (Petrie, 1990; Koutitonsky and Bugden, 1991). The Atlantic water will discussed using T-S diagrams in section 6.1.2.

In general, in regard to the seasonal evolution of T and S at fixed depths, a common pattern may be observed: generally, surface T are low in May, increase to a surface maximum around August and cool down for the rest of the ice-free season; whereas, salinity follows an opposite trend. At a depth of 30 m, the seasonal range of temperature is decreased and its maximum occurs later (around October), whereas salinity variations are even weaker. At a 75 m depth (50 m for the Shallows), both T and S are essentially constant throughout the ice-free months. Typical standard errors (Efron and Tibshirani, 1986; Umoh and Thompson, 1994) may be estimated by $\sigma/(n)^{1/2}$ (where σ is the standard deviation and n is the number of monthly observations) and are generally less than 1°C and 0.4 in the upper 30 meters, for T and S respectively (see table 6.1 for typical values). Largest standard deviations occur near the surface, but standard errors should be used with caution in months/areas with few observations since they depend strongly on n.

	T	01	03	06	10	16	S	01	03	06	10	16
June	0m	0.37	0.36	0.47	0.41	0.41	0m	0.10	0.12	0.26	0.18	0.24
	30m	0.34	0.29	0.15	0.28	0.19	30m	0.07	0.06	0.11	0.11	0.08
Aug	0m	0.28	0.29	0.36	0.37	0.27	0m	0.15	0.10	0.27	0.14	0.16
	30m	0.41	0.57	0.26	0.39	0.22	30m	0.09	0.07	0.13	0.11	0.09
Oct	0m	0.34	0.50	0.47	0.76	0.52	0m	0.20	0.22	0.16	0.12	0.15
	30m	0.51	0.55	0.34	1.00	0.79	30m	0.19	0.16	0.12	0.13	0.16

Table 6.1: *Typical standard errors (°C & PSU) of upper-layer monthly T (left) and S (right) at the 0m and at 30m (top & bottom numbers respectively) for some areas (01, 03, 06, 10 and 16) and months.*

Regional features will be examined in a counterclockwise sense around the Gulf. The first aspect of interest is the difference in surface T and S (SST, SSS) between section 01 (Cabot Strait - Cape Breton side) and 02 (Newfoundland side). In accordance with the commonly believed flow pattern (El-Sabh, 1976) in the Strait, there is lighter surface waters flowing seaward near Cape Breton with a compensating inflow of saltier waters at depth, which extends to the surface near Newfoundland (Koutitonsky and Bugden, 1991). Although displaying similar patterns, the first graphs of figures 6.1 to 6.5 (areas 01 & 02) depict saltier (31 vs 30 in July-August) and slightly colder (14 vs almost 15 °C) surface summer waters for area 02 (Newfoundland side of Cabot Strait). This seems to suggest the influence at the surface of shelf water advected into the Gulf, as well as the arrival of the maximum freshwater runoff near the Strait region by August (El-Sabh, 1976). Areas 03 and 04 (Esquiman Channel, Newfoundland and Québec shores, respectively) display monthly T and S depth distributions analogous to those at Cabot Strait, except that the cold intermediate layer (CIL) is slightly colder along the Newfoundland shore than it is in Cabot Strait. It is even colder along the Québec shore. This feature can be seen in the temperature graphs of areas 01 to 04 by following the 0 °C isotherm: the tongue of "cold" water enclosed within this isotherm, going from the surface (in Jan-Mar) and deepening in early summer to form the cold intermediate layer (June and July for the Esquiman locations). A possible explanation for this is the intrusion of cold Labrador water from the Strait of Belle-Isle. Petrie et al. (1988) suggested that up to 35% of the winter intermediate layer water could be accounted by this incoming cold water. Sea surface salinities show a slow but steady increase (1 to 1.5 PSU) from area 01 to area 04. This monthly T and S depth structure persists in areas 05 and 06, with only slight differences in isotherm and isohaline locations from the previous graphs. A word of caution should be added about these two regions (Jacques Cartier Passage, 05, and the Northwest Gulf, 06). Important runoff effects, as well as frequent occurrence of coastal upwelling, constitute characteristic features of the GSL north shore. Furthermore, large eddying motions (Anticosti Gyre: El-Sabh, 1976) associated with strong north-south T and S gradients exist just west of Anticosti Island (areas 06 & 08). These "sub-area" oceanographic processes are important for the overall circulation in the Gulf and, although the T and S graphs for areas 05, 06 and 08 (and, to variable extent, in the other regions of this study) give good indications of the average thermohaline state likely to occur within these sections, one should also keep in mind the possible existence of local T and S gradients of scales smaller than the area size.

Regions 07 and 08 are distinctive since they are influenced by a strong freshwater surface pulse. Important vertical, as well as strong horizontal, density gradients are generated, leading to the formation of a major circulation feature of the Gulf - the Gaspé current (Koutitonsky and Bugden, 1991). Although this research focusses essentially on the Gulf of the St.Lawrence, the T and S statistics for the lower estuary (area 07) were also computed and will be discussed briefly. As expected, the upper waters there are well stratified. The monthly average SSS reaches a Gulf-wide low of around 26 in May-June as a consequence of high spring runoff from the St.Lawrence River. The summer SST is low due to upwelling and the vertical mixing with deeper and colder waters (Petrie, 1990). These cold and fresh surface characteristics persist into area 08, hugging the Gaspé coast as they move downstream, but are less dramatic there in part due to mixing with neighbouring waters (areas 06 and 09). The central regions (09 and 10) show a warmer/fresher surface layer in the summer overlying an intermediate cold layer and deep salty bottom waters. Summer SST/SSS conditions of area 10 are slightly warmer/fresher than those of area 09, probably because of the influence of the nearby Magdalen Shallows warm waters as well as the advection of freshwater runoff from sections 07-08. Upwelling is also believed to occur along the south shore of Anticosti Island, thus affecting the surface conditions of area 09 by bringing colder water into the upper-layer. At the mouth of Baie des Chaleurs (BdC - area 11), complex dynamical situations may greatly affect the water mass composition. Indeed, according to prevailing atmospheric and oceanic conditions, the Gaspé current may sometimes separate itself from the peninsula and continue past the entrance of the Baie, well into area 11 (and part of 12), or it may remain "attached" to the coast, thus intruding partially into BdC (Gan, 1995). In general, both the Gaspé current and runoff from the BdC contribute strongly to the time-depth evolution of the thermohaline state of region 11.

Finally, the remaining four regions (areas 12, 13, 15 and 16) cover the Magdalen Shallows. There, the Gulf's warmest waters are found (monthly average SST of around 16 °C in mid-summer - excluding again areas 14 and 17)[4]. A rapid decrease of temperature with depth is also observed as it reaches 1 °C, in some places at a depth of only 30m, in June. Although the area is poorly sampled during the ice season (the corresponding parts of the graphs show indeed rather bizarre contour lines, or no data at all), it is fair to say that, as the net surface heat flux reverses in the fall and the wind speed increases, most of the water column between 0 and 50 m becomes well-mixed. The surface salinity for the areas 12, 13, 15 and 16 is slightly lower than for the neighbouring sections of the central GSL (09, 10, 01 and 02). This can be attributed to the fact that part of the freshwater transported from areas 07 and 08 by the Gaspé current flushes the Shallows towards the Atlantic.

- <u>The next 5 pages (fig. 6.1-5) display the monthly depth distribution of T and S for the 15 usual areas.</u>

[4]: Petrie (1990) reports that area 17 exhibit the warmest waters for the GSL.

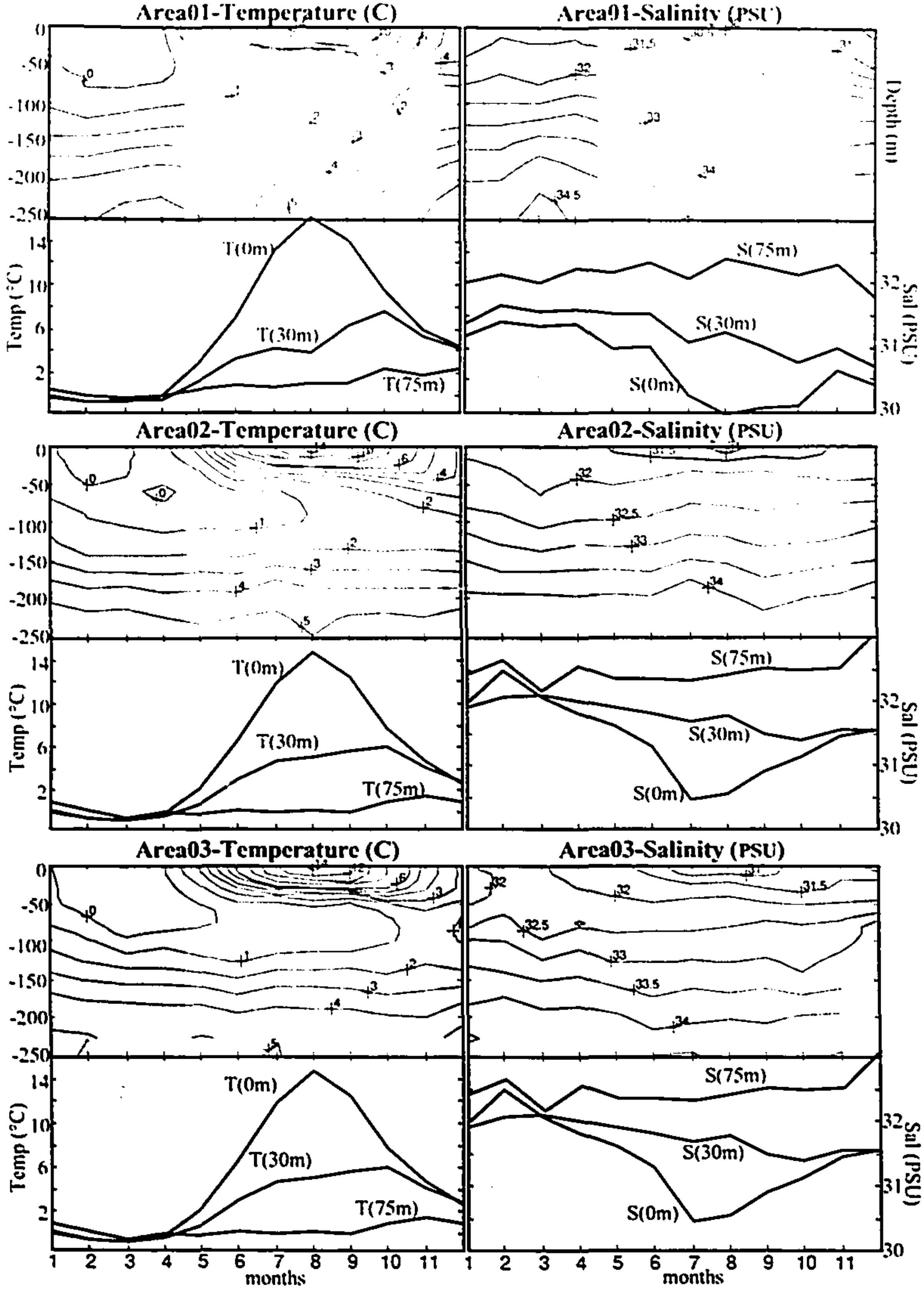

Fig. 6.1: *Monthly-depth distribution of T and S for areas 01, 02 and 03.*

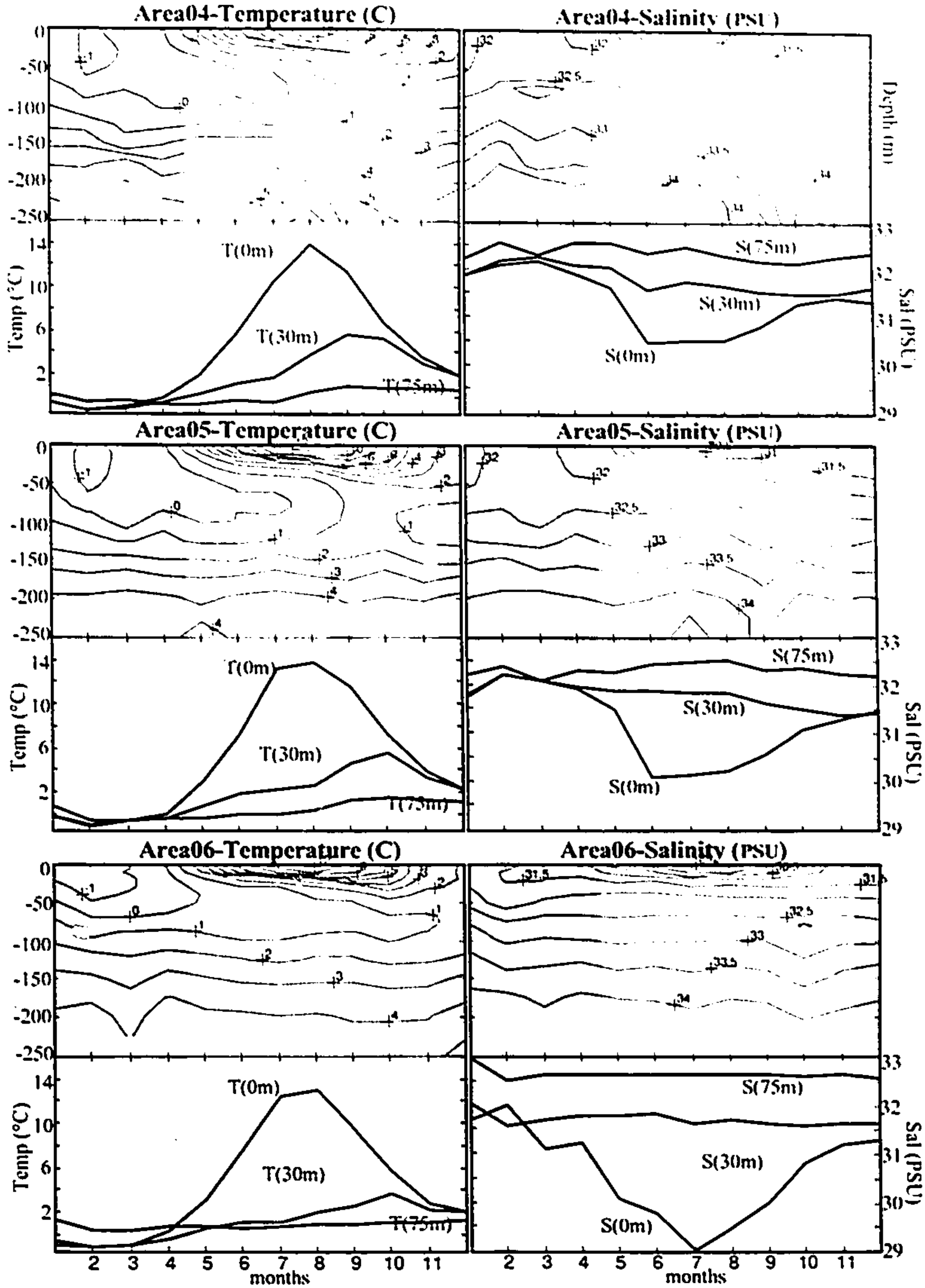

Fig. 6.2: *same as fig. 6.1. for areas 04, 05 and 06.*

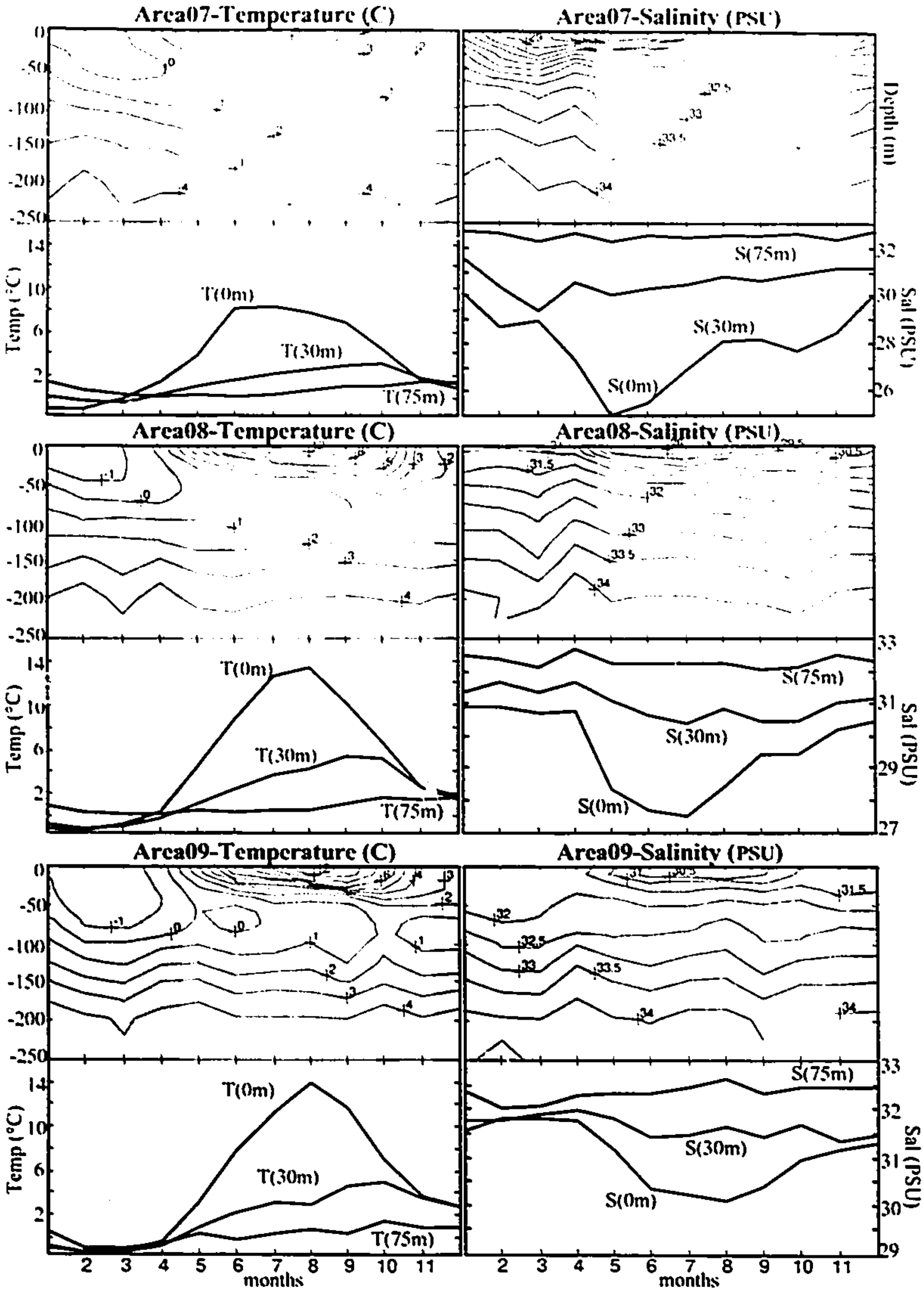

Fig. 6.3: *same as fig. 6.1, for areas 07, 08 and 09.*

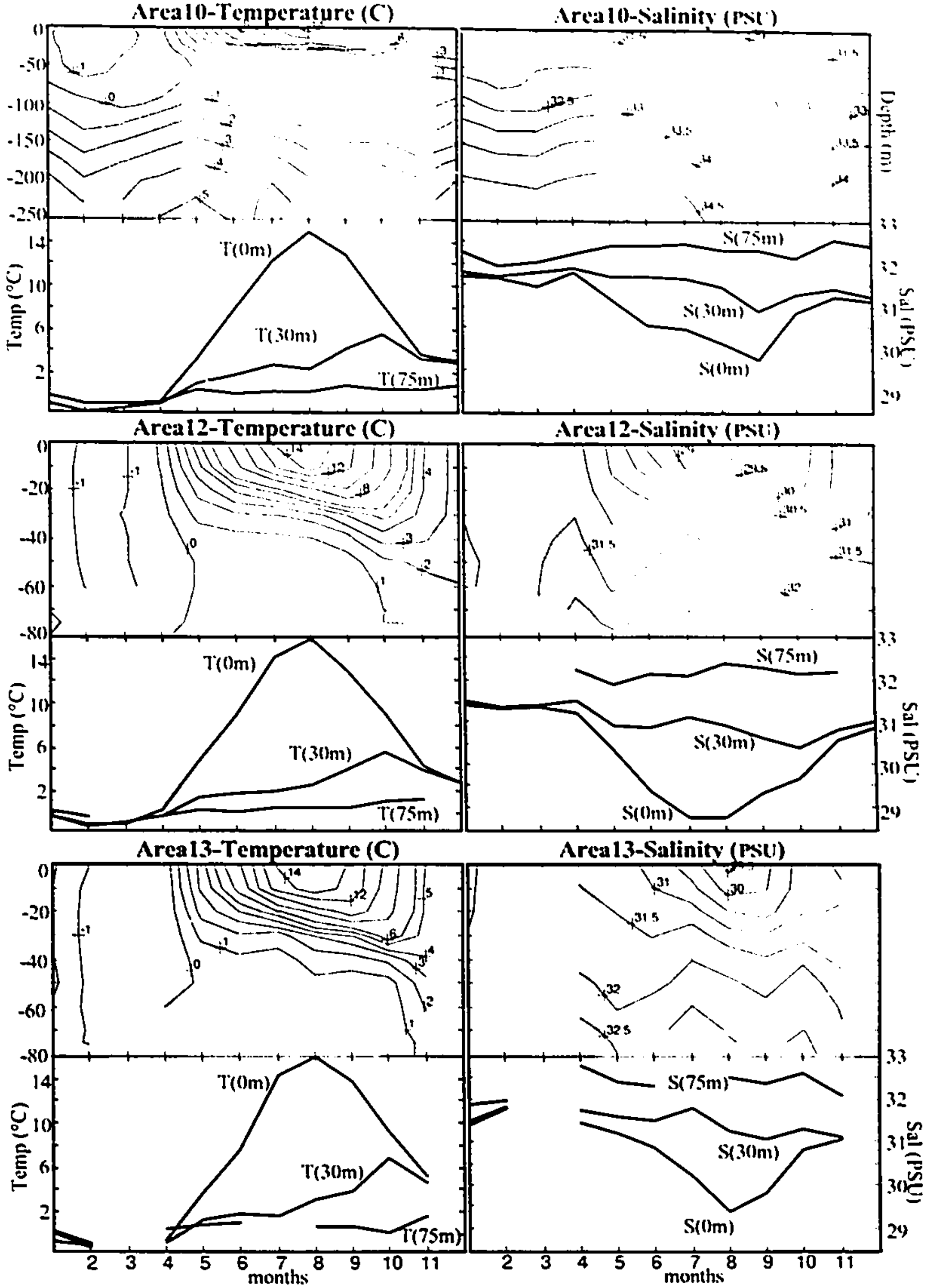

Fig. 6.4: *same as fig. 6.1. for areas 10, 12 and 13.*

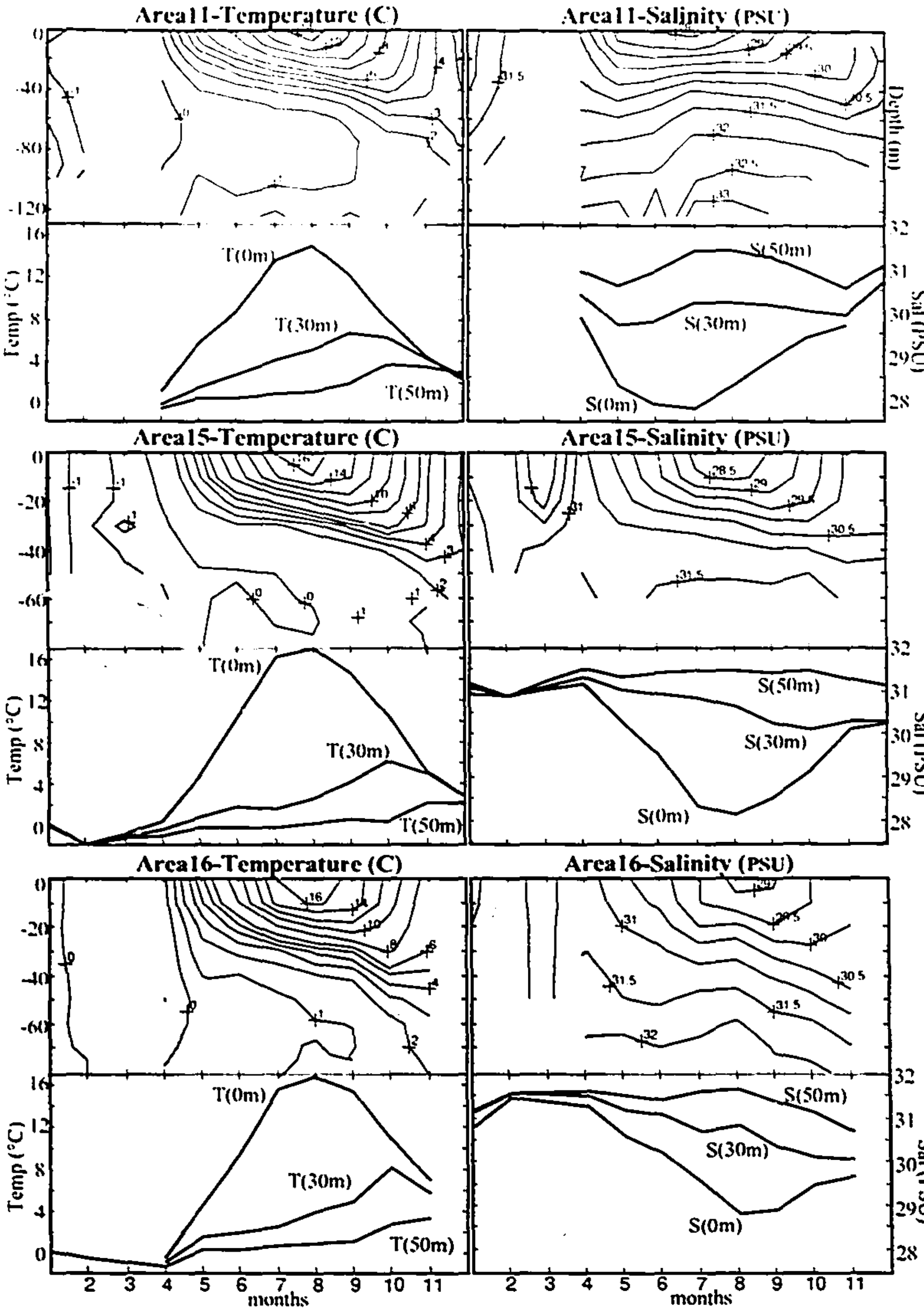

Fig. 6.5: *same as fig. 6.1. for areas 11, 15 and 16.*

6.1.2 Gulf-wide and Composite T-S Relationships

The previous section, which discussed the monthly-depth distributions of temperature and salinity for 15 sub-regions of the GSL, revealed the existence of interesting hydrographic features in relation to the various water masses interacting in the Gulf and their respective evolution over the annual cycle. Another very useful way of characterising the GSL average water properties is to plot the climatological means of temperature versus its salinity counterpart on what is called a T-S diagram (Pickard and Emery, 1990). In this section, T-S diagrams are constructed from climatological T and S values, first for all months, all depths and the entire Gulf, and then in a composite fashion in order to depict the property differences between winter and summer waters as well as between three distinct vertical layers (0-75m, 75-150m, and > 150m).

Gulf-wide Features:

Figure 6.6 displays the characteristic T-S diagram for the GSL based on climatological values of T and S described in the previous section[5]. Although several researchers have, in the past, studied the formation and evolution of the various water masses of the Gulf, it seems Forrester (1964) was one of the few to produce such T-S plots for the GSL. Figure 6.6 was compared to Forrester's original temperature-salinity relationships and examined to gain more insight into the origin of the Gulf's waters as well as their winter-to-summer and surface-to-depth differences. The first important aspect, found on the lower right corner of figure 6.6, is the obvious presence of a well defined salty (33-35 PSU) and dense ($\sigma_T \approx 26.5$-27 kgm^{-3}) water mass whose temperatures vary between 3 and 6°C. This essentially constitutes the deepest layer of the Gulf and is typical of the Atlantic waters near the Scotian Shelf edge (Petrie and Drinkwater, 1993). At the very base of the same figure, the coldest temperatures found in the GSL characterize the CIL. As described earlier, the T and S values range from 2 to -1.7°C and 30 to 33, respectively. Finally, the cloud of scattered T-S values filling-up the remaining space on the graph represent the surface waters of the entire Gulf over the annual cycle. These T-S points cover a much wider range of temperatures and salinities as opposed to the intermediate and deep layers because of the different regional features of the Gulf (upwelling, runoff, etc.) as well as the much larger influence of atmospheric processes.

[5]: Composite T-S diagrams for the 15 sections were also constructed from unaveraged T-S values, but not included in the thesis since they yielded similar T-S relationships to the climatological ones.

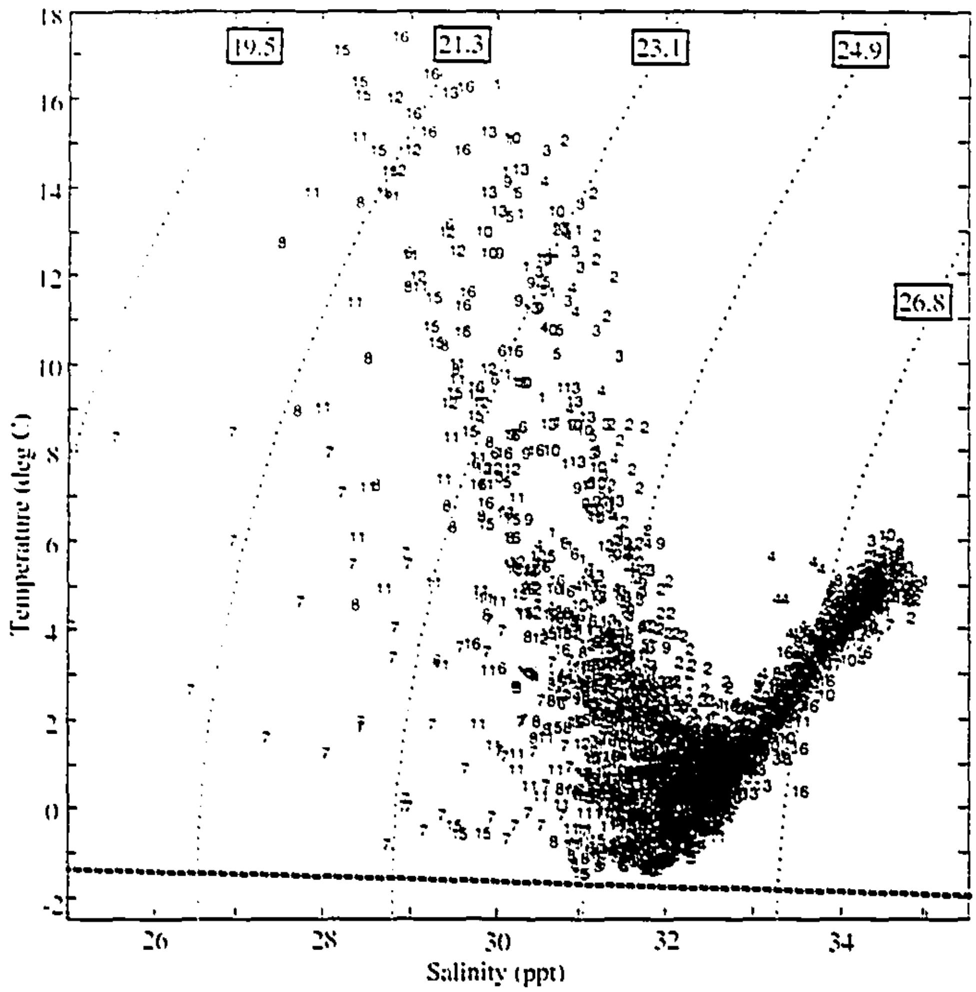

Fig. 6.6: *Climatological Gulf-wide T-S diagram (dashed lines are isopycnals and the freezing point of sea water is denoted by the thicker dashed line in the lower portion of the graph; the #'s correspond the respective GSL area).*

Specific Features:

We now extend Forrester's (1964) approach and form 12 T-S subdiagrams according to three time periods (Feb-Mar, Jul-Aug, and all year) and four depth segments (0-75m, 75-150m, 150-...m, and all depths). The two seasonal extremes (summer and winter) as well as the three distinct GSL layers (deep, intermediate and surface) are clearly distinguished in figure 6.7. In the first column of the figure, the four depth-based climatological T-S diagrams for the months of February and March are shown. The previously discussed Atlantic water mass is shown in the deep layer panel. A rather similar relationship between the 75-150m and the surface masses can be observed from the first two graphs. This further confirms the fact that the summer surface layer eventually cools down sufficiently in the fall to merge almost completely with the intermediate layer during the winter. Evidently, the July-August temperatures and salinities of the 0-75m layer exhibit a much warmer and broader T-S envelope (as depicted by the first panel on the middle column of fig. 6.7), but show little change for the intermediate and deep layers. Indeed, there are only slight T-S variations in the intermediate and deep layer diagrams between February-March and July-August (the two middle panels of the first and second column of figure 6.7). This is in agreement with the idea that the seasonal cycle of the atmospheric forcing affects almost exclusively the upper-layer and that waters below are likely to be influenced solely by extraseasonal fluctuations (Bugden, 1991). In general, these T-S relationships agree well with those produced much earlier by Forrester, but have the advantage of clearly distinguishing the different T-S characteristics related to the three chosen vertical layers.

Transitional Areas Suggested by Pingree and Griffiths (1980):

One interesting aspect concerning the climatological T-S relationships is the ability to characterize water mass changes from year to year and/or within certain regions of the Gulf. One such example, which is of particular interest to both physical and biological oceanographers, is the shallower area of Jacques Cartier Passage (JCP - see fig. 6.8), between Havre St-Pierre and the northwestern end of Anticosti Island (from here on, denoted "JCP area"). Pingree and Griffiths (1980), using the Simpson-Hunter (1974) approach, defined zones likely to be influenced by tidal mixing. The JCP area was classified as a frontal region ($S < 1.5$ - see Pingree and Griffiths, 1980, for a definition), despite a M_2 tide of modest amplitude throughout the GSL. However, this classification was solely based on the results of a M_2 tide model, hence surface buoyancy fluxes

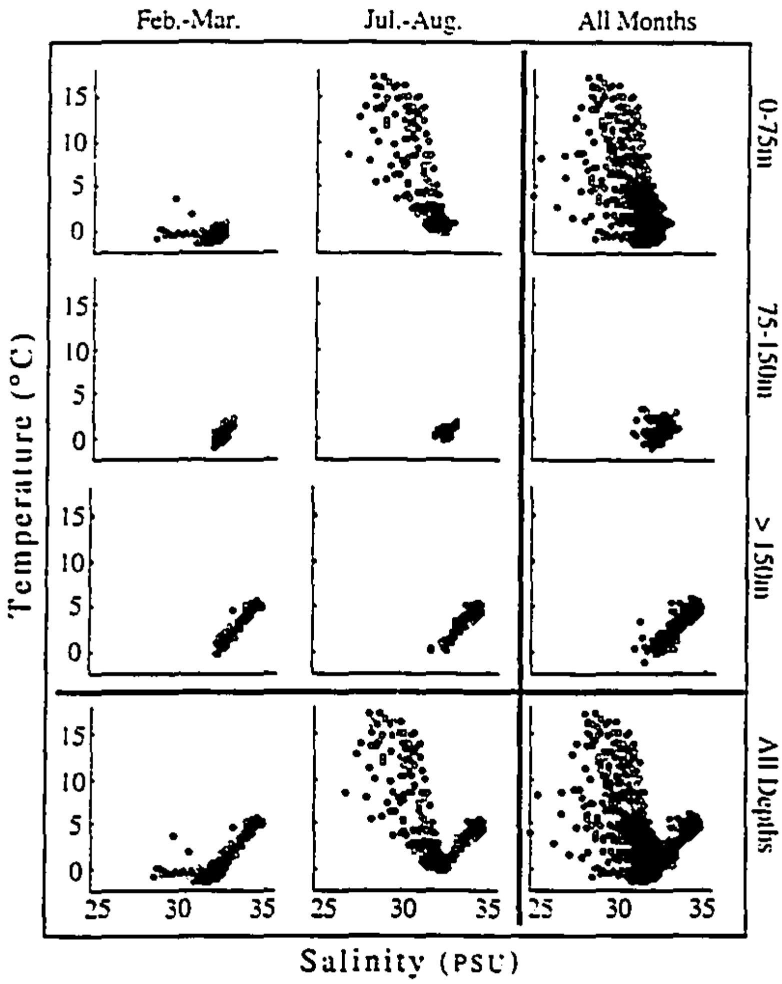

Fig. 6.7: *Composite T-S diagram for Febuary-March, July-August, and for all months, as well as for the upper 75m, the mid 75-150m, the deeper than 150m waters, and for the entire water column.*

and wind mixing effects were not taken into account. In fact, Pingree et al. (1978) note that wind mixing is sometimes more effective than tide alone in setting up vertical circulations. For example, there may be situations where the wind pattern (direction) would be favourable for upwelling but the intensity of the associated wind stress too weak to overcome the ambient upper water stratification. In this case, the addition of tidal mixing may be sufficient to destabilize the water column and induce upwelling events (Pingree et al., 1978; Pingree and Griffiths, 1980). Consequently, we will first look at T-S relationships in the JCP area for the months of June to September and compare them to the monthly averaged ones of area 05. Monthly averaged temperature and salinity profiles will then be examined.

The 4 middle panels of figure 6.8 display T-S relationships in the JCP area for the months of June, July, August and September (individual T-S observations are denoted by the small circles; also shown are the monthly averaged T-S relations for that sector - thin solid line - as well as the corresponding monthly climatological T-S relation for area 05 - thick solid line). Concerning the surface temperatures, those in the JCP area are generally colder than the monthly averaged SST of area 05, and this temperature difference increases from June to September, i.e.: SST_{JCP} is approximately 1°C colder than SST_{05} in June, 2°C to 3°C colder in July-August, and even colder (< 5°C) than SST_{05} in September. For the salinity, June surface values are much fresher in the JCP area than in area 05 (~1 PSU), but SSS_{JCP} are approximately only 0.5 PSU fresher in July-August, such that the situation is completely reversed in September where SSS_{JCP} are roughly 1 PSU saltier than SSS_{05}. These surface temperature and salinity differences can be translated into surface density differences as followed: in June, surface waters of area 05 are heavier than those of the JCP region (~1 kg/m^3), whereas in September, sea surface density of JCP area is approximately 1.5 kg/m^3 lighter than that of area 05; during July-August, surface waters roughly have the same density. At a depth of 50 m, monthly averaged water characteristics of both JCP region and area 05 merge into one common water type (T_{50m} ~ 1° to 2°C, S_{50m} ~ 32 to 32.3 PSU). It is difficult to say that the waters in shallow region of Jacques Cartier Passage are "well-mixed" by looking at these T-S diagrams. Although the monthly T-S properties of JCP area for the 10 m to 50 m interval are in general more tightly

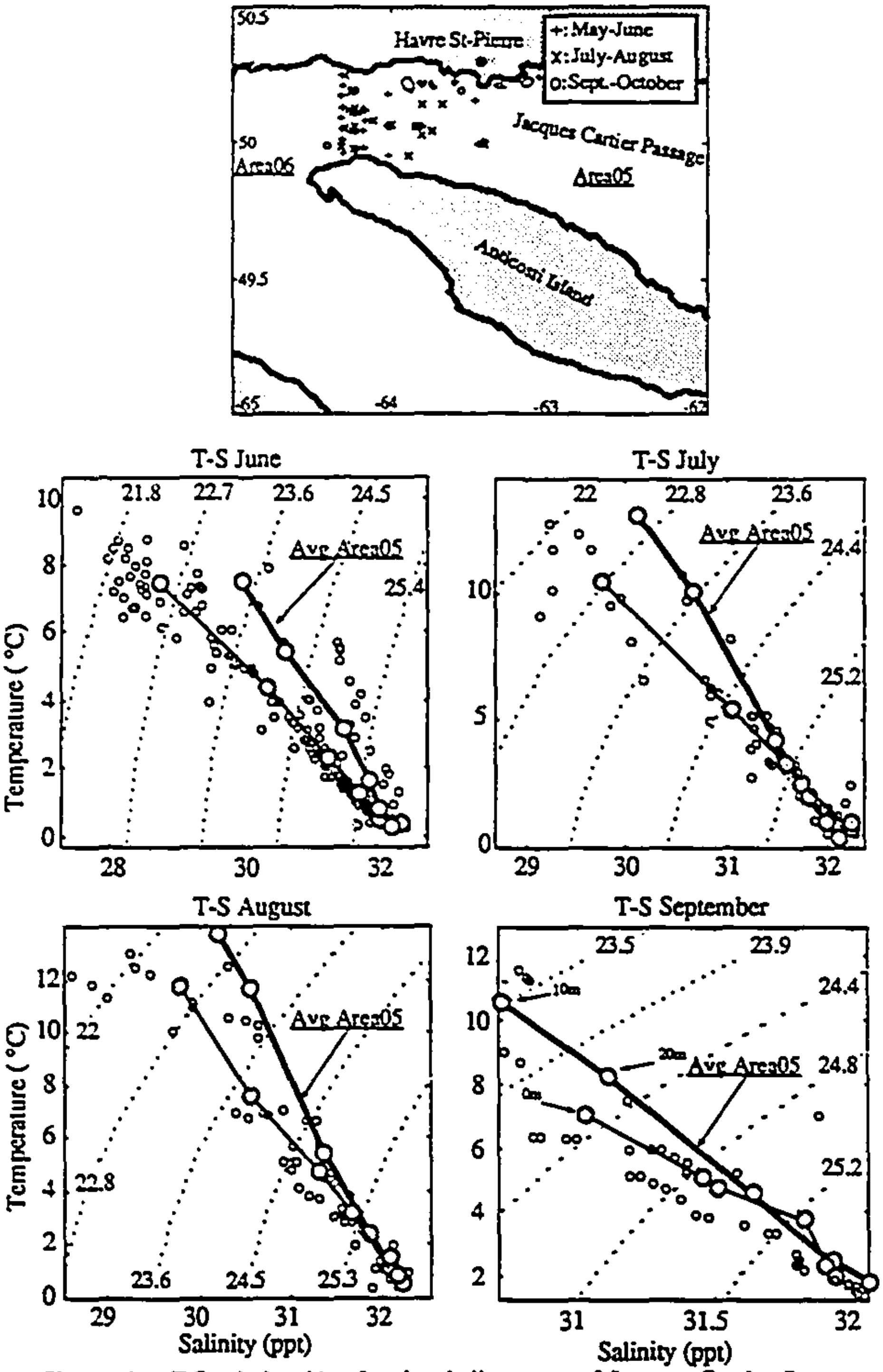

Figure 6.8: *T-S relationships for the shallow area of Jacques-Cartier Passage, between Havre St-Pierre and Anticosti Island (shown on the upper picture), for the months of June, July, August and September. The upper diagram displays the monthly locations of T-S observations plotted for comparisons with climatology. The 4 middle panels show the T-S observations (o), the monthly averaged T-S relations for that sector (thin solid line) as well as the corresponding monthly climatological T-S relation for area 05 (thick solid line). Dotted lines on all 4 panels correspond to iso-sigma-T (kg/m³).*

clustered than the climatology of area 05, the water mass characteristics are highly variable throughout these 4 months, and T-S properties there are also expected to be influenced (hence aliased in terms of the T-S data used here) by episodic processes (synoptic, tidal, etc.) of smaller temporal scales than monthly means (Bourque and Kelley, 1995).

Looking at profiles of temperature and salinity allows us to investigate the depth dependence these properties, hence assess more easily the degree of vertical mixing (Figure 6.9 shows monthly averaged T and S profiles for June, July, August and September, for both the JCP region and the area 05). In June, both T_{JCP} and S_{JCP} profiles follow closely the area 05 climatology for the lower section on the water column (~ 25 m to 50 m). However, the mixed-layer of JCP area is much shallower and more stratified than its area 05 counterpart. The situation changed during the July-August period, when the upper 10 m of JCP region is still more stratified than area 05, but the lower portion of both T and S profiles are now more vertically homogenous (more homogenous than they were in June, also more than those of area 05 for July-August). Finally, in September, the upper-layer situation is now reversed such that upper waters of area 05 are more strongly stratified than in the shallow region of Jacques Cartier Passage. Even more interesting is the degree of vertical homogeneity of both the temperature and salinity profiles of JCP sector: they show differences of only ~ 0.6 PSU and ~ 3°C between 10 m and 40 m. This seasonal variation may perhaps be explained as follow: in the early months of the ice-free season (May, June) the surface waters near the north shore are strongly stratified because of the runoff from neighbouring rivers (Koutitonsky and Bugden, 1991). Moreover, during this time, the winds are decreasing and the surface heat input increasing, both contributing to a shallower and more stratified upper-layer. The effects of reduced winds and increased surface heat input continue on in early July but this trend soon reaches an optimum (minimum winds and maximum heat input) and starts reversing in August. Meanwhile, runoff from rivers has decreased from its June maximum (Bugden, 1981) such that, in September, increased winds and decreased surface input of heat and freshwater work together to weaken the stratification and favour vertical mixing. In comparison with the climatology of area 05, one may argue that the river runoff should influence more strongly the coastal JCP area throughout the 4 analyzed months. Assuming that the wind mixing and the surface heat input are similar for both areas (JCP and 05), the more vertically "well-mixed" conditions observed in JCP area (during August, but mainly in September) could be the result of

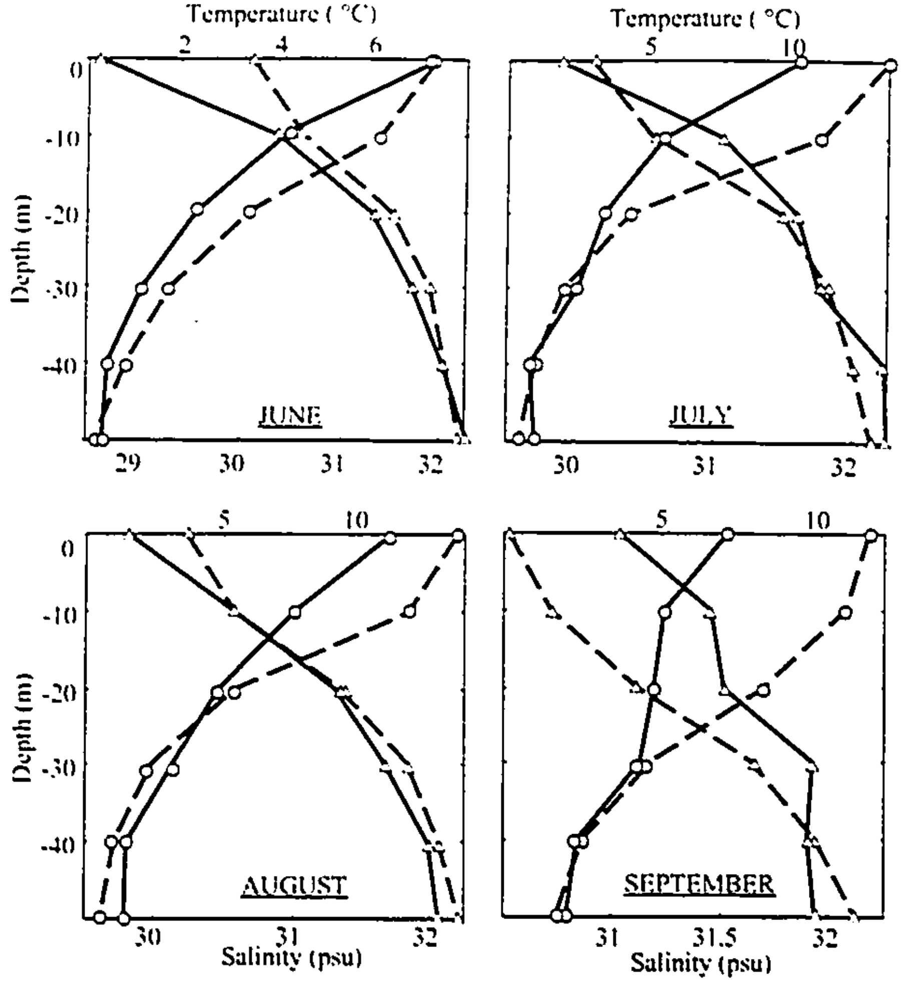

Standard Deviations Of T (left) & S (right)

Depth (m)	T JUN	T JUL	T AUG	T SEP	S JUN	S JUL	S AUG	S SEP
0	2.0	2.6	1.2	2.7	1.4	0.9	0.7	0.3
-10	1.9	2.1	2.3	3.8	1.0	0.5	0.7	0.4
-20	0.9	1.5	1.3	3.7	0.4	0.3	0.3	0.5
-30	0.6	1.2	0.9	3.5	0.2	0.2	0.1	0.1
-40	0.3	0.1	0.2	1.5	0.2	0.1	0.1	0.2
-50	0.3	0.7	1.3	0.5	0.2	0.2	0.4	0.2

Number Of Observ.

Depth (m)	JUN	JUL	AUG	SEP
0	49	10	11	14
-10	53	17	10	11
-20	50	16	12	3
-30	47	6	5	3
-40	44	3	4	6
-50	20	9	8	3

Figure 6.9: *Monthly averaged temperature (o, top scale) and salinity (Δ, bottom scale) profiles for June, July, August and September. Solid lines correspond to the averaged T and S profiles for the shallow area of Jacques-Cartier Passage, between Havre St-Pierre and Anticosti Island (see previous fig. for diagram). Number of observations and standard deviations, for each 10m interval, are also tabulated (for the Mingan-Jacques-Cartier Passage area only). The dashed lines are the monthly T and S climatologies for area 05.*

combined tidal mixing and coastal upwelling, as proposed by Pingree and Griffiths (1980). Finally, since it was also postulated by Pingree and Griffiths (1980) that locally increased tidal mixing could result in increased biological productivity, it is interesting to compare monthly averaged surface chlorophyll data for both area 05 and the shallow zone of Jacques Cartier Passage. The results displayed in the table below show a marked increased in surface Chl*a* (often indicative of increased primary biological productivity;) for JCP area in comparison with area 05. Although it is impossible to truly assess the proportion of increased Chl*a* values directly related to increased wind and tidal mixing, the shallow zone of Jacques Cartier Passage seem to have more favourable conditions for primary production.

	May	June	July	Aug.	Sept.	Oct.
AREA 05	1.71	1.26	1.59	1.42	2.92	2.13
JCP Area	4.48	2.65	2.53	3.00	4.33	4.42

Table 6.2: *Monthly means of surface* Chl*a* *concentrations* (mg Chl*a* /m^3).

6.2 Climatology of Mixed-Layer Depth, Heat Content and Upper-Layer Static Stability

As mentioned previously, the upper-layer of the ocean plays a central role in the storage and exchange of energy with the atmosphere and the waters below, as well as being of critical importance for the primary biological productivity (Pickard and Emery, 1990; Mysak and Lin, 1990). Three important physical quantities often used to describe the energetics and biological relevance of the upper ocean are the mixed-layer depth (MLD), the heat content of the upper water column (HC) and the upper-layer static stability (E). This section briefly explains how these values were computed and describes their corresponding monthly climatology for the 15 areas in the Gulf during the ice-free months (May to November inclusive).

First, the heat content has been calculated for the upper 100 meters of the entire Gulf except for the five areas covering the Magdalen Shallows (11, 12, 13, 15 and 16) where it was done for the first 50 meters from the surface. As before, each profile (per area and per month) were used to compute an upper-layer heat content value, and monthly averages were then produced for each of the 15 GSL regions. The quantity HC was obtained by

$$HC\,\big|_{0\,m}^{100} = \int_{0\,m}^{100} \rho\, C_p T\, dz,$$

where $\rho, C_p = f(T,S,z)$, $T,S = f(z)$ and T is in °K

and the integration was performed using Simpson's Rule (so that the error is $O[dz^5 \times T'''']$, where T'''' is the 4th derivative of T; Kincaid and Cheney, 1990). The empirical formulae used for the heat capacity and the density of sea water were obtained directly from the UNESCO algorithms[6]. Comparisons were done with H.C. calculated with a constant heat capacity (4025 J kg^{-1} °K^{-1}) and results did not change significantly.

The determination of the mixed-later depth is, in itself, rather difficult and subjective (Jim F. Price, W.H.O.I., personal communication). If the ocean behaved as nicely as the schematic pictures of chapter 2, than the MLD could be deduced easily. However, this is often not the case: the upper few meters are not always homogenous, and the sharp transition zone (thermocline, or pycnocline) may not necessarily be well defined. The motivation for using T alone is now explained. The first difficulty arose from the 10m vertical resolution in the interpolated dataset. Given this rather coarse resolution (in terms of mixed-layer depth), we hope that, in processing a large enough number of profiles, the resulting average MLD would tend to the real one, for we could only assess within what 10m interval was the MLD (i.e. ± 5m). Consequently, using T profiles alone has a net advantage in that there are far more "valid" temperature profiles in the database than there are density ones (because the profiles of density required both T and S to be present simultaneously). The next step is to assess whether T alone is a valid candidate for determining MLD. While both T and S contribute to density, during the winter months (and early spring), stratification is mainly dominated by salinity effects. However, during the warm season, this situation reverses such that upper-layer temperature and density profiles strongly covaried. This may also be appreciated from a buoyancy flux point of view (B, as defined in chapter 2), since B depends more strongly on thermal effects during the summer conditions (Gill, 1981). In addition, after "visualization" (and intercomparisons) of all interpolated T, S (and density, when present) profiles in the database for the ice-free

---

[6]: (Ref: Millero et. al., J. Geophys. Res. 78 (1973), 4499-4507; Millero, et al (1980) Deep-Sea Res., 27a,255-264; Millero and Poisson (1981), Deep-Sea Res., 28a pp 625-629. Above references are also found in UNESCO report 38 (1981))

period, we concluded that temperature was indeed a representative "tracer" of "how deep is the upper 'well-mixed' layer" in the ice-free months.

The final step consisted in finding an appropriate "thermal" criterium defining the ML extent. Several such schemes have been used in the past: Defant, according to Wyrtki (1964) used a critical temperature gradient of 0.02 °C/m to determine the depth of the thermocline, while Wyrtki considered its depth to correspond with a 0.5 °C change from the surface; Bathen (1972) used a statistical method combining both a temperature departure from the surface and a critical T gradient; Levitus (1982) used a net temperature change of 0.5 °C from the surface in combination with a density departure (from the surface) of 0.125 kg/m^3; Lamb (1984) defined the MLD base to be the level where T was less than 1°C from the surface, whereas Rao et al. (1989) defined the MLD as the depth where T was less than 1 °C from the 10 m value; Lukas and Lindstrom (1991) considered gradients of temperature, salinity as well as density to determine the depths of thermocline, halocline and pycnocline, respectively.

In this study, we compared 3 temperature-based methods to define the MLD: a dT/dz criterium, as well as two schemes based on temperature from the surface. These methods (defined below) were applied to all complete (no data gaps within the upper 100 m) temperature profiles.

$$\mathrm{MLD}_1 \sim z_{\mathrm{mobile}}\left(dT/dz\big|_{\max}\right)$$
$$\mathrm{MLD}_2 \sim z_{\mathrm{mobile}}\left(T_{(0)} - T_{(z)} \geq 1°C\right)$$
$$\mathrm{MLD}_3 \sim z_{\mathrm{mobile}}\left(T_{(0)} - T_{(z)} \geq 2°C\right)$$

Upon examination of these results, we concluded that the T gradient method was not appropriate since it was more representative of the middle of the thermocline, and not the extent of the mixed-layer (and hence probably yielded too deep MLDs). Consequently, we opted for the 2 other methods, noting that, although these yielded reasonable mixed-layer depth estimates, they exhibited the same seasonal cycle (slow shallowing followed by more rapid deepening) as that obtained by the gradient method. Finally, we defined the base of the mixed-layer, for the ice-free months, as the depth where the temperature was 1°C less than the SST (same criterium used by Lamb, 1984)[7]. Monthly means of MLD will be displayed in figure 6.12, whereas their monthly standard deviations as well as the

[7]: It is informative to note that Lamb, 1984, in a climatological study of the MLD in the north Atlantic, was faced with the exact same problem, i.e.: the use of T alone in determining MLD due to too small a number of S profiles.

number of T profiles used to compute it are presented in the following table:

	May	June	July	August	September	October	November
01	11.8 (25)	7.0 (28)	5.4 (20)	2.0 (22)	4.7 (27)	5.9 (18)	18.0 (31)
02	14.2 (24)	6.9 (20)	4.6 (19)	2.2 (26)	5.4 (21)	9.1 (17)	18.0 (35)
03	15.0 (14)	6.1 (23)	4.4 (23)	5.2 (24)	5.4 (23)	11.5 (16)	18.0 (28)
04	14.8 (13)	6.0 (26)	4.3 (20)	4.4 (21)	6.1 (22)	13.2 (19)	17.0 (25)
05	15.2 (12)	3.8 (19)	1.9 (11)	2.1 (16)	8.3 (12)	11.5 (11)	23.1 (26)
06	3.7 (11)	0.9 (16)	1.7 (15)	2.1 (15)	5.2 (11)	9.2 (13)	21.6 (27)
07	4.8 (11)	1.7 (15)	0.7 (21)	2.1 (15)	6.4 (14)	11.3 (8)	14.1 (8)
08	5.1 (19)	2.7 (30)	1.8 (26)	3.0 (27)	5.9 (33)	13.2 (23)	20.9 (29)
09	12.0 (13)	4.0 (18)	1.5 (6)	3.7 (16)	5.0 (9)	13.6 (8)	19.2 (30)
10	8.3 (15)	5.0 (16)	4.6 (11)	3.2 (15)	4.8 (16)	6.1 (5)	15.4 (19)
11	3.0 (21)	4.1 (28)	2.1 (23)	3.6 (23)	4.7 (30)	13.6 (19)	23.4 (8)
12	6.2 (18)	3.4 (20)	2.2 (15)	2.1 (22)	4.0 (24)	8.0 (11)	19.5 (19)
13	8.6 (14)	4.5 (12)	1.8 (4)	1.5 (7)	3.5 (12)	7.0 (5)	17.7 (8)
15	3.9 (8)	2.8 (14)	1.5 (5)	1.4 (10)	4.0 (14)	7.3 (6)	16.5 (18)
16	5.5 (19)	4.1 (22)	2.6 (12)	1.5 (21)	4.4 (17)	7.7 (10)	15.6 (14)

Table 6.3: *Monthly MLD standard deviations (m; left) and number of T profiles used (in parenthesis).*

In general, standard MLD errors ranged from 1m to 4m roughly (and exceptionally up to 8m in November), with the minimum monthly mixed-layer variance observed in August, and corresponding, on average, to shallowest MLDs.

The static stability[8] (E) is a measure of ocean stratification. It is very similar to the buoyancy frequency (N), but it includes the additional effects of compressibility. In this study, E was calculated directly from the monthly means of T and S, according to the following definition (Pond and Pickard, 1991):

$$E = -\frac{1}{\rho}\frac{\partial \rho}{\partial z} - \frac{g}{C^2},$$

where g is the gravitational acceleration, and C is the speed of sound. Although the compressibility effects (as expressed by the sound speed term) were rather small, they were nevertheless included in the calculation. Since E is not an integrated value, like HC, but rather depends of vertical density gradient, several versions of it may be calculated (e.g., E

[8]: Although E was defined as evaporation in chapter 2 (in Gill's, 1981, definition of surface buoyancy flux), its value has not been computed in this study. Consequently, to follow the notation of Pond and Pickard (1991), the static stability is designated by E.

at the surface; E across the thermocline; E maximum, etc.). For purpose of comparison with the JGOFS data (see chapter 3 and the appendix), three variations of E have been used to deduce area-based monthly climatologies, namely: E_{0-30} (the static stability computed between the surface and a depth of 30 m), E_{MLD} (E computed at a depth 5 m below the mixed-layer) and E_{max} (the maximum E value of the water column). The first parameter (E_{0-30}) provides a mean of determining how stable are the surface waters throughout the GSL (while neglecting the effects of currents). The second parameter (E_{MLD}) measures the ability of deeper waters to be entrained into the mixed-layer. E_{max} usually corresponds to the middle of the thermocline, and has seasonal features (minima, maxima, regional distribution, etc.) very similar to those of E_{MLD} and E_{0-30}.

Gulf-wide Features

Figure 6.10-11 display typical monthly evolution - May to November - for the mixed-layer depth, the upper heat content and mixed-layer static stability in some regions of the Gulf (northeast: area 03; northwest: area 06; central: area 10; and southern GSL: area 16.). In general, the mixed-layer remains deep until the ice cover disappears, but it undergoes a shallowing trend during the first 3-4 months of the ice-free season. The MLD values range from 5 m to 15 m during the June-August period. As expected, and observed elsewhere in the open ocean (chapter 2), this period of shallow MLD corresponds to the Gulf's weakest wind regime (chapter 4) and strongest net heat flux (into the ocean, chapter 5). Afterward, increased wind mixing, along with a decreasing surface heat flux deepens the MLD throughout the Gulf. In regard to the heat content of the upper waters, it depends directly on the extent of the mixed-layer as well as its temperature. Consequently, whereas the MLD remains rather shallow during the early summer, its waters warm-up. As a result, HC values over the Gulf exhibit a steady increase until August-September followed by a decrease during the last months of the ice-free season. Again, a distinct seasonal cycle is evident for the mixed-layer static stability (E_{MLD}), where values are minimal in May, but increase to reach maximum stratification values in July-August, and decrease again until the end of the ice-free regime. The lower 4 panels of fig. 6.11 show typical monthly-depth distributions of stratification (E), again for areas 3, 6, 10 and 16. From this, we notice that the seasonal variation of E_{max} strongly follows that of the thermocline (just below the MLD), i.e.: maximum E values are shallow for the first part of the ice-free season (15m to 25m) and decrease rapidly during the August-November period. moreover, E_{max} values are

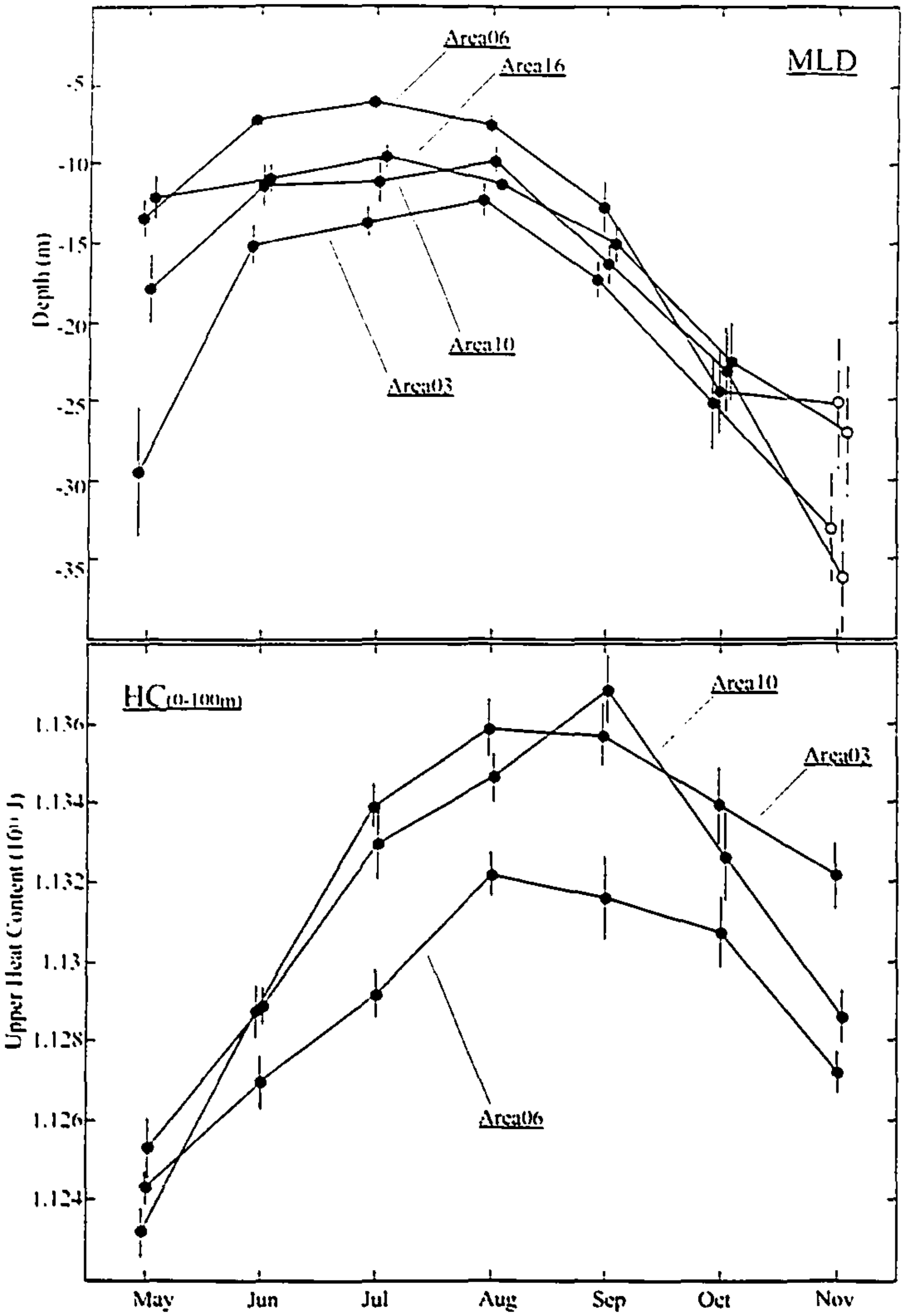

Figure 6.10: *Typical monthly mixed-layer depths (MLD, top) and upper heat content (HC, bottom) for 4 regions of the GSL: (northeast: area 03; northwest: area 06; central: area 10; and southern GSL: area 16). The standard errors are denoted by the vertical bars. (Data points are slightly offset for visual purpose. Due to the low water temperatures of November, MLD values for this month are considered less accurate).*

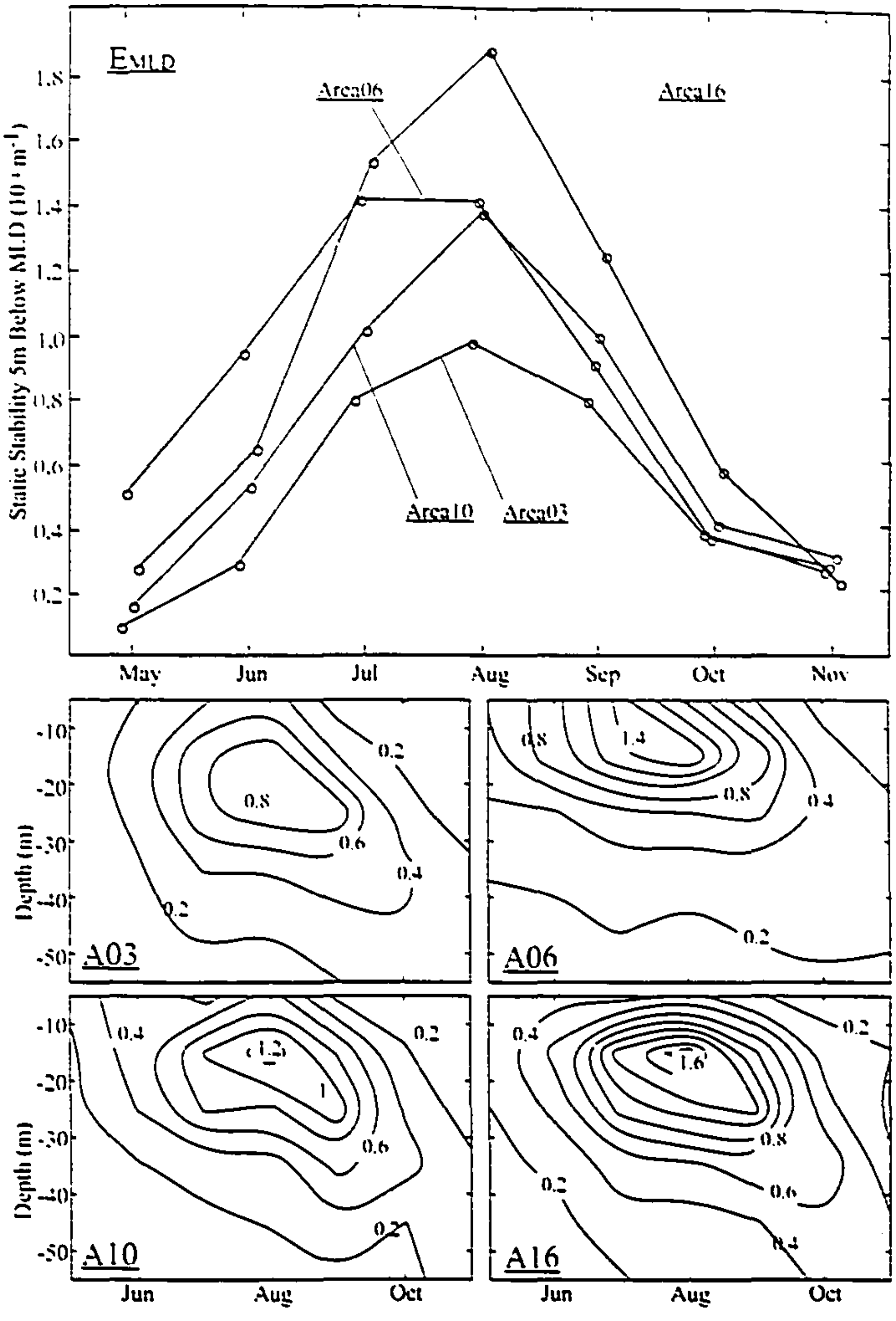

Figure 6.11: *Typical monthly patterns of static stability (m⁻¹) for 4 regions of the GSL: (northeast: area 03; northwest: area 06; central: area 10; and southern GSL: area 16.). The top panel displays the static stability (E) 5m below the mixed-layer, whereas the bottom 4 graphs show the monthly-depth distributions of E (10^{-4} m⁻¹).*

maximum in July-August and stratification is weaker throughout the water column during the early and late months of the ice-free season.

Specific Features

While all areas on figs. 6.12-15 show comparable seasonal cycles of MLD, HC and E, subtle differences can be observed concerning the extreme values of these variables, as well as their time of occurrence during the ice-free season. For upper heat content, regions covering Cabot Strait (01 & 02) show, on average, maximum HC values throughout the ice-free months. Minimum HC values are usually observed in the Estuary and the Gaspé Coast areas (07 & 08, as well as 05 and 06 for most months). This is in accordance with the relatively shallow MLD and cold surface waters. One interesting point is the warmer August-to-October upper 100 m on the Cape Breton side (01), likely to be the result of outgoing waters from the Shallows and central GSL. In general, the maximum HC occurs in August-September, except for area 05 where the largest HC happens in October. The seasonal cycle of the upper heat content closely follows that of SST. Finally, as we shall see in the next sections, although it is difficult to infer any useful information from the absolute HC fields, it is the rate of change of the upper heat content (dHC/dt) that is important in examining the heat budget, hence the thermal structure, of the Gulf upper layer. Regarding the MLD and $E_{0\text{-}30}$ fields, they appear to covary closely for most months. For example, during the first half of the ice-free season, the western region of the Gulf (areas 06, 07, 08 & 11) exhibits shallow mixed-layer depths as well as strongly stratified upper waters (most likely the result of fresh water runoff from the Estuary and the Baie des Chaleurs). Furthermore, when compared to the Shallows areas (12, 13, 15 & 16) the northeastern regions of the Gulf (02, 03, 04, and 01 for some months) are characterized by deeper MLD and weaker $E_{0\text{-}30}$ values for the June-August period. In general, the greatest (intraregional) MLD variability occurs during the early and late months of the ice-free season, while mixed-layer depths are rather shallow and relatively similar throughout the Gulf (excluding the Estuary - area 07) in September. Finally, the upper-layer static stability patterns of most areas are in agreement with the commonly believed scenario of a fresh water pulse originating from the Estuary/Baie des Chaleurs and being slowly advected through the Shallows towards Cabot Strait (Koutitonsky and Bugden, 1991).

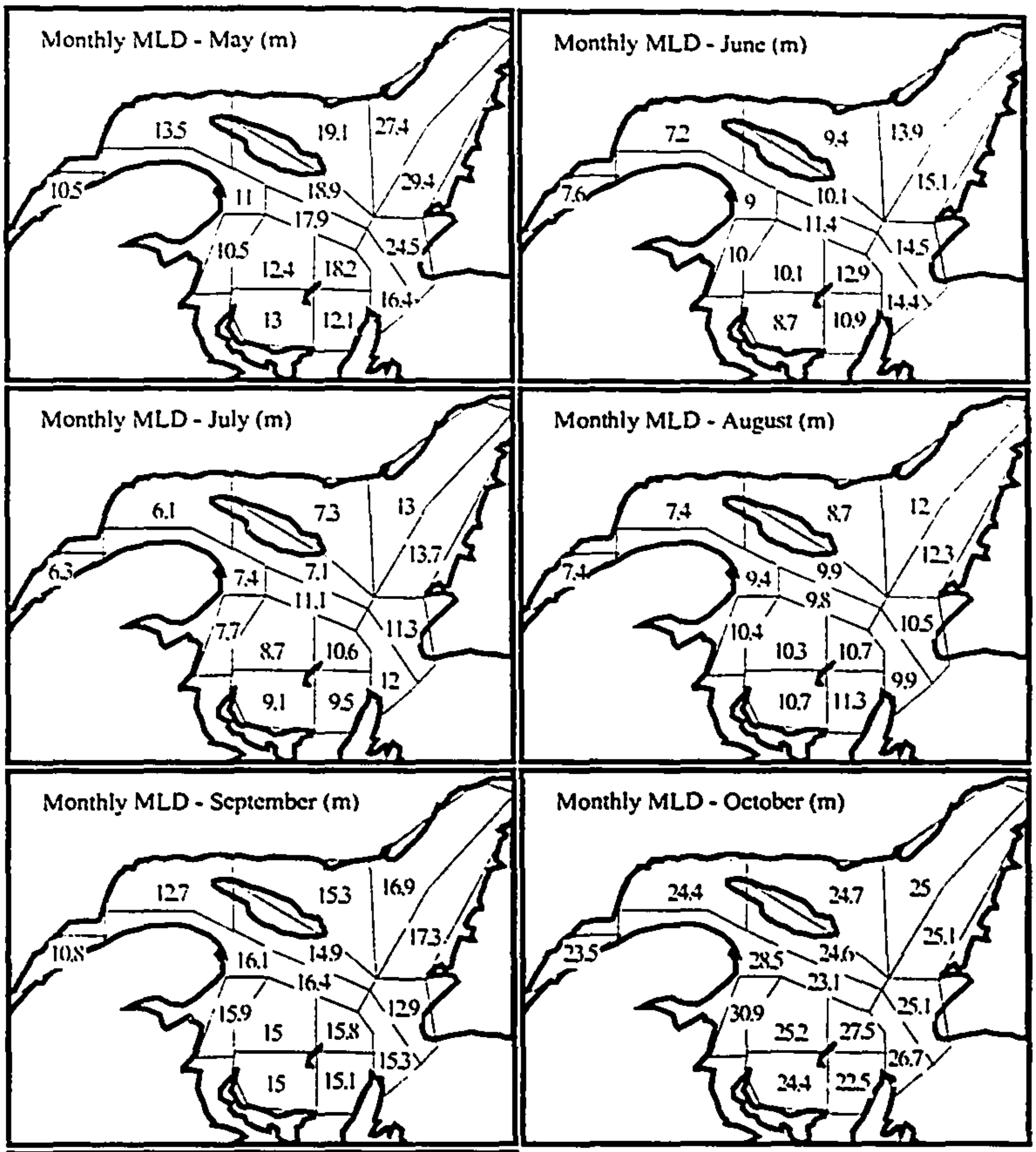

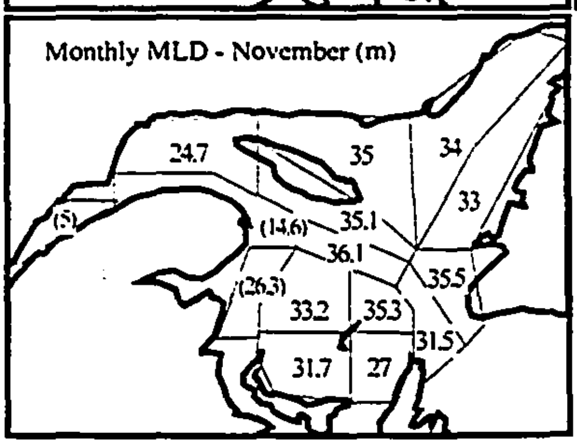

Figure 6.12: *Monthly Mixed-Layer Depth (MLD) climatology (m). (Due to the low water temperatures of November, values in parathenthesis for this month are suspicious).*

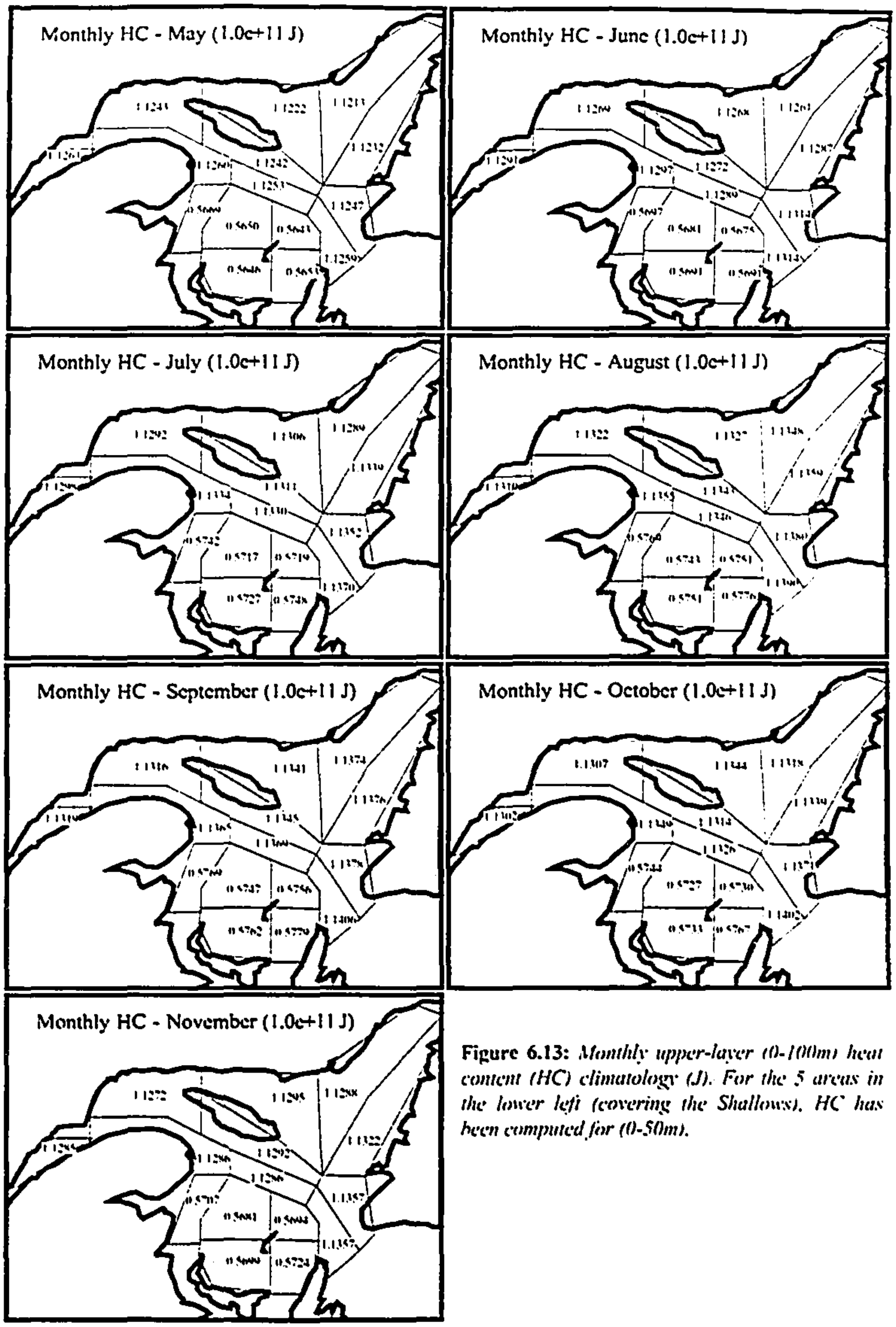

Figure 6.13: *Monthly upper-layer (0-100m) heat content (HC) climatology (J). For the 5 areas in the lower left (covering the Shallows), HC has been computed for (0-50m).*

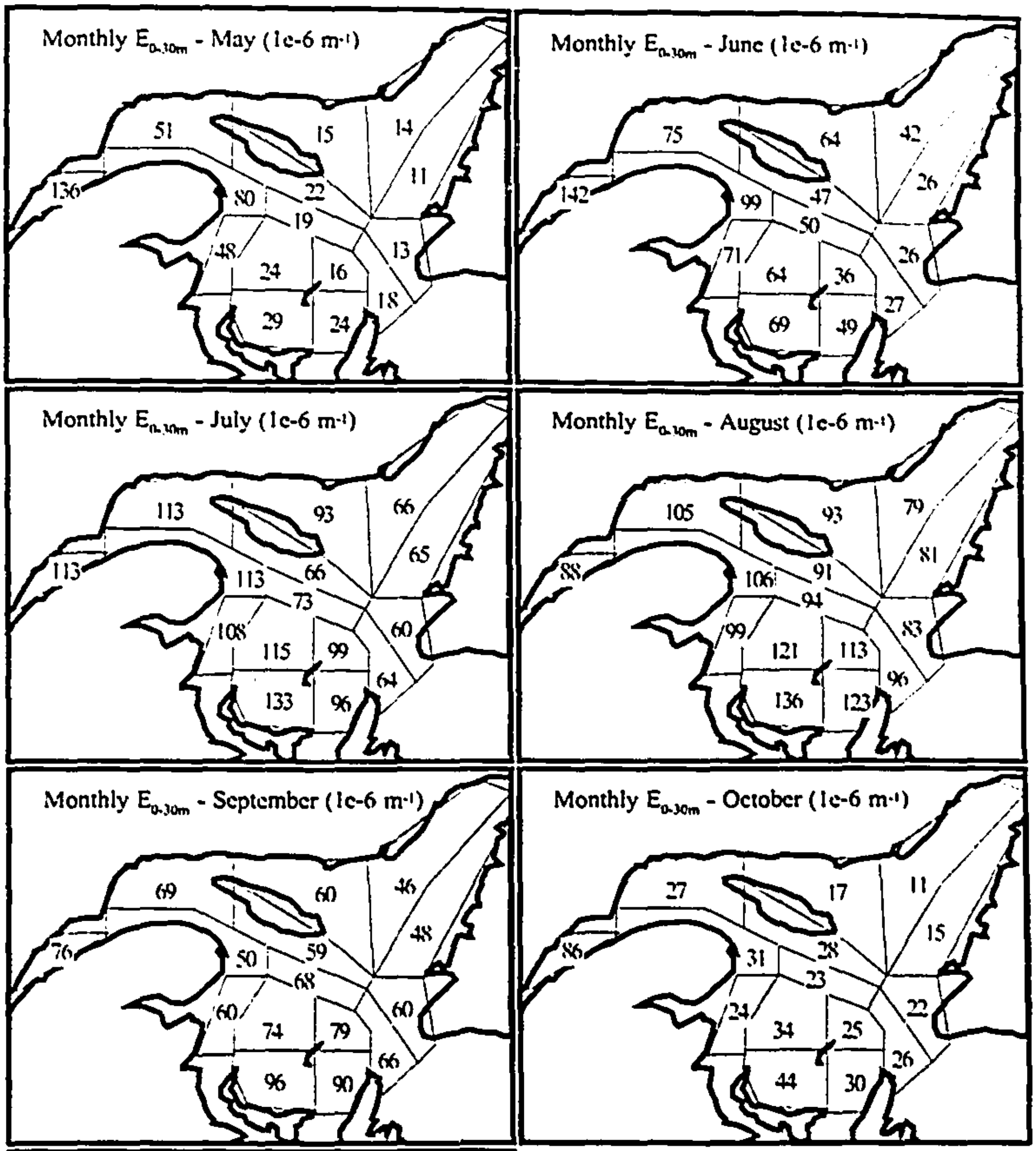

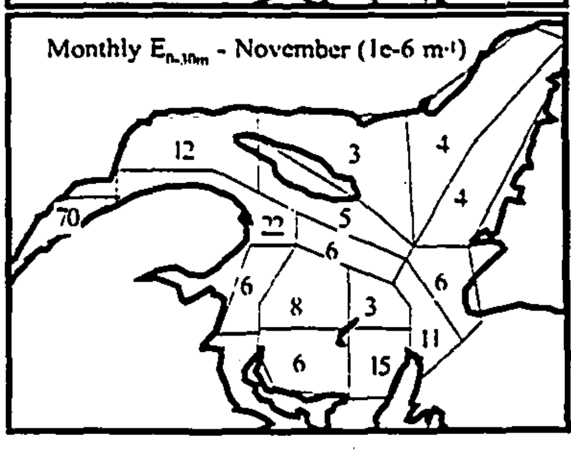

Figure 6.14: *Monthly upper-layer (0-30m) static stability (E) climatology (1/m).*

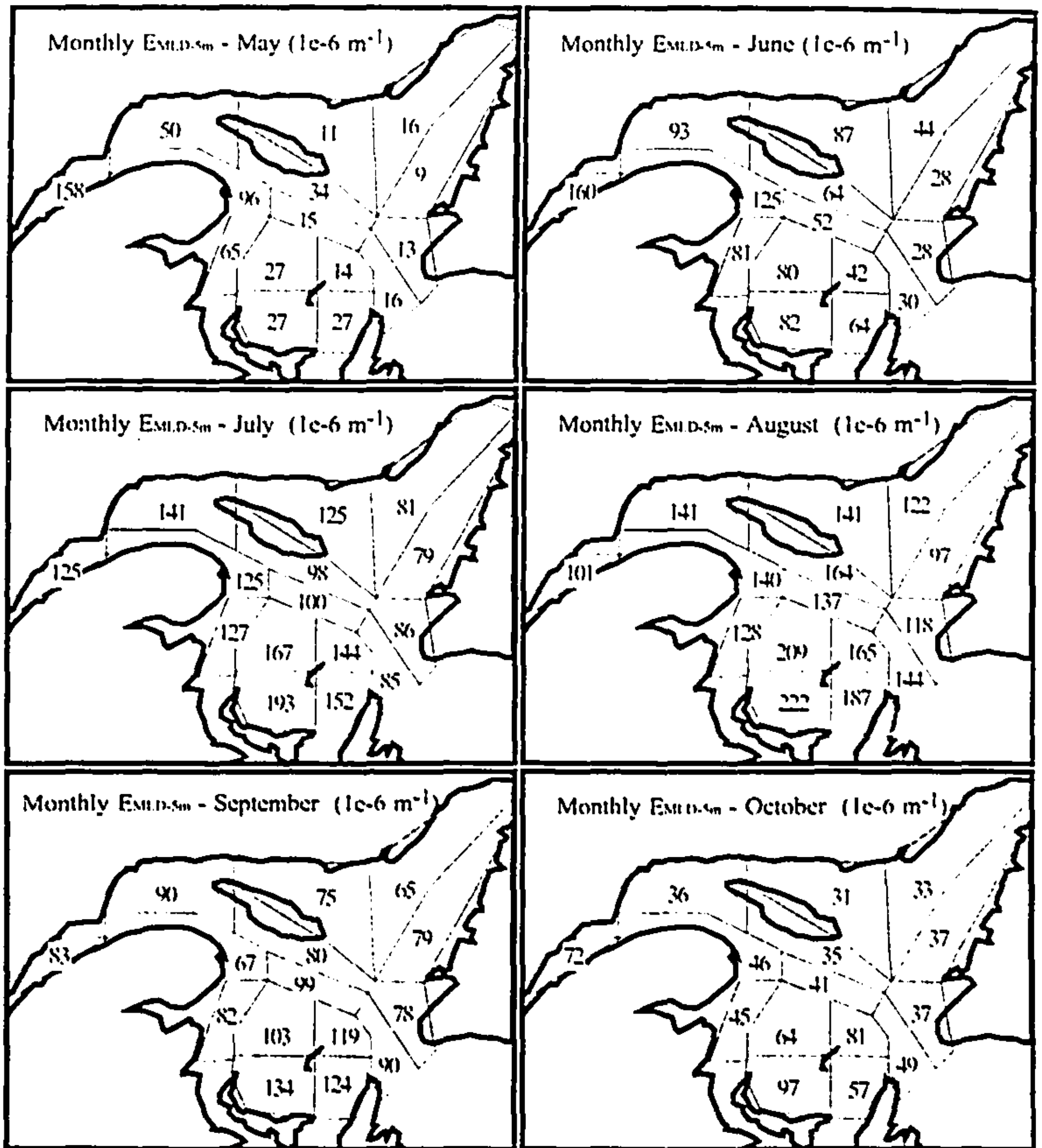

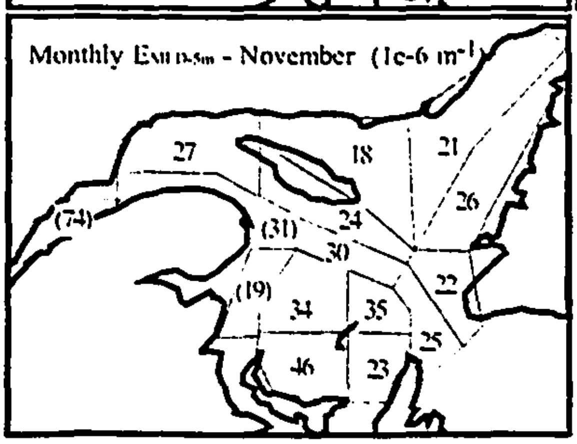

Figure 6.15: *Monthly climatology of static stability (E_{MLD-5m}) 5m below the mixed-layer. Values in parathenthesis during November are suspicious due to uncertain MLD values.*

6.3 Seasonal Evolution of the Upper-Layer Thermohaline Structure

In this section, the seasonal evolution of the upper-layer thermohaline fields are investigated using simple 1D calculations. First, a modified vertical heat diffusion model with parametrized eddy diffusivity is developed and used to examine the monthly temperature-depth fields of the upper 100m. Then, the mixed-layer depth seasonal cycle is analyzed in the context of wind mixing and surface heat flux effects. Finally, the stratification of the upper 50m for the ice-free period is calculated, and its monthly rate of change is compared with the effects of surface wind mixing and heat input.

6.3.1 Modified 1D Heat Diffusion Model with Parametrized Vertical Eddy Diffusivity

As a result of various atmospheric and oceanic processes, the upper-layer thermal structure (during the ice-free season) provides useful information about the oceanography of Gulf of St.Lawrence. For example, it is a useful indicator of the mixed-layer depth for most months/regions. It also provides important information about the stratification patterns throughout the GSL (minima, maxima, spatiotemporal distribution, etc.), which is of great value when studying near-surface biological activity. However, as explained in chapter 2, its structure is the result of several processes occurring on very short time scales (hours to days). Consequently, due to the lack of complete and unaliased time series, it becomes very difficult to accurately study its temporal evolution. Nonetheless, Umoh and Thompson (1994) proposed an original approach to this problem. In modifying the thermal diffusion equation (Umoh, 1992) and using a parametrized vertical turbulent diffusivity (K_v), they were able to incorporate several oceanographic features into a simplified 1D model, while using only monthly temperature and surface heat flux data. Following their approach, we developed a similar heat diffusion model and, with some additional approximations, we applied it to the GSL upper-layer T fields during the ice-free months. The model is now briefly described with a discussion of the results obtained. Model limitations are also discussed. The thermal structure is assumed to obey a simplified heat equation of the form (Umoh, 1992)

$$\frac{\partial T_{(z,t)}}{\partial t} = \frac{\partial}{\partial z}\left(K_{v(z,t)}\frac{\partial T}{\partial z}\right) + \begin{cases}\text{advection}\\ \text{horiz. diffusion}\\ \text{upwelling, etc..}\end{cases},$$

where K_v is the vertical turbulent diffusivity, and the bracketed right-end term consists of the remaining processes not explicitly modelled (horizontal diffusion and advection, upwelling, etc.). To estimate this "source-sink" term[9], Umoh and Thompson (1994) derived a method in which they related the term to the imbalance between the net surface heat flux (Q_{net}) and the local heat storage rate (dHC/dt). In multiplying the heat equation by ($\rho\, c_p$) and integrating it from the surface to some depth (100m in this case), we obtain the following heat budget equation (Frankignoul and Reynolds, 1983),

$$\underbrace{\frac{\partial HC}{\partial t}}_{\#1} \; \underbrace{- \; Q_{net}}_{\#2} = \underbrace{- \; \rho c_p K_v \frac{\partial T}{\partial z}\bigg|_{100m}}_{\#3} \; \underbrace{- \; \rho c_p \int_{100}^{0} \begin{Bmatrix} \text{advection} \\ \text{horiz. diffusion} \\ \text{upwelling, etc..} \end{Bmatrix} dz}_{\#4} \quad .$$

in which the term #1 represents the heat imbalance, and the term #4 includes the heat flux at the bottom as well as the depth integration of various effects (advection, upwelling, diffusion, etc.). With proper estimation of the bottom boundary condition (either set to zero or estimated) this relation represents the "depth-integrated" heat imbalance corresponding to the term #4 of the heat budget equation. Figure 6.16 displays the relation between dHC/dt and Q_{net} for various locations in the Gulf. From the main graph, we realize that, although the heat storage rate is very well correlated with the net surface heat flux, there remains some regional/temporal discrepancies from a "perfect zero" difference, as denoted by the departure from the correlation slope as well as by the variability shown in the top left panel of figure 6.16. However, various spatio-temporal redistribution schemes (e.g.: maximum at the surface with an exponential decay with depth; maximum in May with a slow decay during the summer of this heat imbalance; etc.) were tried and did not significantly improve the simulations. For this reason, the effects of the "heat imbalance" related processes (term #4 of the heat budget equation) have been not been included in the following results.

Concerning the model, one of its attracting features is the parametrization of vertical turbulent diffusivity. Umoh and Thompson (1994) realized the importance of seasonally varying K_v and proposed a parametrization of the form $K_v = K_o(1+aN^p)^{-1}$, where N is the buoyancy frequency and a,p are two adjustable parameters. Later, in a study of air-sea heat fluxes on the Newfoundland Shelf, Umoh et al. (1995) tried to include the mixing

[9]: Although we tested the same formulation as Umoh and Thompson (1994) in the GSL, we found it did not significantly improve the simulation results and, for reasons that will be explained in the text, decided to neglect its effects. Consequently, the reader should refer to the original manuscript of Umoh (1992) or Umoh and Thompson (1994) for a complete derivation.

Figure 6.16: *Monthly heat storage rates (dH/dt) and net surface heat fluxes (Qnet) for some regions (Cabot Str.: 01 and 02; northeast: 03; northwest: 06; and central GSL: 10). The top-left panel shows the monthly evolution of both Qnet (solid line) and dH/dt (dashed), whereas the main graph displays their linear regression. The small number beside each circle corresponds to the respective area #. The thick dashed line in the center represents the correlation (r=1), and the other thin dashed lines denote the 95% confidence interval of the model.*

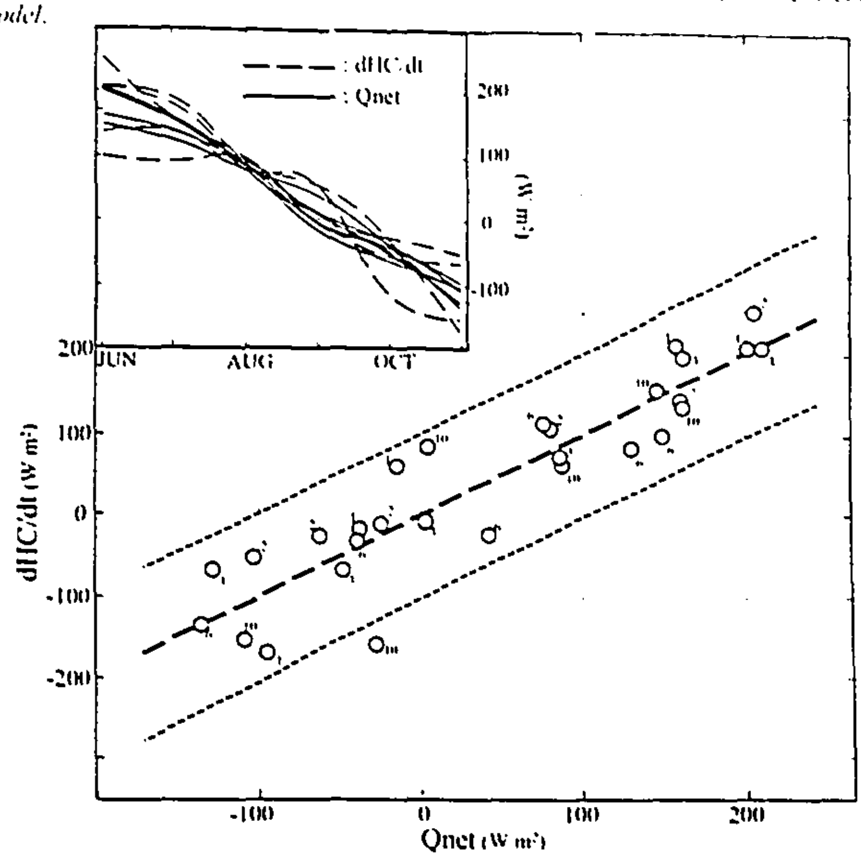

effects of the winds in replacing the constant K_o in the above parametrization with $K_w U^2 \exp(z/d_w)$. U is the long term mean wind speed and K_w, d_w are adjustable parameters. In this study, three parametrization schemes have been tested for K_v:

$$K_v = \begin{cases} K_o \text{ (constant)} \\ K_o(1+aN^2)^{-1} \quad \text{(method 1)} \\ aU_*^3(4\kappa N^2 z)^{-1} \quad \text{(method 2)} \end{cases}$$

The first two schemes are the same as those used by Umoh and Thompson (1994). The third parametrization (method 2) was developed from a constant stress layer approximation (Oakey, 1985), in substituting the TKE dissipation, ε, in $K_v = \varepsilon/4N^2$ (Osborn, 1980) by $\varepsilon = U_*^3 / kz$ (Oakey, 1985; Anis and Moum, 1995). Consequently, K_v of method 2 was parametrized as $aU_*^3 / 4kN^2z$, where U_*, k and N are the wind friction velocity, the buoyancy frequency and the von Karman's constant, respectively, and a is the only adjustable parameter, which may be thought of as an "enhancement" parameter to account for the constant stress scaling discrepancies near the surface (Anis and Moum, 1995). This approach has a few advantages over those proposed by Umoh and Thompson (1994) and by Umoh et al. (1995): first, it involves only one adjustable parameter, a; also, it is derived directly from turbulent boundary layer theory (assuming a constant stress layer); finally, it incorporates the wind mixing effects via monthly averaged values of 12hourly U_*^3 time series, which is more representative of mixing than the 2nd or 3rd power of the monthly averaged wind speed (see chapter 4 for details). Concerning the implicit details of the model, they are similar to those of Umoh (1992), namely: the heat equation is expressed in finite difference form using a stable, second order accurate, scheme (a.k.a. Crank-Nicholson - Kincaid and Cheney, 1991) on 10m x 1month computational grid; the model is forced by calculated surface heat fluxes (z = 0m, chapter 5) and observed temperatures (at z = 100m, and at t = May for the initial condition); it is run cyclically until a steady state is reached; and the monthly heat flux during the winter months are interpolated between Q_{net} of November and May using larger scale estimates made by Bugden (1981). Finally, the diffusivity parameters are adjusted by minimizing the root mean square (RMS) error difference between observed and modeled temperatures for the ice-free season, such that:

$$\overline{Err}_{RMS} = \sqrt{\frac{1}{N}\sum_{1}^{N=7\times 11}\left(T(z,t)_{model} - T(z,t)_{observ.}\right)^2},$$

where N = 7 months X 11 vertical levels = 77 grid points.

Regions	$K_v = K_0$	K_v (method 1)	K_v (method 2)
Area 01	(°C) 6.09	3.50	3.99
Area 02	4.92	2.88	3.76
Area 03	4.20	2.55	3.94
Area 04	3.16	1.55	2.19
Area 05	7.18	3.44	3.56
Area 06	1.25	0.70	0.75
Area 10	4.34	2.16	2.80

Table 6.4: *Simulation errors (°C) for various regions and/or Kv.*

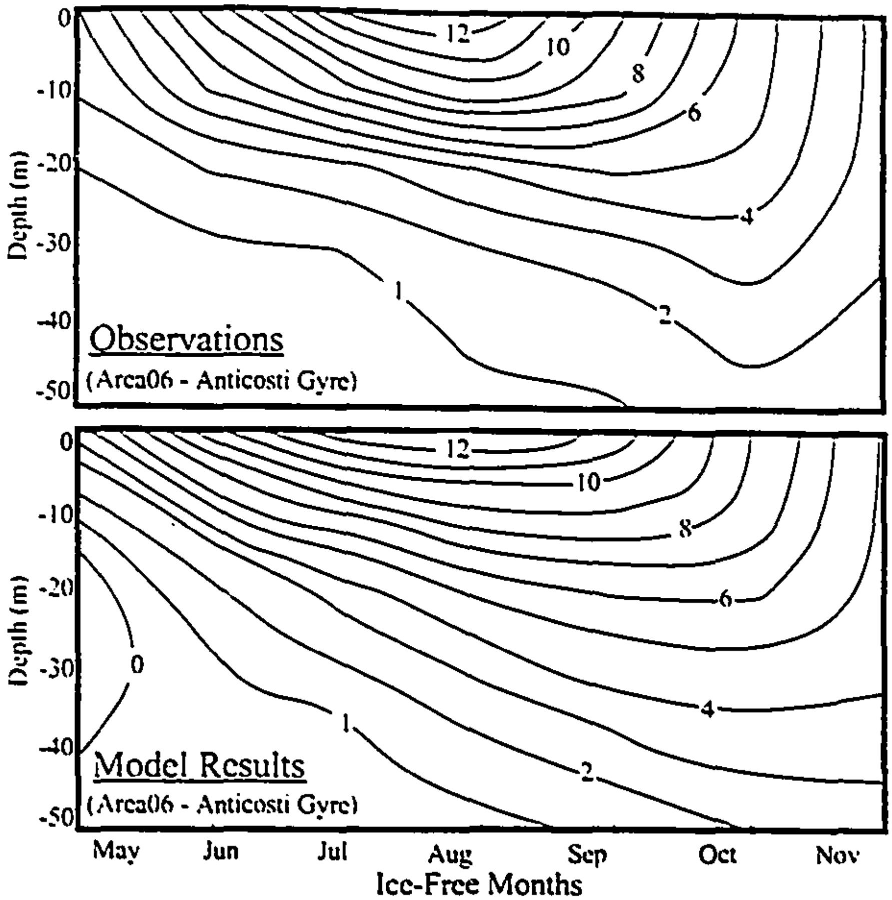

Figure 6.17: *Monthly-depth distributions of temperature for area 06 - Anticosti Gyre - as predicted from a 1D modified heat diffusion calculation, and as observed from climatology. The top panel shows the climatology for the upper 50m during the ice-free months. The lower graph displays the model results using a constant-stress parametrization for the vertical eddy diffusivity and no advection. The RMS error for this simulation was less than 0.8 °C (see text for details).*

RMS error for various simulations are tabulated above (table 6.4) and figure 6.16 shows the observations and the model results for the Anticosti Gyre region simulation. On table 6.4, it is obvious that the variable $K_v(z,t)$ - method 2 - yielded better results than the constant K_0, and that the results obtained using the K_v parametrization of Umoh and Thompson (1994) outperformed both methods. Also interesting is the rather large interregional variability of the simulation errors. Table 6.4 presents the results for 3 diffusivity schemes, all excluding the effects of advection. From this, it is clear that some regions agree very closely with the simplified 1D simulations whereas, for other areas, the present heat diffusion model assumptions perhaps oversimplified the reality. For the constant K_0 scenario, the eddy diffusivity values ranged from 0.8×10^{-4} to 2.65×10^{-4} m^2/s.

Figure 6.17 displays the results for the best simulation. From this picture, we note that the simulated SST are in rather close agreement with observations but that the model seems to have problems in reproducing a cold intermediate layer (this last point was even more obvious among the other simulations). Umoh and Thompson (1994) investigated the necessary conditions allowing the formation of a similar feature (i.e.: a cold intermediate layer) on the Scotian Shelf and found that both surface heat forcing and advection (via a heat imbalance parametrization) were required. Concerning the advection of a salinity minimum leading to the previously discussed upper-layer stability patterns, although it was not modeled explicitly, it was nonetheless taken into account since the K_v parametrization methods 1 and 2 both use, in their formulation, the monthly-depth distributions of buoyancy frequency (deduced from climatology). Finally, although this simplified heat diffusion model reproduced surprisingly well the upper layer thermal structure for some regions, it suffers from several problems. Perhaps its greatest difficulties arise from the uncertain heat budget during the 5 winter months. As mentioned earlier, not only was there some heat imbalance between dHC/dt and Q_{net}, but the interpolated heat flux fields between November and May are rather uncertain. Consequently, we cannot be sure if the model simulations were done with an excess or a deficit of heat.

6.3.2 Simplified 1D Calculations of Mixed-Layer Depth Seasonal Cycle

As explained earlier, the mixed-layer seasonal evolution is mainly the result of short scale episodic events, such as storms (Price et al., 1986). Consequently, a complete and accurate modelling of the upper-layer spatio-temporal structure often requires complete and accurate small scale time series (of winds, air and sea temperatures, salinity, heat fluxes, ocean currents, etc.). Nevertheless, the equation governing the 1D evolution of the mixed-layer depth is relatively simple while containing useful information as to which mechanisms cause MLD to deepen or shoal. In his 1D layer model of the seasonal pycnocline, Stigebrandt (1985) defines the conservation equation for the MLD as follows:

$$\underset{\#1}{\frac{dMLD}{dt}} = \underset{\#2}{w_e} + \underset{\#3}{\begin{cases}\text{advection,}\\ \text{horiz. diffusion,}\\ \text{upwelling, etc..}\end{cases}} \quad \text{for } w_e \geq 0,$$

in which the term #3 denotes some of the effects (advection, upwelling, horizontal diffusion, etc.) that were not explicitly included in this equation. The entrainment velocity, w_e, is then expressed as combination of wind mixing effects (first term on the right) and surface buoyancy flux (second term), such that:

$$w_e = \left(\frac{2m_o U_*^3}{g \frac{\Delta\rho}{\rho} MLD} \right) - \varepsilon\, g \left(\frac{\alpha Q_{net}}{\rho c_p} + \beta Q_{fresh} S_{surf} \right),$$

where the symbols follow the notation used throughout this thesis. Based on a literature survey and previous experimental and hydrographic results, Stigebrandt (1985) proposed $m_o \approx 0.6$, and ε to be equal to 0.05 when the buoyancy term is negative (right-end term in the above equation), and $\varepsilon = 1$ otherwise. As a first approximation, we can neglect the haline effects on the buoyancy flux and take the monthly averaged values of the remaining term in the w_e equation. In this way, we can compute monthly averages of dMLD/dt based on the mixed-layer depth climatology and compare the results with the monthly averaged wind and buoyancy forcing fields, as expressed by the entrainment relation. Since we are no longer dealing with an initial value problem in which the errors are cumulative, assessment of the seasonal MLD deepening rate is possible through simple linear regression.

Monthly values of both calculated and observed dMLD/dt for some regions of the Gulf are displayed in figure 6.18 (top left panel) as well as their linear regression (main graph). From this, it is obvious that both calculated and observed MLD change rates covary, with a linear regression coefficient, $r = 0.84$. From the top left panel, we notice that the largest discrepancies between the observations and this simple 1D calculations occur in June, coinciding with the strongest effects of fresh water runoff on the upper-layer stratification. During this early period, the MLD deepening rates are too strong in comparison with the climatological rates, hence suggesting that buoyancy flux from fresh water runoff is important, especially in late spring and early summer, and should be considered. However, for the remainder of the ice-free period both MLD deepening rates are in surprisingly close agreement despite the simplicity of this 1D calculation. Consequently, strictly from a monthly MLD deepening point of view, assuming a one dimensional vertical behaviour for the mixed-layer depth seems to be a valid approximation (even more so from July on).

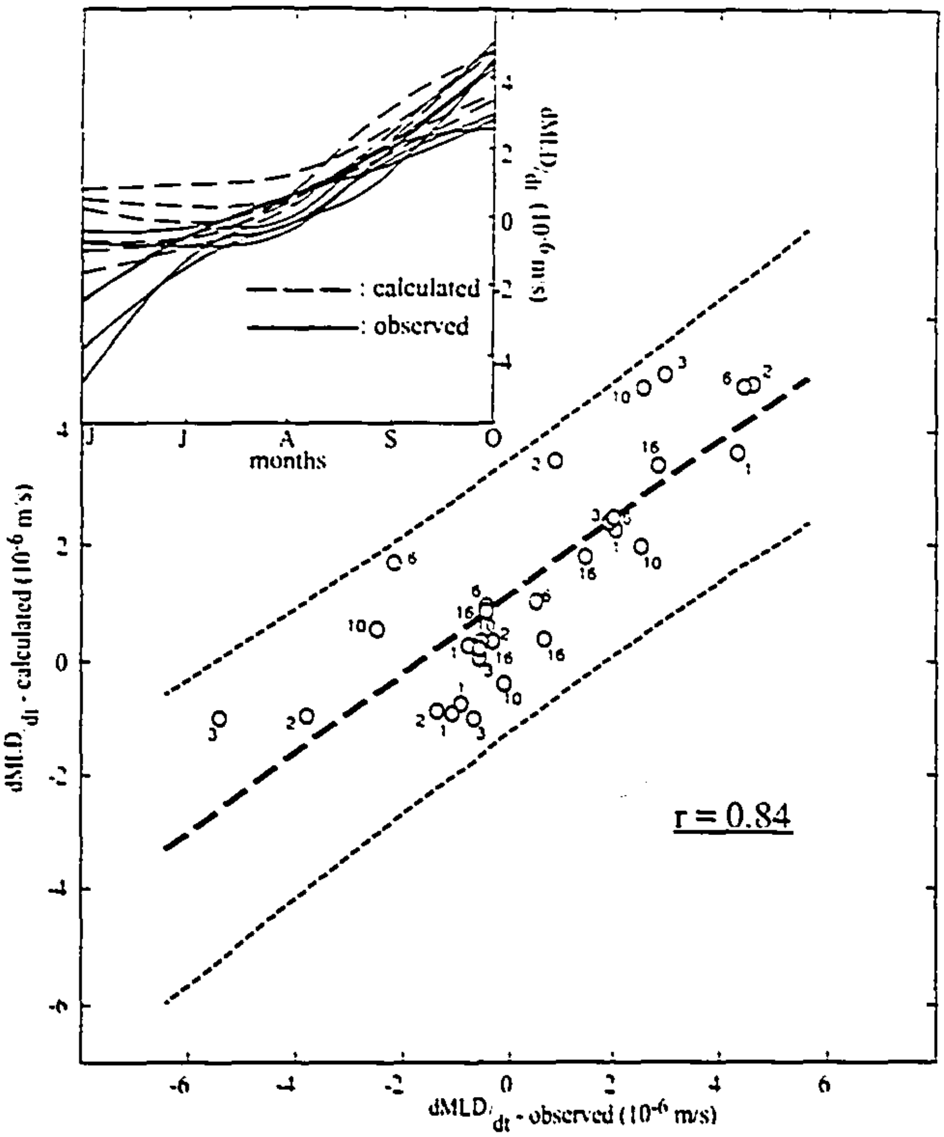

Figure 6.18: *Monthly mixed-layer change rates (dMLD/dt) - as predicted from 1D relationships and observed from climatology - for some regions of the Gulf (Cabot Str.: 01 and 02; northeast: 03; northwest: 06; central: 10; and southern GSL: 16). The top-left panel shows the monthly evolution of both observed (solid line) and calculated (dashed) dMLD/dt values (in m/s), whereas the main graph displays their linear regression. The small number beside each circle corresponds to the respective area #. The thick dashed line in the center represents the correlation (r=0.84), and the other thin dashed lines denote the 95% confidence interval of the model.*

6.3.3 Simplified 1D Calculations of Stratification Seasonal Cycle

Once again using one dimensional upper-layer calculation, the effects of both temperature and salinity will be examined in the context of stratification. Simpson and Bowers (1981) used potential energy arguments based on Kraus and Turner (1967) to model the water column density structure. In their formulation, the stratification was expressed as changes in the potential energy (PE) relative to the well mixed condition, and is defined by:

$$PE = \int_{h}^{0m} (\rho - \overline{\rho}) g z \, dz, \quad \text{where} \quad \overline{\rho} = \int_{h}^{0m} \rho \, dz .$$

Increases in PE occur as a result of wind stirring and tidal mixing, while PE decreases with increasing stratification due to surface heating, river discharge and runoff. Consequently, the change rate of PE (hence stratification) is defined by (Simpson and Bowers, 1981):

$$\frac{dPE}{dt} = -\left(\frac{\alpha\, g h\, Q_{net}}{2c_p}\right) + \zeta\, \rho_a U^3 + \begin{cases}\text{advection,} \\ \text{tidal mixing,} \\ \text{runoff, etc..}\end{cases}$$

where h is the depth of the water column, ρ_a is the air density and ζ is a constant including the wind drag coefficient and a wind mixing efficiency parameter. In their initial formulation, since they tested their model mainly in shelf seas, Simpson and Bowers (1981) assumed h to be the water column depth, tidal mixing effects to be important but to neglect advection, river runoff and rainfall. They also realized that the mixing efficiencies of both tidal mixing and wind stirring varied seasonally as a function of upper-layer stability. However, since this 1D stratification calculation is performed here in the context of monthly data (as for the previous two sections), simplifications will be made such that the analysis is restricted to the upper 50 m. Moreover, following the results of Pingree and Griffiths (1990), effects of tidal mixing will be neglected, along with those of advection, runoff and rainfall.

From these two simplified relations, monthly PE change rates were obtained via calculations and observations, and compared. Figure 6.19 displays the monthly evolution of dPE/dt (calculated and observed) for some regions of the Gulf (top left panel) as well as their mutual linear regression. Again, from the high correlation (r = 0.85), we realize that this simplified calculation of monthly PE change rates covary with the observational trend. However, important discrepancies are observed from the monthly evolution of both quantities. More specifically, the calculated values of dPE/dt are larger than the observations for most of the areas and months. Two causes are possible: first, since runoff tends to render the upper layer more stratified, its omission is reflected in the results; moreover, as pointed out by Simpsons and Bowers (1981), the effects of wind mixing should not depend solely on the wind speed, but vary with the water column stratification. Finally, although simple in its formulation, we realize that this 1D potential energy calculation does reproduce well the seasonal rate of change of the upper-layer stratification.

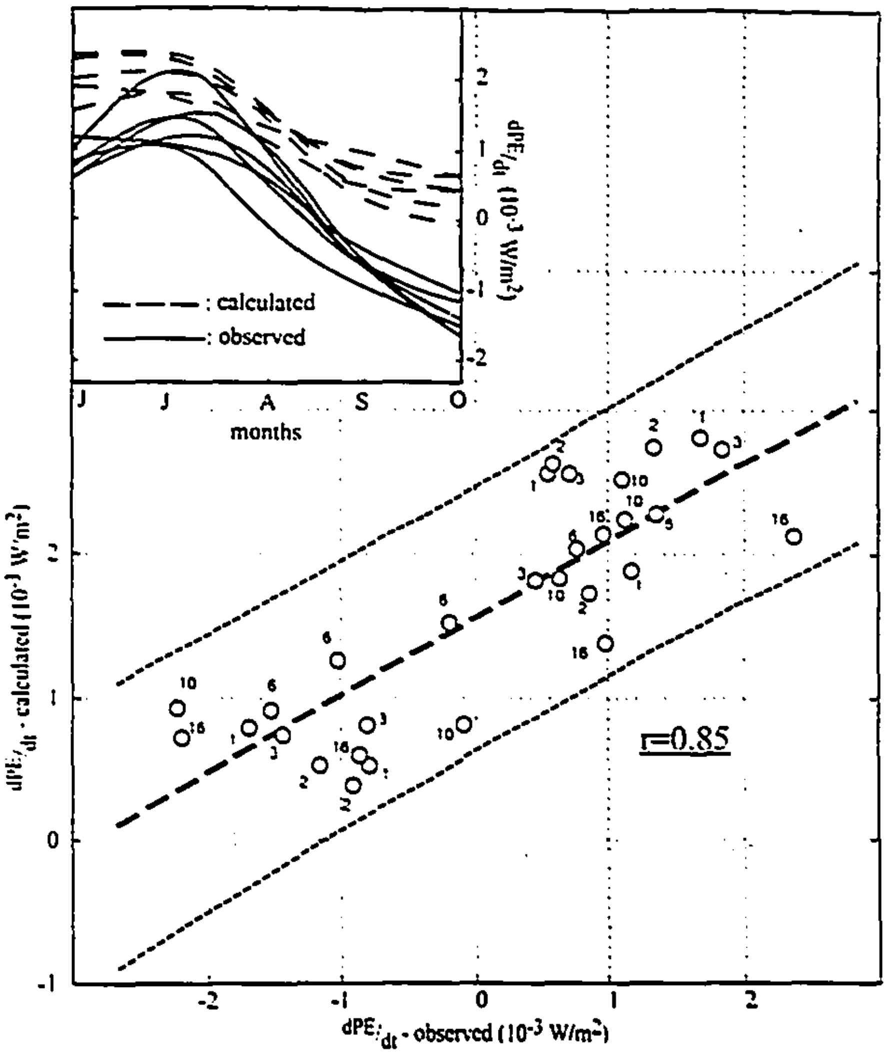

Figure 6.19: *Monthly "relative" potential energy change rates (dPE/dt) - as predicted from 1D relationships and observed from climatology - for some regions of the Gulf (Cabot Str.: 01 and 02; northeast: 03; northwest: 06; central: 10; and southern GSL: 16). The top-left panel shows the monthly evolution of both observed (solid line) and calculated (dashed) dPE/dt values (in W/m2), whereas the main graph displays their linear regression. The small number beside each circle corresponds to the respective area #. The thick dashed line in the center represents the correlation (r=0.85), and the other thin dashed lines denote the 95% confidence interval of the model.*

6.4 Preliminary Study of the Interannual Variability

Although this thesis essentially focuses on seasonal aspects of the upper-layer, this section will make use of the small number of good time series available (Ta, Ug, SST), as well as the satellite-derived monthly SST maps in recent years to present some aspects of the year to year changes. This is not a complete study of the extraseasonal climatic variability but rather a brief and preliminary examination of the longer time scales fluctuations of some oceanographic fields. The relation between anomalous mixed-layer depths and wind mixing will first be presented, followed by a correlation analysis of the sea surface and air temperature anomalies. Finally, the previously described heat diffusion model will be applied to the 1987 and 1990 years.

6.4.1 Mixed-Layer Depth and Wind Mixing Anomalies

We now investigate the year to year variations in the monthly averaged mixed-layer depth throughout the GSL. Both wind mixing and net surface heat flux influence the monthly evolution of MLD. Hence, anomalous mixed-layer values may be related to anomalies in these fields (E_w and Q_{net}). However, since several parameters are involved the Q_{net} calculations, all covering a different time window in their respective dataset, it is not possible to reproduce net heat flux values for all the years where MLD anomalies (MLD', the prime denoting the departure from the monthly mean) were calculated. On the other hand, the geostrophic wind dataset constitutes rather good time series for it is sampled in a continuous fashion, twice daily every day for the last 45 years. Consequently, MLD' can be compared with wind mixing anomalies (both U_g' and E_w') for two different seasonal time periods, i.e.: the earlier months of the ice-free season (May, June and July) and the later months (Sep, Oct, Nov). The first period (MJJ) corresponds to a strong positive surface heat flux and fresh water input, processes which oppose the deepening effect of wind mixing, whereas the later months (SON) are associated with weak negative Q_{net} values which helps the mixing action of the wind deepen further the mixed-layer (Turner, 1981). Table 6.5 shows the correlation coefficients between monthly anomalies of mixed-layer depth (MLD'), geostrophic wind (Ug') and water mixing energy (Ew') for the early (MJJ) and late ice-free season (SON) for some regions of the GSL (Cabot Strait: area 01, northeast Gulf: area 03, northern GSL: area 05, northwestern GSL: area 06, central and southern Gulf: areas 10 and 16.). As can be seen, mixed-layer depth anomalies did not correlate well with anomalies in the geostrophic wind nor with those of E_w. This may be

Area #	MLD' -vs- Ug' (MJJ)	MLD' -vs- Ug' (SON)	MLD' -vs- Ew' (MJJ)	MLD' -vs- Ew' (SON)
01	0.10	0.28	-0.01	0.05
03	0.20	-0.16	0.04	-0.22
05	-0.28	0.25	-0.48	0.25
06	-0.13	0.23	0.21	0.18
10	0.14	0.12	0.23	0.12
16	0.10	0.37	-0.09	0.30
GSL	0.06	0.14	-0.02	0.07

Table 6.5: *Correlation coefficients between monthly anomalies of mixed-layer depth* (MLD'), *geostrophic wind* (Ug') *and water mixing energy* (Ew') *for the early* (MJJ) *and late ice-free season* (SON).

explained by the rather poor temporal resolution of the MLD series (but it is difficult to assess truly). Although the monthly averages of U_g and E_w were computed from 12 hourly time series, only a few MLD observations were used to produce the MLD' for specific months and regions in most cases. Since the mixed-layer response to wind mixing is non-linear (as seen in the previous sections) and MLD may vary substantially over a very short time (e.g. 20 to 30 m increase in 2 days, as shown in chapter 2), this results in a highly aliased signal for the MLD' time series. Hence, a true representation of the mean mixed-layer depth for a specific month/region cannot be achieved with a few scattered hydrographic observations without aliasing the MLD values.

6.4.2 SST and Air Temperature Anomalies

In this section, we investigate monthly anomaly time series of SST (SST') and T_a (T_a') for 6 of the GSL areas. The air temperature time series are those of weather stations neighbouring the hydrographic areas analyzed, and are shown in Table 6.6. These 6 areas were chosen for their larger number of monthly SST' observations as well as for their proximity to a weather station. Correlation analysis was done for both SST and temperature at a depth of 30 m but, since the 30 m anomaly time series behaved similar to that of the sea-surface[10], only the sea-surface results will be reported in this study.

Area #	01	02	06	11	12	16
Station name	Sydney	Stephenville	Sept-Iles	Chatham	Grindstone Is.	Grindstone Is.

Table 6.6: *6 GSL areas and corresponding weather stations chosen for the air-sea temperature correlations*

[10]: For e.g., anomalies of SST and T at 30m, for area 01, were significantly correlated (r = 0.9).

SST' and T_a' were linearly correlated at zero lag and at a lag of one month (where SST' was lagging T_a' by a month, i.e.: SST'_{jun} -vs- Ta'_{may}). The motivation for performing a lag correlation originated from looking at the monthly climatologies for both air and surface water temperatures (chapters 4 and 6), and noticing that both summer seasonal cycles followed one another closely with a lag of one month (which is probably due to the larger thermal inertia/response of water, as noted in Table 2.1). The analysis was done individually for each area and month, for combinations of areas and combinations of months, and for all the anomalies grouped together, as shown in Table 6.7.

	area01	area02	area06	area11	area12	area16	All 6 areas
May - no lag	- 0.35	- 0.41	0.02	- 0.21	0.07	- 0.07	- <u>0.21</u>
" (1month lag)	—	—	—	—	—	—	—
Jun - no lag	- 0.15	- 0.05	0.02	0.15	- 0.12	0.31	0.03
" (1month lag)	0.06	0.50	0.44	0.01	0.28	0.17	<u>0.20</u>
July - no lag	0.25	- 0.05	- 0.10	0.25	0.61	0.42	<u>0.24</u>
" (1month lag)	0.58	0.36	0.12	0.47	0.51	0.69	<u>0.46</u>
Aug - no lag	0.19	- 0.29	- 0.09	0.37	0.18	0.18	0.12
" (1month lag)	0.76	0.63	0.39	0.37	0.78	0.71	<u>0.61</u>
Sept - no lag	- 0.28	- 0.18	0.31	0.23	0.16	0.58	0.13
" (1month lag)	- 0.13	- 0.44	0.15	0.36	0.17	0.44	0.13
Oct - no lag	0.58	0.14	0.25	- 0.06	0.09	0.16	0.15
" (1month lag)	0.49	0.71	0.56	0.16	0.55	0.46	<u>0.40</u>
Nov - no lag	0.23	0.17	0.33	- 0.27	0.05	0.17	<u>0.16</u>
" (1month lag)	0.60	0.67	0.57	0.08	0.60	0.22	<u>0.53</u>
All 7 months	0.06	- 0.04	0.16	0.09	0.13	<u>0.22</u>	<u>0.09</u>
" (1month lag)	<u>0.40</u>	<u>0.41</u>	<u>0.35</u>	<u>0.27</u>	<u>0.43</u>	<u>0.41</u>	<u>0.37</u>

Table 6.7: *Coefficients of linear correlation between anomalies of SST and air temperature (with and without a one month lag). Underlined coefficients were found statistically significant at the 95% level.*

In general, it is fair to say that the air temperature anomalies correlated somewhat better with SST' at a one month lag than at no lag, as expressed from the tabulated coefficients of Table 6.7. Although the linear coefficients are moderate (around 0.4), they seem to agree with earlier results proposing that air temperature and SST trends were correlated (El-Sabh, 1973). However, air temperature anomalies alone cannot account for the entire variability observed in the sea-surface thermal fields, and it should be remembered that the net heat flux, as reported by Phillips (1981), is the main physical parameter influencing the SST for regions away from the coast, where horizontal currents are moderate. Consequently, correlation analysis with the air temperature can only "see" part of the variability for there are several other physical parameters entering the net surface heat budget (chapter 2), all interacting in a complex fashion.

6.4.3 Monthly Composites of AVHRR-derived SST Fields for 1987 and 1990 - a Case Study

In this last section, monthly AVHRR-derived SST fields are analyzed for the ice-free seasons of 1987 and 1990. The motivations for using these are as follow: the monthly maps (as described and shown in appendix 3) constitute monthly fields of very good quality for they have a spatial resolution of approximately 11km, they were produced from monthly averaged "pixels" and hence truly represent the average SST for each month , they had only a few "bad pixels" per images, and their quality has been assessed carefully by the algorithms/operators of NOAA/NASA (refer to the appendix for more details.). The data display interesting regional SST differences between the two analyzed years. Complete monthly atmospheric forcing data (Ta, Cn, U, r, etc.) were also available for 1987 and 1990.[11] Below, some qualitative comparisons are given between these SST fields and the corresponding atmospheric fields, followed by a monthly heat diffusion model analysis.

SST differences between 1987 and 1990 ice-free months:

Although no overall trend can easily be established between 1987 and 1990 (for warmer regions during a month are often found colder during another), some interesting (and common) hydrographic features can be observed: presence of cold water through the Strait of Belle-Isle; warm surface waters covering the Magdalen Shallows; weak signatures of colder waters along the GSL north shore and, to a lesser extent, along the southern coast of Anticosti Island, etc. Consequently, these SST fields can also be compared with the monthly climatological maps discussed earlier. A first attempt was made to explain the local surface temperature differences between various 1987 and 1990 months by spatial correlations with corresponding air temperature fields. These fields were computed using

[11]: They were also "free of charge" via the NOAA/NASA Pathfinder AVHRR Oceans dataset program, and 1987 & 1990 were the only two years available at the time (i.e., in which the quality analyses were completely done by the NOAA/NASA Pathfinder AVHRR Oceans dataset program).

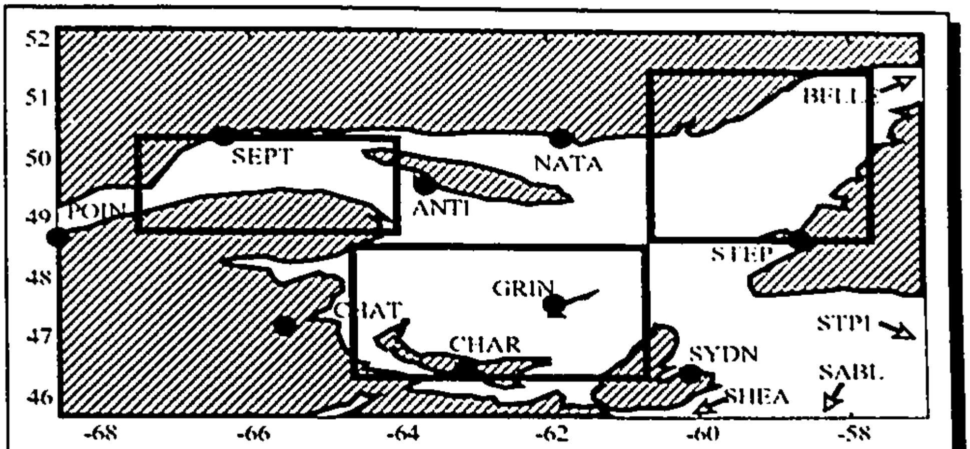

fig. 6.20: *Locations of the 3 regions of interest as well as the weather stations.*

AES data archived for the same weather stations mentioned in chapter 4 and using additional monthly temperature records from 5 more stations scattered around the GSL (the use of these 5 extra stations was possible since only two recent years were needed for the analysis - 1987 and 1990). These fields are displayed in the appendix, along with the monthly satellite-derived cloud fractions. To capture some regional aspects (in both SST and T_a fields), the GSL was segmented into three large areas - the North-West (NW), the North-East (NE), and the South-Central GSL (SC) - as shown in figure 6.20.

	NW	NE	SC	GSL
May	0.57	0.05	0.31	-0.27
June	-0.33	0.56	0.07	0.55
July	0.16	0.55	0.08	0.32
Aug	0.40	0.03	0.56	0.77
Sep	0.31	-0.25	-0.62	-0.13
Oct	-0.02	-0.08	0.37	0.16
Nov	-0.10	0.19	-0.08	0.11
ALL	0.40	0.29	0.25	0.30

Table 6.8: *Correlation coefficients between air temperature and SST for the 1990-1987 difference.*

Afterward, each AVHRR-SST observation was correlated with its corresponding T_a value and correlations were also performed between temperature differences, i.e.:

(SST90-SST87) versus (Ta90-Ta87) for each month/location and for the entire GSL as well. Unfortunately, no significant relation was found between both fields, at zero lag as well as at +/- 1 and 2 months lag (see table 6.8). One possible explanation for this might be that the sea surface gains (or loses) energy via the net surface heat flux which is function of air temperature and several other factors (see chapters 2 and 5). Hence, the heat flux contributions associated with only air temperature might not be sufficient to strongly influence the SST behaviour.

Model Results for the 1987 & 1990 Case Study

Following the rather poor correlation results between air and sea surface temperatures, heat flux fields were computed for the ice free months of both years and the resulting monthly Q_{net} fields averaged over the three regions, and a more complete heat transfer study was undertaken using the modified 1D thermal diffusion model described earlier. To perform the analysis, simulations were done several times in order to find the optimal eddy diffusivity parameters (different for all three areas, but similar for each month). Since only surface temperatures were available, K_v as well as the initial and bottom boundary conditions used corresponding climatological values. This is a rather coarse approximation given that K_v depends strongly on N, and that upper-layer stratification was found to follow closely SST fields (see earlier sections of this chapter). Nevertheless, simulations were performed and the results are displayed on figure 6.21. For this, we note that the model's SSTs were generally higher than the observations. More specifically, sea surface simulations for the NW area were the worst (with observed temperature differences as high as 5°C), whereas those for area NE and SC did a little better overall. Also interesting to note for the northeast and south-central cases are the relatively good agreement between the observed and simulated SST difference trends (i.e., $SST90_{obs.}$-$SST87_{obs.}$ versus $SST90_{model}$ - $SST87_{model}$). In conclusion, although the model did very poorly in simulating the northwestern sea surface temperatures, the relatively better NE and SC results - indicative of heat flux influence on SST differences - should be considered with caution since the model was forced with observed ice-free surface heat fluxes but with arbitrary "climatological" subsurface temperatures.

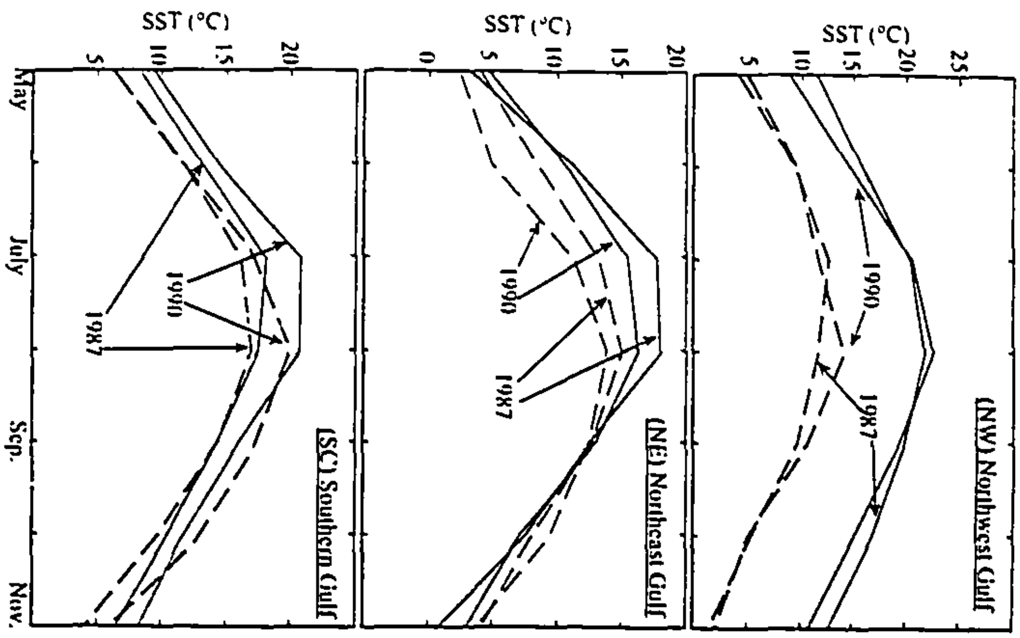

Figure 6.21: *1987 and 1990 monthly sea surface temperatures averaged over 3 regions of the Gulf (NW: 48.75N to 50.00N, 68.00W to 64.00W; NE: 48.50N to 51.00N; 60.75W to 57.50W; and SC: 46.00N to 48.50N; 64.50W to 60.75W.). The dashed lines denote the monthly averaged SST as observed from the NOAA-AVHRR composite images (see text for details), whereas the solid lines display the results of a 1D modified heat diffusion calculation.*

6.5 Summary

In conclusion, the monthly evolution of the upper-layer vertical thermohaline structure and related quantities have been described in this chapter. Their overall behaviour seem to agree "qualitatively" with the usual theory, as briefly reviewed in chapter 2. More precisely, monthly depth distributions of T and S were used throughout the Gulf (15 areas) to assess the seasonal evolution of the upper-layer (i.e.: T, MLD and ρ). Using simple 1D calculations (heat diffusion, MLD, stratification), it was also found that the upper-layer could be relatively well modeled for most areas by considering only the vertical processes, but that the inclusion of horizontal effects, especially the slow advection of buoyancy from runoff, would lead to better results, particularly in the western and northern Gulf. Finally, although the waters in the JCP area "more vertically homogenous" (in T-S terms) than those of area 05, the present data/results do not permit us to conclude that they are "tidally well-mixed", as Pingree and Griffiths (1980) suggested.

Chapter 7
Discussion and Conclusions

This study consists of analyzing several datasets in order to produce a much improved picture of the climatological state of the Gulf's surface layer. Furthermore, an investigation of the air-sea interactions taking place over the GSL was undertaken and the implications of such atmosphere-ocean processes were discussed. The results presented here form, to the author's knowledge, the best up-to-date picture of the climatological monthly surface fields (SST, SSS, MLD, H.C., Q_{net}) for the GSL and should be used as a base for further oceanographic/climate studies in the Gulf of St-Lawrence.

7.1 Comparison with Existing Climatologies

Since there are concerns about reliability when dealing with large historical datasets, one must often rely on comparisons with existing studies on similar physical fields. Consequently, this section will briefly summarize the results presented in the previous chapters in light of several other investigations.

Petrie's (1990) monthly box T and S distributions:

The starting point of this research consisted in reproducing the monthly T and S charts published by Petrie (1990). Doing so would allow verifications to be made on the possible causes of errors if discrepancies were to occur. Moreover, since dubious oceanic profiles were present in the historical database, using Petrie's monthly means as a basis for comparison permitted efficient non-statistical filtering of the entire dataset (see chapter 3). Finally, a novel interpolation technique was used in order to preserve the smaller scale upper-layer structure of the profiles. Again, the resulting climatologies were compared with those obtained by Petrie.

In conclusion, the monthly-depth distributions of temperature and salinity computed in this study (section 5.1) corresponded, after a long and thorough filtering, very closely to those previously obtained by Petrie, with the exception that the profiles were interpolated to finer depth intervals within the first 100 meters from the surface. Moreover, no significant differences were noticed in the monthly means as a result of the different interpolation technique. However, when looking at time series and/or individual vertical profiles (see section 3.4), particularly for the temperature case, obvious advantages were noted when using the method of parametric-cubic curves to perform the vertical interpolation.

Petrie's (1990), Vigeant's (1987) and Bugden et al's. (1982) SST and SSS maps:

More confidence in the validity of the database resulted from these initial comparisons and filtering procedures, thus making possible the computations of related climatological fields. Horizontal maps of monthly surface temperatures and salinity were then obtained. Comparisons were again necessary in order to validate the results. The SST and SSS fields in this study were produced using an objective mapping technique.

As a first step, comparison could be made with Petrie's surface maps of T and S. This proved to be helpful but insufficient since these fields had been obtained by contouring the 17 surface means onto the entire Gulf map. Consequently, they lacked proper horizontal coverage, especially in areas of important surface gradients (e.g. Esquiman Channel towards Strait of Belle-Isle). Vigeant's SST and Bugden et al.'s SSS maps (in Koutitonsky and Bugden, 1991) were then chosen as a better means of comparing the results of chapter 5.

In general, both SSS and SST maps compared well with those of Vigeant and Bugden et al., preserving the overall thermohaline features of the Gulf. On the other hand, it was observed that the results presented in section 5.4 reproduced better the small scale and local surface characteristics known to exist in the GSL. For example, the regions along the Gulf's north shore and along the south side of Anticosti Island experience frequent coastal upwelling events (Koutitonsky and Bugden, 1991), thus exhibiting colder surface features (see the remote sensing image of July SST in Koutitonsky and Bugden, 1991). Because of the excellent spatial coverage of observations in the database (hydrographic observations as well as satellite-derived SST), these features have been preserved in the results of this study. Intrusions of cold water along Québec's shore of the Esquiman Channel were also apparent. Finally, in regard to the salinity maps, although the spatial coverage was not nearly as good as that for temperature, especially in the northwest sector, local characteristics such as the sligthly fresher surface waters along the central part of the Gulf's north shore (area 05) could be observed. In conclusion, although the main features remain unchanged, SST and SSS maps presented in chapter 5 display a more detailed horizontal structure than earlier climatological fields.

Bugden's (1981) heat fluxes:

After having constructed the monthly means of T and S, the second major aspect of this research consisted in calculating the heat budget at the air-sea interface of the Gulf. In this case, Bugden's (1981) work was used as a reference for comparison. In his paper, he produced monthly surface heat fluxes for four large subsections of the GSL, namely: the Estuary, the Shallows, the Northeast and the Northwest regions. The results presented in this thesis correspond fairly well with those of Bugden, despite his coarser segmentation. The advantage of the Q_{net} maps presented in chapter 5 is that they preserve smaller scale features imbeded in the heat flux fields.

Forrester's (1964) T-S envelope:

Chapter 6 showed composite and segmented T-S diagrams for the Gulf. The only known source of such relationships for the entire GSL was that of Forrester (1964). The T-S envelopes compared well. Moreover, T-S relationships plotted in section 5.2 also included diagrams corresponding to specific time and depth intervals. This allowed a rapid visualization of the winter-to-summer differences in water masses as well as information on their vertical structure.

Bugden's (1991) and Petrie and Drinkwater (1993) T-S time series:

Although they have not been formally included and analysed in the present work, time series of temperature and salinity anomalies have been produced for all 15 sections of the Gulf and 5 selected depths. When comparing these temporal series with those of Budgen for the deep central region of the Laurentian Channel and with those of Petrie and Drinkwater for areas near the Gulf's entrance (Cabot Str.), the same climatic trends (T & S variability) were observed.

7.2 Extensions and Improvements from this Research

One of the main purpose of this thesis was to improve our knowledge of the Gulf ocean climatology. This section will briefly survey some aspects of the work which contributed to this goal.

The first aspect of this research concerns the quality of the oceanic dataset. The database provided by K. Drinkwater is believed to be the most complete historical dataset of temperature and salinity profiles for the Gulf of St.Lawrence. Moreover, as in any climatological analysis, erronous data necessitates editing before use. A large part of this work had already been done at B.I.O. so that the filtering described in section 3.2 was a much easier task than anticipated. Moreover, the addition of 7 years of monthly satellite-derived observations (SST and Chl*a*) at a 18km resolution considerably improved the dataset in both spatial and temporal coverage.

Regarding the monthly surface Chl*a* averages: although the analysis is curently underway and is therefore not included in the present document, it is believed that this climatology for the Gulf of St.Lawrence will be of value to the JGOFS study in the Gulf and others.

Another important feature regarding these results deals with the interpolation of hydrographic profiles to preselected vertical levels. Not only did these interpolated profiles have a finer upper-layer resolution (10 meters), but it is believed that the technique and constraints employed to perfom this task were an improvement on the other methods commonly used (e.g. Petrie, 1990; Reynaud, 1994).

Because of the above points, one would expect the resulting climatologies to be an improvement. Although the overall features were similar to those of the previous studies, the new fields revealed physical characteristics not present in previous climatologies (e.g. the absence of cold upwelling waters along the north shore of the GSL in Petrie, 1990). Some of the results showed little or no difference with those of other studies which further confirms their veracity. This was confirmed by the small relative errors associated with the optimal interpolation.

Another novel aspect of this research consists was the use of an 8-year satellite cloud cover climatology in the computation of the surface heat budget. As mentioned in chapter 4, several problems were associated with cloud data from weather stations around the Gulf. It is believed that the use of satellite cloud cover observations (C_n) should improve considerably the estimates of short and long wave surface radiative fluxes, Q_{sw} and Q_{lw}, which both use C_n in their parametrizations. Consequently, making use of these newly formed cloud cover fields as well as the updated monthly maps of sea surface temperature also bring greater confidence to the computed monthly surface heat fluxes. These constitute an improvement on the heat flux calculations performed by Bugden (1981).

Finally, it is believed that calculations of other physical parameters (monthly averaged depth of the mixed-layer, heat content of the upper water column, estimation of the mixing energy input from the wind, upper-layer static stability) could also help better understand the various physical processes occuring in the Gulf.

In general, these improvements in our knowledge of the Gulf's climatological state form a sound basis for further comparisons and/or investigations of the dynamics and climatic variability of the Gulf of St.Lawrence.

7.3 Limitations of the Present Study

One important aspect of this research consists in assessing the causes of shortcomings in the results. First, it is somewhat difficult to evaluate the precision of T and S observations contained in the oceanic dataset. These hydrographic measurements have been taken throughout the century in many locations and in a wide variety of climatic conditions. Moreover, as one would expect, these measurements are often highly localized in both time and space (e.g. post war period, ice-free months, calm weather, etc.). One must therefore rely on existing knowledge of the Gulf's thermohaline state as well as exercise great deal of caution and care in order to filter out dubious oceanic profiles. As previously described in chapter 3, a great effort was done to render the entire dataset suitable for climatological studies while keeping as many profiles intact as possible. In general, although no quantitative estimate of the data precision/error has been obtained, it is believed that the observations used here were indeed adequate for the analyses performed. Moreover, the effort in estimating the spatial correlation of SST and Chl*a* allows the resulting interpolated field to be used with more confidence.

Another area of uncertainty concerns the computation of Q_{sw} and Q_{lw}. Both the incoming shortwave and outgoing longwave energy fluxes depend on the amount of cloud present, as explained in chapter 2. Although the cloud data used were considered quite reliable, other atmospheric factors influence these radiative fluxes and could not be taken into consideration in this study. There also exists a wide variety of empirical formulations to account for the effect of cloud cover, and it is rather difficult to evaluate which one should be used. Consequently, although great care has been taken regarding the quality of these data, and that widely used and conservative parametrizations of Q_{sw} and Q_{lw} were chosen (i.e. empirical formulations that do not underestimate nor overestimate the influence of C_n), it is again rather difficult to assess the precision obtained when computing such surface energy fluxes.

Concerning the fluxes of sensible and latent heat, these were computed from the so-called bulk aerodynamical method which, to estimate their turbulent transfer coefficients, makes use of empirical formulations. Here, the uncertainties lie in the choice of computation schemes for C_e and C_h. As mentioned in chapter 6 and reported by Blanc (1985) in a review paper on turbulent transfer coefficients, there is no universally accepted method of calculating C_e and C_h (in terms of the ambient air-sea state) and very large variations occur when chosing one algorithm over another (section 6.4). Once again, it is not possible to fully quantify the uncertainties associated with such computations and, as in the case of Q_{lw} and Q_{sw}, the choice of C_e and C_h was strongly motivated by its wide use as well as its average value within a broad spectrum of possible values from all existing empirical schemes. There is also some imprecision in using geostrophic winds as well as land-based air temperatures interpolated over the Gulf (section 4.1 and 4.2) to obtain Q_e and Q_h, but these errors are rather small compared to the uncertainties associated with the turbulent transfer coefficients.

Finally, the author thinks that a more detailed investigation should be perfomed in order to correlate all previously mentioned fields within the framework of air-sea interaction models. Moreover, time series of such atmospheric and oceanic parameters have been produced and, although they have not been formally analyzed[1] in the present work, they could yield additional knowledge of the Gulf's past interannual/interdecadal climatic variations, and the relative importance of various physical processes.

[1]: The variability of MLD and SST have been investigated in the previous chapters using only simple correletions. A more thorough analysis of the specific interannual/interdecal fluctuations (e.g. Bugden, 1991; Petrie and Drinkwater, 1993) should include additional forcing parameters, such as runoff, storm tracks and frequencies, ice cover, etc.

In conclusion, it is fair to say that there exists no simple explanation of the exact seasonal structure of the mixed-layer. The processes involved are numerous, complex and interact strongly with one another, thus requiring the use of numerical models. Nevertheless, it is known that an ice cover, altering the air-sea interaction and acting as an insulator, is usually present from December to April (Déry, 1992). Upon melting in the spring, the upper-layer begins to warm, due to a positive net heat flux from the atmosphere an dprovides an in-situ buoyancy flux (chapter 6). The surface layer reaches a maximum temperature around the month of August, followed by progressive cooling until the next ice season. During the approximately seven ice-free months, the wind action modifies the surface layer. Over the year, the strongest winds occur during the winter and the weakest winds are observed around June-July (chapter 4). Finally, air temperature plays a central role in the intensity and direction of the air-sea transfer of heat. It also follows an annual cycle similar to that of the surface water, except that it is warmer than the sea in the spring and early summer, but cools-off more rapidly and becomes colder than its oceanic counterpart in late summer-early fall. As Koutitonsky and Bugden (1991) report, the Gulf of St.Lawrence seems to "respond as an integrated physical oceanographic system" ... "forced at various temporal and spatial scales". It is therefore unrealistic to expect an accurate understanding and prediction of a small yet important part of it - the upper mixed-layer - without considering all ranges of motions and their complex interactions.

7.4 Future Work

The primary objective of this research was to produce an improved picture of the climatological state of the Gulf's surface waters, and to examine features of the air-sea interaction processes. One might expect these results to be of importance to further oceanographic studies of the Gulf of St.Lawrence. A few research topics that the author believes could benefit from the present work, and thus help improve our understanding of the Gulf's oceanography and climate are as follows.. This research was primarily concerned with the Gulf's surface waters and, consequently, the objective analysis performed on the dataset restricted itself to the generation of monthly SST and SSS fields. It would be straightforward to continue this analysis throughout the entire water column (at preselected standard levels) and for all twelve months of the year in order to fully map the Gulf's monthly mean thermohaline state. Once these objective fields of temperature and salinity (thus density) would be available, a diagnostic calculation of GSL circulation via inverse methods could also be performed. Reynaud (1994) successfully did this for the northwestern Atlantic Ocean (45°-70°N,30°-70°W). Although his area of interest included the Gulf of St.Lawrence, the resolution of his density fields was not adequate to resolve the main features. Given the versatility present in today's numerical models, it would also be possible to undertake a study of the mixed-layer and circulation as well as investigating the climatic fluctuations in order to assess their physical causes.

Although some aspects of interannual variability was considered in chapter 6, much work remains to be done in order to fully integrate all important physical parameters within some sort of a multivariate analysis. The limitations do not lie in statistical theory but rather in the completeness (spatial and temporal) of the various datasets. As explained in chapter 6, the typical seasonal evolution of the mixed-layer corresponds quite well with that found by several other authors (Philips, 1981; Turner, 1981) in terms of wind mixing (E_w) and net heat flux (Q_{net}). The problem lies in forming time series for all variables involved in E_w and Q_{net} in order to study the interannual behavior of the surface layer (as well as to estimate the random errors of some fields). And even if these series were available, it must be remembered that all these variables interact together in a complex fashion. The complexity of non-linear multivariate analysis of the variance could perhaps be avoided by studying the GSL as an integrated system (Koutitonsky and Bugden, 1991) using dynamical numerical models, in combination with accurate climatological fields.

As a final note: work is currently being done by the author in linking all hydrographic, atmospheric and biological variables (for both climatology and the JGOFS cruises) into a stratification-phytoplankton model (Prestidge and Taylor, 1995).

References

Achtemeier, G.L., 1987 : On the concept of varying influence radii for a successive corrections objective analysis. *Mon. Weat. Rev.*, **115**, 1760-1771.

Ahrens, C.D., 1991: *Meteorology today: an introduction to weather, climate, and the environment.* West Publ. Co., USA. 577 pp.

Alexander, R. C., and J.-W. Kim, 1976: Diagnostic model study of the mixed-layer depths in the summer north pacific. *J. Phys. Oceanogr.*, **6**, 293-298.

Anis, A., and J.N. Moum, 1995: Surface wave-turbulence interactions: scaling $\varepsilon(z)$ near the sea-surface. *J. Phys. Oceanogr.*, **25**, 2025-2045.

Anonymous, 1984: *Canadian climatic atlas of Canada: a series of maps portraying Canada's climate. Series 3.* Ottawa, Atmospheric environment service - Canadian climate program, c1984.

Anonymous, 1988: *World Weather Disc: climate data for planet earth.* Seattle, Wash., Weather Disc Assoc., c1988 (CDROM disc).

Anonymous, 1991: *The environmental atlas of the St.Lawrence - A river, estuaries and a gulf: Broad hydrographic divisions of the St.Lawrence.* The St.Lawrence Centre, Montreal, Environment Canada, En 40-386/1-4-1991E.

Anonymous, 1994: JPL Physical Oceanography Distributed Active Archive Center (PO.DAAC) Data Availability, Version 1-94, JPL Publication **90-49**, rev. 5.

Bathen, K.H., 1972: On the seasonal changes in the depth of the mixed-layer in the north Pacific ocean. *J. Geophys. Res.*, **77**, 7138-7150.

Besner, M., 1994: Méthode pour estimer des variables horaires à partir d'observation de navires et de stations terrestres. *Rapport Technique, Division des Services Scientifiques, Environnement Canada, Région du Québec.* "Unpublished Manuscript", Montreal.

Blanc, T. V., 1985: Variation of bulk-derived surface flux, stability, and roughness results due to the use of different transfer coefficient schemes. *J. Phys. Oceanogr.*, **15**, 650-669.

Bourque, M. C., and D. Kelley, 1995: Evidence of wind-driven upwelling in Jacques-Cartier Strait. *Atmos.-Ocean*, **33**, 359-387.

Bratseth, A.M., 1986: Statistical interpolation by means of successive corrections. *Tellus*, **38a**, 439-447.

Brown J. W., O. B. Brown, and R. H. Evans, 1993: Calibration of AVHRR Infrared channels: a new approach to non-linear correction, *Journal of Geophysical Research*, **98** (NC10), 18,257-18,268.

Budyko, M. I., 1974: *Climate and Life*. Academic Press, New-York, 508p.

Bugden, G. L., 1981: Salt and heat budgets for the Gulf of St.Lawrence. *Can. J. Fish. Aquat. Sci.*, Vol. 38, 1153-1167.

Bugden, G. L., B. T. Hargrave, M. M. Sinclair, C. L. Tang, J.-C. Therriault, and P. A. Yeats: 1982. *Fresh water runoff effects in the marine environment: the Gulf of St.Lawrence example*. Can. Tech. Rep. Fish. Aquat. Sci. 1078: 88p.

Bugden, G. L., 1991: Changes in the temperature-salinity characteristics of the deeper waters of the Gulf of St.Lawrence over the past several decades. p.139-152. In *The Gulf of St.Lawrence: small ocean or big estuary?*. J.-C. Therriault (ed.) Can. Spec. Publ. Fish. Aquat. Sci. 113.

Bunker, A.F., 1976: Computations of surface energy flux and annual air-sea interaction cycles of the North Atlantic. *Mon. Weat. Rev.*, **104**, 1122-1140.

Cayan, D.R., 1990: *Variability of latent and sensible heat fluxes over the ocean*. Ph.D. Thesis, University of California, San-Diego, 199pp.

Cayan, D.R., 1992a: Variability of latent and sensible heat fluxes estimated using bulk formulae. *Atmos.-Ocean*, **30**, 1-42.

Cayan, D.R., 1992b: Latent and sensible heat fluxes anomalies over the northern oceans: driving the sea surface temperature.*J. Phys. Oceanogr.*, **22**, 859-881.

Csanady, G., 1982: *Circulation in the coastal ocean*. D. Reidel Publ. Co., Boston, USA, 279 pp.

Daley, R., 1991: *Atmospheric data analysis*. Cambridge Univ. Press., USA, 457 pp.

Daoust, M., 1991: *Interannual temperature variability and cyclone frequency over eastern Canada and the New England states; A case study: winter seasons 1931-32 to 1984-1985*. Ph.D. Thesis, McGill University, Montreal, 183pp.

de Lafontaine, Y., S. Demers, and J. Runge, 1991: Pelagic food web interactions and productivity in the Gulf of St.Lawrence. p.99-123. In *The Gulf of St.Lawrence: small ocean or big estuary?*. J.-C. Therriault, ed. Can. Spec. Publ. Fish. Aquat. Sci. 113.

Denman, K.L., 1973: A time-dependant model of the upper ocean. *J. Phys. Oceanogr.*, **3**, 173-184.

Denman, K.L., and M. Miyake, 1973: Upper layer modification at ocean station Papa: Observations and simulation. *J. Phys. Oceanogr.*, **3**, 185-196.

Denman,K.L., and H.J.Freeland, 1985: Correlation scales, objective mapping and a statistical test of geostrophy over the continental shelf. *J. Mar. Res.*, **43**, 517-539.

Déry, F., 1992: *Interannual and intraseasonal variability of the ice cover in the Gulf of St.Lawrence, 1963-1990.* M.Sc. Thesis, McGill University, Montreal, 220pp.

de Szoeke, R. A., and P. B. Rhines, 1976: Asymptotic regimes in mixed-layer deepening. *J. Mar. Res.*, **34**, 111-116.

De Tracey, B., 1993: *Modelling interannual sea ice variability in the Gulf of St.Lawrence.* M.Sc. Thesis, McGill University, Montreal, 108pp.

Dey, C.H., and L.L. Morone, 1985: Evolution of the National Meteorological Center global data assimilation system: January 1982-December 1983. *Mon. Wea. Rev.*, **113**, 304-318.

Dobson, F.W., 1971: Measurements of atmospheric pressure on wind-generated sea waves. *Fluid Mech.*, **48**, 91-127.

Donelan, M., 1990: Air-sea interaction. Chap. 7, pp. 239-287, in *The sea*, Vol. 9, Part A, B. Le Mehaute, and P. Hanes (Eds), Wiley.

Drinkwater, K. F., B. Petrie, and W. H. Sutcliffe, Jr., 1979: Seasonal geostrophic volume transport along the Scotian Shelf. *Estuarine Coastal Mar. Sci.*, **2**, 17-27.

Dunbar, M.J., D.C. Maclellan, A. Filion, and D. Moore, 1980: *The biogeographic structure of the Gulf of St.Lawrence.* McGill Univ., Mar. Sci. Center, MS. Rep. **32**: 142p.

Duxbury, A.C., and A.B. Duxbury, 1991: *An introdution to the world's oceans.* W.C.Brown Publ., USA, 446pp.

Efron, B., and R. Tibshirani, 1986: Bootstrap methods for the standard errors, confidence intervals, and other measures of statistical accuracy. *Stat. Sc.*, **1**, 54-77.

Ekman, V. W., 1905: On the influence of earth's rotation on ocean currents. *Arkiv for Matematik, Astronomi och Fysik*, **2**, No.11, p.52.

El-Sabh, M.I., 1973: Seasonal and long-term variations of the water properties in the Gulf of St.Lawrence. *In* M.El-Sabh [ed] *Proc. Workshop Physical Sciences in the Gulf and Esturary of St.Lawrence.* 128-158.

El-Sabh, M.I., 1976: Surface circulation patterns in the Gulf of St.Lawrence. *J. Fish. Res. Board Can.*, **33**, 124-138.

Ellison, T. H., and J. S. Turner, 1959: Turbulent entrainment in stratified flows. *J. Fluid Mech.*, **6**, 423-448.

Fernando, H. J. S., 1987: Comments on "Wind direction and equilibrium mixed-layer depth: General theory". *J. Phys. Oceanogr.*, **17**, 169-170.

Forrester, W.D., 1964: *A quantitative temperature-salinity study of the Gulf of St.Lawrence*. Rep. 61-11, Bedford Inst. of Oceanogr., N.S., 61pp.

Frankignoul, C., and R.W. Reynolds, 1983: Testing a dynamical model for mid-latitude sea-surface anomalies. *J. Phys. Oceanogr.*, **13**, 1131-1145.

Friehe, C. A., and K. F. Schmitt, 1976: Parametrization of air-sea interface fluxes of sensible heat and moisture by bulk aerodynamical formulas. *J. Phys. Oceanogr.*, **6**, 801-809.

Frouin, R., and C.Gauthier, 1988: Downward longwave irradiance at the ocean surface from satellite data: methodology and in situ validation. *J. Geophys. Res.*, **93** (C1), 597-619.

Galbraith, P. S., 1992: *Relating overturns to mixing and buoyancy flux*. Ph.D. Thesis, Dalhousie University, Halifax, Nova-Scotia.

Gan, J. P., R.G. Ingram, R.J. Greatbatch, and P.Chen, 1995: Upper ocean modelling in a coastal bay. *J. Geophys. Res.*, **100**, 15,977-15,997.

Gan, J.P., 1995: *Upper Ocean Modelling in Baie Des Chaleurs*. Ph.D. Thesis, McGill University, Montreal, 160pp.

Garrett, C., and B. Petrie, 1981: Dynamical aspects of the flow through the strait of Belle-Isle. *J. Phys. Oceanogr.*, **11**, 376-393.

Garwood, R W., Jr., P. Gallacher, and P. Muller, 1985: Wind direction and equilibrium mixed-layer depth: General theory. *J. Phys. Oceanogr.*, **15**, 1325-1331.

Garwood, R. W., Jr., P. Muller, and P. C. Gallacher, 1985: Wind direction and equilibrium mixed-layer depthin the tropical pacific. *J. Phys. Oceanogr.*, **15**, 1332-138.

Garwood, R. W., Jr., P. Muller, and P. C. Gallacher, 1987: Reply to "Comments on "Wind direction and equilibrium mixed-layer depth: General theory" *J. Phys. Oceanogr.*, **17**, 171-172..

Gill, A. E., and P. P. Niiler, 1973: The theory of the seasonal variability in the ocean. *Deep-Sea Res.*, **20**, 141-177.

Gill, A. E., and J. S. Turner, 1976: A comparison of seasonal thermocline models with observation. *Deep-Sea Res.*, **23**, 391-401.

Gill, A. E., 1981: *Atmos.-Ocean Dynamics*. Int. Geophys. Ser., Vol. 30, Academic Press, 662pp..

Gilman, C., and C. Garrett, 1994: Heat flux parametrizations for the Mediterranean Sea: the role of atmospheric aerosols and constraints from the water budget. *J. Geophys. Res.*, **99**, 5119-5134.

Grant, H. L., R. W. Stewart, and A. Moillet, 1962: Turbulence spectra from a tidal channel. *J. Fluid Mech.*, **12**, 241-268.

Grant, H. L., A. Moillet, and W. M. Vogel, 1968: Some observations of the occurence of turbulence in and above the thermocline. *J. Fluid Mech.*, **34**, 443-448.

Gregg, M. C., 1987: Diapycnal mixing in the thermocline: A review. *J. Geophys. Res.*, **92**, 5249-5286.

Gregg, M. C., 1991: The study of mixing in the ocean: A brief history. *Oceanography*, April, 39-45.

Hakkinen, S., and D.J. Cavalieri, 1989: A study of oceanic surface heat fluxes in the Greenland, Norwegian and Barents seas. *J. Geophys. Res.*, **94**, 6145-6157.

Haltiner, G. J., and R. T. Williams, 1980: *Numerical prediction and dynamic meteorology*. John Wiley & Sons Inc., 477pp, 2nd Ed..

Haney, R.L., 1971. Surface thermal boundary condition for ocean circulation model. *J. Phys. Oceanogr.*, **1**, 241-248.

Haney, R. L., and R. W. Davies, 1976: The role of surface mixing in the seasonal variation of the ocean thermal structure. *J. Phys. Oceanogr.*, **6**, 504-510.

Herfst, F.J., 1984: *Wind regimes in the St.Lawrence River valley*. M.Sc. Thesis, University of Toronto, Toronto, 152p.

Houghton, H.G., 1985: *Physical meteorology*. MIT, Cambridge, USA, 442pp.

Hsiung, J., 1986: Mean surface energy fluxes over the global ocean. *J. Geophys. Res.*, **91**, 10585-10606.

Kato, H., and O. M. Phillips, 1969: On the penetration of a turbulent layer into stratified fluid. *J. Fluid Mech.*, **37**, 643-655.

Kidwell, K., 1991: *NOAA Polar Orbiter User's Guide*. NCDC/NESDIS, National Climatic Data Center, Washington, D.C..

Kim, J.-W., 1976: A generalized bulk model of the oceanic mixed-layer. *J. Phys. Oceanogr.*, **6**, 686-695.

Kincaid, D.R., and E.W. Cheney, 1991: *Numerical analysis*. Brooks/Cole, California.

Kistler, R.E., and D.F. Parrish, 1982: Evolution of the NMC data assimilation system: September 1978-January 1982. *Mon. Weat. Rev.*, **110**, 1335-1341.

Kondo, J., 1975. Air-sea bulk transfer coefficients under diabatic conditions. *Boundary-Layer Meteorol.* **9**: 91-112.

Koutitonsky, V.G., B. Côté, and C. Toro, 1986: Modélisation hydrodynamique de la circulation en relation avec les débarquements de maquereaux dans le Golfe du St-Laurent. *INRS-Océanologie*. Rap. Sci. pour Centre Champlain des Sciences de la Mer, Québec, 129p.

Koutitonsky, V. G., and G. L. Bugden, 1991: The physical oceanography of the Gulf of St.Lawrence: A review with special emphasis on the synoptic variability of the motion. p.57-90. In *The Gulf of St.Lawrence: small ocean or big estuary?*, J.-C. Therriault (ed.) Can. Spec. Publ. Fish. Aquat. Sci. 113.

Kraus, E. B., and J. S. Turner, 1967: A one-dimensional model of the seasonal thermocline: II. The general theory and its consequences. *Tellus*, **19**, 98-106.

Kraus, E. B., 1972: *Atmos.-Ocean interaction*.Clarendon press, Oxford, 275 pp.

Krauss, W., 1981: The erosion of a thermocline. *J. Phys. Oceanogr.*, **11**, 415-433.

Kundu, P. K., 1980: A numerical investigation of mixed-layer dynamics. *J. Phys. Oceanogr.*, **10**, 220-236.

Lamb, P. J., 1984: On the mixed-layer climatology of the north and tropical Atlantic. *Tellus*, **37A**, 292-305.

Large, W. G., and S. Pond, 1980: Open ocean momentum flux measurements in moderate to strong winds. *J. Geophys. Res.*, **11**, 324-336.

Lauzier, L.M., and W.B. Bailey, 1957: Features of the deep waters of the Gulf of St.Lawrence. *Bull. Fish. Res. Board Can.* **III**, 213-250.

Lauzier, L.M., R.W. Trites, and H.B. Hachey, 1957: Some features of the surface layer of the Gulf of St.Lawrence. *Bull. Fish. Res. Board Can.* **III**, 195-212.

Lauzier, L.M., and R.W. Trites, 1958: The deep waters in the Laurentian Channel. *Bull. Fish. Res. Board Can.* **15**, 1247-1257.

Lentz, S. J., 1992: The surface boundary layer in coastal upwelling regions. *J. Phys. Oceanogr.*, **22**, 1517-1539.

Lepage, S., and R.G. Ingram, 1991: Variation of upper layer dynamics during breakup of the seasonal ice cover in Hudson Bay. *J. Geophys. Res.*, **96**, 12,711-12,724.

Lesieur, M., 1987: *Turbulence in fluids*. Martinus Nijhoff Publishers, Dordrecht, Netherlands.

Levitus, S., 1982: *Climatological atlas of the world ocean*. NOAA Prof. Pap. **13**, Natl. Oceanic and Atmos. Admin., Washington D.C., USA, 173p.

Lin, C.A., K. Higuchi, and R. Michaud, 1992: Interannual variability of the surface heat budget of the northern north Atlantic and north Pacific oceans. *Theor. Appl. Climatol.*, **45**, 161-165.

Liu, P. C., and D. J. Schwab, 1987: A comparison of methods for estimating U_* from given $U(z)$ and air-sea temperature differences. *J. Geophys. Res.*, **92**, 6488-6494.

Liu, W.T., K.B. Katsaros, and J.A. Businger, 1979: Bulk parametrization of air-sea exchanges of heat and water vapor including the molecular constraints at the interface. *J. Atmos. Sciences*, **36**, 1722-1735.

Lorenc, A.C., 1986: Analysis methods for numerical weather prediction. *Tellus*, **112**, 1177-1194.

Lukas, R., and E. Lindstrom, 1991: The mixed-layer of the western equatorial Pacific Ocean. *J. Geophys. Res.*, **96**, suppl., 3343-3357.

Madden, R.A., and R.W. Katz, 1994: *Applications of statistics to modelling the earth's climate system*. NCAR Technical Note, **NCAR/TN-409**, Boulder, USA, 123 pp.

Marcotte, D., 1991: Cokriging with MATLAB, *Computers & Geosc.*, **17**, 1265-1280.

McCormick, M. J., and G. A. Meadows, 1988: An intercomparison of four mixed-layer models in a shallow inland sea. *J. Geophys. Res.*, **93**, 1234-1245.

McClain E. P., W. G. Pichel, and C. C. Walton, 1985: Comparative performance of AVHRR based multichannel sea surface termperatures, *J. Geophys. Res.* , **90**, 11587-11601.

McIntosh, P.C., 1990: Oceanographic data interpolation: objective analysis and splines. *J. Geophys. Res.*, **95**, 13,529-13,541.

McMillin, L. M., and D. S. Crosby, 1984: Theory and validation of the multiple window sea surface temperature technique. *J. Geophys. Res.*, **89** (C3), 3655-3661.

McPhee, M.G., 1979: The effects of the oceanic boundary layer on the mean drift of packed ice: application of a simple model. *J. Phys. Oceanogr.*, **9**, 388-400.

McPherson, R.D., K.H. Bergman, R.E. Kistler, G.E. Rash, and D.S. Gordon, 1979: The NMC operational global data assimilation system. *Mon. Weat. Rev.*, **107**, 1445-1461.

Michaud, R., and C.A. Lin, 1992: Monthly summaries of merchant ship surface marine observations and implications for climate variability studies. *Clim. Dyn.*, **7**, 45-55.

Miller, J. R., 1976: The salinity effect in a mixed-layer ocean model. *J. Phys. Oceanogr.*, **6**, 29-35.

Monin, A. S., and A. M. Yaglom, 1972: *Statistical fluid mechanics*. MIT Press, Cambridge, Massachusetts.

Munk, W. H., and E. R. Anderson, 1948: Notes on a theory of the thermocline. *J.Mar. Res.*, **7**, 276-295.

Mysak, L. A., and C. A. Lin, 1990: Role of the oceans in climatic variability and climatic change. *The Canadian Geographer*, 4, 352-369.

Niiler, P. P., 1975: Deepening of the wind-mixed layer. *J. Mar. Res.*, **33**, 405-422.

Niiler, P. P., and E. B. Kraus, 1977: One-dimensional models of the upper ocean, in *Modelling and prediction of the upper layers of the ocean*, edited by E. B. Kraus, pp. 143-172, Pergamon, Elmsford, New York.

Oakey, N. S., 1985: Statistics of mixing parameters in the upper ocean during JASIN phase 2. *J. Phys. Oceanogr.*, **15**, 1662-1675.

Oberhuber, J. M., 1993: Simulation of the Atlantic circulation with a coupled sea ice-mixed layer-isopycnal general circulation model. Part I: Model description. *J. Phys. Oceanogr.*, **23**, 808-828.

Osborn, T.R., 1980: Estimates of the local rates of vertical diffusion from dissipation measurements. *J. Phys. Oceanogr.*, **10**, 83-89.

Paduan, J. D., R. A. de Szoeke, and R. A. Weller, 1989: Inertial oscillations in the upper ocean during the mixed-layer dynamics experiment (MILDEX). *J. Geophys. Res.*, **94**, 4835-4842.

Paulson, C.A., and J.J. Simpson, 1977: Irradiance measurements in the upper ocean. *J. Phys. Oceanogr.*, 7, 952-956.

Payne, R.E. 1972: Albedo of the sea surface. *J. Atmos. Sciences*. **29**, 959-970.

Peixoto, J.P., and A.H. Oort, 1991: *Physics of climate*. AIP Press, NY, USA, 520pp.

Perry, A. H., and J. M. Walker, 1977: *The ocean-atmosphere system* . Longman, NewYork, 160pp.

Petrie, B., B. Toulany, and C. Garrett, 1988: The transport of water, heat and salt through the Strait of Belle-Isle. *AAtmos.-Ocean*, **26**, 234-251.

Petrie, B., 1990: *Monthly means of temperature, salinity and sigma-T for the Gulf of St.Lawrence*. Can. Tech. Rep. Hydr. Ocean Sc. No. 126, 137 pp.

Petrie, B., and K. Drinkwater, 1993: Temperature and salinity variability on the Scotian Shelf and in the Gulf of Maine: 1945-1990. *J. Geophys. Res.*, **98**, 20079-20089.

Phillips, O. M., 1981: *The dynamics of the upper ocean*. Cambridge Univ. Press, USA

Pickard, G.L., and W.J. Emery, 1990: *Descriptive physical oceanography: an introduction, 5th edition*. Pergamon Press, 320p.

Pingree, R. D., P.M. Holligan, and G.T. Mardel, 1978: The effects of vertical stability on phytoplankton distributions in the summer on the northwest European Shelf. *Deep-Sea Res.*, **25**, 1011-1028.

Pingree, R. D., and D. K. Griffiths, 1980: A numerical model of the M2 tide in the Gulf of St. Lawrence. *Oceanologica Acta*, 3, 221-225.

Pollard, R. T., and R. C. Millard, Jr., 1970: Comparison between observed and simulated wind-generated inertial oscillations. *Deep-Sea Res.*, **17**, 813-821.

Pollard, R. T., P. B. Rhines, and R. O. R. Y. Thompson, 1973: The deepening of the wind-mixed layer. *Geophys. Fluid Dyn.*, **3**, 381-404.

Pollard, R. T., T. H. Guymer, and P. K. Taylor, 1983: Summary of the JASIN 1978 field experiment. *Phil. Trans. Roy. Soc. London*, **A308**, 221-230.

Pond, S., and G.L. Pickard, 1991: *Introductory dynamical oceanography, 3rd edition*. Pergamon Press, 329p.

Preisendorfer, R.W., 1988: *Principal component analyses in meteorology and oceanography*. Elsevier, USA.

Prestidge, M.C., and A.H. Taylor, 1995: A modelling investigation of the distribution of stratification and phytoplankton abundance in the Irish Sea. *J. Plankt. Res.*, **17**, 1397-1420.

Price, J. F., C. N. K. Mooers, and J. C. Van Leer, 1978: Observation and simulation of storm-induced mixed-layer deepening. *J. Phys. Oceanogr.*, **8**, 584-599.

Price, J. F., 1979: Obsevation of a rained-formed mixed-layer. *J. Phys. Oceanogr.*, **9**, 643-649.

Price, J. F., 1981: Upper ocean response to a hurricane. *J. Phys. Oceanogr.*, **11**, 153-175.

Price, J. F., R. A. Weller, and R. Pinkel, 1986: Diurnal cycling: Observations and models of the upper ocean response to diurnal heating, cooling, and wind mixing. *J. Geophys. Res.*, **91**, 8411-8427.

Prinsenberg, S. J., 1982: One-dimensional mixed-layer model for Hudson bay and James bay. *Government of Canada, Fisheries and Oceans*. "Unpublished Manuscript".

Prinsenberg, S. J., 1983: Effects of hydroelectric developments on the oceanographic surface parameters of Hudson bay. *Atmos.-Ocean*, **21**, 418-430.

Rao, R.R., R.L. Molinari, and J.F. Festa, 1989: Evolution of the climatological near-surface thermal structure of the Tropical Indian Ocean, 1: Description of mean monthly mixed layer depth, and sea surface temperature, surface current, and surface meteorological fields. *J. Geophys. Res.*, **94**, 10,801-10,815.

Reed, R.K., 1977: On estimating the insolation over the ocean. *J. Phys. Oceanogr.*, **7**, 482-485.

Reynaud, T., 1994: *Dynamics of the northwestern Atlantic ocean: a diagnostic study*. Ph.D. Thesis, McGill University, Montreal, 266pp.

Roche-Mayzaud, O., J.-C. Therriault, J.A.Runge, and Y. deLafontaine, 1991: Variations de l'activité des enzymes digestives et de la ponte chez les femelles de *Calanus finmarchicus* dans le Golfe du St-Laurent. p.57-90. In *The Gulf of St.Lawrence: small ocean or big estuary?*. J.-C. Therriault (ed.) Can. Spec. Publ. Fish. Aquat. Sci. 113.

Rodi, W., 1987: Examples of calculation methods for flow and mixing in stratified fluid. *J. Geophys. Res.*, **92**, 5305-5328.

Roebber, P.J., 1989: The role of surface heat and moisture fluxes associated with large-scale ocean current meanders in maritime cyclogenesis. *Mon. Weat. Rev.*, **117**,1676-1693.

Rogers, R. R., and M. K. Yau, 1989: *A short course in cloud physics* . Intl. Series in Natural Series, Pergamon Press, Oxford, 292pp.

Rose, G. A., 1988: *Temporal and Spatial Variability in Onshore Cod (Gadus morhua)*. Ph.D. Thesis, McGill University, Montréal, Québec.

Rose, G. A., and W. Leggett, 1988: Atmosphere-Ocean coupling in the Northern Gulf of St.Lawrence: frequency-dependent wind-forced variations in nearshore sea temperatures and currents. *Can. J. Fish. Aquat. Sci.*, **45**, 1222-1233.

Rossow, W. B., et al., 1988: *ISCCP Documentation of Cloud Data*. WMO/TD-No. 266.

Rossow, W. B., and R. A. Schiffer, 1991: ISCCP cloud data products. *Bull. Amer. Meteor. Soc.*, **72**, 2-20.

Saunders, P.M., 1977: Wind stress on the ocean over the eastern continental shelf of North America. *J. Phys. Oceanogr.*, **7**, 555-566.

Schiano, M.E., 1996: Insolation over the western Mediterranean Sea: a comparison of direct measurements and Reed's formula. *J. Geophys. Res.*, **101**, 3831-3838.

Seckel, G.R., and F.H. Beaudry, 1973: The radiation from sun and sky over the north Pacific ocean (abstract). *EOS Trans. AGU.*, **54**, 1114.

Simpson, J.H., and J.R. Hunter, 1974: Fronts in the Irish Sea. *Nature*, **1250**, 404-406.

Simpson, J.H., and D. Bowers, 1981: Models of stratification and frontal movement in shelf seas. *Deep-Sea Res.*, **28A**, 727-738.

Smith, S.D., and E.G. Banke, 1975: Variation of the sea surface drag coefficient with wind speed. *Quart. J. Roy. Meteor. Soc.*, **101**, 655-673.

Smith, S.D., 1980: Wind stress and heat flux over ocean in gale force winds. *J. Phys. Oceanogr.*, **10**, 709-726.

Smith, S. D., 1988: Coefficients for sea surface wind stress, heat flux, and wind profiles as a function of wind speed and temperature. *J. Geophys. Res.*, **93**, 15,467-15,472.

Smith, S. D., 1990: Reply to Wu's comments on "Coefficients for sea surface wind stress, heat flux, and wind profiles as a function of wind speed and temperature. *J. Geophys. Res.*, **95**, 1,777-1,778.

Stevenson, J. W., 1979: On the effect of dissipation on seasonal thermocline models. *J. Phys. Oceanogr.*, **6**, 496-503.

Stigebrandt, A., 1985: A model for seasonal pycnocline in rotating systems with application to the Baltic Proper. *J. Phys. Oceanogr.*, **15**, 1392-1404.

Stowe, L. L., E. P. McClain, R. Carey, P. Pellegrino, G. G. Gutman, P. Davis, C. Long, and S. Hart, 1991: Global distribution of cloud cover derived from NOAA/AVHRR operational satellite data. *Adv. Space Research*, **3**, 51-54.

Sutcliffe Jr., W.H., R.H. Loucks, and K.F. Drinkwater, 1976: Coastal circulation and physical oceanography of the Scotian Shelf and the Gulf of Maine. *J. Fish. Res. Board. Can.*, **33**, 2,747-2,757.

Swail, V.R., 1985: Geostrophic wind climatology of Canadian marine areas. Canadian Climate Center Report No. 85-9.

Tennekes, H. and J. L. Lumley, 1972: *A first course in turbulence*. MIT Press, Cambridge, MA, 300 pp.

Thiébaux, H.J., and M.A. Pedder, 1987: *Spatial objective analysis: with application in atmospheric science*. Academic Press, NY, USA, 290 pp.

Thompson, R. O. R. Y., 1976: Climatological numerical models of the surface mixed-layer of the ocean. *J. Phys. Oceanogr.*, **6**, 496-503.

Toro, C., 1991: *Three-dimensional diagnostic modelling of the density-driven circulation in the Gulf of St.Lawrence*. Ph.D. thesis, Université du Québec à Rimouski, UQAR, Rimouski, 286 pp.

Tremblay, J., and L.M. Lauzier, 1940: L'originne de la nappe d'eau froide dans l'estuaire du St-Laurent. *Natur.Can.* **67 (11)**, 7-23.

Trites, R. W., 1972: The Gulf of St.Lawrence from a pollution point of view, p.52-72 In M.Ruivo [ed.] *Marine pollution and Sea life*. FAO, Fishing New Books, London.

Trites, R. W., and A. Walton, 1975: *A canadian coastal sea - the Gulf of St-Lawrence*. Rep. BI-R-75-15, Bedford Inst. of Oceanogr., N.S., 61pp.

Turner, J. S., and E. B. Kraus, 1967: A one-dimensional model of the seasonal thermocline: I. A laboratory experiment and its interpretation. *Tellus*, **19**, 88-97.

Turner, J. S., 1981: Small-scale mixing processes. Chap. 8, pp. 236-262, in *Evolution of physical oceanography*, B. A. Warren, and C. Wunsch (Eds), MIT Press.

Umoh, J.U., 1992: *Seasonal and interannual variability of sea temperature and surface heat fluxes in the northwest Atlantic*, Ph.D. Thesis, Dalhousie Univ., Canada, 237pp.

Umoh, J.U., and K.R. Thompson, 1994: Surface heat flux, horizontal advection, and the seasonal evolution of water temperature on the Scotian Shelf. *J. Geophys. Res.*, 99, 20,403-20,416.

Umoh, J.U., J.W. Loder, and B. Petrie, 1995: The role of air-sea heat fluxes in annual and interannual ocean temperature variability on the eastern Newfoundland Shelf. *Atmos.-Ocean*, 33, 531-568.

Vigeant, G., 1984: *Cartes climatologiques du St-Laurent (fleuve et Golfe)*. Serv. Env. Atmos. Canada, Ville St-Laurent, Québec, Canada, 15p.

Warren, S. G., C. J. Hahn, J. London, R. M. Chervin, amd R. L. Jenne, 1986: *Global distribution of total cloud cover and cloud type amounts over land*. NCAR Tech. Note, NCAR/TN -273 +STR, National Center for Atmospheric Research, Boulder, Colorado, 200p.

Warren, S. G., C. J. Hahn, J. London, R. M. Chervin, amd R. L. Jenne, 1988: *Global distribution of total cloud cover and cloud type amounts over the ocean*. NCAR Tech. Note, NCAR/TN -317 +STR, National Center for Atmospheric Research, Boulder, Colorado, 212p.

Weiler, J.D.M., and J.R. Keeley, 1980: *Monthly sea surface temperature for the Gulf of St.Lawrence*. Tech. Rep. 7, Mar. Env. Data Service, Fisheries and Oceans, Ottawa, 43pp.

Wyrtki, K., 1964: The thermal structure of the eastern Pacific ocean, *Deutsch. Hydrogr. Zeit., Suppl. Ser. A*, **8**, 6-84.

Woods, J.D., and W. Barkmann, 1986: The response of the upper ocean to solar heating. I: The mixed-layer. *Quart. J. R. Met. Soc.*, **112**, 1-27

Woods, J.D., and V. Strass, 1986: The response of the upper ocean to solar heating. II: The wind-driven current. *Quart. J. R. Met. Soc.*, **112**, 29-42

Wu, J., 1990: Comments on "Coefficients for sea surface wind stress, heat flux, and wind profiles as a function of wind speed and temperature. *J. Geophys. Res.*, **95**, 1,777-1,778.

Zverev, A.S., 1972: *Practical Work in Synoptic Meteorology* . Hydrometeorological Publishing House, Leningrad.

Appendix 1

The Parametric-Cubic Curves for Vertical Interpolation

After having established the general characteristics and main advantages of the parametric-cubic interpolation method, this section will now explain its geometric and algebraic foundations. As it will be explained, the construction of the parametric-cubic curves (PCC) requires the use of tangent vector and local coordinate axis. More specifically, four combinations and slight modifications of these construction tools are possible. These are:

1.	Tangent bisector vectors (2)	Double local coordinate (X) axis
2.	Weighted tangent bisector vectors (2)	Double local coordinate (X) axis
3.	Tangent bisector vectors (2)	Single local coordinate (X) axis
4.	Weighted tangent bisector vectors (2)	Single local coordinate (X) axis

Since only one form of the parametric-cubic (PC) curve was chosen and that a complete explanation of this geometric theory lies outside the scope of this study, only the most general form of parametric-cubics (#3, tangent bisectors + single local X-axis), the one used for this research, will be derived.

The PCC method was devised as a naturally malleable alternative to cubic-splines by research professor P.J. Zsombor-Murray (unpublished) at the McGill Research Center for Intelligent Machines - Robotic Mechanical Systems Lab. This novel technique for construction of linked, smooth, piecewise cubic splines (curves) uses only the point sequence to be interpolated, P_{i-1} to P_{i+2}.

The PC curves can be expressed mathematically in both algebraic and geometric form. The algebraic relations relating the position vector $\bar{p}$ in terms of the parameter **u** for both two-dimensional curve and three-dimensional surface can expressed as:

$$\bar{p} \triangleq \begin{bmatrix} \bar{p}_x \\ \bar{p}_y \\ \bar{p}_z \end{bmatrix} = \bar{U}\bar{A}$$

where $\vec{U}$, the parametric vector of cubic order, is $\vec{U} \triangleq [u^3\ u^2\ u\ 1]$ and $\vec{A}$ corresponds to the algebraic matrix of coefficients that generates the 2D (3D) curve (surface) as the parameter **u** is incremented.

$$\vec{A} \triangleq \begin{bmatrix} a_{3x} & a_{3y} & a_{3z} \\ a_{2x} & a_{2y} & a_{2z} \\ a_{1x} & a_{1y} & a_{1z} \\ a_{0x} & a_{0y} & a_{0z} \end{bmatrix}$$

For the 2D case of oceanic vertical interpolation (T-depth and S-depth equivalent to the x-y plane), the 'z' coefficients

$$a_{3z} = a_{2z} = a_{1z} = a_{0z} = 0.$$

Although these algebraic expressions are relatively simple, the difficulties arise when trying to decide which matrix $\vec{A}$ will generate the best (smooth, continuous) 3D (2D) surface (curve). In order to determine the adequate matrix coefficients that will produce the desired surface, once combined with the incremental parametric vector, it is first appropriate to look at the geometric form of the PCC and try to understand how they are constructed graphically.

Again, the position vector defining the PC surface can be expressed by

$$\vec{p} \triangleq \begin{bmatrix} \vec{p}_x \\ \vec{p}_y \\ \vec{p}_z \end{bmatrix} = \vec{F}\,\vec{B} \text{ and } \vec{F} = \vec{U}\,\vec{M}$$

where the parametric vector is $\vec{U} \triangleq [u^3\ u^2\ u\ 1]$ and $\vec{M}$, an invariant matrix, equals

$$\vec{M} \triangleq \begin{bmatrix} 2 & -2 & 1 & 1 \\ -3 & 3 & -2 & -1 \\ 0 & 0 & 1 & 0 \\ 1 & 0 & 0 & 0 \end{bmatrix}.$$

The geometric matrix, $\vec{B}$, is formed by the two points vectors to be interpolated, P_0 and P_1, and their corresponding tangent bisector vectors, P_0'' and P_1'', as

$$\vec{B} \triangleq \begin{bmatrix} \vec{p}_{0x} & \vec{p}_{0y} & \vec{p}_{0z} \\ \vec{p}_{1x} & \vec{p}_{1y} & \vec{p}_{1z} \\ \vec{p}''_{0x} & \vec{p}''_{0y} & \vec{p}''_{0z} \\ \vec{p}''_{1x} & \vec{p}''_{1y} & \vec{p}''_{1z} \end{bmatrix}.$$

Once again, for the planar 2D case, the 'z' components simply have to be set to:

$$\vec{p}_{0z} = \vec{p}_{1z} = \vec{p}''_{0z} = \vec{p}''_{1z} = 0.$$

In order to better understand what exactly these various vectors represent and how they come into the construction of the PCC, we can refer to the next figure illustrating a sequence of 4 points, P_{i-1} to P_{i+2}, from which the middle two (P_i and P_{i+1}) need to be linked (interpolated). The basic characteristic of the PC curve is to join the two middle points with a smooth cubic curve while preserving the general direction prescribed by the sequences P_{i-1} to P_{i+1} and P_i to P_{i+2}. To do so, two unit vectors, $\hat{t}_0$ and $\hat{t}_1$, tangent to the general orientation of the point series, are placed at each ends of the interval to be interpolated, P_i and P_{i+1}. The parametric-cubic spline that will then be constructed will have to satisfy the following two boundary conditions for its end points:

- 1. It must be continuous at both interpolating ends.
- 2. It must also be tangent to the two vectors, $\hat{t}_0$ and $\hat{t}_1$, at P_i and P_{i+1}.

As depicted by the next figure, these two tangents simply correspond to the bisector vectors prescribed by half the angle between the $\overline{P_{i-1}P_i}$ and $\overline{P_i P_{i+1}}$ segments for $\theta/2$ and between $\overline{P_{i-1}P_i}$ and $\overline{P_i P_{i+1}}$ for $\phi/2$.

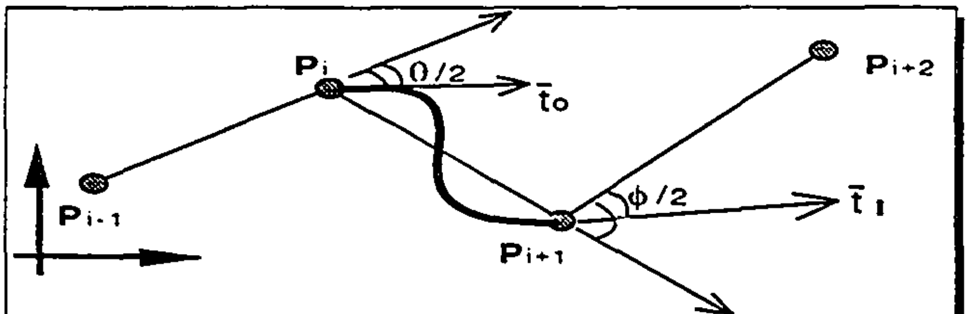

Geometric construction of the PCC for the 4 points sequence with the corresponding vectors.

Consequently, these two unit tangent bisector vectors are defined by :

$$\hat{t}_0 = \frac{\dfrac{\vec{p}_i - \vec{p}_{i-1}}{|\vec{p}_i - \vec{p}_{i-1}|} + \dfrac{\vec{p}_{i+1} - \vec{p}_i}{|\vec{p}_{i+1} - \vec{p}_i|}}{\left|\dfrac{\vec{p}_i - \vec{p}_{i-1}}{|\vec{p}_i - \vec{p}_{i-1}|} + \dfrac{\vec{p}_{i+1} - \vec{p}_i}{|\vec{p}_{i+1} - \vec{p}_i|}\right|}$$

$$\hat{t}_1 = \frac{\dfrac{\vec{p}_{i+1}-\vec{p}_i}{|\vec{p}_{i+1}-\vec{p}_i|} + \dfrac{\vec{p}_{i+2}-\vec{p}_{i+1}}{|\vec{p}_{i+2}-\vec{p}_{i+1}|}}{\left|\dfrac{\vec{p}_{i+1}-\vec{p}_i}{|\vec{p}_{i+1}-\vec{p}_i|} + \dfrac{\vec{p}_{i+2}-\vec{p}_{i+1}}{|\vec{p}_{i+2}-\vec{p}_{i+1}|}\right|}$$

From this, it is obvious to note that $\hat{t}_0$ and $\hat{t}_1$ are effectively obtained by first, adding the unit vectors corresponding to the $\overline{P_{i-1}P_i}$ and $\overline{P_i P_{i+1}}$ segments for $\hat{t}_0$ and $\overline{P_{i-1}P_i}$ and $\overline{P_i P_{i+1}}$ for $\hat{t}_1$, and then dividing the resulting vector by its magnitude, thus becoming unit length. A second type of vector is also used in the construction of the PCC. The local X-axis, $\hat{i}$, represent some sort of coordinate axis, specific to the series to be interpolated, P_i to P_{i+1}. This unit length vector "pinned" to the first interval end, P_i, and defined relatively simply by

$$\hat{i} = \frac{\hat{t}_0 + \hat{t}_1}{|\hat{t}_0 + \hat{t}_1|},$$

has no "direct" geometric influence on the PC curve. Instead, it is involved in the magnitude determination of the tangent vectors $\vec{p}_0''$ and $\vec{p}_1''$, as expressed by:

$$\vec{p}_0'' \triangleq k_0\, \hat{t}_0$$

$$\vec{p}_1'' \triangleq k_1\, \hat{t}_1$$

$$k_0 = k_1 = \frac{(\vec{p}_{i+1} - \vec{p}_i)\bullet \hat{i}}{\hat{t}_0 \bullet \hat{i}}$$

The local X-axis constitutes perhaps the only "artifice" that can be modulated to vary the PC curvature radii. As mentioned earlier, combinations of one or two of these local "coordinate axis" and variations on their unit/non-unit length form the 4 possible types of PCC mentioned. They nevertheless remain much "less artificial" than most spline methods for several reasons. First, their mathematical foundation is essentially geometric, making use of no statistical or other artificial "tuning" parameter. Furthermore, the PCC construction truly relies on the four points sequence, P_{i-1} to P_{i+2}, thus involving no off-constructs to shape the curve segment. Finally, the entire PCC theory, "geometric cousin" to the (more familiar) Bézier curves (Zsombor-Murray, personal communication), constitutes a particular case of the common B-splines whose mathematical formulation and numerical behavior are quite elegant and rigourous (Kincaid and Cheney, 1991). Thes are two last points to be noted about the particularities of the interpolating scheme used to process the oceanic data. The parametric-cubic curves were chosen as the best overall method for the present situation, but were slightly improved by adding a few numerical criteria. First, it was expected that any interpolated value between its two end, P_i and P_{i+1}, would lie in between these two end values. Consequently, if for some reason, the interpolation algorithm yielded an intermediate point outside the range cover by the observation interval, then the linear method was substituted for that interval. Although this situation occured very rarely, the linear method was used occasionally when two measurements were almost similar (isoT and isoS). Also, it was noticed that due to the specific structure of the upper mixed-layer, a minimum number of observations were necessary for the interpolation to yield physically realistic results. Therefore, a set of criteria were established for each month and area where a mixed-layer was expected to be present. These required that, for the upper 100 meters, a minimum number of observational points as well as a certain vertical density of measurements be present for the interpolation routine to proceed.

Appendix 2

Horizontal Distribution of Surface Salinity Data

SSS - MAY

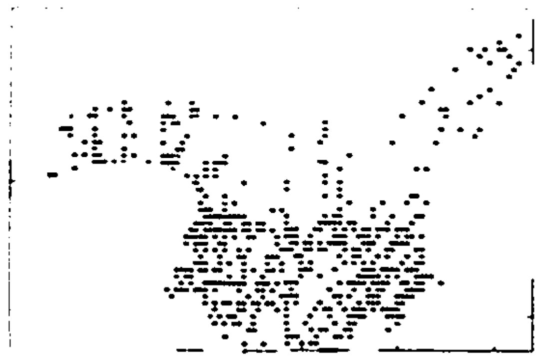

SSS - JUN

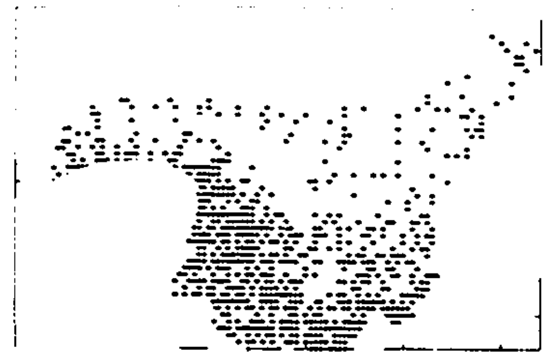

SSS - JUL

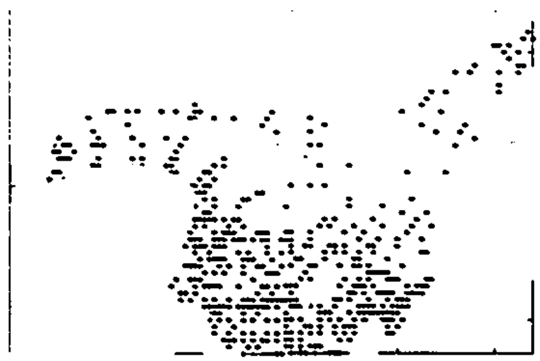

SSS - AUG

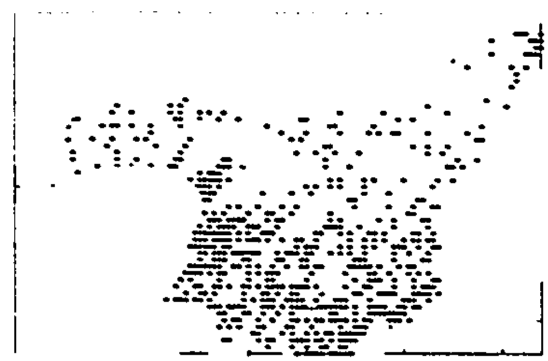

SSS - SEP

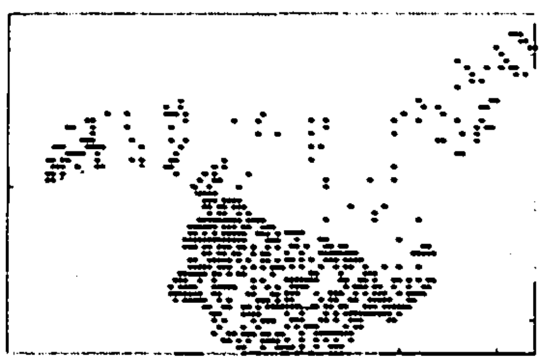

SSS - OCT

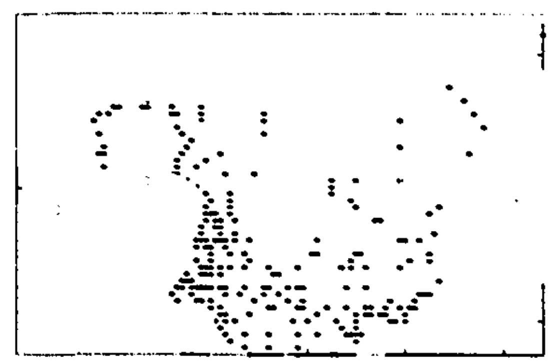

SSS - NOV

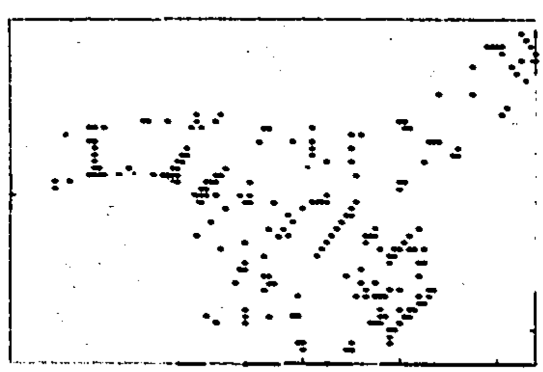

Appendix 3

Monthly Composites of AVHRR-derived SST Fields for 1987 and 1990, and Corresponding Atmospheric Fields

The NOAA/NASA Pathfinder AVHRR SST data:

The NOAA/NASA Pathfinder AVHRR Oceans datasets is global, multichannel, sea surface temperature data derived from the Advanced Very High Resolution Radiometers (AVHRR) on the NOAA/TIROS operational meteorological satellites (NOAA-7, 9, and 11) which provide a continuous daily and composite dataset from July 1981 through the present[1]. "The AVHRR Ocean Pathfinder data are processed in an equal-area grid based on one developed by the International Satellite Cloud Climatology Project (ISCCP). The bin size is approximately 9.28 km on a side. Since the data were originally sampled at approximately 4 km resolution, bin values are averages. Each of the series of NOAA satellites operates in a near-polar, sun-synchronous orbit. The orbital period is ~102 minutes, giving 14.1 orbits per day (Kidwell, 1991). The 110.8° cross-track scan equates to a swath width of about 2700 km. AVHRR was designed for multispectral investigations of meteorological, oceanographic, and hydrologic parameters, measuring emitted and reflected radiance in four or five spectral bands, spanning the visible portion of the spectrum to the thermal infrared. Coverage is global, twice daily, at an instantaneous field of view (IFOV) of ~1.4 milliradians, giving a ground field of view of ~1.1 km at nadir for a nominal altitude of 833 km.

The history of SST computation from AVHRR radiances is discussed at length by McClain et al. (1985). Briefly, radiative transfer theory is used to correct for the effects of the atmosphere on the observations by utilizing "windows" of the electromagnetic spectrum where little or no atmospheric absorption occurs. Channel radiances are transformed

---

[1]: A more detailed description of the NOAA-series satellites, the AVHRR instrument, and the AVHRR Global Area Coverage (GAC) Level-1B data can be found in the Polar Orbiter Users Guide (Kidwell, 1991), which can be obtained from NOAA/NESDIS, and from which the following information is reproduced.

(through the use of the Planck function) to units of temperature, then compared to a-priori temperatures measured at the surface. This comparison yields coefficients which, when applied to the global AVHRR data, give estimates of surface temperature which have been nominally accurate to 0.3 °C. Recently, the AVHRR thermal vacuum test data have been examined in detail (Brown et. al., 1993) in order to quantify drift in the calibration coefficients of the channels. Through this work, the nonlinear SST algorithm has been modified with a time-dependent term. Processing has been further modified by dividing the earth into three regimes of atmospheric water vapor. Regression coefficients are computed independently for each of these regimes, to compensate for the well-known limitations of AVHRR SST retrievals in tropical areas, which are an artifact of high humidity. The AVHRR Level-1B sensor counts in the visible channels (1 and 2) are first converted to Rayleigh-corrected radiances and then to optical depth for use in removing the effects of the atmosphere and viewing and illumination geometry. Channels 3-5 are transformed to units of "brightness temperature", using the Planck black body function and a newly-determined (Brown et al., 1993) correction for sensor calibration non-linearity in the longer-wavelength channels. The algorithm used is essentially the nonlinear SST with a modification for sensor calibration drift with time.

In order to be considered a match, the pixel location and in-situ measurement must differ by no more than 0.1 degree spatially, and temporally by no more than 30 minutes. Temperature retrievals as detailed above are determined for all pixels. Several tests are then performed to assign an estimate of the goodness of each retrieval, in the form of a flag value with four possible values. The "satellite" test is a channel 4/5 threshold (used to detect how "bright" a pixel is), combined with a spatial homogeneity test. The "Reynolds" test is a comparison of the initial temperature retrieval to the Reynolds blended SST climatology. If a pixel passes all of these, it is considered "best", and assigned a quality flag of 3. Passing the Reynolds test but failing the satellite test generates a 2 (or "mediocre" quality), failing the Reynolds test and passing the satellite test generates a 1, and failing all tests gives a quality flag of zero. The next phase is declouding, effected through the creation of composite images over 3 weeks before and after the target week, and a mean computed from these. The composite means are used to fill a central weekly mean image which contains the day being declouded (if the central mean image is missing values, and if there is a mean pixel of sufficient quality). If the weekly means from week(n-1) or week(n+1) cannot be used to fill empty values in the central (week n) mean, a spatial interpolation is done. The completely-filled weekly image is then compared to the daily image, and simple thresholding is used to indicate partial or complete cloudiness. Repeating this process generates a cloud mask for every day of data. Finally, a semi-automated quality-assurance (QA) scheme has been developed which examines AVHRR SST retrievals for temporal and spatial consistency. This is carried out in a two-part statistical post-processor, followed by a visual inspection. The automated portion of the analysis serves to guide an operator in the visual inspection phase, greatly reducing the time necessary to characterize spurious findings. The data quality information thus gained is passed to the end-user in the form of additions to the processing flags, as well as comments which are included in each image file. This combination forms a qualitative and quantitative description of anomalies found in the data."

Monthly Composites of AVHRR-derived SST Fields for 1987 and 1990:

The following 7 figures display monthly composites SST fields over the GSL for the ice-free months of 1987 and 1990. These two years were chosen because of the limited data availibility for monthly composites. As will be noticed, they nonetheless depict rather different oceanographic features and are of considerable interest given the availaibility of air temperature and cloud cover fields for these two years. (white pixels were plotted when the data quality was not sufficient to compute monthly mean values - composites).

- **fig. A3.1a:** (COLOR PLATE 1) AVHRR-derived SST fields - May 1987 and 1990.
- **fig. A3.1b:** (COLOR PLATE 2) same as fig. A3.1a - June 1987 and 1990.
- **fig. A3.1c:** (COLOR PLATE 3) same as fig. A3.1a - July 1987 and 1990.
- **fig. A3.1d:** (COLOR PLATE 4) same as fig. A3.1a - August 1987 and 1990.
- **fig. A3.1e:** (COLOR PLATE 5) same as fig. A3.1a - September 1987 and 1990.
- **fig. A3.1f:** (COLOR PLATE 6) same as fig. A3.1a - October 1987 and 1990.
- **fig. A3.1g:** (COLOR PLATE 7) same as fig. A3.1a - November 1987 and 1990.

NOAA/AVHRR SST May87 (deg C)

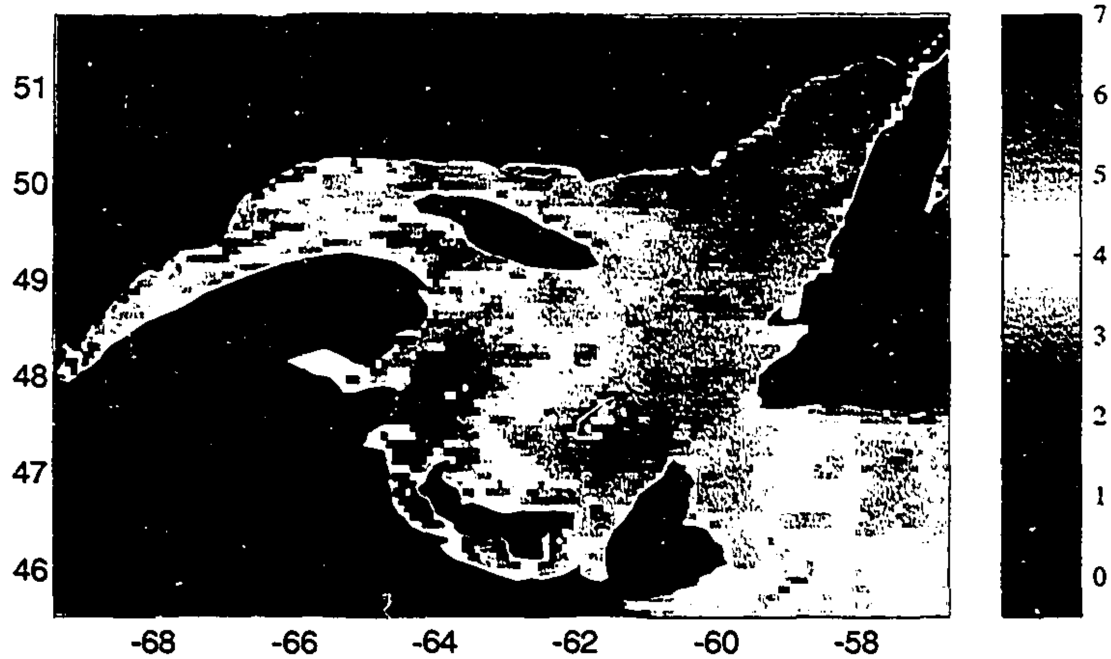

NOAA/AVHRR SST May90 (deg C)

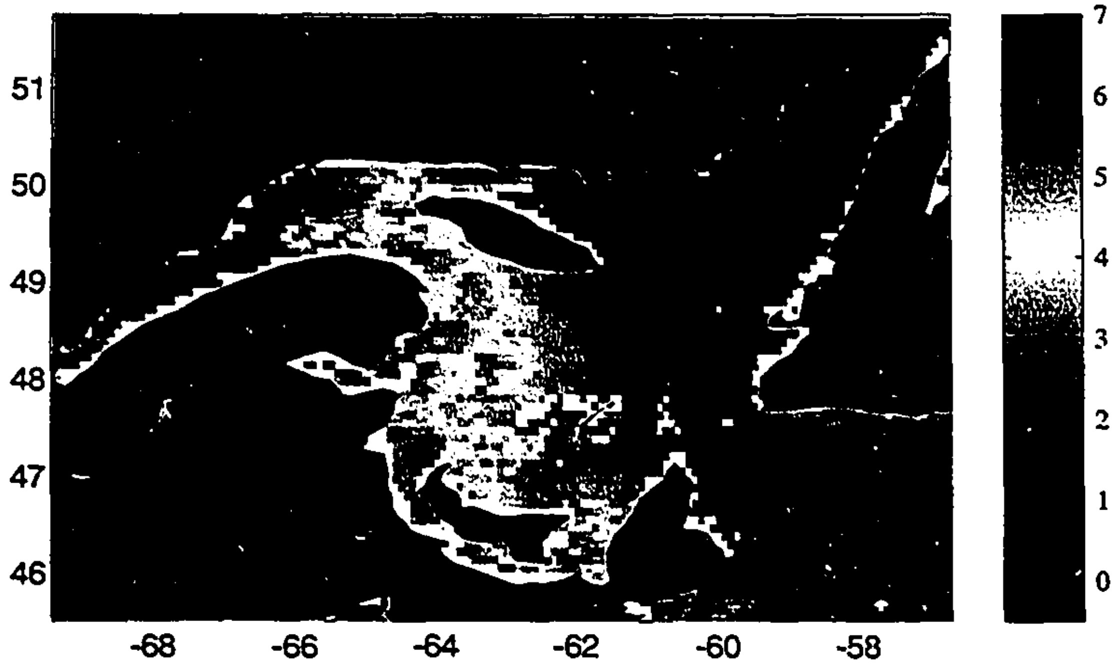

NOAA/AVHRR SST Jun87 (deg C)

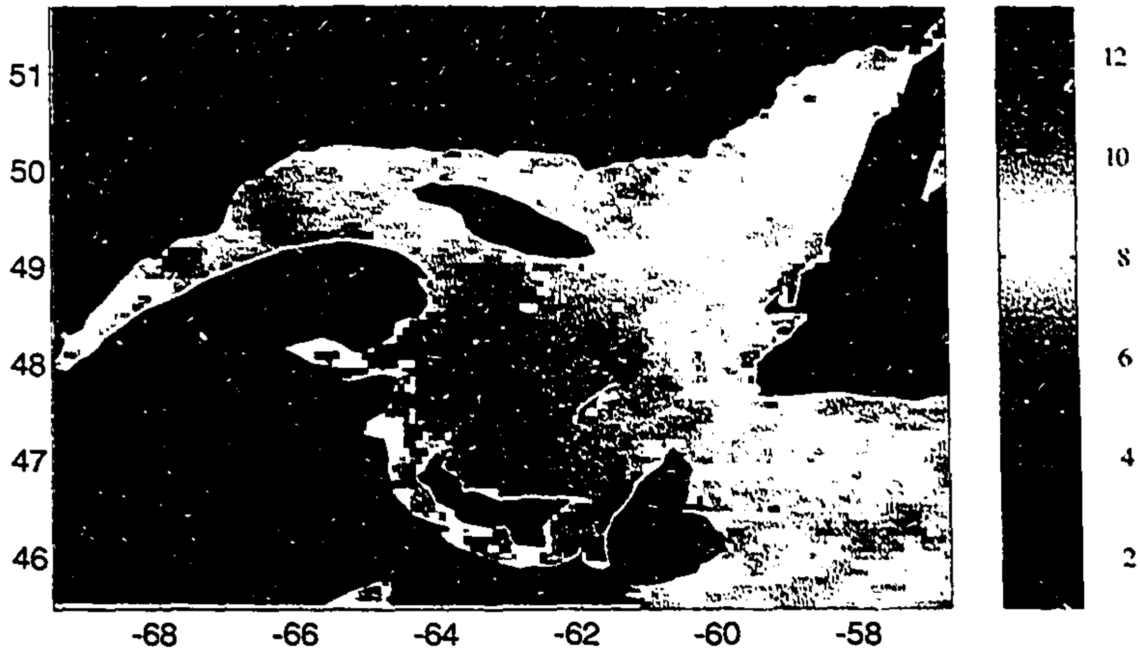

NOAA/AVHRR SST Jun90 (deg C)

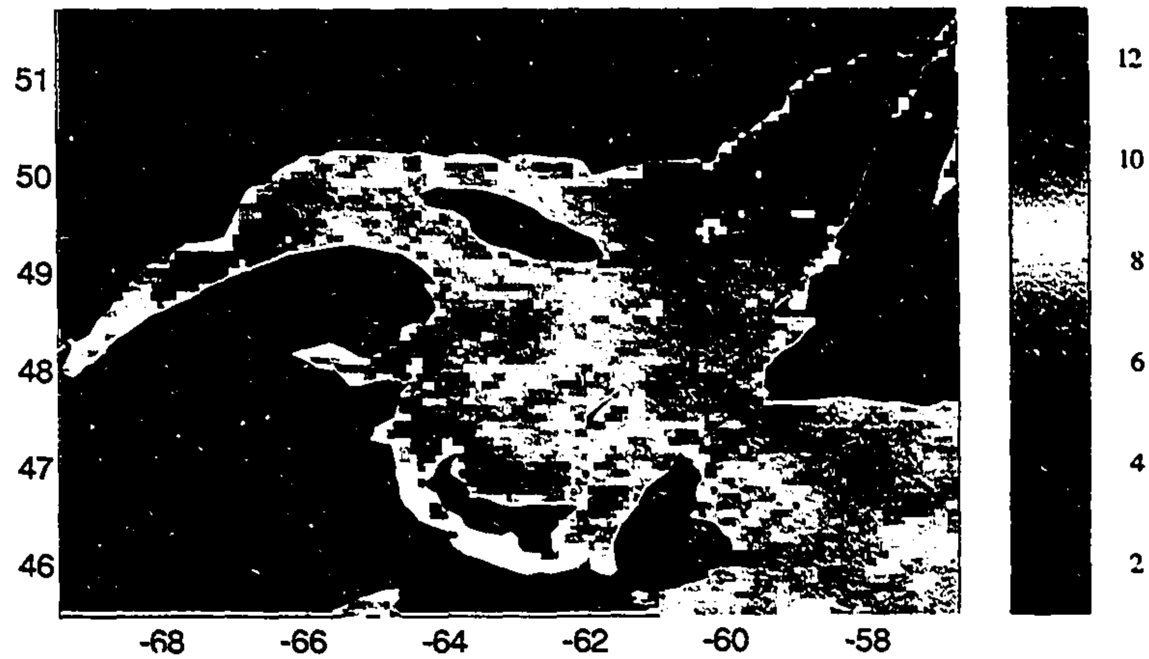

NOAA/AVHRR SST Jul87 (deg C)

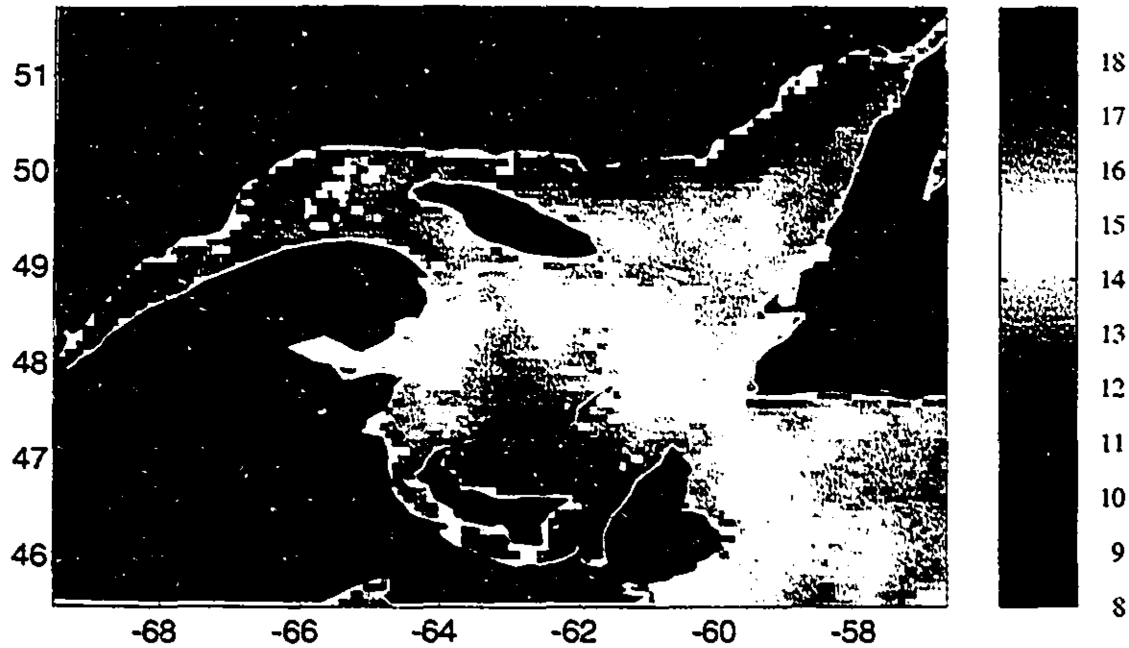

NOAA/AVHRR SST Jul90 (deg C)

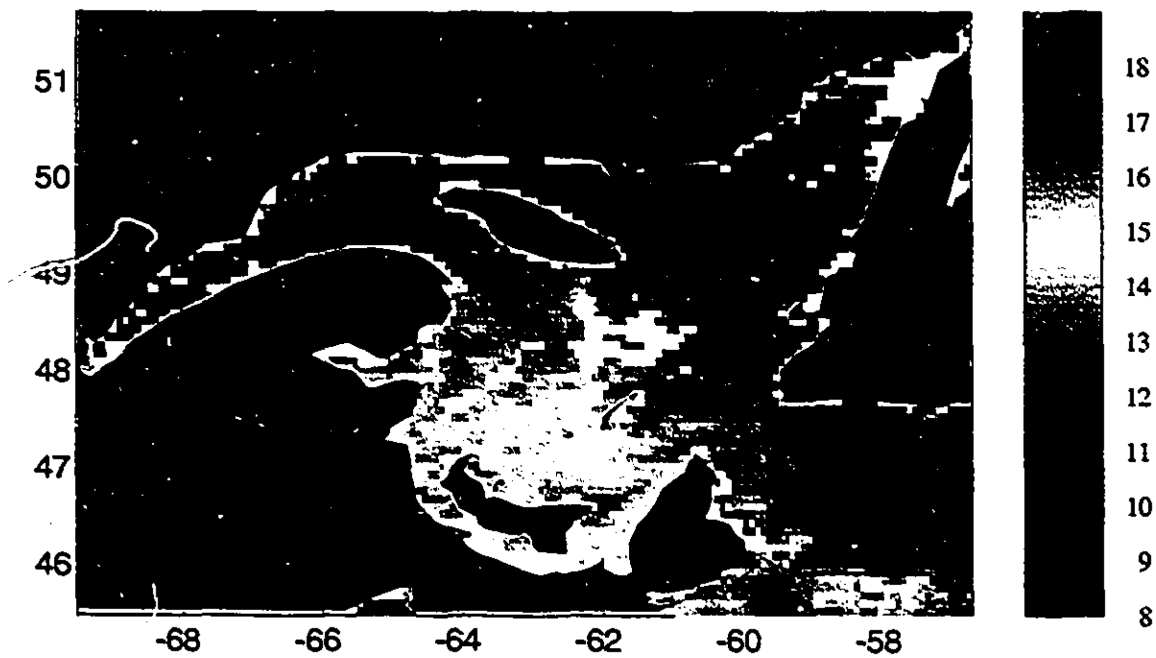

NOAA/AVHRR SST Aug87 (deg C)

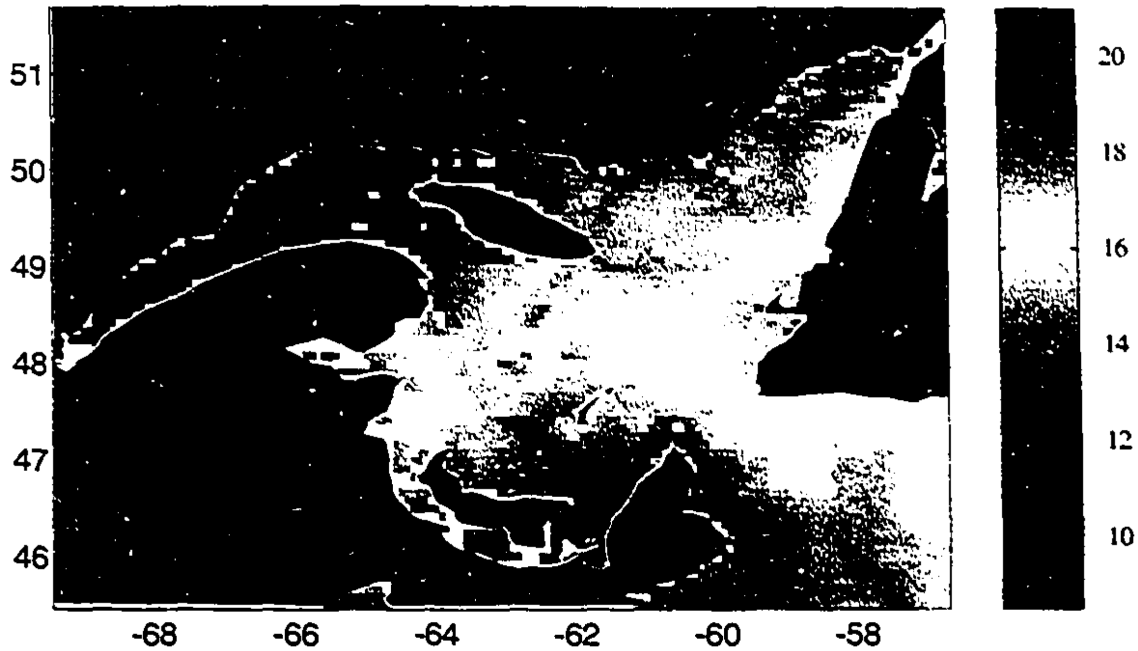

NOAA/AVHRR SST Aug90 (deg C)

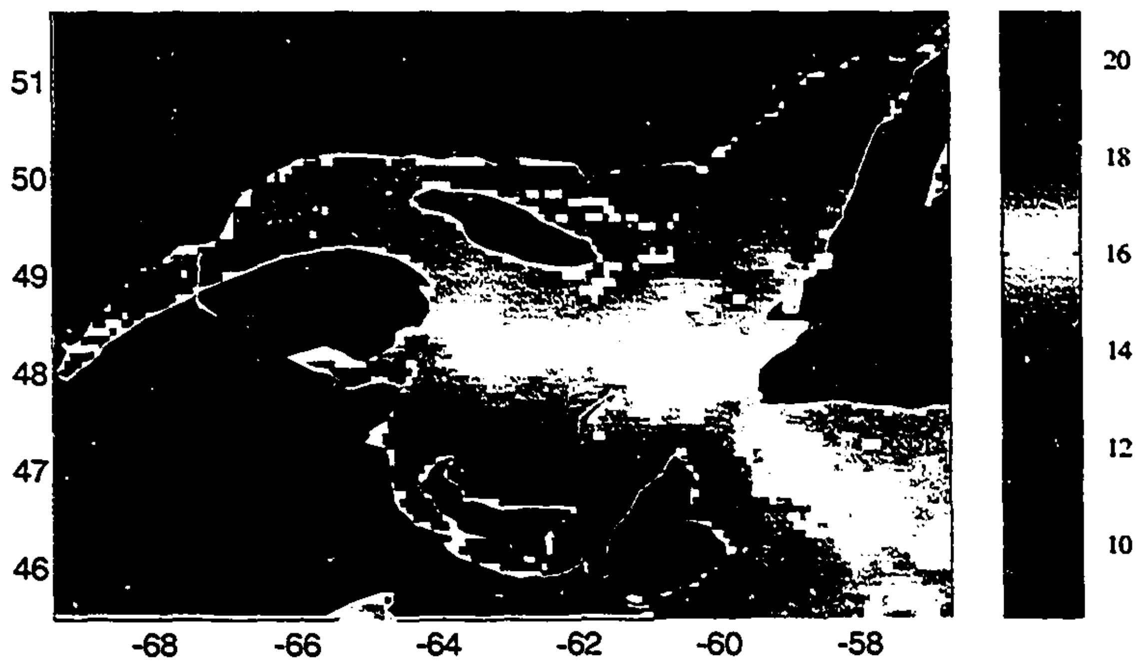

NOAA/AVHRR SST Sep87 (deg C)

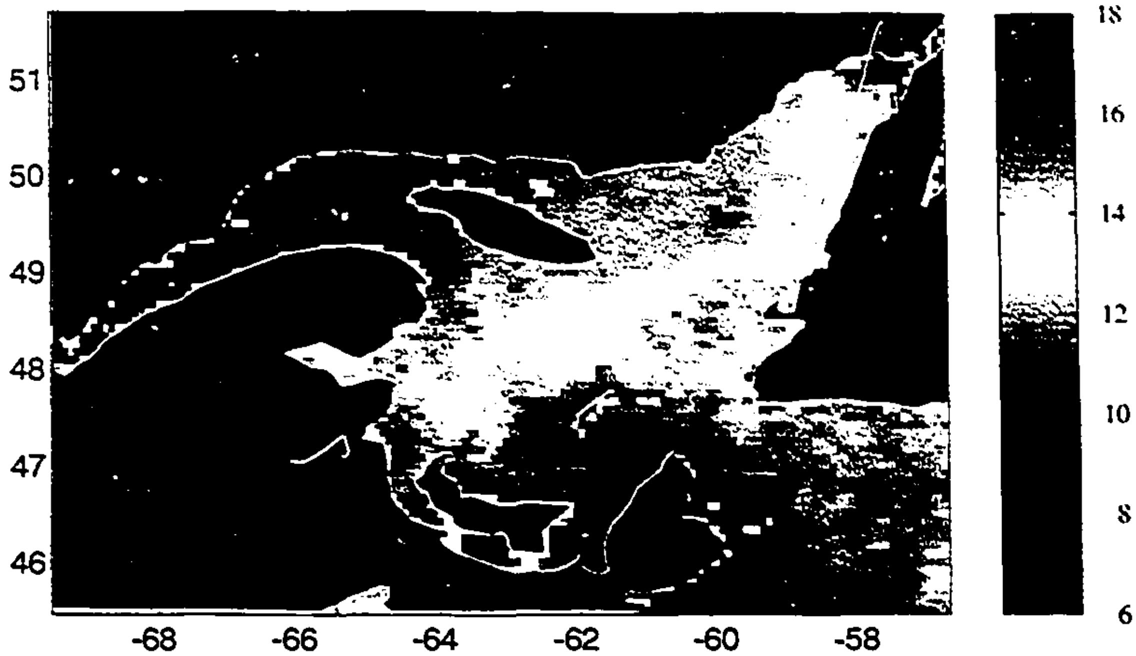

NOAA/AVHRR SST Sep90 (deg C)

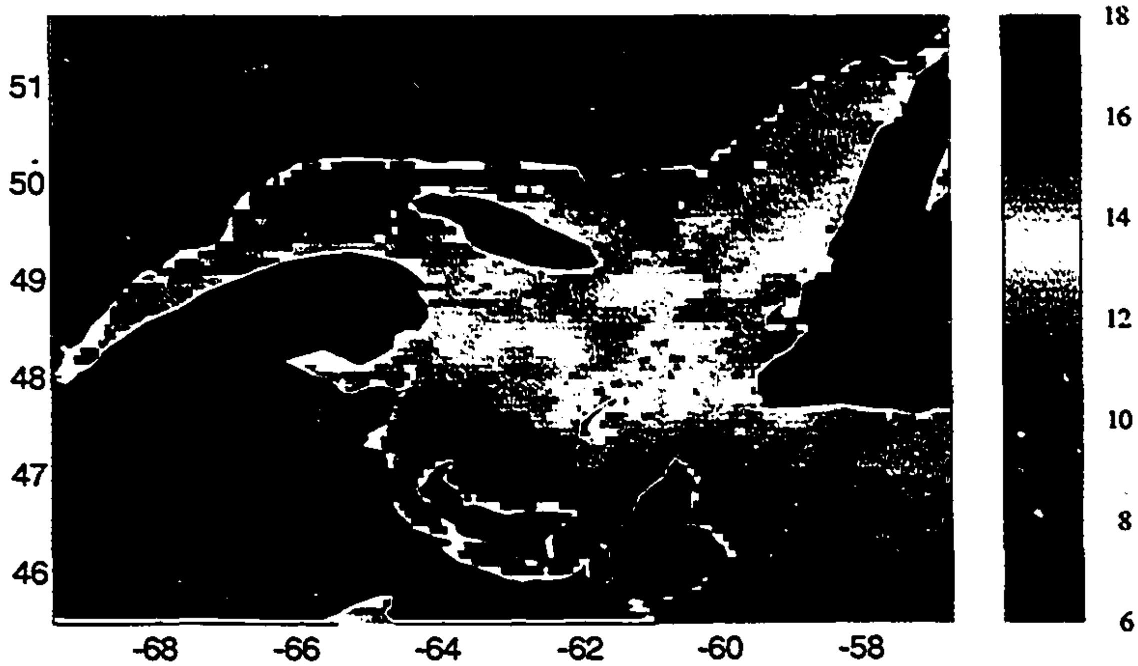

NOAA/AVHRR SST Oct87 (deg C)

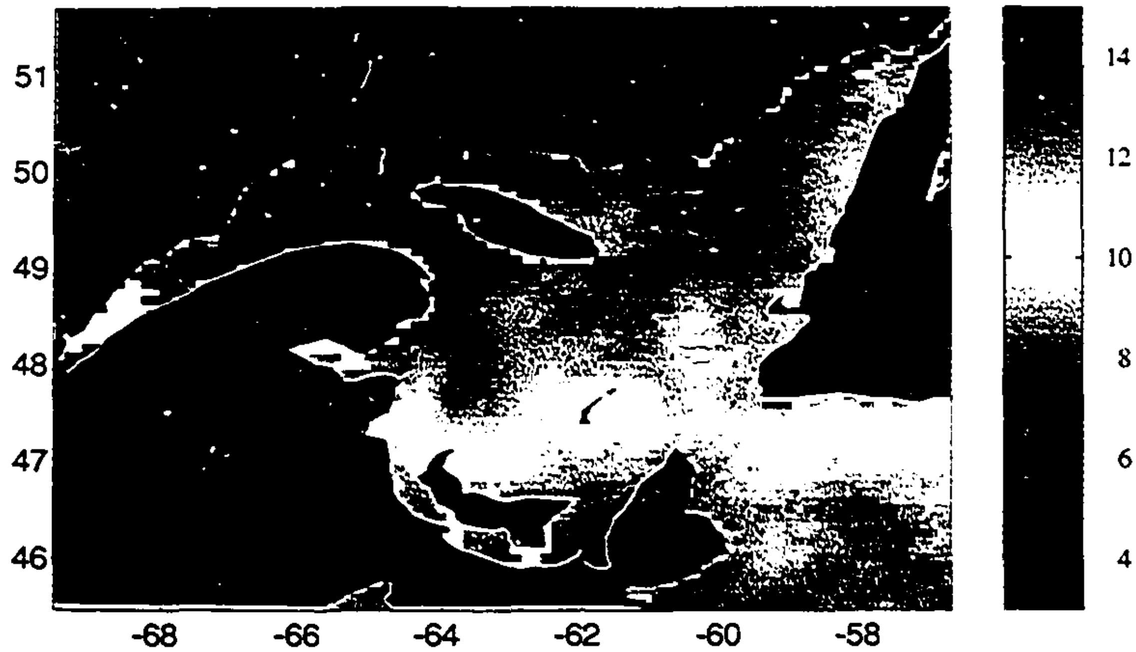

NOAA/AVHRR SST Oct90 (deg C)

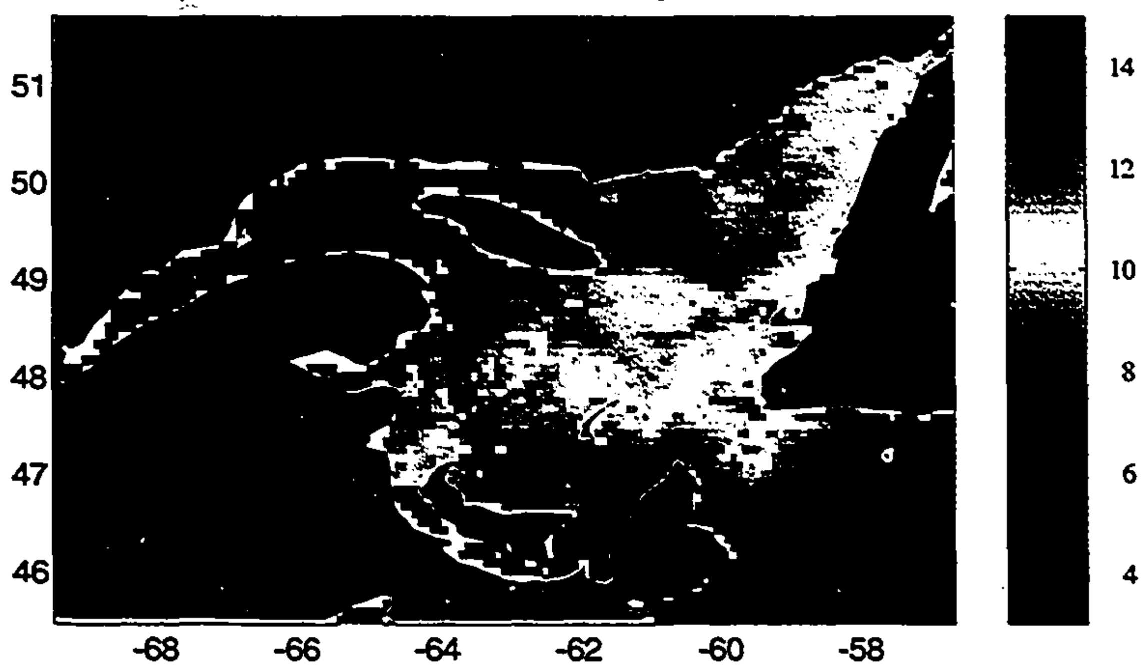

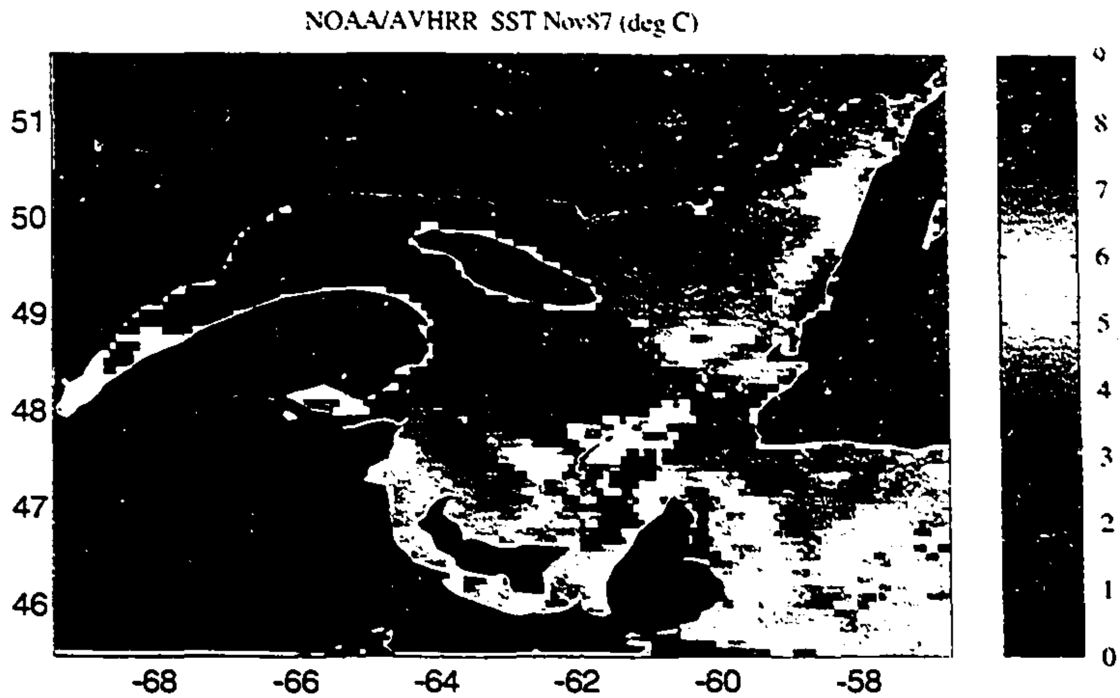
NOAA/AVHRR SST Nov87 (deg C)
51
50
49
48
47
46
-68
-66
-64
-62
-60
-58
8
7
6
5
4
3
2
1
0

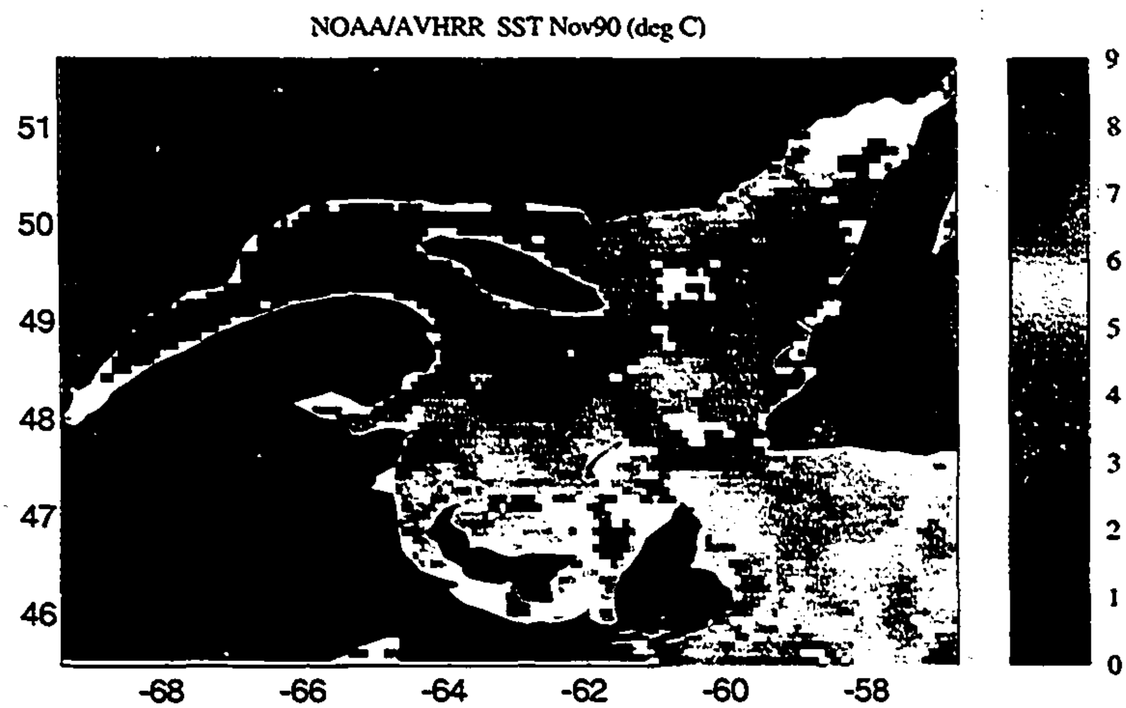
NOAA/AVHRR SST Nov90 (deg C)
51
50
49
48
47
46
-68
-66
-64
-62
-60
-58
9
8
7
6
5
4
3
2
1
0

Appendix 4

Hydrographic Data during the Canadian JGOFS Cruises

As explained earlier, one of the goal of this thesis was to produce various climatologies in order to assess hydrographic changes observed in other studies. Canadian JGOFS is one such research project in which hydrographic (physical, biological, etc.) measurements will be compared with their climatological conterparts. This analysis is being done currently by researchers at McGill and at other universities. Consequently, this section will briefly show the averaged thermohaline state of the water column for each station/cruise (see chapter 3) as well as some climatological comparisons.

The next three pages display averaged vertical profiles T, S and E for all 6 stations in the GSL (see chapter 3 for a description of cruise dates and station locations). The small number besides each profile corresponds to the cruise #. The graphs display typical hydrographic and atmospheric conditions encountered for some stations/cruises, as well as the corresponding climatology.

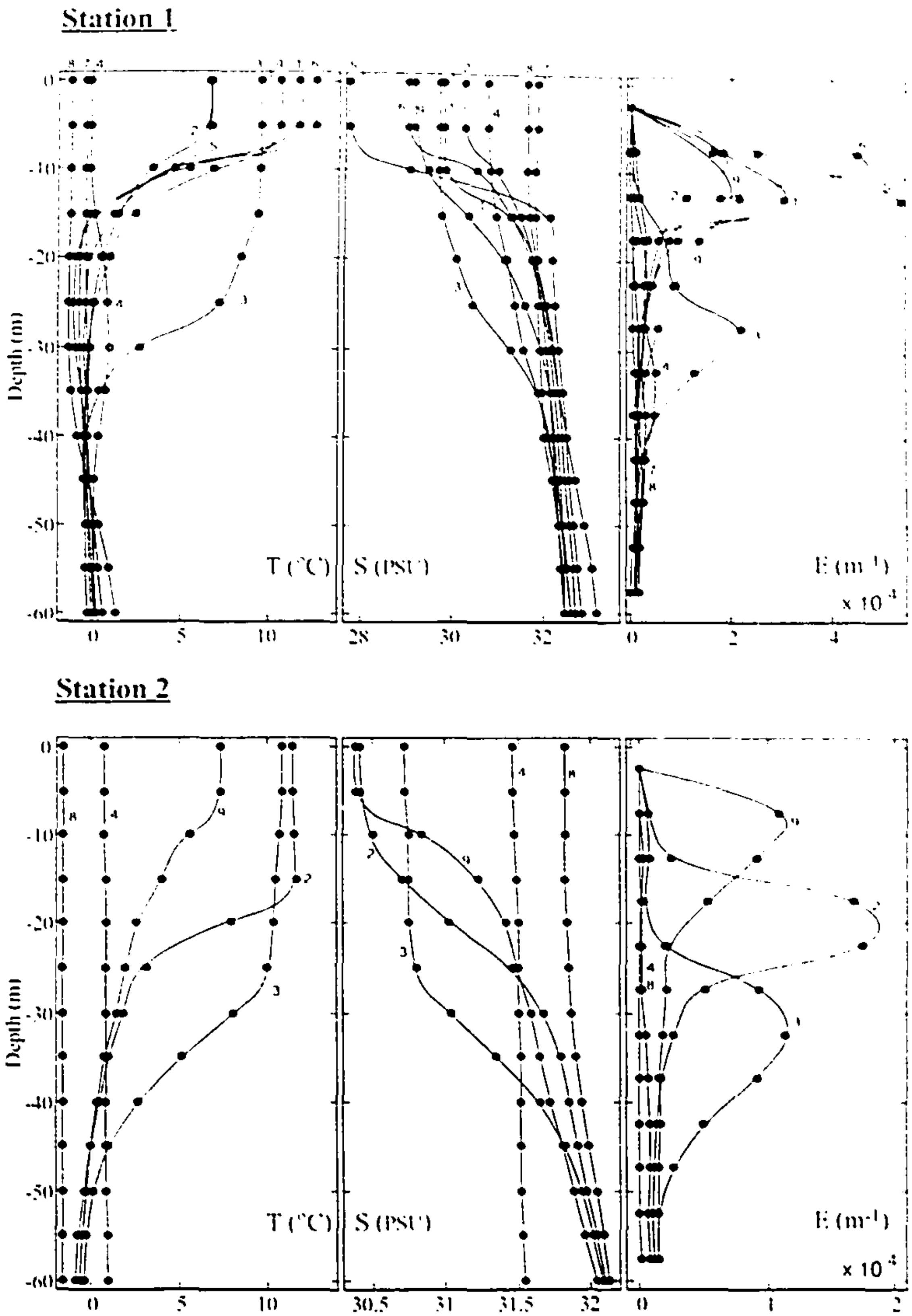

Fig. A4.1: *T, S, and E for stations 1 and 2 during the 9 JGOFS cruises.*

Station 3

Station 4

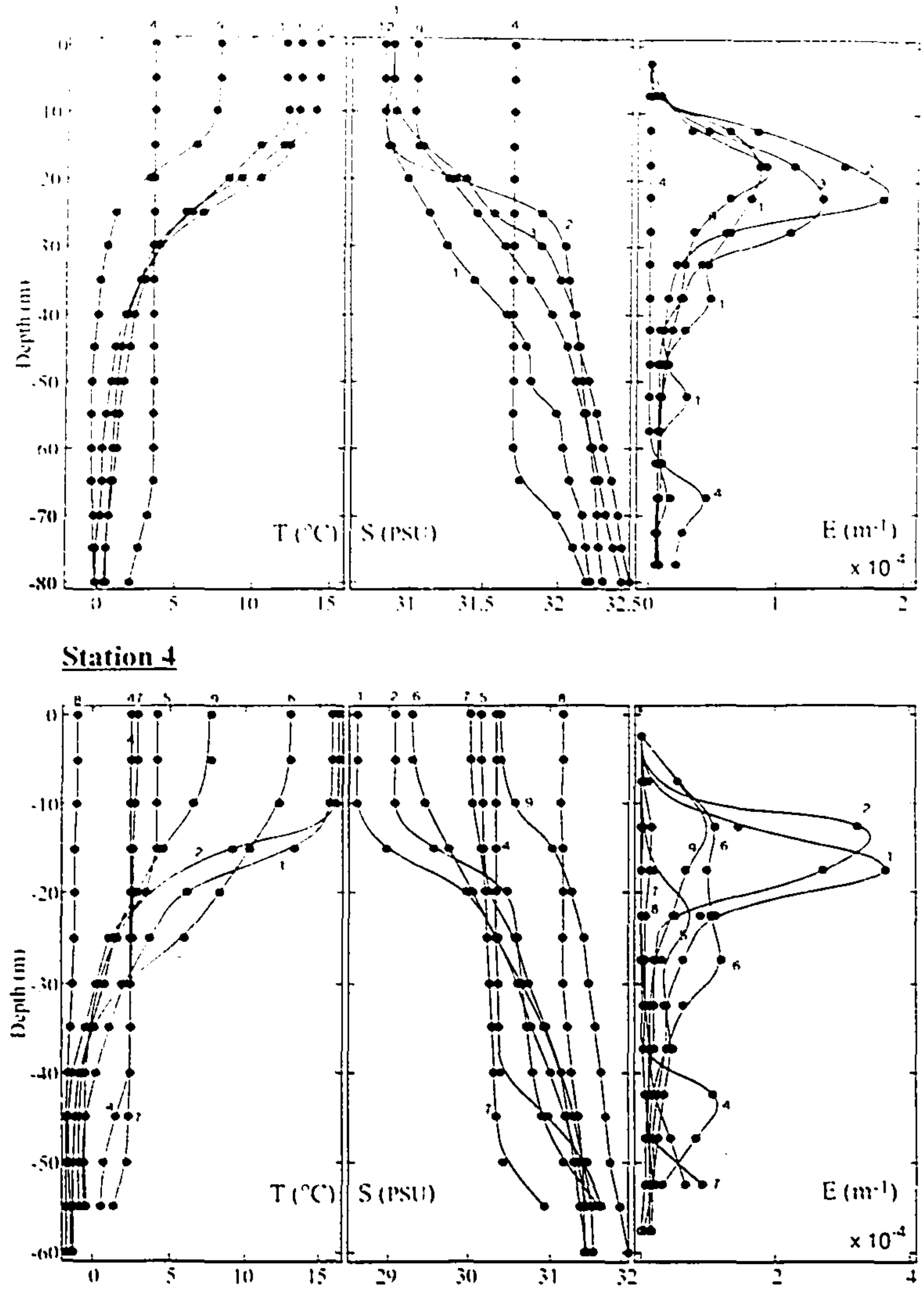

Fig. A4.2: *T, S, and E for stations 3 and 4 during the 9 JGOFS cruises.*

Station 5

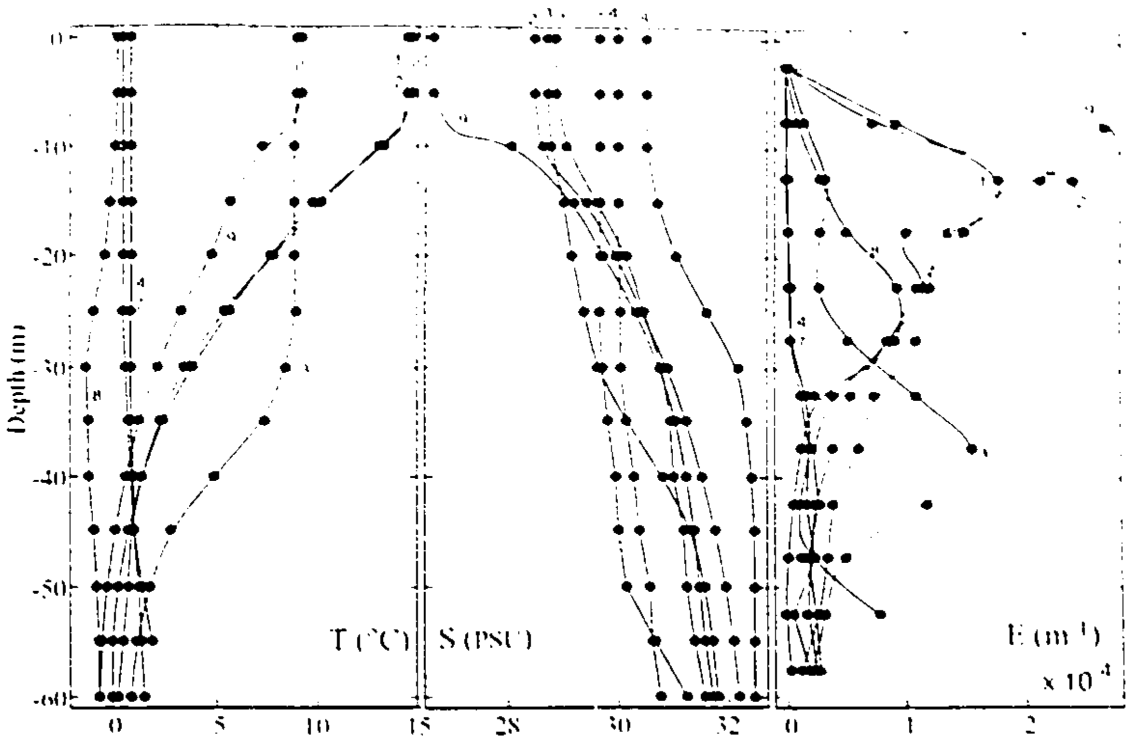

Station 6

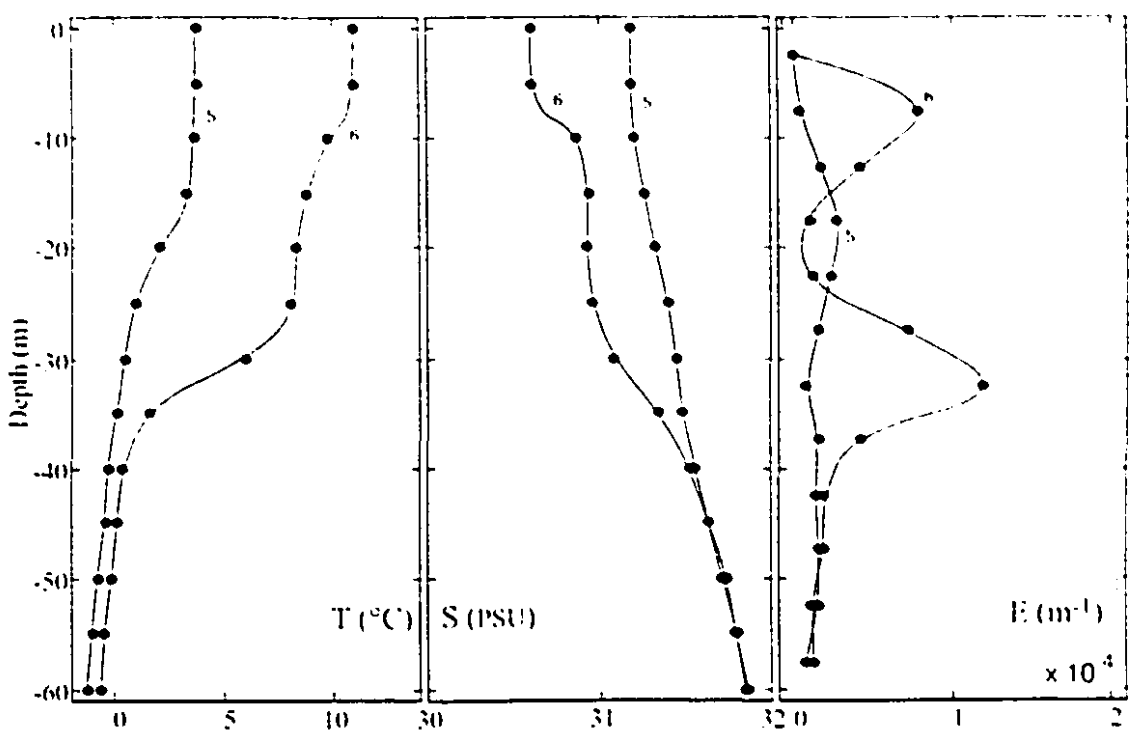

Fig. A4.3: *T, S, and E for stations 5 and 6 during the 9 JGOFS cruises.*

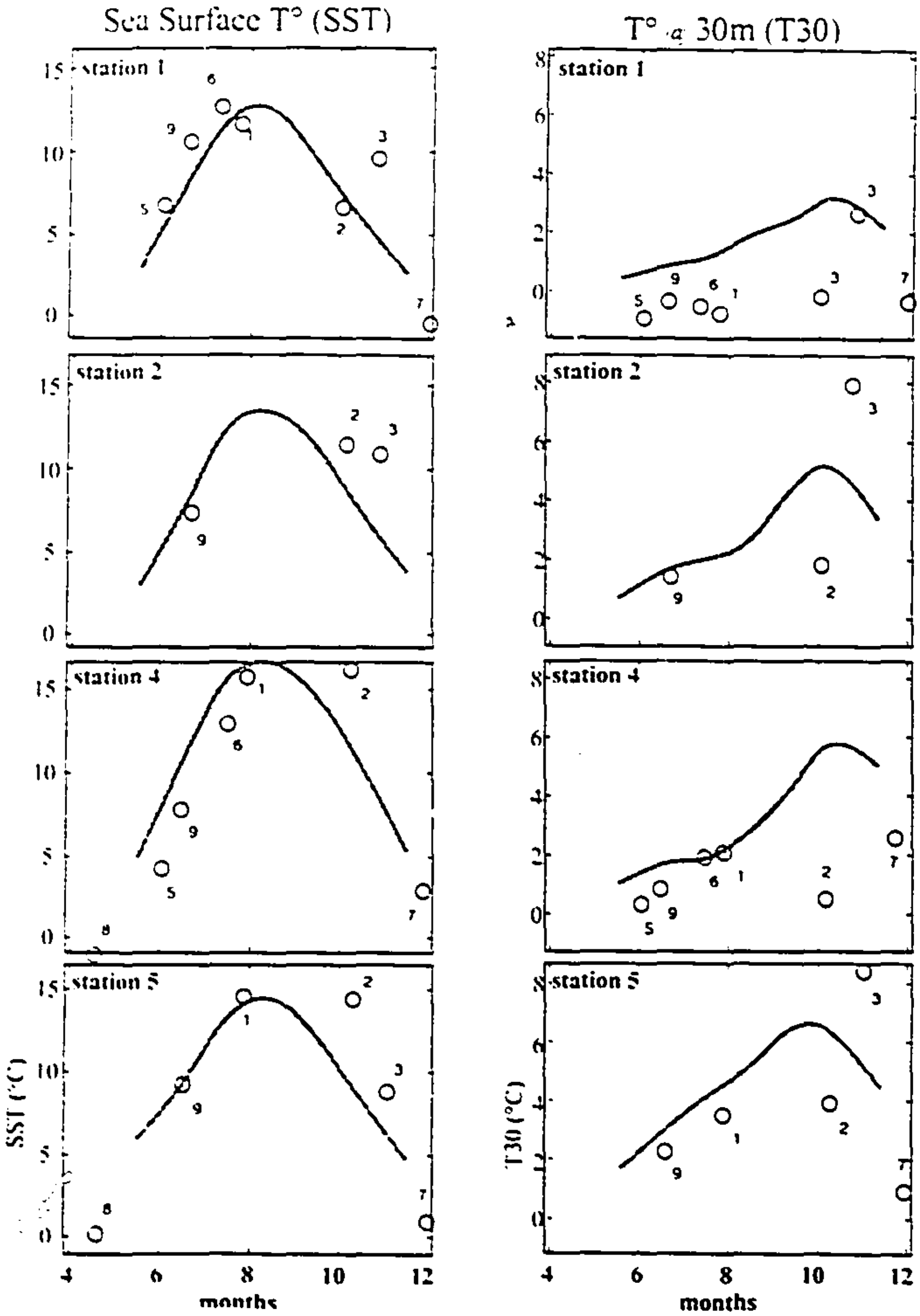

fig. A4.2: *Temperature at the surface and at 30m for stations 1, 2, 4 and 5 for all 9 CJGOFS cruises (solid line corresponds to the local climatology).*

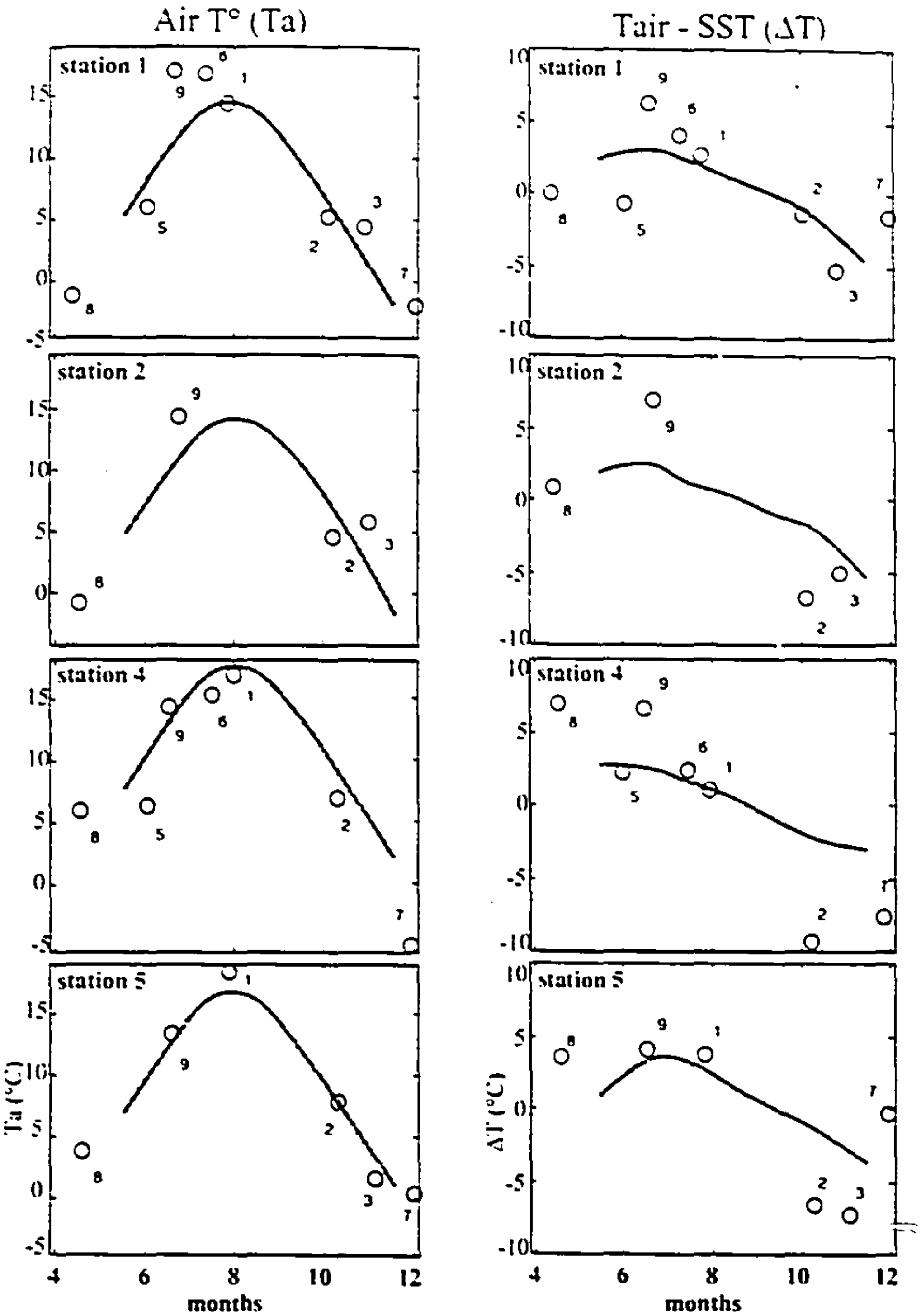

fig. A4.3: *Air temperatures and air-sea temperature differences for stations 1, 2, 4 and 5 for all 9 CJGOFS cruises (solid line corresponds to the local climatology).*

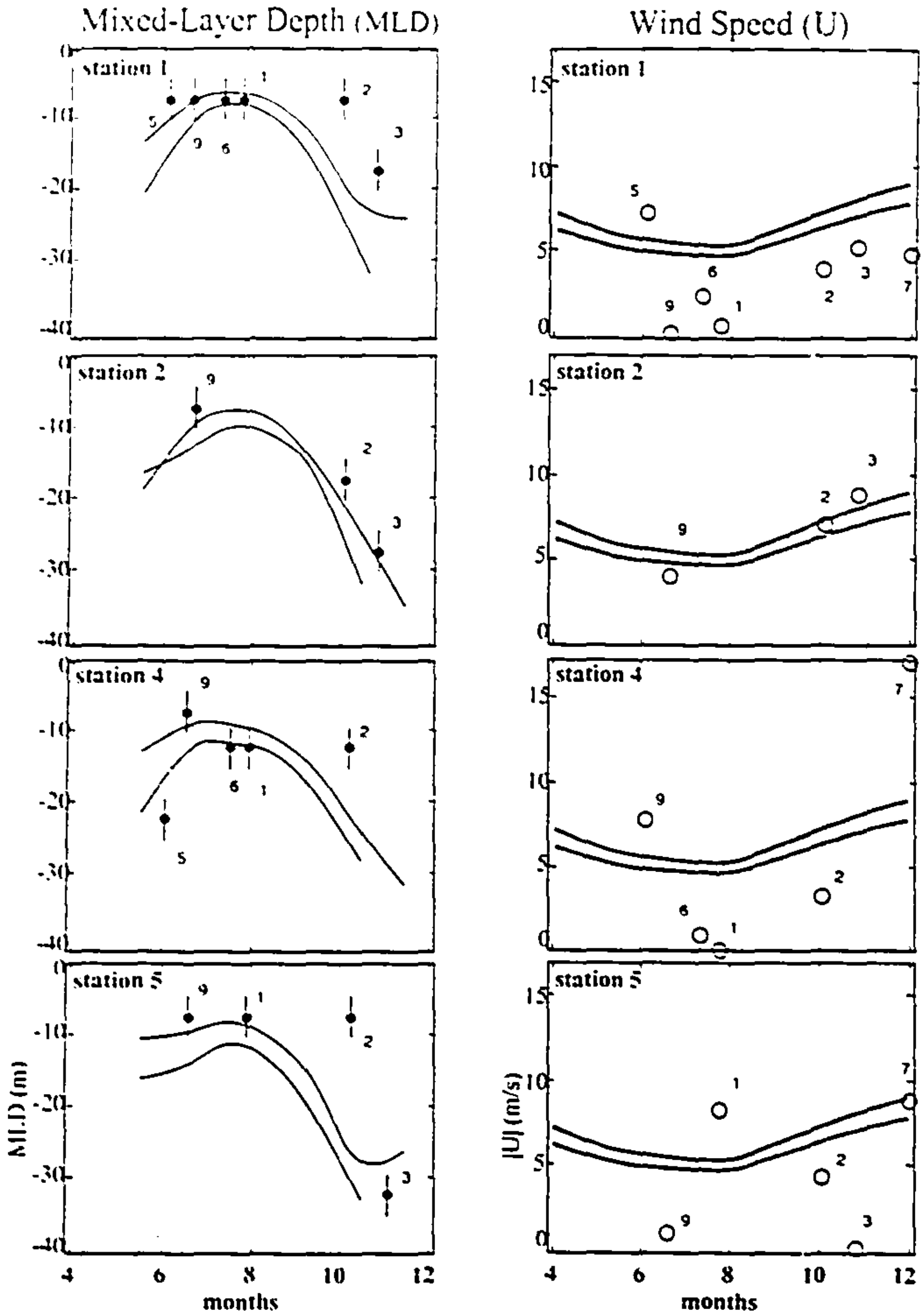

fig. A4.4: *Mixed-layer depth and wind speed for stations 1, 2, 4 and 5 for all 9 CJGOFS cruises (solid line corresponds to the local climatology).*